**ALLOSTERIC INTERACTIONS WITHIN CANNABINOID RECEPTOR 1 (CB$_1$)
AND DOPAMINE RECEPTOR 2 LONG (D$_{2L}$) HETEROMERS**

by

Amina Mustafa Bagher

Submitted in partial fulfilment of the requirements
for the degree of Doctor of Philosophy

at

Dalhousie University
Halifax, Nova Scotia
August 2017

TABLE OF CONTENTS

LIST OF TABLES

LIST OF FIGURES

ABSTRACT

G protein-coupled receptors (GPCRs) have long been recognized as essential membrane receptors mediating a vast array of functions in eukaryotes. GPCRs have more complex signaling than originally envisioned due to the fact that GPCRs can associate to form homomeric complexes or associate with other GPCRs to form heteromeric complexes. Allosteric communication within complexes influences the range of receptor function. Cannabinoid receptor 1 (CB_1) and dopamine receptor 2 long (D_{2L}) are GPCRs that are co-localized in specific neuronal populations in the basal ganglia. These receptors play crucial roles in the coordination of movement. I hypothesized that CB_1 and D_{2L} receptors associate in heteromeric complexes and that CB_1 and D_{2L} ligands promote bidirectional allosteric interactions within heteromeric complexes. I confirmed that CB_1 and D_{2L} receptors form homodimers and that each homodimer was coupled to a $G\alpha_i$ protein. CB_1 and D_{2L} receptors formed higher order oligomeric complexes; the minimum functional heteromeric complex was composed of a CB_1 and D_{2L} homodimer each coupled to a $G\alpha_i$ protein. Activation of either CB_1 or D_{2L} receptors by the agonists, arachidonyl-2-chloroethylamide (ACEA) or quinpirole, respectively, resulted in fast and transient conformational changes among CB_1, D_{2L} and $G\alpha_i$ proteins indicative of receptor activation. Treating cells co-expressing CB_1 and D_{2L} receptors with both ACEA and quinpirole switched CB_1 and D_{2L} receptors coupling and signaling from $G\alpha_i$ to $G\alpha_s$, enhanced β-arrestin1 recruitment and co-internalization. The high-affinity D_{2L} receptor antagonist, haloperidol, was also able to switch CB_1 coupling from $G\alpha_i$ to $G\alpha_s$ but, unlike D_2 agonists, haloperidol inhibited β-arrestin1 recruitment to CB_1 and inhibited complex internalization. Allosteric interactions within CB_1/D_{2L} heteromeric complexes were ligand dose-dependent and bidirectional. CB_1/D_{2L} heteromers were detected in the globus pallidus of C57BL/6J mice. Chronic exposure to the cannabinoid CP 55,940 increased CB_1/D_{2L} heteromers while the D_2 antagonist haloperidol reduced CB_1/D_{2L} heteromers in the globus pallidus of C57BL/6J mice indicating that functional heteromers existed *in vivo* and were affected by chronic drug exposure. The concept of bidirectional allosteric interaction within CB_1/D_2 heterotetramers has significant implication for the understanding of the complex physiology and pharmacology of CB_1 and D_{2L} receptors.

LIST OF ABBREVIATIONS USED

AC	Adenylyl cyclase
ACEA	Arachidonyl-2-chloroethylamide
AEA	N-arachidonoylethanolamine, or anandamide
ANOVA	Analyses of variance
BiFC	Bimolecular fluorescence complementation
BiLC	Bimolecular luminescence complementation
BRET	Bioluminescence resonance energy transfer
$BRET_{Eff}$	BRET efficiency
$BRET_{Max}$	$BRET^2$ signal to reach a maximum saturated value
$BRET_{Min}$	BRET minimum
BSA	Bovine serum albumin
cAMP	Cyclic adenosine monophosphate
CB_1	Type 1 cannabinoid receptor
CB_1-VC	CB_1 fused to the EYFP Venus C-terminal
CB_1-VN	CB_1 fused to the EYFP Venus C-terminal
CB_2	Type 2 cannabinoid receptor
CI	Confidence interval
CNS	Central nervous system
CODA-RET	Complemented donor-acceptor resonance energy transfer
CREB	Cyclic AMP response element binding protein
CTx	Cholera toxin
D_{2L}	Type 2 dopamine receptor long isoform
D_{2s}	Type 2 dopamine receptor short isoform
DMED	Dulbecco's Modified Eagle's Medium
DMSO	Dimethyl sulfoxide
DS	Dopamine System
ECS	Endocannabinoid System
ELISA	Enzyme-linked immunosorbent assay
ERK	Extracellular-signal regulated kinase

EYFP	Enhanced yellow fluorescent protein
FAAH	Fatty acid amide hydrolase
FBS	Fetal bovine serum
FP	Forward primer
FRET	Fluorescence resonance energy transfer
G protein	Guanine nucleotide binding protein
GABA	γ-aminobutyric acid
GDP	Guanosine diphosphate
GFP^2	Green fluorescent protein^2
GPCR	G protein coupled receptor
GRK	G protein receptor kinase
GTP	Guanosine triphosphate
HALO	Haloperidol
HD	Huntington's disease
HEK 293A	Human embryonic kidney 293A cells
HERG	Human *ether-a-go-go* related gene
I.p.	Intraperitoneal
L-AP4	L-2-amino-4-phosphonobutyric acid
L-DOPA	Levodopa
MAPK	Mitogen activated protein kinase
mGluR6	Metabotropic glutamate receptor 6
mHtt	Mutant huntingtin protein
MSNs	GABAeric medium spiny neurons
N	GPCR oligomerization state
O.D.	Optical density
PBS	Phosphate-buffered saline
PBST	Phosphate-buffered saline with 0.1% tween-20
PCR	Polymerase chain reaction
pCREB	Phosphorylated CREB
pERK	Phosphorylated ERK
PFA	Paraformaldehyde

PLA   Proximity ligation assay

PTx   Pertussis toxin

QF-IHC   Quantitative fluorescence immunohistochemistry

qRT-PCR   Real-time quantitative polymerase chain reaction

RET   Resonance energy transfer

Rluc   *Renilla* luciferase

RNA   Ribonucleic acid

RP   Reverse primer

RT-PCR   Reverse transcription polymerase chain reaction

SDS-PAGE   Sodium dodecyl sulfate polyacrylamide gel electrophoresis

SEM   Standard error of the mean

SRET   Sequential resonance energy transfer

SULP   Sulpiride

THC Δ^9-tetrahydrocannabinol

TRPV1   Transient receptor potential vanilloid type 1

Acknowledgements

In the name of ALLAH (GOD), the most merciful, the most compassionate

"The more you thank Me, the more I give you." Quran, 14:7

CHAPTER 1

INTRODUCTION

1.1 Overview

G protein-coupled receptors (GPCRs) are the largest family of transmembrane receptors. GPCRs mediate intracellular signaling *via* G protein-dependent and G protein-independent signaling pathways. The complexity and diversity of GPCR signaling are much greater than first envisioned because GPCRs can physically interact to form homo- and heteromeric complexes. Allosteric interactions across homo- and heteromeric complexes have profound impacts on GPCR ligand binding, G protein coupling, receptor trafficking and internalization. Cannabinoid receptor 1 (CB_1) and dopamine receptor 2 long (D_{2L}) are GPCRs that are co-expressed in the basal ganglia and play crucial roles in controlling movement. Antipsychotics, acting as D_{2L} receptor antagonists, are clinically used to treat psychotic disorders in a variety of clinical settings and to control excessive involuntary movement in Huntington's disease (HD). Heteromerization between CB_1 and D_{2L} receptors has been confirmed in heterologous expression systems and striatal neurons. Concurrent activation of both receptors was proposed to alter G protein coupling relative to the effects of independently activating each receptor. The global aim of this thesis was to understand the physical and functional interactions between CB_1 and D_{2L} receptors within heteromeric complexes. The focus has been placed on elucidating the allosteric interactions within CB_1/D_{2L} heteromers following the application of CB_1 agonists and D_2 ligands (agonists and antagonists) using a heterologous expression system and cells endogenously expressing both receptors. Specifically, we examined the effects of CB_1 and D_{2L} ligand co-application on G protein coupling, G protein-dependent downstream signalling, and β-arrestin recruitment. Furthermore, we aimed to understand the stoichiometry of $CB_1/D_{2L}/Gα$ proteins within heteromeric complexes. Finally, we examined the expression of CB_1/D_{2L} heteromers in the globus pallidus of C57BL/6J mice following chronic CB_1 and/or D_{2L} ligand treatment. The studies presented in this thesis will improve understanding of the allosteric interactions within CB_1/D_{2L} heteromers and the impact of co-administration of cannabinoids on the therapeutic effects of

antipsychotics (D_2 antagonists). This work will guide efforts to improve treatment for patients suffering from movement disorder and psychosis.

1.2 G-protein Coupled Receptors (GPCRs)

GPCRs are the largest family of signal transduction transmembrane receptors, with class A GPCRs being the largest subfamily within the group (Bockaert, 1991; Gether 2000; reviewed in Katritch *et al.,* 2013). These receptors and signal transduction pathways play essential roles in various physiological functions as well as in pathologies. Therefore, GPCRs are considered a highly 'druggable' class of receptors and are the targets of a wide range of pharmacological therapies. GPCRs possess seven membrane-spanning regions, coupled to heterotrimeric guanine nucleotide binding proteins (G proteins). G proteins are comprised of a Gα subunit bound to a G$\beta\gamma$ dimer. GPCRs can generate diverse signaling responses based on their coupling to specific Gα subtypes. The three primary subtypes include 1) Gα_s, which activates adenylyl cyclase (AC) and increases cyclic adenosine monophosphate (cAMP), 2) Gα_i, which inhibits AC and decreases cAMP; and 3) Gα_q, which activates the phospholipase C (PLC) signaling pathway resulting in an increase in intracellular calcium (Ca^{2+}) (Strathmann and Simon, 1990; Levitzki and Bar-Sinai, 1991; Nurnberg *et al.,* 1995).

The dynamics of GPCR and G protein interaction are still not completely understood. Two models have been proposed to explain the interactions between GPCRs and G proteins and the subsequent activation of G proteins (Limbird, 1983; Gilman 1987; Bockaert, 1991; Brady and Limbird, 2002; reviewed in Oldham and Hamm, 2007; Goricanec *et al.,* 2016; Toyama *et al.,* 1017). The classic model of GPCR- mediated signal transduction was believed to occur through the interaction and activation of different types of Gα protein (Limbird, 1983; Gilman 1987; Bockaert, 1991; Brady and Limbird, 2002). This model implies that the four components of the interacting functional complex including GPCR, Gα, G$\beta\gamma$, and AC are freely mobile and can interact by random 'collision coupling' (Tolkovsky and Levitzki 1978; reviewed in Oldham and Hamm, 2008). In this model, GPCR-mediated signal transduction begins with agonist binding to the orthosteric ligand-binding site at the receptor promoting conformational

2

changes and the transition of the receptor from the inactive to the active state leading to G protein recruitment in its guanosine diphosphate (GDP)-bound Gαβγ form (Fig. 1.1). Activated G protein coupled-GPCRs trigger guanylyl nucleotide exchange from GDP to guanosine triphosphate (GTP) on the Gα subunit, which leads to rapid dissociation of Gα and Gβγ into active subunits to allow effector activation. Activated Gα binds and activates differenet second messengers depending on the subtype of coupled Gα protein with the receptor. Finally, signaling is terminated when GTP is hydrolyzed to GDP by intrinsic GTPase activity of the Gα subunit, which promotes dissociation of Gα from AC and reconstitution of Gαβγ heterotrimeric protein (reviewed in Cabrera-Vera, 2003; Oldham and Hamm, 2007).

The second model of GPCR-mediated signal transduction suggests that GPCRs are "pre-assembled" with their cognate heterotrimeric G protein (Braun and Levitzki, 1979; Klein *et al.,* 2000; Philip *et al.,* 2007). The pre-assembly of GPCR and cognate G protein occur early during the biosynthesis of the receptors in the endoplasmic reticulum and the pre- assembled GPCR/G protein complex is trafficked together to the cell membrane (Dupré *et al.* 2007). The pre-assembly between GPCR and G protein has been confirmed using biochemical approaches such as co-immunoprecipitation (Smith and Limbird, 1981), crystallographic analysis (Rasmussen *et al.,* 2007; Scheerer *et al.,* 2008) and resonance energy transfer (RET)-based approaches (Galés *et al.,* 2005, 2006; Nobels *et al*., 2005; Ayoub *et al.,* 2007, 2010; Audet *et al.,* 2008; Levoye *et al.,* 2009; Qin *et al.,* 2011). The use of RET, bioluminescence resonance energy transfer (BRET) and fluorescence resonance energy transfer (FRET) facilitated the study of the interaction between GPCR and G protein in real time in living cells. RET approaches allow for the determination of the proximity and relative conformation between chromophores fused to a GPCR and a G protein (either Gα or Gβγ protein, reviewed in Ayoub *et al*., 2012). RET approaches have been used to confirm the pre-assembly of various family A GPCR with their cognate Gα$_i$-protein such as α$_{2A}$-drenergic receptor with Gα$_{i1}$ (Galés *et al.,* 2006) and Gα$_o$ (Nobels *et al*., 2005), protease-activated receptor 1 and 2 with Gα$_{i1}$ (Ayoub *et al.,* 2007, 2010), δ-opioid receptor and Gα$_{i1}$ (Audet *et al.,* 2008), muscarinic M4 receptors and Gα$_o$ (Nobels *et al*., 2005), chemokine CXCR4 and CXCR7 (Levoye *et al.,*

Figure 1.1: The Life Cycle of a GPCR. GPCRs are translated on ribosomes associated with the endoplasmic reticulum and transported *via* secretory vesicles to the Golgi apparatus and eventually to the plasma membrane. Signal transduction at GPCRs begins with agonist binding to the receptor, which catalyzes the exchange of guanosine diphosphate (GDP) for guanosine triphosphate (GTP) on the α-subunit of heterotrimeric G proteins (Gαβγ). This allows the activated G protein to act on downstream effectors and produce biological responses. Signaling is then turned off by the hydrolysis of GTP to GDP by the Regulator of G protein Signaling (RGS) proteins. Receptors are internalized following phosphorylation of the intracellular domain of the receptor by G protein kinase (GRK) and then subsequent recruitment of β-arrestin protein (Arr). Internalized receptors are either degraded by the lysosome or recycled back to the cell surface. Figure 1.1 was modified from Wilkie, 2001.
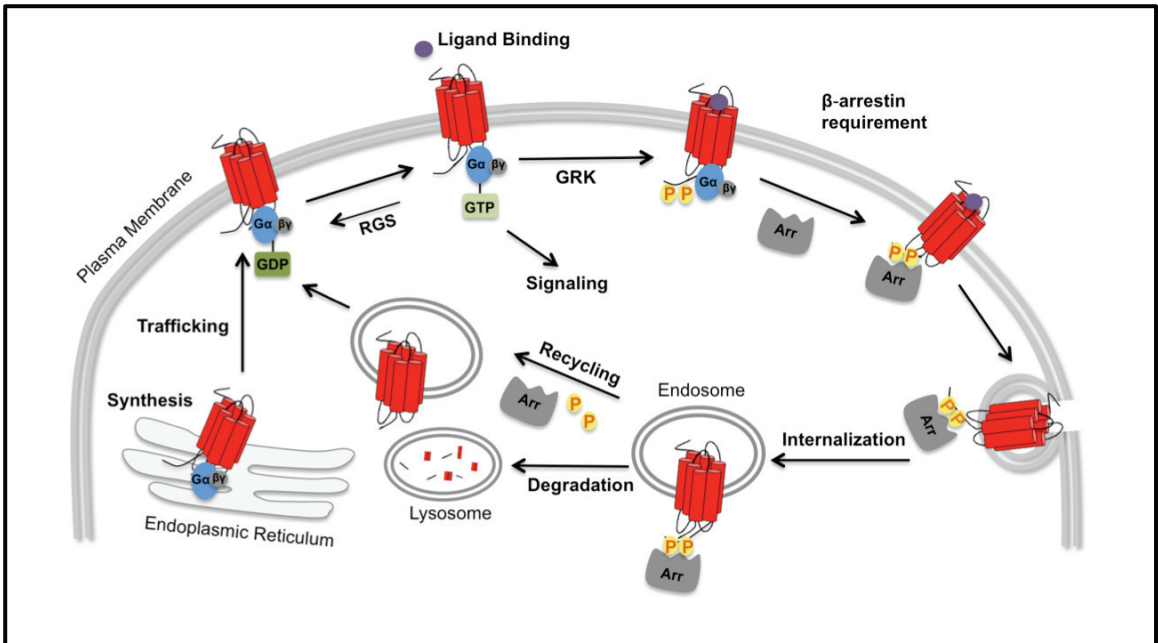
2009) receptors, and muscarinic receptor M3 and Gα_q (Qin *et al.,* 2011). RET experiments indicate that binding of an agonist to GPCRs results in rapid conformational changes with rearrangement and/or reorientation of Gα within the pre-assembled GPCR-G protein complex, rather than recruitment of G proteins to GPCR. Such conformational changes result in agonist dose-dependent increase/decrease in RET signal between tagged GPCR and Gα protein (Galés *et al.,* 2005, 2006; Levoye *et al.,* 2009; Levoye *et al.,* 2009; Denis *et al.*, 2012). The agonist-dependent increase in RET signals is followed by the return of RET signals to basal levels indicating the return of GPCR/Gα protein complexes to the inactive conformation rather than dissociation of GPCR from Gα protein (Bunemann *et al.*, 2003; Galés *et al.,* 2006). Moreover, the pre-assembly model suggests that Gα and G$\beta\gamma$ subunit dimers remain associated and pre-assembled to GPCR during activation of GPCRs by agonists (Galés *et al.,* 2006). It has become increasingly clear that GPCRs mediate ligand-dependent cell signaling is far more complex than can be simply explained by the activation of different Gα subtypes since GPCRs are able to couple and activate multiple downstream effector proteins (reviewed in Bosier and Hermans, 2007; Kenakin and Christopoulos, 2013; Ferré *et al.,* 2014, 2015).

After G protein-dependent activation, the primary pathway leading to GPCR desensitization involves the phosphorylation of the intracellular carboxy terminus of the receptor by a G protein receptor kinase (GRK) (Benovic *et al.*, 1985; Lefkowitz, 1993; reviewed in Gurevich *et al.,* 2012; Smith and Rajagopal, 2016). Following receptor phosphorylation, β-arrestin is recruited to the receptor, which blocks the G protein binding site on the receptor thereby desensitizing the GPCRs to the initial stimuli (Ferguson *et al.*, 1996; Lohse *et al.,* 1990; DeGraff *et al.,* 2002; Marion *et al.,* 2006; reviewed in Smith and Rajagopal, 2016). β-arrestin further serves as a scaffold protein, allowing for the formation of clathrin-coated pits followed by endocytosis of the GPCR/β-arrestin complex (Anderson, 1998; Luttrell *et al.*, 2001). The GPCR may then be recycled to the plasma membrane or targeted to lysosomes for degradation (Anderson, 1998; Luttrell *et al.*, 2001; Luttrell and Lefkowitz, 2002).

In addition to the primary roles of β-arrestins in the termination of G protein-dependent signal and receptor internalization, β-arrestins are involved in G protein independent signaling. β-arrestins scaffold and regulate several downstream effectors

(reviewed in Smith and Rajagopal, 2016). In particular β-arrestins scaffold and activate the mitogen-activated proteins (MAPs) including extracellular signal–regulated kinases (ERK1 and ERK2) (Tohgo *et al.*, 2002; Lefkowitz and Shenoy, 2005; Shenoy *et al.*, 2006). Unlike the transient G protein-dependent ERK signaling (peak 2-5 min), β-arrestin-dependent ERK phosphorylation develops slowly (peak 5-10 min) and persists for extended periods (over 30 min) due to the long-lasting association between the receptor and β-arrestin (Ahn *et al.,* 2004; Shenoy *et al.,* 2006; DeWire *et al.*, 2007).

GPCRs do not exist in either active conformations capable of activating G proteins or in inactive conformations unable to activate G proteins. Rather GPCRs can adopt multiple active conformations, and each active conformation favors binding and stimulation of specific effector proteins (Kenakin, 2010; Kenakin and Christopoulos 2013). Biased agonism or functional selectivity is the result of an orthosteric ligand-dependent shift in the conformation of a receptor that favors interaction with specific effector proteins at the expense of other possible effector proteins (Kenakin, 2010; Kenakin and Christopoulos, 2013). For example, different orthosteric cannabinoid agonists that bind the type 1 cannabinoid receptor (CB_1) can preferentially stabilize different active conformations of the receptor resulting in alteration of the coupling of the receptor to different G proteins (reviewed in Laprairie *et al.,* 2017).

To further increase the complexity of GPCR signaling, the pharmacology of GPCR orthosteric ligands can be modulated by the binding of allosteric modulators. Allosteric modulators are molecules that bind to a site distinct from that of the orthosteric agonist-binding site on a GPCR (conduit) and induce conformational changes within the GPCR that are transmitted from the allosteric binding site to the orthosteric binding site (Fig. 1.2A). Allosteric modulators lack intrinsic efficacy and are unable to activate the receptor in the absence of orthosteric agonist (guest) (Wootten *et al.,* 2013; van der Westhuizen *et al.,* 2015). The binding of the allosteric modulators can either enhance (positive allosteric modulator), or diminish (negative allosteric modulator) the efficacy and potency of orthosteric ligand-dependent signaling through the GPCR (Wootten *et al.,* 2013; van der Westhuizen *et al.,* 2015). G proteins and other effector proteins that physically bind GPCRs also have allosteric modulatory properties that can modify orthosteric ligand binding (reviewed in Leach *et al.*, 2007; Darren *et al.*, 2013; Gentry *et*

al., 2015). The assembly of homo- and heteromeric complexes influences the conformation of each receptor within the complex (Vilardaga *et al.,* 2008; Maier-Peuschel *et al*., 2010; Bourque *et al*., 2017; Devost *et al.,* 2017; Sleno *et al*., 2017). Taken together, it is now accepted that orthosteric-ligand dependent biased agonism and allosteric modulation due to ligand binding and protein- protein interactions contribute to the diversity of signaling responses. This view is in contrast to early simple models of GPCR function that were based on the classic "one receptor - one G protein -one signaling response" model. The demonstration that many GPCRs physically associate to form homo- and heteromers, and that these interactions have the ability to modulate nearly every aspect of receptor pharmacology and function provides further evidence that GPCR signaling is increasingly more complex than previously assumed.

1.2.1 GPCR Oligomerization

It is now well accepted that class A GPCRs physically associate to form homo and heteromers or higher order oligomeric complexes in heterologous expression systems (reviewed in Rios *et al*., 2001; Milligan 2004, 2009; Ferré*,* 2015; Franco *et al*., 2016; Gaitonde and González-Maeso, 2017). The evidence of GPCR oligomerization emerged during 1970-1980 with the observation of functional interactions among GPCRs. These interactions involve ligand binding to one receptor altering the ligand binding of another receptor. Negative cooperativity among the β_2 adrenergic receptors (β_2AR) was observed in 1975 in the frog erythrocyte membrane preparation (Limbird *et al.,* 1975). The observed cooperativity effects were proposed to be due to the formation of β_2AR homomers (De Lean *et al*., 1980; Chidiac *et al.,* 1997). Subsequently, the formation of β_2AR homomers was confirmed using differential epitope tagging and co-immunoprecipitation (Hébert *et al.,* 1996) and using BRET (Angers *et al.,* 2000). Since these findings, GPCRs oligomerization has been a major subject of research, and increasing evidence suggests that class A GPCRs exist as homo- and heteromers when expressed in a heterologous expression system (reviewed in Milligan 2004, 2009; Ferré*,* 2015; Franco *et al*., 2016; Gaitonde and González-Maeso, 2017). Interestingly, more recent evidence has provided evidence for the existence of GPCR heteromers in native tissues and animal models (reviewed in Franco *et al*., 2016; Gomes *et al.,* 2016).

Figure 1.2: Allosterism Across GPCR Monomers and Oligomers. **(A)** The GPCR monomers can act as the conduit of the allosteric modulator. Small molecule allosteric modulators bind to a region of the receptor that is distant from the orthosteric ligand-binding site. Allosteric modulators can affect the binding and function of orthosteric ligands (guest). In addition, G proteins and other effector proteins that physically bind GPCRs can have allosteric modulatory properties that modify orthosteric ligand binding and receptor functions. **(B)** GPCR oligomers can have two types of allosteric interactions. GPCR oligomers can be considered as the conduit of the allosteric modulator where the orthosteric ligand of the first GPCR protomer acts as an allosteric modulator to alter the functions of the second orthosteric ligands (guest) bound to the second GPCR protomer (left panel). The second type of allosteric interaction within GPCR oligomers is called ligand-independent allosteric modulation. In this case, one of the GPCR protomer acts as the allosteric modulator, in the absence of ligand, and the second GPCR protomer becomes the conduit that binds the guest ligand (right panel). Figure 1.2 was modified from Kenakin and Miller, 2010.

A)

GPCR Monomer
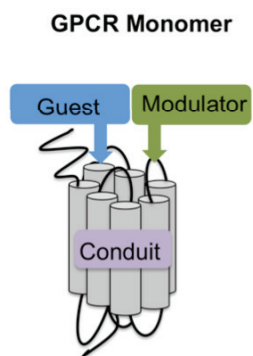
B)
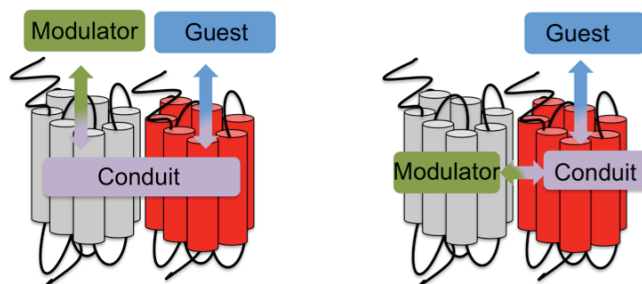
GPCR Oligomer

1.2.2 Functional Consequences of GPCR Oligomerization

Oligomerization of class A GPCRs can affect nearly every aspect of GPCR functions including biosynthesis, trafficking, ligand pharmacology, signal transduction and internalization (Fig. 1.3). Therefore, GPCR homomerization can play important roles in the modulation of GPCR functions and is a vital mechanism to increase the diversity and specificity of GPCR signaling (reviewed in Milligan, 2004, 2009; Terrillon and Bouvier, 2004; Gurevich *et al*., 2008; Smith and Milligan, 2010; Ferré *et al*., 2014, 2015; Franco *et al.,* 2016; Gaitonde and González-Maeso, 2017). Several studies have demonstrated that family A GPCR homo- and hetero-oligomerization play a crucial role for proper trafficking of the receptors to the plasma membrane. GPCR oligomers form in the endoplasmic reticulum and appear to be present through all phases of receptor trafficking (Dupré *et al.,* 2006; Herrick-Davis *et al*., 2006). For example, olfactory receptors reach the cell surface when co-expressed with the α_{1B} adrenergic receptor or the β_2 receptor, but not if expressed as single receptors (Hague *et al.,* 2004; Bush *et al.,* 2007; Hall, 2009). Similar observations have been reported for other GPCRs and confirm that homo- and heteromerization of GPCRs is required for the proper maturation and trafficking of GPCRs from the endoplasmic reticulum to the cell membrane (Kobayashi *et al.*, 2009; reviewed in Milligan, 2004, 2009; Terrillon and Bouvier, 2004; Gurevich *et al*., 2008; Smith and Milligan, 2010; Ferré *et al*., 2014, 2015). GPCR oligomerization can also affect receptor desensitization and internalization following agonist activation. Most commonly, activation of one receptor in a heteromer will lead to a cross-internalization and a cross-desensitization of the second receptor (Pfeiffer *et al.* 2002; Hillion *et al.,* 2002; Fiorentini *et al*., 2008). These observations suggest that GPCR oligomers internalize as intact entities instead of disassociating prior to receptor internalization (reviewed in Prinster *et al.*, 2004; Terrillon and Bouvier, 2004). GPCR heteromerization has also been found to play a role in the recycling of internalized receptors back to the plasma membrane (Pfeiffer *et al*., 2003; Terrillon *et al.,* 2004; Ellis *et al*., 2006: Grant *et al.,* 2008). Together, this evidence indicates that oligomerization plays a significant role in the proper trafficking of GPCRs throughout their entire life-cycle starting early during receptor synthesis in the endoplasmic reticulum and being maintained throughout trafficking to the plasma membrane, agonist-induced internalization, and during recycling

Figure 1.3: Functional Consequences of GPCR Oligomerization. **(1)** GPCR oligomerization plays an important role in receptor maturation and correct trafficking from the endoplasmic reticulum to the plasma membrane. **(2)** Ligand binding to GPCR oligomers can modulate GPCR oligomer formation. **(3)** Ligand binding to one GPCR protomer can allosterically modulate the affinity between the ligand and associated protomer within oligomeric complexes. **(4)** Allosteric interaction within oligomeric complexes might result in enhancing or suppressing downstream signaling or altering G protein coupling. The three Gα subtypes include Gα_i, which inhibits adenylyl cyclase (AC) and decreases cyclic adenosine monophosphate (cAMP), Gα_s, which activates AC and increases cAMP, and Gα_q, which activates the phospholipase C (PLC). PLC cleaves phosphatidylinositol 4,5-bisphosphate (PIP2) into diacylglycerol (DAG) and inositol 1,4,5-triphosphate (IP$_3$). **(5)** GPCR oligomerization can affect GPCR localization, the rate of internalization and subsequent recycling. $+/-$ indicates an increase or decrease, respectively. Figure 1.3 was modified from Schellekens *et al.,* 2013.

13
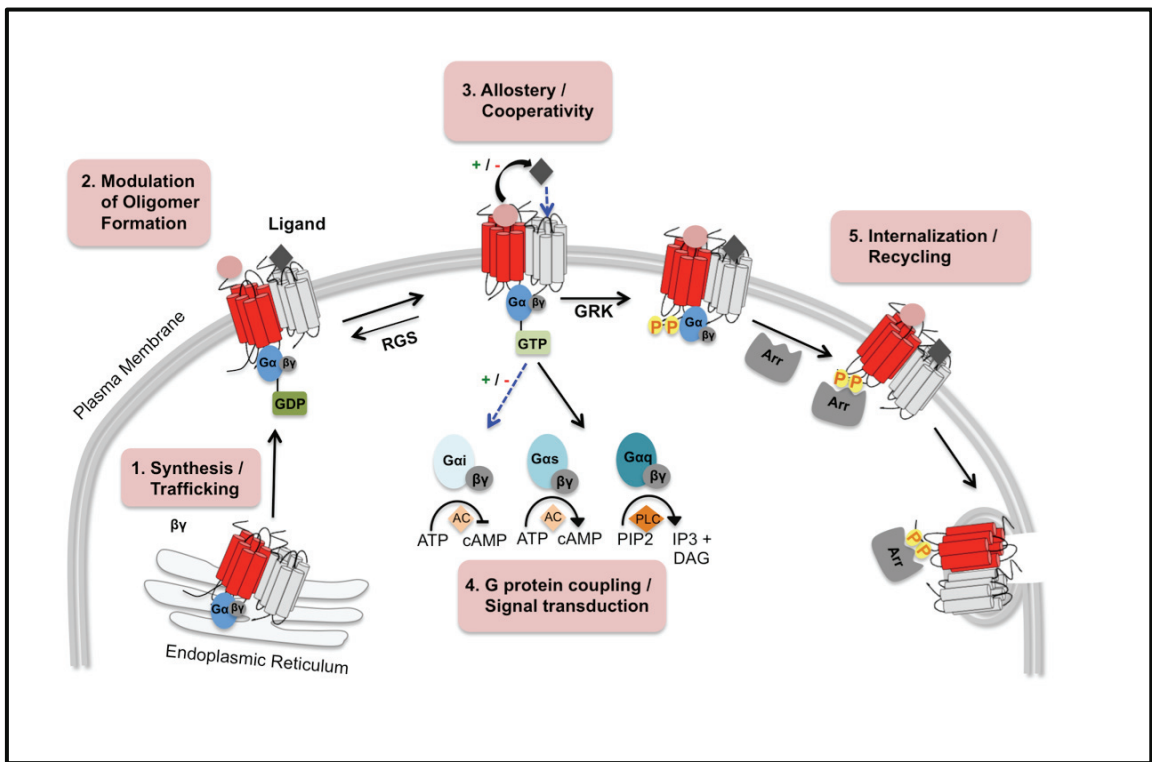
back to the plasma membrane.

Specific ligand binding has been shown to modulate GPCR oligomer formation. Some studies have suggested that GPCRs either form stable interactions while other studies suggested that the interactions between GPCRs are transient. With the ability to detect oligomerization using RET techniques, several studies reported ligand-induced changes in BRET or FRET signals. These changes in BRET or FRET signals were suggested to represent the formation or disassociation of GPCR oligomers leading to the conclusion that GPCR oligomer formation is dynamic in nature (Angers, 2000; Rocheville, 2000; Cornea *et al.*, 2001; Milligan and Bouvier, 2005; Alvarez-Curto *et al.*, 2010; Elisa *et al.*, 2010; Urizar *et al.*, 2011). However, because BRET and FRET are dependent not only on the number of interacting receptors but also on the relative orientation of the donor and acceptor molecules, it is possible that ligand-induced changes in BRET and FRET are more likely caused by conformational changes than alterations in the number of interacting receptors (Pfleger and Eidne, 2005; Milligan and Bouvier, 2005; Alyarez-Curto, 2010; Ayoub, 2009, 2012). More recent studies using single-molecule total internal reflectance fluorescence microscopy together with SNAP-tag technique reported that GPCR oligomerization is highly dynamic, with the constant formation or disassociation of GPCR oligomers; however, ligand treatment did not modify GPCR oligomerization (Hern *et al.,* 2010; Kasai *et al.,* 2011; Calebiro *et al.,* 2013). In contrast, using post-imaging acquisition spatial intensity distribution analysis of standard laser scanning confocal microscopy images demonstrated that the serotonin 5-HT$_{2C}$ receptors form mainly homodimers, and antagonist treatment decreased the number of homodimers (Ward *et al.*, 2015). Altogether, the effects of acute ligands treatment on GPCR oligomerization are still controversial and might be receptor-dependent.

As mentioned earlier, the first evidence of GPCR oligomerization was the negative cooperativity observed in radioligand binding experiments (Limbird *et al.,* 1975; De lean *et al.*, 1980; Chidiac *et al.,* 1997). Since then, several studies have reported either negative or positive cooperativity of GPCR homo- and heteromers in relation to ligand binding and intrinsic efficacy (Albizu *et al.,* 2006, 2010; reviewed in Ferré *et al.,* 2014). The negative or positive cooperativity effects of ligand binding are a particular type of allosteric communication between GPCR protomers, within homo or hetero-oligomeric

complexes (Kenakin and Miller, 2010; Kenakin and Christopoulos, 2013). Kenakin and Miller (2010) proposed two models to describe allosteric modulations within GPCR oligomers with respect to ligand binding and efficacy. In the first model, the GPCR oligomers (at least two protomers) are considered as the conduit of the allosteric modulator; the orthosteric ligand of the first GPCR protomer acts as an allosteric modulator to alter the affinity and/or efficacy of the second orthosteric ligand (guest) binding to the second GPCR protomer (Fig. 1.2B). In this model, binding of the allosteric modulator to one of the GPCR protomers leads to either an increase or decrease in the affinity and/or efficacy of the guest ligand, which binds to the second GPCR protomers within homo or hetero-oligomeric complexes (Kenakin and Miller, 2010). An example of this model is the adenosine A_{2A} receptor (A_{2A})/D_2 heterotetramer, where the A_{2A} receptor ligand decreases the affinity and signaling of dopamine at the D_2 receptor (Ferré *et al*., 1992; Azdad, 2009; Bonaventura *et al.,* 2015). Similarly, CB_1 ligands can allosterically potentiate the binding and signaling of the δ-opioid receptor agonists (Bushlin *et al.,* 2012; Rozenfeld *et al.,* 2012).

The second model of allosteric modulation within GPCR oligomers with respect to ligand binding and efficacy is known as ligand-independent allosteric modulation in which one of the GPCR protomer acts as the allosteric modulator and the second GPCR protomer becomes the conduit that binds the guest ligand (reviewed in Ferré *et al.,* 2014, 2015). In this model (Fig. 1.2B), the first GPCR protomer acts as the allosteric modulator of the orthosteric ligand binding to the conduit (second GPCR protomer) (reviewed in Ferré *et al*., 2014, 2015). For instance, the dopamine D_2 receptor acts as the allosteric modulator that reduces the binding of SCH-442416 to A_{2A} receptors within A_{2A}/D_2 heterotetramers (Orru *et al*., 2011; Bonaventura *et al*., 2015). Numerous mathematical models have been developed to analyze the complex ligand binding curves generated from ligand binding to GPCR oligomers. (Casadó *et al.,* 2007, 2009; Rovira *et al.,* 2009; Giraldo, 2013; reviewed in Ferré *et al.,* 2014, 2015).

Allosteric communication between GPCR protomers within GPCR heteromeric complexes might contribute to activation of distinct signaling pathways known as functional selectivity or biased signaling (reviewed in Ferré *et al.,* 2014). Physical interactions between GPCR protomers allosterically induce conformational changes in

each of the individual GPCR protomers (Vilardaga *et al.,* 2008; Hlavackova *et al.,* 2012; Sleno *et al.,* 2017). In some cases, GPCR oligomerization might preferentially stabilize each of the individual GPCR protomers in conformations that favor coupling to specific G proteins (Kenakin and Miller, 2010). Several examples of switches in G protein coupling following GPCR heteromerization have been reported including G protein switching at angiotensin AT_1/CB_1 heteromers (Rozenfield *et al.,* 2011), dopamine D_1/histamine H_3 heteromers (Ferrada *et al.,* 2009), the dopamine D_2/ghrelin $GHSR_{1a}$ heteromers (Kern *et al.,* 2012, 2015). Other studies have reported that GPCR heteromerization may only potentiate or inhibit receptor signaling through distinct pathways rather than altering G protein coupling (reviewed in Milligan, 2004, 2009; Terrillon and Bouvier, 2004; Gurevich *et al*., 2008; Smith and Milligan, 2010; Ferré *et al*., 2014, 2015). Allosteric communication within GPCR heteromeric complexes may result in unique pharmacological properties of GPCR heteromers versus homomers.

1.2.3 Stoichiometry of GPCR/G Protein Complexes Within Homo- and Heterooligomeric Complexes

One question that has not been resolved in the field of GPCR oligomerization is the number of GPCR subunits involved in the formation of oligomeric complexes. For GPCR homomers, at least two GPCRs (homodimers) interact (Banères and Parell, 2003; Herrick-Davis *et al.,* 2005). Strong support for the formation of GPCR homodimers also comes from morphological evidence obtained using atomic force microscopy for rhodopsin receptors in native tissue (Fotiadis *et al.,* 2003; Liang *et al.,* 2003). However, several lines of evidence suggeste that higher order homooligomeric complexes can exist (reviewed in Bouvier and Hébert, 2014; Ferré *et al.,* 2014, 2015). The use of protein complementation approaches together with BRET have allowed several investigators to demonstrate that GPCRs could form higher order homooligomeric complexes in systems expressing $\beta_2 AR$ receptors (Rebois *et al.,* 2008), dopamine receptor 2 short (D_{2s}) (Gua *et al*., 2008), and A_{2A} receptor (Vidi *et al.,* 2008). FRET was also used to show that higher order homo-oligomeric structures could be formed following expression of M_2 muscarinic receptors (Pisterzi *et al.,* 2010) and the $\beta_2 AR$ receptors (Fung *et al*., 2009). However, recent studies suggest that GPCR homodimers are the predominant species

(Herrick-Davis *et al.* 2013; reviewed in Bouvier and Hébert, 2014; Ferré *et al.,* 2014, 2015). This model is supported by evidence obtained using RET, fluorescence correlation spectroscopy and analysis of single fluorescence-labeled receptor molecules by total internal reflection fluorescence microscopy (Calebiro *et al.,* 2013; Herrick-Davis, *et al.,* 2013; Mazurkiewicz *et al.,* 2015; Ward *et al.,* 2015; Navarro *et al.,* 2016). Crystal structures of the β_2AR receptor (Rasmussen *et al.,* 2007), CXCR4 chemokine receptors (Wu *et al.,* 2010), μ and κ opioid receptors (Manglik *et al.,* 2012, Wu *et al.,* 2012), and β_1 adrenergic receptor (Haung *et al.,* 2013) have demonstrated the presence of receptor homodimers. Moreover, each GPCR homodimer was reported to couple to one heterotrimeric G protein to form a functional signaling complex (Han *et al.,* 2009; Jastrazebka *et al.,* 2013; Navarro *et al.,* 2016). Asymmetric binding of heterotrimeric G protein to homodimers has been reported, where one heterotrimeric G protein binds to one protomer within the homodimeric complexes (Damian *et al.,* 2006; Han *et al.,* 2009; Zylbergold and Hébert, 2009; Jastrazebka *et al.,* 2013; Pellissier *et al.,* 2011; Jonas *et al.,* 2015; Mishra et al., 2016). Therefore, the minimal composition of the functional unit is a homodimer interacting with one heterotrimeric G protein. Higher order homo-oligomeric complexes are also possible. GPCR heteromers are formed when two or multiple homodimers (each coupled to their cognate G protein) interact (reviewed in Ferré, 2015) to form a heterotetramer (Elisa *et al.,* 2010; Mishra *et al.,* 2014; Guitart *et al.,* 2014; Bonaventura *et al.,* 2015; Cordomí *et al.,* 2015; Navarro *et al.,* 2016). Specifically, Guitart *et al.* (2014) reported that the dopamine receptor type 1 (D_1) and dopamine receptor type 3 (D_3) receptors form heterotetramers composed of D_1 and D_3 homodimers as demonstrated using BRET combined with bimolecular fluorescence complementation (BiFC) and bimolecular fluorescence luminescence complementation (BiLC) assays. The same approach has also been used to uncover the tetrameric structure of A_{2A} and D_2 heteromers (Bonaventura *et al.,* 2015). A more recent study, using microscope-based single-particle tracking and molecular modeling, reported that A_1 and A_{2A} form mainly heterotetramers composed of two homodimers, while A_1 and A_{2A} homomers, homotrimers and homotetramers were scarce (Navarro *et al.,* 2016). Overall, GPCR heterotetramers are formed from at least two homodimers and one homodimer-associated G protein (reviewed in Cordomí *et al.,* 2015).

1.3 The Endocannabinoid System (ECS)

The endocannabinoid system (ECS) is a lipid signaling system comprised of endogenous ligands (endocannabinoids), enzymes for their synthesis and degradation and two well-characterized GPCRs, cannabinoid receptors CB_1 and CB_2 (reviewed in Howlett *et al.*, 2004; Pacher *et al.,* 2006; Mechoulam and Parker, 2013). Endocannabinoids are lipid mediators derived from arachidonic acid. The primary endocannabinoids are N-arachidonoylethanolamine (Anandamide or AEA) and 2-arachidonoylglycerol (2-AG) (Devane *et al.*, 1992; Mechoulam *et al.,* 1995; Sugiura *et al.*, 1995). Unlike classical neurotransmitters, the endocannabinoids are not stored in vesicles but are synthesized on demand postsynaptically in response to specific signals, such as increases in intracellular calcium or activation of phospholipase Cβ by $G_{q/11}$-coupled metabotropic receptors (Di Marzo *et al.*, 1998; Stella and Piomelli 2001; Piomelli*,* 2003). The enzyme necessary for the synthesis of AEA are *N*-acyltransferase (NAT) and *N*-acylphosphatidylethanolamide-phospholipase D (NAPE-PLD) (Cadas *et al.,* 1996; Di Marzo *et al.*, 1999), while the main enzyme required for the synthesis of 2-AG is diacylglycerol lipase (DAGL) (Stella *et al.,* 1997). Degradation of AEA and 2-AG occurs locally by fatty-acid amide hydrolase (FAAH) and monoacylglycerol lipase (MGL), respectively (Egertová *et al.,* 1998; Cravatt *et al.,* 1996; McKinney and Cravatt, 2005; Blankman *et al.,* 2007; Ahn *et al.,* 2008).

1.3.1 The Cannabinoid Receptor 1 (CB_1)

CB_1 is the most abundant GPCR in the central nervous system (CNS) and is expressed at high levels in the basal ganglia, hippocampus, cerebral cortex, amygdala and cerebellum and at lower levels throughout the CNS (Matsuda *et al.,* 1990; Herkenham *et al.*, 1990; Mailleux and Vanderhaeghen, 1992). Accumulating evidence has confirmed that CB_1 is also expressed in the periphery in many tissues including the cardiovascular system, reproductive system, intestine, smooth muscle, and eye (Pertwee *et al.,* 1996; Sugiura *et al.,* 1998; Straiker *et al.,* 1999; Stamer *et al.,* 2001; Wang, 2003). The widespread distribution of CB_1 allows for its participation in the regulation of a variety of central and peripheral physiological functions, including modulation of neurotransmitter release, energy metabolism, and cardiovascular, respiratory and reproductive function

(reviewed in Iversen, 2003; Pacher *et al*., 2006; Vemuri *et al.,* 2008; Smith *et al*., 2010; Kirilly *et al.,* 2012; Pertwee, 2012; Aizpurua-Olaizola, 2017)

The human CB_1 gene (*CNR1*) is located on chromosome 6 locus q14-q15. Alternative splicing of human CB_1 within the coding region (exon 4) results in the formation of the full-length CB_1 (472 amino acids), CB_{1a} (411 amino acids) (Shire *et al.*, 1995) and CB_{1b} (439 amino acids) (Ryberg *et al.*, 2005). CB_{1a} is shorter than CB_1 by 61 amino acids at its N-terminus, while CB_{1b} is shorter than CB_1 by 33 amino acids at the N-terminal tail (Shire *et al.,* 1995; Ryberg *et al.,* 2005). Overlap in the distribution patterns of the mRNAs of the three CB_1 protein variants in different regions of the human brain and the periphery has been reported (Shire *et al.,* 1995; Ryberg *et al.,* 2005; Xiao *et al.*, 2008; Gustafsson *et al.*, 2008; Bagher *et al.,* 2013).

In the CNS, CB_1 is located presynaptically where it plays a modulatory role in the regulation of noradrenaline, acetylcholine, dopamine, γ-aminobutyric acid (GABA), glutamine, serotonin, and glycine release (Fig. 1.4) (Abood and Martin, 1992; Di Marzo *et al.,* 1998; Wilson and Nicoll, 2001; Howlett *et al.*, 2004; Castillo *et al.,* 2012). Endocannabinoids synthesized postsynaptically diffuse retrogradely to activate presynaptic CB_1 receptors, resulting in inhibition of voltage-gated Ca^{2+} channels (VGCC) and activation of G protein-coupled inwardly rectifying K^+ channel (GIRKs) suppressing the release of many different neurotransmitters. Some evidence also suggests the CB_1 receptors are also expressed postsynaptically on GABAergic neurons and non-retrograde CB_1 signaling has been observed (Hohmann *et al.,* 1999; Ong and Mackie, 1999; Bacci *et al.,* 2004; Nyiri *et al.,* 2005). Repetitive activation of GABAergic interneuron triggers increases in intracellular Ca^{2+}, synthesis of AEA/2-AG, and activation of postsynaptic CB_1 receptors that couple to GIRKs. This autocrine activation of postsynaptic CB_1 receptors leads to postsynaptic hyperpolarization and reducing excitability (Bacci *et al*., 2004; Marinelli *et al*., 2008, 2009; reviewed in Castillo, 2012).

In addition to signaling *via* $Gα_{i/o}$, CB_1 receptors have been shown to signal through both $Gα_s$ and $Gα_{q/11}$ pathways to increase cAMP levels, and cytosolic $[Ca^{2+}]$, respectively (Demuth and Molleman, 2006; Bosier *et al.,* 2010; Turu and Hunyady, 2010; reviewed in Hudson *et al*., 2010a; Laprairie *et al*., 2017). In addition to Gα protein

Figure 1.4: Diagram of CB$_1$ Retrograde Inhibition of Neurotransmitter Release and Postsynaptic Signaling. An increase in intracellular calcium levels in the postsynaptic terminal activates N-acyltransferase (NAT) or diacylglycerol lipase (DGL), leading to the synthesis of anandamide (AEA) and 2-arachidonyl glycerol (2-AG), respectively, from cellular phospholipids. AEA and 2-AG are released into the synaptic cleft and traverse in a retrograde fashion to activate CB$_1$ receptors located on the presynaptic terminal. Activation of CB$_1$ receptors inhibits voltage gated-calcium channel (VGCC) and activates G protein-coupled inwardly rectifying K$^+$ (GIRK) channels, in addition to causing other presynaptic changes that hyperpolarize the presynaptic membrane and lowers the probability of Ca^{+2} dependent neurotransmitter release. In addition, AEA/ 2-AG activate postsynaptic CB$_1$ receptors to stimulate GIRK channels, which leads to hyperpolarization and inhibition of neuronal firing. Figure 1.4 was modified from Hosking and Zajicek, 2008 and Castillo *et al.*, 2012.
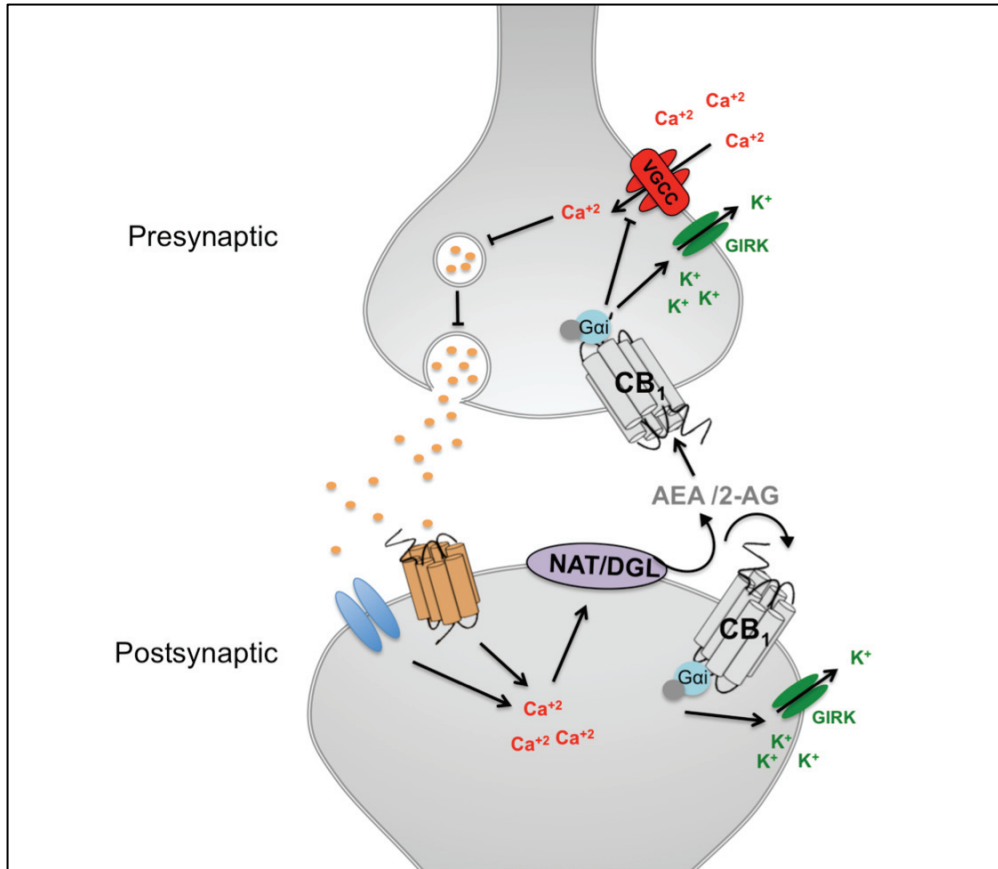
dependent signaling, CB_1 can also signal *via* $G\alpha$ protein-independent pathways including β-arrestin 1 and 2. Ligand-dependent coupling of CB_1 to β-arrestin may influence the dwell time of receptors at the plasma membrane, and receptor internalization, recycling, and degradation (Jin *et al.*, 1999; Bakshi *et al.,* 2007; van der Lee *et al.,* 2009; Laprairie *et al.,* 2014). Ligand-dependent coupling of CB_1 to β-arrestin also affects β-arrestin-dependent ERK phosphorylation and signaling kinetics (reviewed in Laprairie *et al.*, 2017; Ibsen *et al.*, 2017).

Similar to other members of the class A GPCR subfamily, CB_1 receptors form both homo-oligomers (Wager-Miller *et al.*, 2002) and hetero-oligomers with other GPCRs. Homomerization of CB_1 has been demonstrated by the observation of a high molecular weight band on non-denaturing sodium dodecyl sulfate polyacrylamide gel electrophoresis (SDS-PAGE) using an antibody directed against the C-terminal tail of CB_1; the observed high molecular weight bands correspond to the molecular weight of a CB_1 homodimer (Wager-Miller *et al.*, 2002). Homomerization of CB_1 was further confirmed using BRET (Hudson *et al.*, 2010; Bagher *et al.,* 2013, 2016). Heteromerization of CB_1 has been demonstrated with several class A GPCRs such as the D_2 dopamine receptor (Glass and Felder, 1997; Kearn *et al.*, 2005), μ-, κ-, and δ-opioid receptors (Rios *et al.,* 2006; Hojo *et al.,* 2008; Ittai *et al.,* 2012), orexin-1 (Ellis *et al.*, 2006; Jäntti *et al.*, 2014), A_{2a} adrenergic receptor (Carriba *et al.,* 2007) $β_2AR$ (Hudson *et al.*, 2010b), angiotensin II (Ang II) receptor (Rozenfeld *et al.,* 2011), CB_{1a} and CB_{1b} (Bagher *et al.,* 2013) . Heteromerization of CB_1 has been reported to affect receptor trafficking, G protein coupling and signaling (Rios *et al.,* 2006; Ellis *et al.* 2006; Carriba *et al.*, 2007; Hudson *et al.,* 2010; Rozenfeld *et al.,* 2011; Bagher *et al.,* 2013). Therefore, such hetero-oligomeric interactions may play a role in the regional and ligand-specific variability in cannabinoid function.

CB_1 orthosteric ligands have been proposed as pharmacotherapeutics for treating neurodegenerative diseases, chronic pain, substance abuse disorders and obesity because CB_1 plays important roles in many physiological and pathophysiological processes (Pacher *et al.*, 2006; Vemuri *et al.,* 2008; Pertwee, 2008, 2012; Aizpurua-Olaizola, 2017). CB_1 can be activated by plant-derived cannabinoid and synthetic compounds in addition to being activated by endocannabinoids. Cannabinoid agonists are divided into four

structurally distinct groups. The first group contains the 'classical cannabinoids' derived from the plant *Cannabis sativa* such as Δ-9-tetrahydrocannabinol (THC) and related synthetic derivatives such as HU-210. The second group contains the non-canonical cannabinoids, which are synthetic derivatives of the classical cannabinoids that lack the dihydropyran ring such as CP 55,940. The third group includes aminoalkylindoles such as WIN 55212-2 and its related compounds. The last group contains the endocannabinoids, which are eicosanoid compounds rather than cannabinoid compounds and includes the endocannabinoids AEA and 2-AG (Bosier *et al.,* 2010). Due to the structural differences of CB_1 agonists, different classes of CB_1 show agonist bias, CB_1 coupling and signaling with various effector proteins including $G\alpha_{i/o}$, $G\alpha_s$ and $G\alpha_q$ proteins and β-arrestin 1 and 2 (reviewed in Laprairie *et al.*, 2017; Ibsen *et al.*, 2017). In addition, CB_1 allosteric modulators have been developed and tested. Several studies have reported that CB_1 positive allosteric modulators provide improved safety and drug-pharmacology profiles over orthosteric CB_1 agonists (Ross, 2007; Morales *et al.,* 2016; Laprairie *et al.,* 2017).

1.4 The Dopaminergic System (DS)

Dopamine is a monoamine neurotransmitter that is produced in the dopaminergic neurons (Johnston, 1968; Hadjiconstantinou *et al.*, 1993; Männistö *et al.*, 1992; Sampaio-Maia *et al.,* 2001; Eriksen *et al.,* 2010). Dopamine has various functions in the CNS, including regulation of locomotor activity, reward, learning, memory, and endocrine function. In the periphery, dopamine helps to regulate cardiovascular function, vascular tone, renal function, hormone secretion and gastrointestinal motility (reviewed in Iversen and Iversen, 2007). In the brain, there are four main dopaminergic pathways including mesolimbic, mesocortical, nigrostriatal, and tuberoinfundibular pathways. The mesolimbic pathway is involved in motivational behavior. This pathway originates from the ventral tegmental area and innervates the nucleus accumbens and parts of the limbic system. The mesocortical pathway also originates from the ventral tegmental area; however, it innervates regions of the frontal cortex involved in learning and memory. The nigrostriatal pathway originates from the substantia nigra compacta and innervates the striatum, where it participates in the control of movement. Finally, the tuberoinfundibular

pathway originates from the cells of the periventricular and arcuate nuclei of the hypothalamus, reaching the pituitary (Missale *et al.,* 1998; Hall *et al.,* 1994; Wang *et al.,* 2009; Beaulieu and Gainetdinov, 2011).

The physiological and pharmacological actions of dopamine are mediated by five dopamine receptors. The dopamine receptors are subclassified into two groups: the D_1-like family (includes D_1 and D_5) and the D_2- like family (includes D_2, D_3, and D_4) receptors (reviewed in Missale *et al.,* 1998; Beaulieu and Gainetdinov, 1995; Vallone *et al.*, 2000). The D_1 and D_5 receptors, members of the D_1-like family, share 80% amino acid sequence similarity and couple with the stimulatory $G\alpha_s$ protein. The D_2 receptor shares 75% sequence similarity with the D3 receptor and only 53% sequence similarity with the D_4 receptor. Receptors in the D_2- like family couple with the inhibitory $G\alpha_i$ protein (reviewed in Missale *et al.,* 1998; Vallone *et al.*, 2000; Beaulieu and Gainetdinov, 2011).

1.4.1 The Dopamine Receptor 2 (D_2)

The dopamine D_2 receptor is encoded by the *DRD2* gene located on chromosome 11q22-23 (Grandy *et al.,* 1989). Alternative splicing of an 87 bp segment within exon 6, between introns 4 and 5, yield two splice variants including the short D_{2S} receptor isoform and the long D_{2L} receptor isoform (Monsma *et al.,* 1989; Dal Toso *et al.*, 1989; Giros *et al.,* 1989). The D_{2L} receptor is characterized by the inclusion of 29 amino acids in the third intracellular loop, which is absent in D_{2S} receptor (Monsma *et al.,* 1989; Dal Toso *et al.*, 1989; Giros *et al.*, 1989). These variants of D_2 receptors have a distinct expression, physiological and signaling properties (Guiramand *et al.,* 1995; Khan *et al.,* 1998; Usiello *et al.*, 2000; Beaulieu *et al.*, 2005; Girault and Greengard, 2004; De Mei *et al.*, 2009; Beaulieu and Gainetdinov, 2011).

D_2 receptors are highly expressed in the brain and the periphery. In the CNS, highest levels of D_2 receptors are found in the striatum, olfactory tubercle, and nucleus accumbens. D_2 receptors are also expressed in the ventral tegmental area, substantia nigra, prefrontal cortex, hypothalamus, amygdala and hippocampus (reviewed in Missale *et al.,* 1998; Vallone *et al.*, 2000; Beaulieu and Gainetdinov, 2011). In the CNS, the D_2 receptors control a variety of physiological functions. In the striatum, these receptors

have been implicated in regulating locomotor activity (Khan *et al.,* 1998; Kelly *et al.*, 1998; Schindler and Carmona, 2002). Additionally, the D_2 receptor has also been implicated in reward and motivation (Di Chiara and Bassareo, 2007; Koob and Volkow, 2010; Soares-Cunha *et al.,* 2016), learning and memory (Miller and Marshall, 2005; Hyman *et al.,* 2006), as well as cognitive functions (Sawaguchi and Goldman-Rakic, 1994; Takahashi *et al.*, 2008).

Agonist binding to the D_2 receptor results in $G\alpha_i$-dependent activation leading to inhibition adenylyl cyclase activity, causing an overall decrease in the levels of cAMP. Moreover, the D_2 *receptor also* increases outward potassium currents, leading to cell hyperpolarization through a mechanism including $G\beta\gamma$ subunits of the G protein (Missale *et al.,* 1998; Neve *et al.*, 2004).   The D_2 receptor also signals *via* β-arrestins, both β-arrestin1 (Kim *et al.,* 2001) and β-arrestin2 (Masri *et al.,* 2008; Huang *et al.,* 2013) to facilitate receptor internalization and G protein-independent ERK phosphorylation.

Similar to CB_1, the D_2 receptor can form both homo- and hetero-oligomers. Homomerization of the D_{2L} receptor was proposed following the observation of high molecular weight bands on SDS-PAGE using rat and human brain striatal membranes following photoaffinity labeling. D_{2L} homodimer, trimer, tetramers, and pentamers were all detected, suggesting that D_2 receptors can form both dimer and higher order homomeric complexes (Zawarynski *et al.,* 1998; Armstrong and Strange, 2001; O'Dowd *et al.*, 2005; George *et al.,*2014). Homomerization of the D_{2L} receptors has also been confirmed using BRET, FRET and co-immunoprecipitation (Lee *et al.*, 2000; Wurch *et al.*, 2001; Gazi *et al.*, 2003; Bagher *et al.*, 2016). Homomerization of the D_{2L} receptor results in negative cooperativity, whereby ligand binding at one D_{2L} receptor, decreases affinity for further ligand binding to another D_{2L} receptor within the oligomeric complex (Armstrong and Strange, 2001; Han *et al.*, 2009). The D_{2L} receptor has also been shown to hetero-oligomerize with other class A GPCRs including the D_1 receptor (Lee *et al.,* 2004; Rashid *et a*l., 2007; Hasbi *et al.,* 2009), A_{2A} receptor (Ferré *et al.,* 1992; reviewed in Ferré *et al.,* 2014, 2015b; Casadó-Anguera *et al.,* 2016), and ghrelin $GHSR_{1a}$ receptor (Kern *et al.,* 2012).

D_2 receptors have been implicated in the etiology of several neurological and neuropsychiatric disorders and drugs acting on these receptors are used to treat several

diseases (reviewed in Noble, 2003; Tost *et al.,* 2010; Rangel-Barajas *et al.,* 2015). Pharmaceutical agents include dopamine agonists, such as pramipexole, ropinirole and retigabine, are used clinically to treat symptoms of Parkinson's disease (reviewed in Brooks, 2000; Stowe *et al*., 2008; Tomlinson *et al*., 2010; Stocchi *et al*., 2016). Clinically, pharmaceutical agents that block the dopamine receptors are used to treat schizophrenia, bipolar disorder, major depression, Huntington's disease, and Tourette's syndrome (Seeman, 2010; Eddy and Rickards, 2011; Frank, 2014). Antipsychotics are classified as "typical" (also known as first-generation) antipsychotics or "atypical" (also known as second-generation) antipsychotics, based on their relative affinity for the different receptors (reviewed in Gerlach, 1991; Kapur and Mamo, 2003; Meltzer, 2013; Murray *et al.,* 2017). Antipsychotic drugs mediate their therapeutic actions by blocking the central mesolimbic and mesocortical dopaminergic pathways. Typical antipsychotics have a high affinity for the D_2 receptors. The antagonism of D_2 in the nigrostriatal pathway is responsible for the extrapyramidal side effect, akathisia, dystonia, and tardive dyskinesia produced by these drugs. In addition to blocking D_2 receptors, these drugs also have various affinities for other receptor types such as $5HT_{2A}$- serotonergic, α_1-adrenergic, $M_{1,2,3}$-muscarinic and H_1-histaminic receptors. Typical antipsychotic drugs include reserpine, chlorpromazine, thioridazine, and haloperidol. Atypical antipsychotics are as potent in inhibiting serotonin $5HT_{2A}$ receptors as they are in inhibiting dopamine D_2 receptors. Examples of atypical antipsychotics include risperidone, clozapine, olanzapine, quetiapine, sertindole and aripiprazole (reviewed in Gerlach, 1991; Kapur and Mamo D, 2003; Meltzer, 2013; Murray *et al.,* 2017). This group of antipsychotics has a lower risk of extrapyramidal side effects but is associated with a higher incidence of metabolic abnormalities including dyslipidemia, metabolic syndrome and weight gain (reviewed in Tschoner *et al.,* 2007; Ücok and Gaebel, 2008; Leung *et al.,* 2012; Scigliano and Ronchetti, 2013).

1.5 Interactions Between the Endocannabinoid System (ECS) and the Dopaminergic System (DS) in the Basal Ganglia

Dopamine is the key neurotransmitter in the basal ganglia that plays a role in the regulation of movement (reviewed in Smith and Villalba, 2008; Nelson and Kreitzer, 2014). The dorsal striatum receives dopamine from the *pars compacta* of the substantia nigra through the nigrostriatal dopaminergic pathway (Fig. 1.5). This dopaminergic pathway regulates voluntary movement as part of the basal ganglia motor loop (reviewed in Missale *et al.,* 1998; Beaulieu and Gainetdinov, 1995; Vallone *et al.*, 2000). The globus pallidus also receives dopaminergic projections from the *para compacta* of the substantia nigra (Mamad *et al.,* 2015; Robison *et al.,* 2015). In the basal ganglia, both dopamine D_1 and D_2 are expressed, whereas D_{2L} receptor is the predominant dopaminergic receptor in the basal ganglia. Specifically, the D_{2L} receptor is expressed postsynaptically on dendritic spines of GABAeric medium spiny neurons (MSNs) projecting from the striatum to the external segments of the globus pallidus (indirect pathway), and on the terminals of these neurons in the globus pallidus. The D_{2S} receptor is expressed presynaptically on dopaminergic terminals, and glutamatergic afferents to the striatum. The D_1 receptor is expressed in the GABAeric MSNs projecting from the striatum to the internal segments of the globus pallidus (direct pathway) (Monsma *et al.,* 1989; Giros *et al.*, 1998; Levey *et al.*, 1993; Khan *et al.,* 1998; Gerfen, 2000; Usiello *et al.*, 2000; Shuen *et al.,* 2008). Activation of the dopaminergic transition in the basal ganglia is associated with an increase in movement; however blocking dopaminergic receptors in the globus pallidus (Hauber and Lutz, 1999; Mamad *et al.,* 2015) or dopamine depletion is associated by hypokinesisa (Lorenc-Koci *et al.*, 1995; Abedi *et al.*, 2013). Alternation in the function of the dopaminergic dystem (DS) in the basal ganglia has been implicated in the pathophysiology of several basal ganglia disorder including Parkinson's disease, Huntington's disease (HD) and schizophrenia (reviewed in Mehler-Wex *et al.*, 2006; Cepeda *et al.,* 2014; García *et al.*, 2016).

Endocannabinod ligands and CB_1 receptors are highly expressed in the basal ganglia (e.g. striatum, globus pallidus and substantia nigra). Specifically, the CB_1 receptor is located presynaptically on terminals of GABAergic interneurons, and also on the glutamatergic afferents to the striatum but not in dopaminergic terminal (Fig. 1.5)

Figure 1.5: ***Distribution of CB₁ and D₂L Receptors in the Basal Ganglia***. **(A)** A simplified diagram of basal ganglia circuits. GABAergic inhibitory pathways are presented in red and glutamatergic excitatory pathways are presented in green. The modulatory dopaminergic nigrostriatal pathway is indicated in blue. GABAergic medium spiny neurons (MSNs) of the indirect movement pathway projecting from the striatum to the external globus pallidus (GPe) are highlighted in red. **(B)** An *Enlarged* view of the boxes present in part A. CB_1 and D_{2L} receptors are co-localized postsynaptically on the dendritic spine of GABAergic MSNs projecting from the striatum to the GPe (right box), as well as being co-localized presynaptically on the axon terminal of the same neurons in the GPe (left box). In addition, CB_1 is expressed presynaptically on terminals of glutaminergic cortical and on GABAergic interneurons. The D_{2s} receptors, but not CB_1 receptors, are expressed presynaptically on nigrostriatal dopaminergic neurons and on terminals of glutaminergic cortical neurons. Figure modified from Ferré *et al*., 2009.

A)

Cerebral cortex

Thalamus

Striatum

Globus pallidus

GPe

GPi

Subthalamic nucleus

Nigrostriatal Dopaminergic Pathway

Substantia nigra

— Glutamate
— GABA
— Dopamine

B)

GABAergic MSN terminal

GABAergic neuron

GABAergic Interneuron

Glutaminergic Cortical Neuron

Dendritic Spine of GABAergic MSN

Dopaminergic Neuron

CB_1

D_{2L}

D_{2s}

29
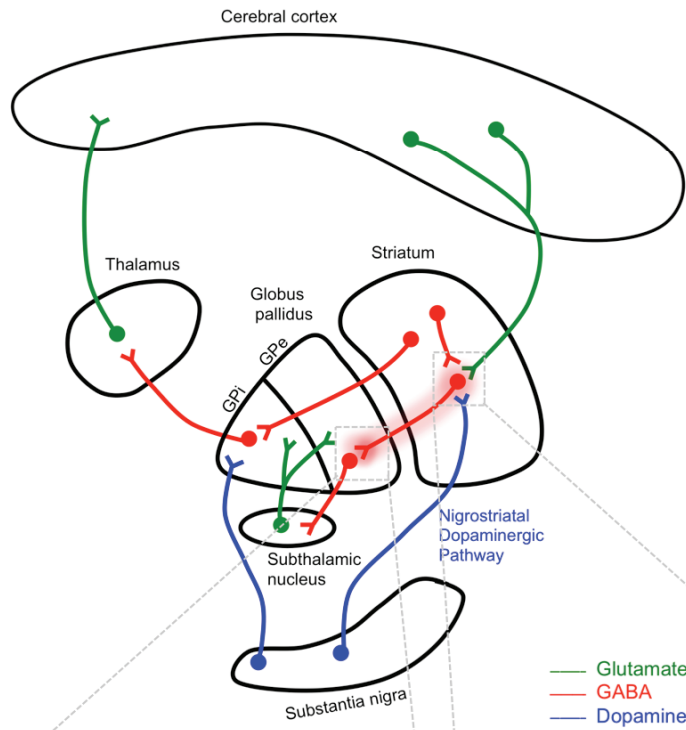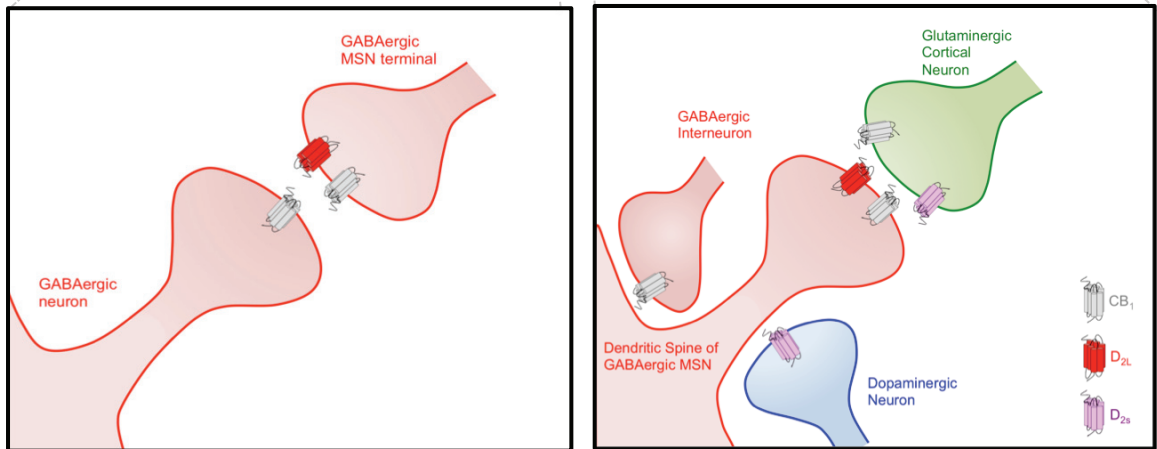
(Herkenham *et al*., 1991; Tsou *et al*., 1998; Köfalvi *et al.,* 2005; Pickel *et al.,* 2006; Uchigashima *et al.,* 2007). In addition, the CB_1 receptor is also located postsynaptically on somatodendritic of GABAergic MSNs of both the direct and indirect pathways (Rodriguez *et al*., 2001; Pickel *et al.,* 2004, 2006), and is highly expressed in the terminals of these neurons in the globus pallidus (Herkenham *et al*., 1991; Julian *et al.,* 2003; Martín *et al*., 2008). The ECS contributes to the regulation of movement (reviewed in Fernández-Ruiz and Gonzáles 2005; Fernández-Ruiz *et al.,* 2009; Kluger *et al.,* 2015). Administration of exogenous cannabinoids results in dose-dependent modulation of motor activities where very low doses of cannabinoids produce stimulatory effects, while high doses of cannabinoids cause dose-dependent motor depression and even catalepsy (reviewed in Fernández-Ruiz and Gonzáles, 2005; Fernández-Ruiz *et al.,* 2010; García *et al*., 2016; Bloomfield *et al.,* 2016). Additionally, cannabinoids were reported to counteract the motor effect of dopamine receptor activation (Aulakh *et al.,* 1980; Moss *et al.,* 1981; Anderson *et al*., 1996; Giuffrida *et al.,* 1999; Andersson *et al*., 2005; Marcelino *et al.,* 2008). For example, a single low-dose of the cannabinoid agonist CP 55940, which did not affect locomotor activity when administered alone, reduced quinpirole-induced hyperactivity (Marcellino *et al.,* 2008). In contrast, the administration of the CB_1 antagonist SR141716A enhanced the stimulation of motor behavior elicited by administration of D_2 agonist quinpirole, confirming the important role of the CB_1 receptor in the control of movement (Giuffrida *et al*., 1999; reviewed in Fernández-Ruiz and Gonzáles, 2005; Fernández-Ruiz *et al.,* 2010; García *et al*., 2016; Bloomfield *et al.,* 2016).

Several mechanisms have been proposed to explain the interactions between ECS and DS in the basal ganglia involving the modulation of movement (Fig. 1.6). Classically, the effects of cannabinoids on movement were believed to be mediated indirectly by modulating the release of dopamine in the basal ganglia (reviewed in García *et al*., 2016). CB_1 is expressed presynaptically on the GABAergic interneurons and glutamatergic neurons, located in close proximity to the dopaminergic neurons in the striatum. Activation of CB_1 receptors by cannabinoid agonists acts as a retrograde feedback on presynaptic glutamatergic and GABAergic nerve terminals, modulating dopamine release (reviewed in Fernández-Ruiz and Gonzáles, 2005; Fernández-Ruiz *et*

Figure 1.6: Different Mechanisms Proposed to Explain the Interactions Between the ECS and DS in the Basal Ganglia. The ECS plays a modulatory role in the control of dopaminergic neurotransmission in the basal ganglia. This influence is indirect and exerted through the actions of endocannabinoids on the presynaptic CB_1 receptor to modulate GABA and glutamate inputs received by dopaminergic neurons. Additionally, there is evidence that certain eicosanoid-related cannabinoids may directly activate the transient receptor potential vanilloid type 1 (TRPV1) receptors, which are expressed in nigrostriatal dopaminergic neurons, allowing a direct regulation of dopamine transmission. In addition, CB_1 and D_{2L} receptors are co-localized postsynaptically on the dendritic spine of GABAergic MSNs projecting from the striatum to the external globus palliduas as well as the axon terminal of the same neurons. It has been proposed that heteromerization between CB_1 and D_{2L} receptors provides another mechanism to facilitate direct interactions between the two systems. Through these direct and indirect mechanisms, cannabinoids may interact with the dopaminergic transmission in the basal ganglia and play a role in the control of movement. Figure 1.6 was modified from García *et al.*, 2015.
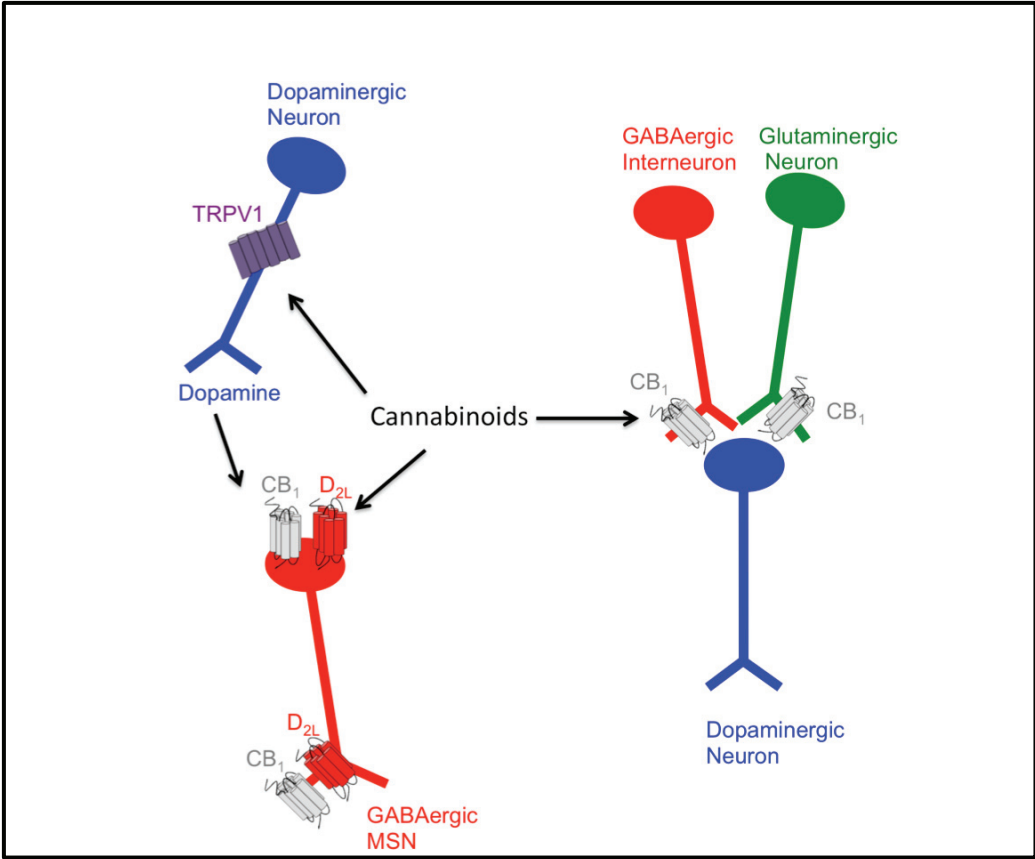
al., 2010; García *et al.,* 2016; Bloomfield *et al.,* 2016). However, accumulating evidence suggests that other cannabinoid receptor(s) and/ or mechanisms might be involved in the interaction between the ECS and DA at the level of the basal ganglia. For example, several researchers have reported that the transient receptor potential cation channel family V member 1 (*TRPV1*) receptors are expressed in the nigrostriatal dopaminergic neurons (Fig. 1.6) (Mezey *et al.,* 2000) and the activation of this receptor can directly modulate dopamine release in the striatum (Marinelli *et al.,* 2003, 2007; Ferreira *et al.* 2009). Specifically, the activation of *TRPV1* receptors with either capsaicin or with other vanilloid agonists produced hypokinesia in rats (Di Marzo *et al.,* 2001). Similarly, the endocannabinoid AEA produced the same behavioral effects (hypokinesia) accompanied by a reduction in the activity of dopaminergic neurons in the striatum; these effects were partially reversed by co-administration of the vanilloid-like receptor antagonist capsazepine. Thus indicating that these effects might also be mediated through the TRPV1, not only the CB_1 receptor following AEA application (de Lago *et al.,* 2004; reviewed in García *et al.,* 2016; Bloomfield *et al.,* 2016).

Another proposed mechanism that might facilitate the interaction between the ECS and the DS in the basal ganglia is through the formation of CB_1 and D_{2L} receptor heteromers in the basal ganglia (Fig. 1.6). CB_1 and D_{2L} receptors are co-localized postsynaptically on the dendritic spine of GABAergic MSN projecting from the striatum to the globus pallidus as well as the axon terminal of the same neurons in the external globus pallidus (Fig. 1.5) (Maneuf and Brotchie 1997; Pickel *et al.,* 2006). The fact that CB_1 and D_{2L} receptors are co-localized suggests that they could form functional heteromers. The formation of CB_1/D_{2L} heteromers would allow for bi-directional interactions between the ECS and DS at the level of GPCR and G protein function (Giuffrida *et al.,* 1999; Meschler and Howlett, 2001; Julian *et al.,* 2003; Martín *et al.,* 2008; Nguyen *et al.,* 2012). Even before heteromerization between these two receptors had been demonstrated *in vitro*, it was observed that co-stimulation of CB_1 and D_2 in striatal neurons leads to an accumulation of cAMP, while stimulation of either receptor alone leads to an inhibition of cAMP (Glass and Felder 1997). This response was suggested to be the result of switching CB_1 coupling from $G\alpha_i$ to $G\alpha_s$ proteins following the co-activation of both CB_1 and D_2 receptors (Kearn *et al.,* 2005). Subsequently, it was

found that co-expression of the D_2 receptor with CB_1 was sufficient to switch CB_1 coupling even in the absence of a D_2 agonist (Jarrahian *et al.,* 2004). Finally, heteromerization between the two receptors was confirmed using co-immunoprecipitation, BRET, FRET, and multicolor BiFC (Kearn *et al.,* 2005; Marcellino *et al.,* 2008; Przybyla and Watts *et al.,* 2010; Khan and Lee, 2014; Bagher *at al.*, 2016). In fact, *in vivo* heteromerization between the two receptors has been recently confirmed in the caudate-putamen of *Macaca fascicularis* brain using *in situ* PLA (Pinna *et al.,* 2014; Bonaventura *et al.,* 2014).

1.5.1 Clinical Relevance: Huntington's Disease

Alteration in the expression and function of CB_1 and D_{2L} receptors has been observed in Huntington's disease (HD) (Blázquez *et al.,* 2011; reviewed in Laprairie *et al.*, 2015). HD is an inherited dominant negative disorder characterized by movement, psychological and cognitive impairments. Other symptoms include weight loss, metabolic dysfunction, muscle wasting and cardiac abnormalities (Newcombe, 1981; Roos *et al.,* 1993; Foroud *et al.,* 1999; Ross 2010, Roos and Tabrizi 2011; Labbadia and Morimoto, 2013). HD is caused by the expression of a single copy of huntingtin (Htt) with an expanded CAG repeat. Translation of the mutant allele yields the mutant Htt (mHtt) protein containing an expanded polyglutamine region near the amino terminus (Huntington's Disease Collaborative Research Group, 1993). The N-terminus of mHtt undergoes protein cleavage and accumulates in the nucleus where it forms aggregates (Vonsatte *et al.*, 1985; Luthi-Carter *et al.*, 2002; Atwal *et al.,* 2007; Hogel *et al.*, 2012). mHtt interferes with a variety of cellular processes including excitotoxic stress, mitochondrial dysfunction, an abnormal inflammatory response in the CNS and the transcriptional dysregulation of a subset of genes (reviewed in Zuccato and Cattaneo, 2014; Sharma and Taliyan*,* 2015). One of the earliest signs of cellular dysfunction in HD brain is a decline in the expression of CB_1 receptors in the basal ganglia (Denovan-Wright and Robertson, 2000; Glass *et al.*, 2000). A significant reduction in CB_1 receptor mRNA and protein were observed in the caudate nucleus, putamen and external segment of globus pallidus of post-mortem human HD brain tissue (Denovan-Wright and Robertson, 2000; Glass *et al.*, 2000; reviewed in Sagredo *et al.,* 2012). Studies using

positron emission tomography and autoradiography demonstrated reduced striatal D_2 receptor density even in asymptomatic HD patients (Richfield *et al.,* 1991; Weeks *et al.,* 1996; van Oostrom *et al.,* 2009). These observations indicate that cannabinoid and dopamine signaling is disrupted early in HD progress. Atrophy of the striatum is the hallmark of HD pathogenesis. GABAergic MSNs of the indirect movement pathway that project from the striatum to the globus pallidus are more susceptible to degradation in HD. The loss of GABAergic MSN is responsible for the development of the involuntary movements (chorea) observed in HD (reviewed in Zuccato and Cattaneo, 2014; Sharma and Taliyan*,* 2015).

Currently, there is no cure for HD. Available therapies aim to reduce the severity of motor symptoms but do not alter disease progression (reviewed in Ross and Tabrizi, 2010; Carroll *et al.,* 2015; Polo *et al.*, 2015; Mason and Barker, 2016; Wyant *et al.,* 2017). Tetrabenazine and deutetrabenazine are the Food and Drug Administration (FDA) approved drugs to control chorea in HD (Hayden *et al.,* 2009; Frank *et al.,* 2014). However, patients who cannot tolerate the side effects of tetrabenazine are prescribed typical or atypical antipsychotic drugs. These drugs are also used in HD patients to control psychosis, delusions, agitation and hallucinations (reviewed in Ross and Tabrizi, 2010; Carroll *et al.,* 2015; Polo *et al.*, 2015; Mason and Barker, 2016; Wyant *et al.,* 2017). Increasing evidence suggests that cannabinoid-based therapies might aid in reducing involuntary movement due to their anti-hyperkinetic properties and may also help in slowing the progression of HD due to their neuroprotective, anti-inflammatory and antioxidant profiles (Blázquez *et al.,* 2011, 2015; Mievis *et al.,* 2011; reviewed in Sagredo *et al.,* 2012; Chiarlone *et al.*, 2014; Naydenov *et al.,* 2014; Laprairie *et al.,* 2016). The effects of co-administration of cannabinoids on dopamine antagonist effects are still unknown. Preclinical studies suggest that co-administration of cannabinoids and D_2 antagonist might have different outcomes than administrating either compound alone. Therefore, a better understanding of the allosteric interaction between the CB_1 and D_{2L} receptors is directly applicable to the current treatments for HD and the design of therapies for HD.

1.6 Research Objectives

Increasing functional, biochemical and pharmacological evidence suggests that CB_1 and D_2 receptors can form heteromers that have distinct functional properties compared to homomers of either parent receptor. Given that allosteric interactions within hetero-oligomeric complexes result in a unique pharmacology, there is a need to better understand the allosteric interactions within CB_1/D_{2L} heteromeric and the stoichiometry of $CB_1/D_{2L}/G$ protein complexes. *In vivo*, CB_1 and D_{2L} receptors are co-localized in the GABAergic MSNs projecting from the striatum to the globus pallidus, as well as on the axon terminals at the globus pallidus where they play important roles in the coordination of movement. Given the interaction between CB_1 and D_2 receptors, we hypothesized that co-localization of CB_1 and D_{2L} receptors in the basal ganglia allows for bidirectional allosteric interactions between CB_1 and D_{2L} ligands within CB_1/D_{2L} heteromers, which may be physiologically and clinically significant. Therefore, in the present work, I address these issues with three primary research objectives:

1- **Understand the stoichiometry of $CB_1/D_{2L}/G$ protein complexes.**

2- **Examine the effect of D_2 ligands (agonist and antagonists) on CB_1 pharmacology, and examine the effect of CB_1 agonists on D_{2L} pharmacology within the CB_1/D_{2L} heteromers in both heterologous expression system and in cell model endogenously expressing both receptors.**

3- **Examine the effects of chronic cannabinoid and/or antipsychotic treatment on locomotion activity and on CB_1/D_2 heteromer expression in the globus pallidus of C57BL/6J mice.**

CHAPTER 2

MATERIALS AND METHODS

2.1 Generation of DNA Constructs

All cDNA plasmid constructs used in this thesis are listed in Table 2.1. For BRET^2 assays, the C-terminus of the D$_{2L}$ receptor (GenBank accession number: NM_000795) was tagged with green fluorescent protein 2 (GFP^2) using the pGFP^2-N3 plasmid to generate the D$_{2L}$-GFP^2 construct. D$_{2L}$ was also tagged at the C terminus with *Renilla* luciferase (Rluc) using the pRluc-N1 plasmid to generate the D$_{2L}$-Rluc construct (PerkinElmer, Waltham, MA). The human D$_{2L}$-pcDNA3.1 (+) plasmid was obtained from the Missouri University of Science and Technology cDNA Resource Center (Rolla, MO). The D$_{2L}$-GFP^2 and D$_{2L}$-Rluc constructs were generated by amplifying the D$_{2L}$ from D$_{2L}$-pcDNA3.1 (+) by PCR using the forward primer (FP) D$_{2L}$-FP and the reverse primer (RP) D$_{2L}$-RP (Tables 2.2 and 2.3). Briefly, to clone the D$_{2L}$ receptor into the pGFP^2-N3 and pRluc-N1 plasmids the D$_{2L}$ receptor was amplified without stop codon from the D$_{2L}$-pcDNA3.1 (+) plasmid by PCR utilizing a high-fidelity *Pfu* DNA polymerase (Thermo Fisher Scientific, ON, Canada) with the FP D$_{2L}$-FP possessing an *EcoR1* restriction site and the RP D$_{2L}$-FP possessing a *Kpn1* restriction site. PCR reactions contained 1 μl of 10 pg/μl D$_{2L}$-pcDNA3.1 (+), 2 mM 10X *Pfu* buffer with MgSO4, 2 mM each deoxyribonucleoside triphosphate and 1 unit of *Pfu* DNA polymerase (Thermo Fisher Scientific). Reactions were subjected to an initial denaturation step at 95°C for 3 m, and then 30 cycles of denaturation at 95°C for 30 s, primer annealing at 58°C for 30 s and extension at 72°C for 2 min with a final extension at 72°C for 10 m. The PCR products were fractionated on a 1% agarose gel containing ethidium bromide and visualized with a UV transilluminator and Kodak EDAS 290 docking station. Bands of the expected size were extracted from the agarose gel using the GenElute™ Gel Extraction Kit (Sigma-Aldrich, ON) and digested with FastDigest *EcoRI* and *Kpn1* (Thermo Fisher Scientific) at 37°C for 15 min. The same restriction enzyme digestions were performed on the pGFP2-N3 and pRluc-N1 plasmids (PerkinElmer, Waltham, MA). The FastDigest enzymes were inactivated by heating for 5 min at 80°C. Fragments were ligated into compatibly

Table 2.1: DNA Constructs Used in This Thesis.

Constructs	Genbank accession number	Description	Source
CB$_1$-pcDNA	NM_016083	Untagged CB$_1$ receptor cloned into pcDNA3.1 Zeo (+) (Invitrogen).	Construct was cloned by AMB.
CB$_1$-GFP^2	NM_016083	CB$_1$ receptor C-terminally tagged with GFP^2 cloned into GFP^2-N3 (PerkinElmer).	Construct was cloned by Dr. Brian Hudson (Hudson *et al.*, 2010).
CB$_1$-Rluc	NM_016083	CB$_1$ receptor C-terminally tagged with Rluc cloned into Rluc-N1 (PerkinElmer).	Construct was cloned by Dr. Brian Hudson (Hudson *et al.*, 2010).
CB$_1$-VC	NM_016083	CB$_1$ receptor C-terminally tagged with EYFP Venus C-terminal hemiprotein cloned into pBiFC-VC155 (Shyu *et al.,* 2006).	Construct was cloned by AMB.
CB$_1$-VN	NM_016083	CB$_1$ receptor C-terminally tagged with EYFP Venus N-terminal hemiprotein cloned into pBiFC-VN173 (Shyu *et al.,* 2006).	Construct was cloned by AMB.
CB$_1$-BP	NM_016083	CB$_1$ blocking peptide that inhibits the interaction between CB$_1$ and D$_{2L}$ cloned into pcDNA3.1 Zeo (+) (Invitrogen).	Construct was cloned by AMB.
CB$_1$-Gα_{i1}-BP	NM_016083	A blocking peptide that binds to the 3rd intracellular loops of CB$_1$ (amino acids 316-344) and blocks the interaction between CB$_1$ and Gα_{i1}. The blocking peptide was cloned into pcDNA3.1 Zeo (+). (Invitrogen).	Construct was cloned by AMB.
D$_{2L}$-pcDNA	NM_000795	Untagged D$_{2L}$ receptor cloned into pcDNA3.1 Zeo (+) (Invitrogen).	Construct was obtained from the Missouri University of Science and Technology cDNA Resource Center (Rolla, MO).

Table 2.1: DNA Constructs Used in This Thesis.

Constructs	Genbank accession number	Description	Source
D_{2L}-GFP^2	NM_000795	D_{2L} receptor C-terminally tagged with GFP^2 cloned into GFP^2-N3 (PerkinElmer).	Construct was cloned by AMB.
D_{2L}-Rluc	NM_000795	D_{2L} receptor C-terminally tagged with Rluc cloned into Rluc-N1 (PerkinElmer).	Construct was cloned by AMB.
$G\alpha_{i1}$-Rluc	001256414	Rluc was inserted between nucleotide 273 and 274 of human $G\alpha_{i1}$. The recombinant $G\alpha_{i1}$-RLuc construct was cloned in pcDNA3.1 (+) (Invitrogen).	Construct was obtained from Dr. Denis Dupré (Ayoub *et al*, 2007).
$G\alpha_s$-Rluc	BC108315.1	Rluc was inserted between nucleotide 564 and 565 corresponding to the α-helical domain of the human $G\alpha_s$. The recombinant $G\alpha_s$-RLuc construct was cloned in pcDNA3.1 (+).	Construct was obtained from Dr. Denis Dupré (Ayoub *et al*, 2007).
$G\beta_1$ pcDNA	NC_000001.11	Untagged $G\beta_1$ cloned into pcDNA 3.1 (+) (Invitrogen).	Construct was obtained from Dr. Denis Dupré (Galés, 2005).
$G\gamma_2$-pcDNA3.1	NM_031754	Untagged $G\gamma_2$ cloned into pcDNA 3.1 (+) (Invitrogen).	Construct was obtained from Dr. Denis Dupré (Galés *et al*, 2005).
HERG-GFP^2	NG_008916.1	HERG sequence was inserted into pGFP^2-N3 plasmid (PerkinElmer).	Plasmid was obtained from Dr. Terry Hébert (Dupré *et al*., 2007).
mGLuR6-GFP^2	NC_000005.10	mGLuR6 sequence was inserted into the pGFP^2-N3 plasmid (PerkinElmer).	Construct was obtained from Dr. Robert Duvoisin.
β-arrestin1-GFP^2	NM_004041.4	β-arrestin1 C-terminally tagged with GFP^2 cloned into pcDNA 3.1 (+) (Invitrogen).	Construct was cloned by AMB.

Table 2.1: DNA Constructs Used in This Thesis.

Constructs	Genbank accession number	Description	Source
β-arrestin1-Rluc	NM_004041.4	β-arrestin1 C-terminally tagged with Rluc cloned into pcDNA 3.1 (+) (Invitrogen).	Construct was obtained from Dr. Denis Dupré (Ayoub *et al*, 2007).
β$_2$AR-GFP^2	NM_000024	β$_2$AR C-terminally tagged with GFP^2 cloned into GFP^2-N3 plasmid (PerkinElmer).	Construct was cloned by Dr. Brian Hudson (Hudson *et al*., 2010).
β$_2$AR-pcDNA	NM_000024	Untagged β$_2$AR cloned into pcDNA3.1 Zeo (+) (Invitrogen).	Construct was cloned by Dr. Brian Hudson (Hudson *et al*., 2010).
β$_2$AR-VN	NM_000024	β$_2$AR C-terminally tagged with EYFP Venus C-terminal hemiprotein cloned into pBiFC-VC155 .	Construct was cloned by Dr. Maha Hammad (Hammad and Dupré, 2010)
β$_2$AR-VC	NM_000024	β$_2$AR C-terminally tagged with EYFP Venus N-terminal hemiprotein cloned into pBiFC-VC155 .	Construct was cloned by Dr. Maha Hammad (Hammad and Dupré, 2010)

digested pGFP^2-N3 and pRluc-N1 plasmids using a T4 DNA ligase overnight at 4°C. The ligation mixture contained 100 ng of each PCR product, 1 μl ligase 10X buffer and 1 unit T4 DNA ligase in 10-μl reaction (Promega Fisher Scientific Ltd., Ottawa, CA). The ligation mix was then transformed into One Shot® TOP10 Chemically Competent *E. coli* (Thermo Fisher Scientific) and plated on agar plates containing either zeocin (25 μg/ml) or kanamycin (30 μg/ml) for selection of D_{2L}-GFP$_2$ and D_{2L}-Rluc constructs, respectively. Plates were incubated overnight at 37°C to allow individual colonies to form. Single colonies were isolated and allowed to grow overnight in 2 ml Luria-Bertani (LB) broth containing either zeocin (25 μg/ml) or kanamycin (30 μg/ml). Plasmids were extracted using a GenElute™ Plasma Miniprep Kit (Sigma-Aldrich, ON), and clones containing appropriate inserts were identified by restriction digestion of each individual DNA sample with *EcoR1 a*nd *Kpn1* followed by gel electrophoresis. A clone containing appropriate sized insert was subjected to bidirectional sequencing using universal FP and RPs (Genewiz, NJ).

Similarly, the CB$_1$ receptor (GenBank accession number: NM_016083) was cloned such that either GFP^2 or Rluc was expressed as fusion proteins on the intracellular C-terminus of each receptor using the pGFP^2-N3 and pRluc-N1 plasmids (PerkinElmer, Waltham, MA). Both the CB$_1$-GFP^2 and the CB$_1$-Rluc constructs were cloned by Dr. Brian Hudson (Hudson *et al.*, 2010b). To clone CB$_1$ cDNA into pcDNA3.1 Zeo (+) (Thermo Fisher Scientific), the CB$_1$ cDNA was amplified from CB$_1$-Rluc by PCR using the following primers: CB$_1$-FP and CB$_1$-RP (Tables 2.2 and 2.3). The PCR products were inserted into the pcDNA3.1 Zeo (+) using *BamH1* and *XhoI* restriction sites to generate CB$_1$-pcDNA. After transforming chemically competent *E.coli,* colonies were selected on agar plates with 50 μg/ml carbenicillin. The CB$_1$ blocking peptide (CB$_1$-BP), spanning amino acids 432-456 of the CB$_1$ sequence that inhibits the interaction between CB$_1$ and D_{2L} receptors, was amplified from CB$_1$-Rluc by PCR using the CB$_1$-BP-FP and the CB$_1$-BP-RP (Tables 2.2 and 2.3; Khan and Lee, 2014). The PCR products were cloned into the pcDNA3.1 Zeo (+) using *BamH*I and *Xho*I restriction sites. A blocking peptide that binds to the 3rd intracellular loops of CB$_1$ (amino acids 316-344), and specifically blocks the interaction between CB$_1$ and $G\alpha_{i1}$ protein (CB$_1$-$G\alpha_{i1}$-BP), was also cloned (Mukhopadhyay and Howlett, 2001). The CB$_1$- $G\alpha_{i1}$-BP was amplified by PCR from

Table 2.2: Primer Sequences Used in RT-PCR and Cloning. Restriction sites are shown in bold.

Primer Name	Primer sequence (5' to 3')	References
β-arrestin-FP	ATAT**GCTAGC**ATGGGCGACAAAGGGACCCGA	Designed by AMB
β-arrestin-RF	ATAT**AAGCTT**TCTGTTGTTGAGCTGTGGAGAGCC	Designed by AMB
CB$_1$-FP	GAT**GGATCC**ATGAAGTCGATCCTAGAT	Designed by AMB
CB$_1$-RP	GGC**CTCGAG**TCAGAGCCTCGGCAGACG	Designed by AMB
CB$_1$-BP-FP	GAT**GGATCC**ATGTGTGAAGGCACTGCGCGCCT	Khan and Lee, 2014
CB$_1$-BP-RP	GGC**CTCGAG**TCATGAGTCCCCCATGCTGTTATC	Khan and Lee, 2014
CB$_1$-Gα$_{i1}$-BP-FP	GAT**GGATCC**ATGAAGAGCATCATCATCCAC	Mukhopadhyay and Howlett, 2001
CB$_1$-Gα$_{i1}$-BP-RP	GGC**CTCGAG**CTTGGCTAACCTAATGTC	Mukhopadhyay and Howlett, 2001
CB$_1$-VN173-FP	CCGGAC**GAATTC**TATGAAGTCGATCCTAATGGCC	Designed by AMB
CB$_1$-VN173-RP	ACAT**GGTACC**ATGCACAGAGCCTCGGCAGAC	Designed by AMB
CB$_1$-VC155-FP	CCGGAC**GAATTC**TTATGAAGTCGATCCTAGATGGCC	Designed by AMB
CB$_1$-VC155-RP	ACAT**GGTACC**CCACAGAGCCTCGGCAGAC	Designed by AMB
D$_{2L}$-FP	CGAC**AAGCTT**ATGGATCCACTGAATCTGTCC	Bagher *et al.,* 2016
D$_{2L}$-RP	TGACAT**GGATCC**CAGCAGTGGAGGATCTTC	Bagher *et al.,* 2016
mouse CB$_1$-FP	GGGCAAATTTCCTTGTAGCA	Blázquez *et al.*, 2011
mouse CB$_1$-RP	GGCTAACGTGACTGAGAAA	Blázquez *et al.*, 2011
mouse D$_{2L}$-FP	TTCAGAGCCAACCTGAAGACACCA	Coronas *et al.,* 1997
mouse D$_{2L}$-RP	GCTTTCTGCGGCTCATCGTCTTAA	Coronas *et al.,* 1997
mouse D$_2$-FP	CTGGAGAGGCAGAACTGGAG	Ikegami *et al.,* 2014
mouse D$_2$-RP	TAG ACG ACC CAG GGC ATA AC	Ikegami *et al.,* 2014

CB$_1$-Rluc using the following primers: CB$_1$-Gα_{i1}-BP-FP and CB$_1$-Gα_{i1}-BP-RP (Table 2.2). The PCR products were cloned into the pcDNA3.1 Zeo (+) using *BamH*I and *Xho*I restriction sites.

The C-terminus fusion constructs of the β$_2$AR with GFP[2], β$_2$AR-GFP[2], and the membrane protein human *ether-a-go-go*-related gene (HERG), HERG-GFP[2], were provided by Dr. Terry Hébert (McGill University, Montreal, CA). These constructs were used as controls as specified (Dupré *et al.*, 2007, Hudson *et al.,* 2010b). The carboxy-terminus GFP[2] construct of the human metabotropic glutamate receptor 6 (mGLuR6)-GFP[2] was obtained from Dr. Robert Duvoisin of the Oregon Health and Science University, Portland, OR, and was generated by the insertion of the mGLuR6 sequence into the pGFP2-N3 plasmid (Hudson *et al.,* 2010). Plasmids encoding Gα_{i1}-Rluc, Gα_s-Rluc, Gβ_1-pcDNA3.1 (+) and Gα_q-pcDNA3.1 (+) were provided by Dr. Denis Dupré (Dalhousie University, Halifax, CA) (Dupré DJ *et al.*, 2006). For the Gα_{i1}-RLuc construct, the Rluc cDNA sequence (GenBank accession number: JQ606807.1) was inserted between nucleotide 273 and 274 of human Gα_{i1} (GenBank accession number: NM_001256414), which corresponds to the loop connecting helices A and B of Gα_i. The recombinant Gα_{i1}-RLuc construct was cloned in pcDNA3.1 (+), as previously described (Ayoub *et al.,* 2007). To generate Gα_s-Rluc construct, Rluc was inserted between nucleotide 564 and 565 corresponding to the α-helical domain of the human Gα_s protein (GenBank accession number: BC108315.1) (Ayoub *et al.,* 2007). For the β-arrestin1-Rluc construct, Rluc was fused to the carboxyl terminus of β-arrestin1 (GenBank accession number: NM_004041.4) (Hamdan *et al.,* 2007). β-arrestin was also tagged at the C-terminus with GFP[2]. The β-arrestin was PCR amplified from β-arrestin-Rluc without its stop codon using the β-arrestin-FP and β-arrestin-RF primers (Tables 2.2 2.3). The PCR products were cloned into *Nhe1* and *HindIII* sites of pGFP[2]-N3 to generate β-arrestin-GFP[2] construct.

For SRET[2] assays combined with BiFC assays, CB$_1$ receptors were cloned into enhanced YFP (EYFP) Venus vector pBiFC-VN173 (Addgene plasmid # 22010) and pBiFC-VC155 (Addgene plasmid # 22011). The pBiFC-VN173 and pBiFC-VC155 vectors were gifts from Chang-Deng Hu (Shyu *et al.,* 2006). The following pairs of primers were used to amplify CB$_1$ from CB$_1$-Rluc to be cloned into pBiFC-VN173: CB$_1$-

Table 2.3: **Primers, Restriction Sites, and Vectors Used to Clone DNA Constructs.**

Primer description in table 2.2

Construct	GenBank accession number	Forward Primer	Forward Primer Restriction site	Reverse Primer	Reverse Primer Restriction Site	Vector	Tag	References
β-arrestin1-Rluc	NM_004041.4 (225-1478)	β-arrestin-FP	*NheI*	β-arrestin-RF	*HindIII*	pGFP^2-N3	C-terminal GFP^2 tag	Construct was cloned by AMB.
CB$_1$-pCDNA	NM_016083 (310-1726)	CB$_1$-FP	*BamH1*	CB$_1$-RP	*XhoI*	pcDNA3.1 zeo (+)	Untagged	Construct was cloned by AMB.
CB$_1$-BP	NM_016083 (1552-1595)	CB$_1$-BP-FP	*BamH1*	CB$_1$-BP-RP	*XhoI*	pcDNA3.1 zeo (+)	Untagged	Khan and Lee, 2014
CB$_1$-Gα$_{i1}$-BP	NM_016083 (1252-1337)	CB$_1$-Gα$_{i1}$-BP-FP	*BamH1*	CB$_1$-Gα$_{i1}$-BP-RP	*XhoI*	pcDNA3.1 Zeo (+)	Untagged	Mukhopadhyay and Howlett, 2001
CB$_1$-VN	NM_016083 (310-1726)	CB$_1$-VN173-FP	*EcoRI*	CB$_1$-VN173-RP	*KpnI*	pBiFC-VN173	EYFP Venus N-terminal hemiprotein tag	Construct was cloned by AMB
CB$_1$-VC	NM_016083 (310-1726)	CB$_1$-VC155-FP	*EcoRI*	CB$_1$-VC155-RP	*KpnI*	pBiFC-VC155	EYFP Venus C-terminal hemiprotein tag	Construct was cloned by AMB.
D$_{2L}$-GFP^2	NM_000795 (236-1566)	D$_{2L}$-FP	*EcoRI*	D$_{2L}$-RP	*KpnI*	pGFP^2-N3	C-terminal GFP^2 tag	Construct was cloned by AMB.
D$_{2L}$-Rluc	NM_000795 (236-1566)	D$_{2L}$-FP	*EcoRI*	D$_{2L}$-RP	*KpnI*	pRluc-N1	C-terminal Rluc tag	Construct was cloned by AMB.

VN173-FP and CB$_1$-VN173-RP. While the following primers pairs were used to amplify CB$_1$ to be cloned into pBiFC-VC155 plasmid: CB$_1$-VC155-FP and CB$_1$-VC155-RP (Tables 2.2 and 2.3). The PCR products were digested with *EcoR*I and *Kpn*I before being inserted into either pBiFC-VN173 or pBiFC-VC155 to generate CB$_1$-VN and CB$_1$-VC, respectively.   All constructs were sequenced to confirm their full cDNA sequence and reading-frame (Genewiz, NJ).

2.2 Material

The CB$_1$ agonist Arachidonyl-2'-chloroethylamide (ACEA) (*N*-(2-Chloroethyl)-5Z,8Z,11Z,14Z-eicosatetraenamide), and CP 55,940 ((-)-cis-3-[2-Hydroxy-4-(1,1-dimethylheptyl)phenyl]-trans-4-(3 hydroxypropyl)cyclohexanol), and CB$_1$-selective antagonist O-2050 (6aR,10aR)hydroxy-3-(1-Methanesulfonylamino-4-hexyn-6-yl)-6a,7,10,10a-tetrahydro-6,6,9-trimethyl-6H-dibenzo[b,d]pyran) were purchased from Tocris Bioscience (Bristol, UK). The D$_2$ agonist quinpirole ((4aR,8aR)-5-propyl-4,4a,5,6,7,8,8a,9-octahydro-1*H*-pyrazolo[3,4-*g*]quinolone),   and   D$_2$-antagonists haloperidol (4-[4-(4-chlorophenyl)-4-hydroxypiperidin-1-yl]-1-(4-fluorophenyl)butan-1-one), sulpiride (N-[(1-ethylpyrrolidin-2-yl)methyl]-2-methoxy-5-sulfamoylbenzamide), and olanzapine (2-Methyl-4-(4-methyl-1-piperazinyl)-10*H*-thieno[2,3-*b*][1,5] benzodiaz epine), β$_2$AR agonist isoprenaline ((*RS*)-4-[1-hydroxy-2-(isopropylamino)ethyl]benzene-1,2-diol), the mGLuR6 agonist L-AP4 ((2S)-2-amino-4-phosphonobutanoic acid), *Pertussis* toxin (PTx) and *Cholera* toxin (CTx) were obtained from Sigma-Aldrich. Drugs were dissolved in 100% ethanol as 10 mM stocks and the final vehicle concentration after dilution was 0.1% (v/v) in assay media. PTx and CTx were dissolved in dH$_2$O (50 ng/mL) and added directly to the media 24 hr prior to drug treatment.

2.3 Cell Culture

The ST*Hdh*$^{Q7/Q7}$ cell line was derived from conditionally immortalized striatal progenitor cells of embryonic day 14 C57BL/6J male mice (Coriell Institute, Camden, NJ) (Trettel *et al.,* 2000; Paoletti *et al.,* 2008). ST*Hdh*$^{Q7/Q7}$ cells endogenously express CB$_1$, D$_{2L}$, D$_3$ and D$_4$ receptors (Lee *et al*., 2007). ST*Hdh*$^{Q7/Q7}$ cells were cultured in tissue culture treated flasks (BD) at 33°C, 5% CO$_2$ in Dulbecco's Modified Eagle's Medium

(DMEM) supplemented with 10% (v/v) Fetal Bovine Serum (FBS), 2 mM L-glutamine, 100 U/ml penicillin and 10 µg/ml streptomycin and 400 µg/ml Geneticin® (Thermo Fisher Scientific) (Trettel *et al.*, 2000; Lee *et al.*, 2007; Laprairie *et al.*, 2013). At confluency, cells were subcultured at a 1:10 ratio. All experiments were carried out using cells between passages 3 and 15. ST*Hdh*$^{Q7/Q7}$ cells normally exist in a dividing state. Serum deprivation causes ST*Hdh*$^{Q7/Q7}$ cells to exit the cell cycle, increase neurite outgrowth and increase expression of DARPP-32 and D$_{2L}$ receptors (Trettel *et al.,* 2000; Paoletti *et al.,* 2008). The phenotype of serum-deprived ST*Hdh*$^{Q7/Q7}$ cells resembles that of striatal MSNs (Paoletti *et al.,* 2008; Blázquez *et al.,* 2011). ST*Hdh*$^{Q7/Q7}$ cells were maintained in serum-containing media. To stop cell division and promote neurite outgrowth, media were aspirated from cells, and the cells were rinsed once with 1X phosphate-buffered saline (PBS). Media lacking serum, but otherwise equivalent to ST*Hdh* media described above, was then added and cells were allowed to grow for an additional 24 h.

The Human Embryonic Kidney 293A (HEK 293A) cells were obtained from the American Type Culture Collection (ATCC, Manassas, VI, USA). Cells were maintained in high glucose DMEM supplied with 10% (v/v) FBS, 100 U/ml penicillin and 10 µg/ml streptomycin. Cells were cultured at 37ºC and 5% CO$_2$. 96-well plate was coated with 0.01% (w/v) poly-D-lysine to provide an adherent substrate for growing cells.

2.4 Transfection

HEK 293A or ST*Hdh*$^{Q7/Q7}$ cells were transfected using Lipofectamine® 2000 reagent (Thermo Fisher Scientific) following the manufacturer's protocol. For BRET^2 experiments, cells were plated in 6-well plate (10 cm^2/ml) with DMEM and 10% (v/v) FBS for 24-48 h, until cells reached 90% confluence. Each well of the 6-well plate received 400 µg of the required plasmid(s) diluted in 250 µl Opti-MEM® Reduced-Serum Medium (Thermo Fisher Scientific). The total amount of DNA/well was kept constant by using a pcDNA3.1+ empty vector as required. Plasmid DNA was mixed with 250 µl Opti-MEM® Reduced-Serum Medium containing 10 µl of Lipofectamine® 2000 reagent. The solution was then incubated at room temperature for 20 min before being added to a well of the 6-well plate containing fresh DMEM media without serum. Cells

were cultured for 48 h. The same method was used to transfect HEK 293A cells used for SRET[2] and BiFC assays. For confocal microscopy and Immunofluorescence assays 24-well plate was used, and for In- and On-Cell Western™ analysis 96-well plate was used (Nunc, Rochester, NY) (Table 2.4).

2.5 In-Cell Western™ Analysis

The In-Cell Western™ (ICW) cell-based assay is an immunofluorescences assay that enables the quantification of protein targets in fixed cells in a microplate well. ICW is a very powerful alternative tool to Western blot. ICW allows for quantitative, precise, and rapid detections of target proteins using a 96-or 348-well format (reviewed in Boveia and Schutz-Geschwnder, 2015). For ICW the cells are permeabilized, which allow antibodies to reach cell surface and cytoplasmic antigens. ICW functional assays have been used to study the dose and time-dependent pharmacology of GPCR ligands, protein levels and post-transcriptional (phosphorylation) states of signaling proteins (Hudson *et al.,* 2010b; Bagher *et al.,* 2013; Laprairie *et al.,* 2013, 2014, 2016). Levels of protein are normalized to the expression of a housekeeping gene (e.g. β-actin or β-tubulin). The ICW analysis was used to measure phosphorylation of the extracellular kinase 1 and 2 (ERK) and cyclic AMP response element binding protein (CREB). The ICW analysis was used to measure total CB_1 and D_{2L} immunoreactivity as an estimate of protein levels.

To carry out ICW, cells were plated on either poly-D-lysine-coated 96-well plate (HEK 293A cells) or normal 96-well plate (ST*Hdh*$^{Q7/Q7}$) and cultured for 24-48 hr until confluency was reached. For ST*Hdh*$^{Q7/Q7}$ cells, cell culture media was then replaced with 100 μl of serum-free DMEM and cells were maintained for 24 hr prior to experiments to allow cell differentiation. For HEK 293A, cell culture media was removed and replaced with 100 μl serum-free DMEM. HEK 293A cells were transfected with 200 ng of the required constructs and cells were cultured for 48 hr to allow for protein expression. To carry out ICW, cells were treated as indicated in each figure by the addition of 100 μl of serum-free DMEM containing 2X the desired final concentration of ligand(s) or vehicle. After the indicated agonist exposure time, the media was removed, and cells were fixed for 20 min with 4% (w/v) paraformaldehyde (PFA) in 0.1 M $NaPO_4$ buffer, pH 7.4. After

Table 2.4: DNA Transfection Protocol for Different Cell Culture Formats Using Lipofectamine® 2000 Reagent.

Culture Vessel	Volume of plating medium	Volume of dilution medium	DNA	Lipofectamine® 2000
6-well	2 mL	2 X 250 μL	4.0 μg	5 μL
24-well	500 μL	2 X 50 μL	0.8 μg	1 μL
96-well	100 μL	2 X 50 μL	0.2 μg	0.25 μL

fixation, cells were washed three times with 1X PBS for 5 min each, permeabilized with 0.1% (v/v) Triton X-100 in PBS for 1 hr at room temperature, and then washed three times with 1X PBS while gently shaken. Non-specific antigen binding to cells was blocked using Odyssey Blocking Buffer (Li-Cor Biosciences, Lincoln, NE, USA) containing 0.1% (v/v) Tween-20 for 90 min at room temperature while gently shaken. Cells were then incubated overnight at 4°C with either rabbit anti-phospho ERK antibody (Tyr 204; Santa Cruz Biotechnology Inc, Santa Cruz, CA, USA, Cat. No: sc-7976) and rabbit anti-total ERK 2 antibody (C-14; Santa Cruz Biotechnology Inc, Cat. No: sc-154) or goat anti-pCREB-1 (Ser 133; Santa Cruz Biotechnology Inc, Cat. No: sc-7978) and rabbit anti-total CREB-1 (C-21; Santa Cruz Biotechnology Inc, Cat. No: sc-186) diluted 1:200 in 20% (v/v) Odyssey Blocking Buffer in 1X PBS.

To measure total CB_1 and D_{2L} protein levels following persistent ligand treatment the following primary antibodies were used: Mouse anti-β-Actin antibody (Sigma-Aldrich, ON) and monoclonal rabbit N-terminal CB_1 antibody (1:500; Cayman Chemical Company, Ann Arbor, MI, USA) or mouse anti-β-Actin antibody (Sigma-Aldrich, ON) and primary monoclonal rabbit N-terminal-D_2 antibody (1:200; Santa Cruz Biotechnology Inc) diluted in 20% (v/v) Odyssey Blocking Buffer in 1X PBS containing 0.1% (v/v) Tween-20. Next day, cells were washed three times with 1X PBS containing 0.1% (v/v) Tween-20 (PBST) for five min each while gently shaken. Cells were incubated for 1 hr with the near infrared (IR) fluorescently tagged secondary antibodies IR800CW-conjugated anti-rabbit IgG secondary antibody (Rockland Immunochemical, Gilbertsville, PA) and Alexa Fluor 680 anti-goat secondary antibody (Thermo Fisher Scientific) or Alexa Fluor 680 anti-mouse secondary antibody (Thermo Fisher Scientific) diluted 1:800 in the 20% (v/v) Odyssey Blocking Buffer in 1X PBS and cells were protected from light and gently shaken. Plates were washed three times with PBST, three times with PBS and once with ddH_2O before being allowed to air-dry. Plates were scanned using the Odyssey infrared imaging system (Li-Cor Biotechnology), with intensity settings of 5 for both 700 nm and 800 nm channel and a focus offset of 5 mm.

To obtain relative phosphorylated ERK (pERK) or phosphorylated CREB (pCREB) values, the background fluorescence of channel 700 and 800 obtained from wells receiving only the secondary antibodies was subtracted from the fluorescence of

channel 700 and 800 obtained from the vehicle and drug- treated wells (Fig. 2.1). The ratios of pERK/total ERK (or pCREB/total CREB) was calculated by dividing background-subtracted fluorescence obtained from phosphorylated protein pERK to background-subtracted fluorescence obtained from total protein total ERK for each well. The ratio of the background-subtracted pERK/total ERK signals was then normalized to the ratios obtained from the wells treated with vehicle. To calculate changes in CB_1 and D_{2L} protein levels following persistent ligand treatment, the background fluorescence was determined from wells receiving only the secondary antibodies and the background was then subtracted from the total receptor expression fluoresces. The ratio of the background-subtracted total signal/ total β-actin fluoresces was then determined for each well.

2.6 On- Cell Western™ Analysis

The On-Cell Western™ (OCW) cell-based assay is used to quantify target protein levels at the cell surface. In OCW, the cell membrane is not permeabilized; therefore, antibody access is restricted to antigens on the cell membrane. The relative signal determined by OCW to ICW signal has been used to study GPCR internalization after ligand treatment. Using antibodies that recognize the extracellular domains of GPCRs (e.g. N-terminal tail of CB_1 or D_{2L}), OCW can measure cell surface expression of GPCRs on intact cells following vehicle or ligand treatment (Miller *et al.,* 2004; Hudson *et al.,* 2010b, Laprairie *et al.,* 2015). Following the detection of the cell surface GPCR, cells were permeabilized (using Triton X-1000), and ICW of total GPCR levels were determined. The ratio of GPCR expression on the cell membrane (OCW, non-permeabilized cell) and total GPCR expression (ICW, permeabilized cells) was measured at different times following drug exposure to determine the rate of GPCR internalization.

To measure cell surface expression of CB_1 and D_{2L} receptors following vehicle or ligand treatment, OCW analysis was employed using the protocol described previously by Miller *et al*. (2004). Cells were plated on either poly-D-lysine-coated 96-well plate (HEK 293A cells) or normal 96-well plate (ST*Hdh*$^{Q7/Q7}$ cells) and cultured for 24-48 hr until cell confluency was observed. Following confluency of ST*Hdh*$^{Q7/Q7}$ cells, cell culture media was replaced with 100 μl of serum-free DMEM and cells were maintained

Figure 2.1: In-Cell Western™ Analysis to Measure ERK Phosphorylation. pERK concentration-response curve measured by In-Cell Western™ from HEK 293A cells expressing CB_1 receptors treated with increasing concentrations of WIN 55,212-2 for 5 min . **(A)** ERK phosphorylation was detected using pERK antibody (800 nm, green), while total ERK was detected using total ERK antibody (700 nm, red). Overlaid image (yellow, 800 and 700 nm) indicate pERK and total ERK signals. **(B)** The concentration-response curve of WIN55,212-2 with pERK signal normalized relative to total ERK. The concentration-response curve was fit to a nonlinear regression with variable slope (four-parameter) model. Figure 2.1 was modified from Bagher *et al.,* 2017 (in press).

A)

phospho-ERK (800 nm)

Total ERK (700 nm)

Overlaid image
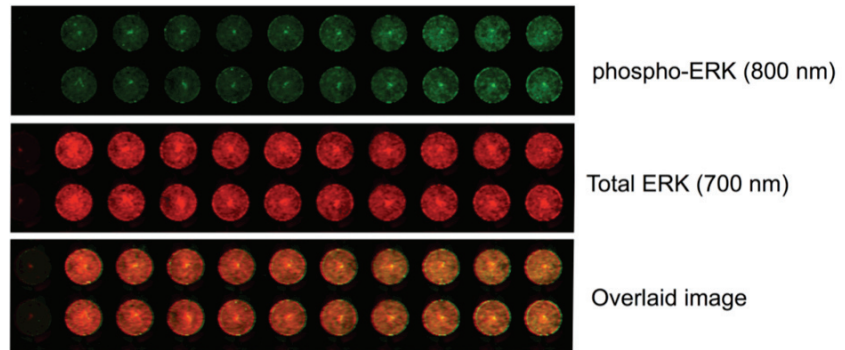
B)
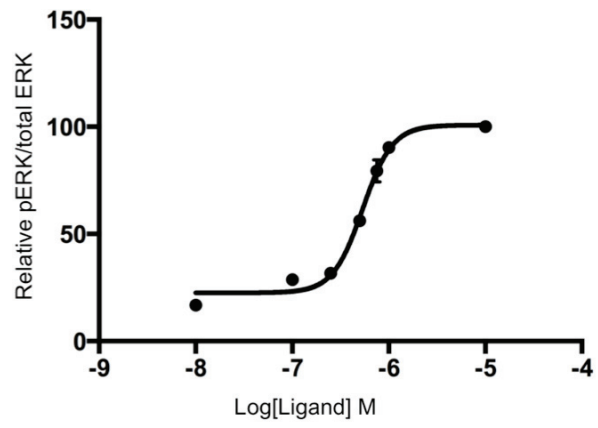
for 24 hr prior to experiments. For HEK 293A, culture media was removed and replaced with 100 μl serum-free DMEM and cells were transfected with 200 ng of the required constructs and cells were cultured for 48 hr prior to OCW.

To measure receptor internalization, cells were treated as indicated by the addition of 100 μl of serum-free DMEM containing 2 X the desired final concentration of ligand(s) or vehicle and cells were incubated for 5-60 min at 37°C in a cell culture incubator maintaining a 5% CO2. Cells were fixed with 4% (w/v) PFA for 20 min at room temperature and washed three times with PBS. Cells were blocked using Odyssey Blocking Buffer (Li-Cor Biotechnology) for 90 min at room temperature while gently shaken. Cells were incubated with primary monoclonal rabbit N-terminal CB_1 antibody (1:1000; Cayman Chemical Company), and primary monoclonal mouse N-terminal-D_{2L} antibody (1:200; Santa Cruz Biotechnology) diluted in 20% (v/v) Odyssey Blocking Buffer in 1X PBS overnight at 4°C. The following day, cells were washed three times with PBS while gently shaken, before being incubated with an anti-rabbit IR800CW-conjugated secondary antibody (Rockland Immunochemicals) and Alexa Flour 680-conjugated anti-mouse IgG secondary antibody (Invitrogen) diluted 1:800 in 20% (v/v) Odyssey Blocking Buffer in 1X PBS. Finally, cells were washed 5 times with PBS and once with ddH_2O while gently shaken. The cell culture plates were scanned using an Odyssey infrared imaging system (Li-Cor Biotechnology) with intensity settings of 5 for both the 700 and 800 nm channels and a focus offset of 3 mm.

After imaging the cell surface expression of the receptors using the Odyssey, total receptor expression was determined. To do this, cells were permeabilized using 0.1% (v/v) Triton X-100 in PBS for 1 hr at room temperature and washed three times with PBST with gentle shaking. Cells were then exposed to primary anti-CB_1 and anti-D_{2L} antibodies, secondary antibodies and scanned following the same protocol described for on OWA. To obtain the percent of basal surface expression, the background fluorescence was determined from wells exposed to the secondary antibodies and the background was then subtracted from the surface and total receptor expression signals. The ratio of the background-subtracted surface/total signals was then determined for each well.

2.7 Bioluminescence Resonance Energy Transfer 2 (BRET^2)

Bioluminescence Resonance Energy Transfer 2 (BRET^2) was used to study protein-protein interactions including the ability of CB_1 and D_{2L} receptors to form homo- and heteromers and the physical interaction between CB_1 or D_{2L} receptors and $G\alpha_i$, $G\alpha_s$, or β-arrestin1 using previously described protocol (Ramsay *et al.*, 2002; James *et al.*, 2006; Bagher *et al.*, 2013). In BRET^2, Rluc is used as the donor protein, while GFP^2 is used as the acceptor protein (Fig. 2.2). BRET^2 utilizes a unique Rluc substrate, coelenterazine 400 a, that emits light between 290-400 nm. If the Rluc molecule is in sufficiently close proximity (approximately 50-100 Å) to the GFP^2 molecule, then there will be a non-radiative resonance energy transfer to the GFP^2, which in turn will lead to its subsequent fluorescent emission at 505-508 nm (Fig. 2.2). The efficiency of energy transfer is dependent upon a number of factors including the relative distance between the donor and acceptor molecules, estimated to be less than 100 Å, and their relative orientation (Pfleger and Eidne, 2005).

To carry out BRET^2 experiments, HEK 293A cells or ST*Hdh*$^{Q7/Q7}$ cells were plated in 6-well plate and transfected with constructs as indicated in each figure. Forty-eight hours post-transfection, the BRET^2 experiment was conducted. Cells were washed twice with cold 1X PBS before being suspended in 90 μl of BRET buffer [1X PBS supplemented with glucose (1 mg/ml), benzamidine (10 mg/ml), leupeptin (5 mg/ml) and a trypsin inhibitor (5 mg/ml)] (James *et al.*, 2006). Cells were dispensed into a white 96-well plate (PerkinElmer). The GFP^2 emission was measured using an FLx800 fluorescence plate reader (BioTek Instruments Inc., Winooski, VT) with excitation and emission filters of 485/20 and 510/20 nm respectively. To carry out BRET^2, cells were treated with 1 μl of either vehicle or ligand as described in the text and figure legends. Following the addition of 10 μl of 50 μM coelenterazine 400a substrate (Biotium,CA, USA), emissions of Rluc and GFP^2 were respectively measured at 405 nm and 510 nm using Luminoskan Ascent plate reader (Thermo Scientific, Waltham, MA), with the integration time set to 10 s and the photomultiplier tube voltage set to 1200 volts. The ratio of 510/405 nm was converted to BRET efficiency (BRET$_{Eff}$) by first determining the 510/405 ratio of each sample, subtracting the minimum 510/405 nm emission

Figure 2.2: Bioluminescence Resonance Energy Transfer 2 (BRET^2). **(A)** GPCRs are tagged at their carboxy-termini with either Rluc or GFP^2. The left panel illustrates when the tagged GPCRs are not interacting. Following the addition of the Rluc substrate coelenterazine 400a it is oxidized by Rluc, causing Rluc to emit blue light at ~ 405 nm, but no energy is transferred to the acceptor GFP^2, and therefore no green light is emitted. The right panel illustrates the emission spectra for co-expressed Rluc and GFP^2 in the presence of coelenterazine 400a when the Rluc and GFP^2 are not in close proximity. When Rluc and GFP^2 are not in close proximity resonance energy transfer does not occur; resulting in a peak at 405 nm from Rluc emission. **(B)** When the tagged GPCRs are interacting, the oxidation of coelenterazine 400a by Rluc emits blue light, which is transferred to the acceptor GFP^2 when it is in close enough proximity to Rluc. This allows resonance energy transfer to occurs, causing GFP^2 excitation, resulting in the emission of green light at ~ 510 nm. The right panel shows the emission spectra for co-expressed Rluc and GFP^2 in the presence of coelenterazine 400a when the Rluc and GFP^2 are sufficiently close to allow for resonance energy transfer to occur. This results in two peaks in the emission spectra; one at ~ 405 nm and one at ~ 510 nm. BRET^2 signals are measured as the ratio of the 510 nm to the 405 nm peaks.

A) No Protein-Protein Interaction
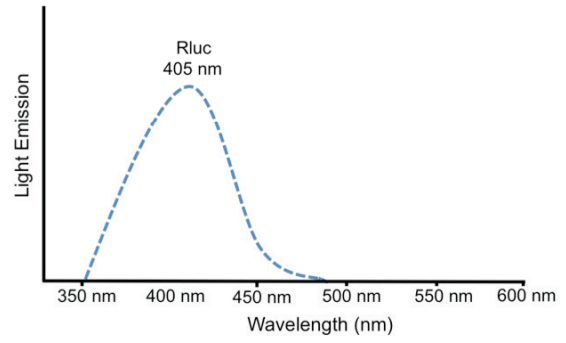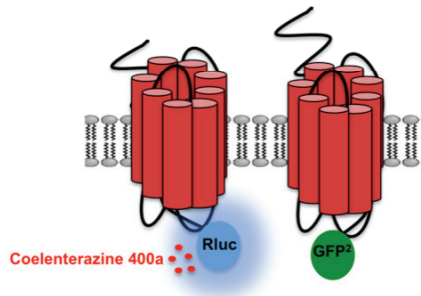
B) Protein-protein Interaction
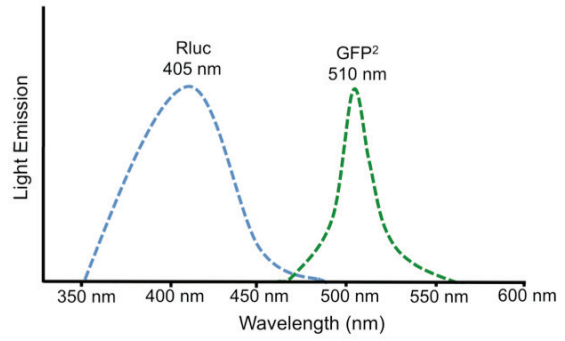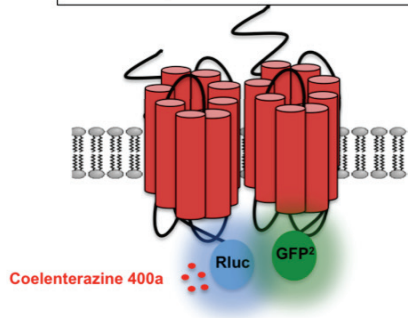
obtained from cells expressing only a Rluc-N1 construct, then dividing by the maximum measurable 510/405 nm ratio obtained from cells expressing a GFP^2-Rluc fusion construct (PerkinElmer).

It is possible that the observed BRET^2 signal may be the result of random collisions of the over-expressed receptors within the cell membrane (Pfleger and Eidne, 2005). BRET^2 saturation assay can distinguish between specific and non-specific interaction (Pfleger and Eidne, 2005). In BRET^2 saturation experiments, cells were transfected with fixed amounts of the BRET^2 donor (Rluc-tagged receptor), together with increasing amounts of BRET acceptor (GFP^2- tagged receptor). BRET$_{Eff}$ values were then plotted against the ratio of GFP^2/Rluc concentration or plotted against the ratio of GFP^2 fluorescence (obtained by directly exciting GFP^2) and Rluc emission as described in specific figure legends. The resulting data were fit to a rectangular hyperbola curve using GraphPad version 6.0 (GraphPad Software Inc. San Diego, CA). If the interaction was specific, the curve was hyperbolic indicating a specific and saturable increase in BRET^2 signal to reach a maximum saturated value (BRET$_{Max}$), where all donor molecules are interacting with acceptor molecules. However, non-specific interactions only resulted in a gradual linear increase in BRET$_{Eff}$. Changes in BRET$_{Max}$ values reflects the relative orientation, distance, and expression levels of both donor and acceptor molecules (Guan *et al*., 2009). An added benefit to the BRET^2 saturation approach is that the amount of receptor required to achieve 50% of BRET$_{Max}$ signal could be defined as BRET$_{50}$ values. The BRET$_{50}$ estimates the affinity of donor and acceptor molecules. In BRET^2 saturation curves that fit a hyperbolic form, B$_{Max}$ and K$_d$ determinations are the BRET$_{Max}$ and BRET$_{50}$ values, respectively (Pfleger and Eidne, 2005; Guan *et al.,* 2009).

The oligomerization state of CB$_1$ and D$_{2L}$ homo- and heteromer was assessed by using a modified form of the Veatch and Stryer model (Vrecl *et al*., 2006; Drinovec *et al.*, 2012). BRET^2 values were fitted to the model curve obtained for simple oligomers with the correction for high-energy transfer efficiencies E (Vrecl *et al*., 2006; Drinovec *et al.*, 2012):

$$\frac{BRET}{\text{BRET}_{Max}} = 1 - \frac{1}{E + (1 - E)\left(1 + \frac{[A]}{[D]}\right)^N}$$

57

Where [D] and [A] are donor and acceptor concentrations and (N) is the oligomerization state ($N=1$ for dimer, $N=2$ for trimer, $N=3$ tetramer). The transfer efficiency (E) was calculated from the emission spectra of donor and acceptor molecules obtained for coelenterazine 400a (Biotium, Hayward, CA, USA) and GFP[2] fluorescence (Vrecl *et al.*, 2006; Drinovec *et al.*, 2012).

BRET[2] experiments were also used to study the interaction between CB_1 or D_{2L} receptors and $G\alpha_i$-Rluc or $G\alpha_s$-Rluc fusion proteins in the absence or presence of ligands. In these experiments, cells were plated in 6-well plate and transfected with the required constructs ($G\alpha_i$-Rluc or $G\alpha_s$-Rluc together with CB_1-GFP[2] and/or D_{2L}-GFP[2]) in addition to un-tagged $G\beta_1$ and $G\gamma_2$ in pcDNA3.1 (+). Forty-eight hour later, cells were collected from each well, washed and resuspended in 900 μl BRET buffer. The resuspended cells were dispensed into ten wells of a white 96-well plate (90 μl/well). For BRET[2] kinetic analyses, the BRET[2] substrate coelenterazine 400a (Biotium, Hayward, CA) was added at time 0 min and light emissions were measured every 25 s for 9 min. Haloperidol was added at 50 s, while vehicle or ACEA was added at 75 s following coelenterazine 400a (Biotium, Hayward, CA, USA) administration. Quinpirole and ACEA were co-applied together at 50 s following coelenterazine 400a (Biotium, Hayward, CA, USA) administration. For all BRET[2] experiments, ligands were present throughout the assay and were not washed out.

2.8 Sequential Resonance Energy Transfer (SRET[2]) Combined with Bimolecular Complementation (BiFC)

The Bimolecular Complementation (BiFC) assay can be used to study protein-protein interactions. BiFC relies on the interaction between two non-fluorescent proteins fragments of the enhanced yellow fluorescent protein (EYFP) Venus, resulting in fluorescence EYFP signals that can be qualified (Fig. 2.3) (Hu *et al.,* 2002; Vidi *et al.,* 2010). BiFC was used to confirm that CB_1 receptors could physically associate to form homodimers when expressed in HEK 293A cells. CB_1 cDNA was cloned into expression vectors producing a CB_1 fused to the EYFP Venus N-terminal (VN) using the pBiFC-VN173 plasmid (CB_1-VN). Similarly, the CB_1 cDNA was cloned to EYFP Venus C-terminal (VC) using pBiFC-VC155 plasmid to produce CB_1 receptor fused to the EYFP

Figure 2.3: Bimolecular Fluorescence Complementation (BiFC). **(A)** GPCRs are tagged at their carboxy-termini with non-fluorescent proteins fragments of the enhanced yellow fluorescent protein (EYFP) Venus, the EYFP Venus N-terminal (VN) or EYFP Venus C-terminal (VC). The left panel illustrates tagged GPCRs that are not interacting. In this case, the two Venus fragments do not come into close proximity and there is no fluorescence. The right panel illustrates the emission spectra for co-expressed Venus-VN and Venus-VC tagged GPCRs when the Venus-VN and Venus-VC tagged are not in close proximity resulting in no detectable signal using an excitation filter of 515 nm and an emission filter of 530 nm. **(B)** The left panel illustrates tagged GPCRs interactions. As a result of the interaction, the two Venus fragments associate and refold allowing fluorescence to occur. The right panel illustrates the emission spectra for co-expressed Venus-VN and Venus-VC tagged GPCRs when the Venus-VN and Venus-VC are in close proximity allowing the two fragments associate, resulting in a detectable signal using an excitation filter of 515 nm and an emission filter of 530 nm.

A)

No Receptor-Receptor Interaction

515 nm

VN   VC

B)

Receptor-Receptor Interaction

VN VC

530 nm

515 nm
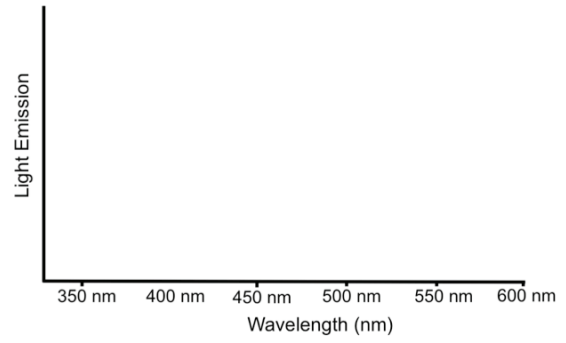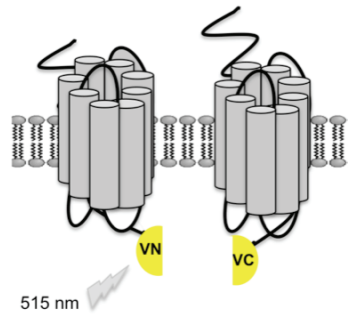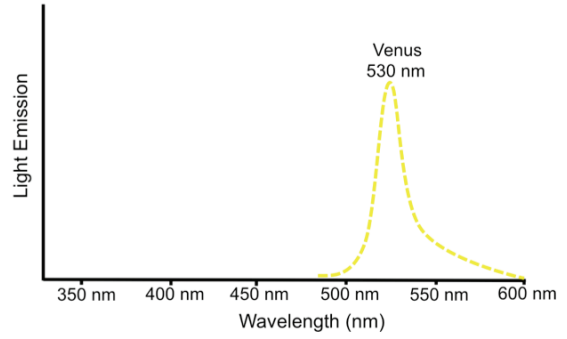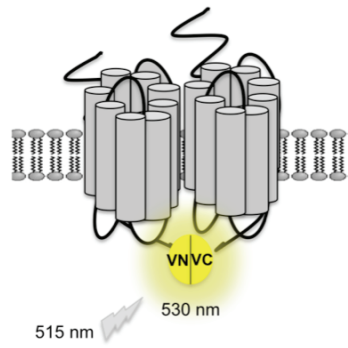
Venus
530 nm

Venus C-terminal using (CB$_1$-VC) (Shyu *et al.,* 2006). To conduct BiFC experiments, HEK 293A cells were plated in a 6-well plate and transfected with the required construct (i.e. cells were transfected with either CB$_1$-VN or CB$_1$-VC alone or in combination at 1:1 ratio). Forty-eight hours post-transfection, cells were washed twice with cold 1X PBS before being suspended in 90 μl of BRET buffer. Cells were dispensed into a white 96-well plate (PerkinElmer) and EYFP Venus fluorescence was measured using FLx800 fluorescence plate reader (BioTek Instruments Inc., Winooski, VT) with an excitation at 515 nm and an emission measured at 530 nm.

Sequential resonance energy transfer 2 (SRET^2) combines both BRET^2 and fluorescence resonance energy transfer (FRET) techniques, which allow identification of heteromers formed by three different proteins (Carriba *et al.,* 2008; Navarro *et al.,* 2013). In SRET^2, the oxidation of Rluc substrate by an Rluc fusion protein triggers acceptor excitation of GFP^2 fusion protein by BRET^2 and subsequent FRET to EYFP fusion protein (Fig. 2.4). SRET^2 combined with BiFC was used to test whether CB$_1$ and D$_{2L}$ form heterotetramers according to previously described methods (Carriba *et al.,* 2008; Navarro *et al.,* 2013). In brief, HEK 293A cells were grown in 6-well plates and transiently transfected with different plasmids encoding fusion proteins (D$_{2L}$-Rluc, D$_{2L}$-GFP^2, CB$_1$-NV, and CB$_1$-CV) as indicated for each experiment. Forty-eight hours later, transfected cells were washed twice with cold 1X PBS before being suspended in 360 μl of BRET buffer. The cell suspension was divided into four equal aliquots (90 μl). The first aliquot was used to measure GFP^2. The expression of GFP^2 protein was quantified by determining the fluorescence resulting from direct GFP^2. 90 μl of cell suspension was dispensed into a white 96-well plate and GFP^2 emission was measured using an FLx800 fluorescence plate reader (BioTek Instruments Inc., Winooski, VT) with excitation and mission filters at 485 nm and 510 nm, respectively. The expression of EYFP Venus (CB$_1$-VN and CB$_1$-VC) was qualified by determining the fluorescence resulting from EYFP Venus using a 515 nm excitation filter and a 530 nm emission filter. The second aliquot of cell suspension was used to measure Rluc protein expression. Rluc expression was quantified by determining the luminescence resulting from Rluc. Cells were distributed (90 μL) in a white 96-well plate and the luminescence was determined immediately after addition of 10 μl of 50 μM coelenterazine 400a (Biotium, Hayward, CA, USA) using a

Figure 2.4: Sequential Resonance Energy Transfer 2 (SRET^2) Combined with Bimolecular Fluorescence Complementation (BiFC). **(A)** GPCRs are tagged at their carboxy-termini with Rluc, GFP^2 or Venus fragments (Venus-VN and Venus-VC). The left panel shows Rluc and GFP^2 tagged GPCRs interacting. Thus, on the addition of the Rluc substrate, coelenterazine 400a, the oxidation of coelenterazine 400a by Rluc-tagged GPCRs triggers acceptor excitation of GFP^2 tagged GPCRs by BRET^2. Since Venus-VN and Venus-VC tagged GPCRs interact together, but not with Rluc and GFP^2 tagged GPCRs, no energy transfer occurs from GFP^2 tagged GPCRs to Venus tagged GPCRs by FRET. In the right panel, emission spectra for co-expressed Rluc and GFP^2 in the presence of coelenterazine 400a when the Rluc and GFP^2 are in close proximity and resonance energy transfer can occur. There is only a peak at 405 nm and 510 nm. **(B)** The left panel shows Rluc, GFP^2 or Venus tagged GPCRs interacting. In the left panel, as a result of this, on the addition of coelenterazine 400a, the oxidation of coelenterazine 400a by Rluc emits blue light and triggers the excitation of the acceptor GFP^2 by BRET^2, which emits green light. Since Venus tagged GPCRs are now in close enough proximity to GFP^2 tagged GPCRs, resonance energy transfer does occur to the acceptor Venus by FRET. In the right panel, emission spectra for co-expressed Rluc, GFP^2 and Venus tagged GPCR^2 in the presence of coelenterazine 400a, when the Rluc, GFP^2 and Venus tagged GPCR^2 are sufficiently close to allow resonance energy transfer to occur by BRET^2 and FRET. There will be three peaks at 405 nm resulting from Rluc emission, at 510 nm resulting from GFP^2 emission and 530 nm resulting from Venus emission. Net SRET^2 signals are measured as the ratio of the 530 nm to the 405 nm peaks.
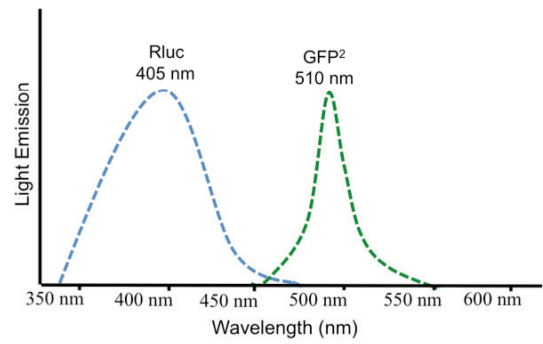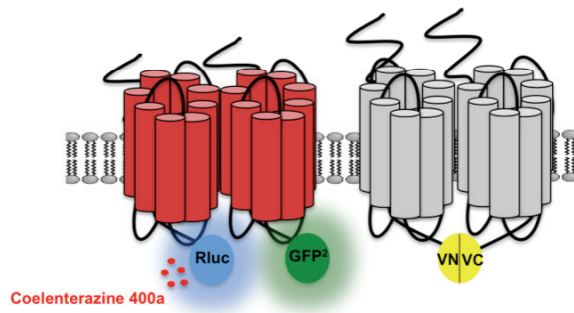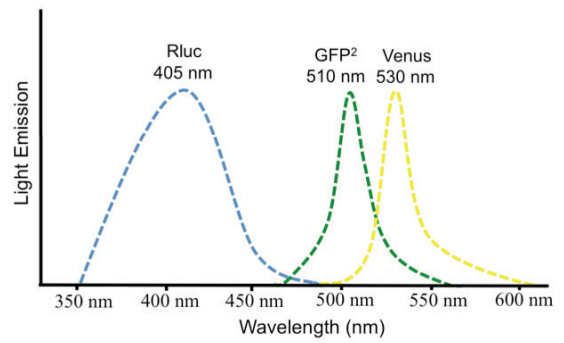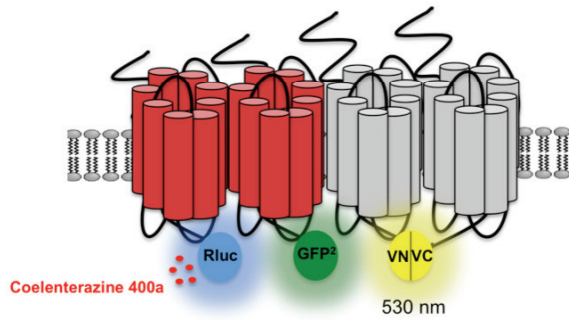
Luminoskan Ascent plate reader (Thermo Scientific, Waltham, MA) with detection filter 405 nm. The third aliquot of cell suspension was used to conduct $SRET^2$ combined with BiFC experiments. Suspended cells (90 μl) were dispensed into a white 96-well plate (Perkin-Elmer). The $SRET^2$ signals were detected immediately following the addition of 10 μl of 50 μM coelenterazine 400a (Biotium, Hayward, CA, USA) using Luminoskan Ascent plate reader (Thermo Scientific, Waltham, MA) with detection filters for 405 nm and wavelength 530 nm. Net $SRET^2$ was defined as [(530 nm emission)/(405 emission)] − correction factor. The correction factor is the value determined from 530 emission/400 emission for cells expressing only Rluc, GFP^2, or EYFP (Carriba *et al.,* 2008; Navarro *et al.,* 2013). To confirm the specificity of the interaction, $SRET^2$ saturation curves were generated by transfecting cells with a constant amount of protein-Rluc and protein-GFP^2 and increasing amounts of EYFP Venus constructs (CB_1-NV and CB_1-CV). From these saturation curves, $SRET_{Max}$ and $SRET_{50}$ values were determined, similar to $BRET^2$ assays (Carriba *et al.*, 2008; Navarro *et al.,* 2013).

2.9 Confocal Microscopy and Immunofluorescence

The co-localization of endogenous CB_1 and D_{2L} in $STHdh^{Q7/Q7}$ cells was observed using confocal microscopy. $STHdh^{Q7/Q7}$ cells were plated onto glass coverslips in a 24-well plate. At 50% confluence, cell culture media was then replaced with serum-free DMEM and cells were maintained for 24 hr prior to experiments. Cells were fixed with ice-cold 100% ethanol for 5 min. After washing the cells three times with 1X PBS, non-specific antibody binding was blocked by treating cells with 1% (w/v) bovine serum albumin (BSA) for 60 min at room temperature. Cells were incubated with primary monoclonal rabbit N-terminal CB_1 antibody (1:500; Cayman Chemical Company) and primary monoclonal mouse N-terminal-D_2 antibody (1:200; Santa Cruz Biotechnology) overnight at 4°C. The next day, the cells were washed three times with 1X PBS and incubated with a Cy3-conjugated anti-mouse immunoglobulin G (IgG) secondary antibody and Cy2-conjugated anti-rabbit secondary antibody (1:500, Jackson Immuno Research Laboratories, West Grove, PA) for 1 hr at room temperature, then washed 3 times with 1X PBS and once with H_2O. Finally, coverslips were mounted on microscopic slides (Fisher Scientific) using Fluorsave reagent® (Calbiochem, San Diego, CA).

Images of cells were acquired with a Nikon Eclipse E800 microscope attached to the D-Eclipse C1 confocal system (Nikon Canada Inc., Mississauga, ON). Cy3 was imaged by a 543 nm Helium-Neon laser (JDS Uniphase, Milpitas, CA), while Cy2 was imaged using a 488 nm air-cooled argon laser (Spectra-Physics Lasers Inc., Mountain View, CA). Images were taken using a 100X oil immersion objective.

2.10 RNA Extraction From Cell Culture

STH$dh^{Q7/Q7}$ cells were cultured in a 24-well plate to approximately 90% confluency. Cells were allowed to differentiate for 24 hr in serum-free DMEM. Trizol® reagent (Thermo Fisher Scientific, ON) was used to extract RNA from STH$dh^{Q7/Q7}$ cells following the manufacturer's protocol. Briefly, the culture media was aspirated, and cells were washed once using 1X PBS. Next, 200 μL of Trizol® was added to each well and samples were mixed by pipetting. Samples were transferred to 1.5 ml microcentrifuge tube, vortexed and incubated on ice for 3 min. Forty μL of chloroform was then added to each tube, mixed well for 15 sec by shaking and samples were centrifuged at 12,000 x g for 20 min at 4°C. The aqueous phase was removed to a new microcentrifuge tube. To precipitate RNAs, 100 μL of isopropanol was added, mixed well by inversion and tubes were placed on ice for 15 min before being centrifuged at 12,000 x g for 10 min at 4°C. The supernatant was discarded and the RNA pellet was washed twice using 200 μL ice-cold 75% (v/v) ethanol, vortexed and centrifuged at 7,500 x g for 5 min at 4°C. The RNA pellet was allowed to air dry for approximately 10 min before being suspended in 10 μL ddH$_2$O. The purity and concentration of the collected RNA were determined by measuring the A260/280 ratio of the samples using a spectrophotometer. RNA samples were stored at -80°C.

2.11 Reverse Transcriptase Reaction

Using RNA isolated from STH$dh^{Q7/Q7}$ cells, first strand cDNA was generated using reverse transcriptase SuperScript® II (Thermo Fisher Scientific, ON) following the protocol supplied by the manufacturer in a 20 μl reaction volume. Briefly, 2 μg of total cellular RNA was added to the reverse transcriptase reaction containing 0.5μM deoxynucleoside triphosphate and 7.5 μM random primers (mostly hexamers; Invitrogen)

in dH$_2$O to a final volume of 13 μl for +RT reactions, or 14 μl for –RT reactions. The reaction was vortexed, incubated at 65°C for 5 min then chilled on ice for 1 min. The following reagents were then added to the reaction: 20% First-Strand Buffer, 5% RNaseOUT$^®$, 5 mM dithiothreitol, and 200 U SuperScript III$^®$ reverse transcriptase (Invitrogen) and the reaction was mixed by pipetting. The reaction was incubated for 1 hr at 50°C, followed by 15 min inactivation at 70°C. The reaction was diluted to a final volume of 40 μL in ddH$_2$O and stored at -20°C.

2.12 Reverse Transcriptase-Polymerase Chain Reaction (RT-PCR)

Reverse Transcriptase Polymerase Chain Reaction (RT-PCR) was used to test whether ST*Hdh*$^{Q7/Q7}$ cells express D$_{2L}$ or D$_{2S}$ mRNAs. PCR primers that span the alternatively spliced exon that distinguished the D$_{2L}$ and D$_{2S}$ isoforms were used to detect D$_{2L}$ or D$_{2S}$ sized variants (Coronas *et al.,* 1997). Amplification using the FP mouse D$_{2L}$-FP and the RP mouse D$_{2L}$-RP (Table 2.2; Coronas *et al.,* 1997) yields two bands of molecular sizes 397 and 310 bp representing D$_{2L}$ and D$_{2S}$ isoforms of the receptor, respectively. The mouse-CB$_1$-FP and the mouse-CB$_1$-RP (Table 2.2) were used to amplify CB$_1$ receptor (Table 2.3) (Blázquez *et al.*, 2011). PCR reactions contained 1 μl cDNA produced from RT reaction, 2 mM of 10X *Pfu* buffer with MgSO4 (final concentration of 2 mM), 2 mM each deoxyribonucleoside triphosphate and 1 unit of *Pfu* DNA polymerase II (Thermo Fisher Scientific, ON) in ddH$_2$O to a final volume of 20 μl. These reactions were subjected to an initial denaturation step at 95°C for 3 min, and then 30 cycles of denaturation at 95°C for 30 s, primer annealing at 56 °C for 30 s and extension at 72°C for 1 min with a final extension at 72°C for 10 min. Products were fractionated on a 2% agarose gel containing 0.5 μg/ml ethidium bromide and visualized with a UV transilluminator and Kodak EDAS 290 docking station.

2.13 LightCycler® SYBR Green qRT-PCR

Real-time Quantitative Polymerase Chain Reaction (qRT-PCR) was used to quantify CB$_1$ and D$_2$ cDNA expression in ST*Hdh*$^{Q7/Q7}$ cells using previously described protocol (Laprairie *et al.,* 2013) using the LightCycler® system and software (version 3.0; Roche, Laval, QC). cDNA abundance was measured using SYBR Green (Roche, Laval,

QC), contained in the PCR buffer, which intercalates with double-stranded DNA and fluoresces green at 520 nm . Fluorescence was then quantified by the LightCycler® on a per-sample basis 46 during each round of PCR amplification of cDNA. The following CB$_1$-specific primers were used in qRT-PCR reactions: mouse-CB$_1$-FP and mouse-CB$_1$-RP primers (Table 2.2) (Blázquez *et al.*, 2011), while mouse-D$_2$-FP and mouse-D$_2$-RF were used for D$_2$ (Table 2.2; Ikegami *et al.,* 2014). qRT-PCR reactions were composed of 2 mM MgCl$_2$, 0.5 µM each of FP and RP, 2 µl of LightCycler® FastStart Reaction Mix SYBR Green I [0.3 mM dNTP, 10% SYBR Green I dye, 1.2 U FastStart Taq DNA polymerase], and 1 µl cDNA to a final volume of 20 µl with ddH$_2$O. The PCR program was: 95°C for 10 min, 50 cycles of 95°C 10 s, a primer-specific annealing temperature (Table 2.2) for 5 s, and 72°C for 10 s. Melting curve analysis of PCR products was performed immediately after the PCR program. The melting curve program was 95°C for 10 s, 60°C for 30 s, a ramp to 99°C at 0.20°C/s, and 40°C for 30 s. All qRT-PCR experiments included sample-matched –RT controls, a no-sample ddH$_2$O control, and a standard control containing 1 µl of product-specific cDNA of known concentration in copies/µl. Expression data were quantified by comparing the crossing points (i.e. the cycle number during PCR amplification at which the amount of product measured began to increase at a logarithmic rate) of each sample to a product-specific standard curve generated by plotting the

crossing points of known standards against their respective concentrations in copies/µl.

2.14 γ-Aminobutyric Acid (GABA) Assay

To qualify GABA levels in ST*Hdh*$^{Q7/Q7}$ cells culture media, a sandwich enzyme-linked immunosorbent assay (ELISA) was used. ELISA was conducted according to manufacturer's instructions (Novatein Biosciences, Boston, MA). In the GABA ELISA kit, the 96-well plate was pre-coated with a monoclonal antibody against Mouse GABA. In brief, ST*Hdh*$^{Q7/Q7}$ cells were plated in 96-well plate and cultured until reached 90% confluence. Cell culture medium was then replaced with 100 µl of serum free DMEM and cells were maintained for 24 hr prior to experiments to allow cell differentiation. Twenty-four hours later, 100 µl/well of serum-free DMEM was added to the wells with cells exposed to specific drug treatment. Cells were incubated at 33°C, 5% CO$_2$ for 30 min or

20 hr; then cell media was collected for analysis of GABA concentration. Next, 50 μl of the collected cell media was added to each sample wells. For controlled defined amounts of GABA (standards) wells, 50 μl of the pre-diluted standards were added to each of the standard wells. GABA standard concentrations ranged from 0.5 μM to 16 μM. 100 μl of the horseradish peroxidase (HRP)-conjugated antibody was added to each well and the plate was mixed well. The plate was incubated for 1 hr at 37°C. Wells were washed five times with 100 μl wash solution for 5 min each to remove all unbound components. The plate was inverted and blotted dry by tapping the plate on absorbent paper towels. Next, 50 μl of Chromogen Solution A and 50 μl Chromogen Solution B were added to each well, sequentially, containing the HRP enzyme substrate tetramethylbenzidine (TMB). The plate was protected from light and incubated for 15 minutes at 37°C to allow the enzyme (HRP) and TMB substrate to react. The enzyme-substrate reaction was terminated by addition of 50 μl of a sulphuric acid stop solution to each well and mixed well. The optical density (O.D.) was measured at 450 nm using SynergyHT fluorescent/luminescent plate reader (BioTek Instruments Inc., Winooski, VT). Background O.D. was collected using a cell-free well and subtracted from each standard and sample reading. For each experiment, a GABA standard curve was created and used to calculate GABA concentration in each sample.

2.15 In situ Proximity ligation Assay (PLA)

In situ proximity ligation assay (PLA) allows for the detection and quantification of protein-protein interactions in intact cells (Fredriksson *et al.,* 2002; Söderberg *et al.*, 2006). *In situ* PLA involves the use of two secondary antibodies attached to oligonucleotides (PLA probes) that can be joined by ligation only if the antibodies have been brought in close proximity by their respective binding to proteins to form protein-protein complexes. The DNA ligation products that form are then used as a template for *in situ* PCR amplification for protein detection (Fig. 2.5) (Fredriksson *et al.,* 2002; Söderberg *et al.*, 2006, 2008).

In situ PLA was used to study the interaction between endogenous CB_1 and D_{2L} receptors in ST*Hdh*$^{Q7/Q7}$ cells following ligand treatment. CB_1/D_{2L} molecular interactions were detected using the Duolink® In Situ Orange Starter Kit Mouse/Rabbit kit (Sigma-

Aldrich, ON). For *in situ* PLA experiments, ST*Hdh*$^{Q7/Q7}$ cells were cultured on glass coverslips (18 mm) on a 24-well plate for 24-48 hr until cells reached 50-60% confluency. Cells were then treated for 18 hr with vehicle or CB$_1$ and/or D$_2$ ligands. Eighteen hours later, the cell culture media was removed from each well, and cells were washed three times using 500 µl 1X PBS then fixed using 4% (w/v) PFA for 20 min at room temperature. After that, the cells were washed three times with 1X PBS and coverslips were transferred to a humidity chamber where background fluorescence was blocked using one drop of Duolink In Situ Blocking Solution (Sigma-Aldrich, ON) for 1 hr at 37°C. The blocking buffer was removed and cells were incubated with the primary rabbit N-terminal CB$_1$ antibody (1:500; Cayman Chemical Company) or the primary monoclonal rabbit N-terminal-D$_2$ antibody (1:200; Santa Cruz Biotechnology) diluted in Duolink *In Situ* Antibody Diluent (Sigma-Aldrich, ON) overnight at 4°C. The next day, the primary antibodies were removed and the coverslips were transferred to a 24-well plate. Cells were washed four times using 200 µl Duolink *In Situ* Wash Buffer A for 10 min each with gentle shaking. While the cells were being washed, the PLA probes, Duolink® *In Situ* PLA® Probe Anti-Rabbit PLUS and the Duolink® *In Situ* PLA® Probe Anti-Mouse MINUS, were diluted 1:5 in the in Duolink *In Situ* Antibody Diluent (Sigma-Aldrich, ON) and allowed to incubate for 20 min at room temperature. The coverslips were returned to the humidity chamber, and 30 µl of the diluted probe solution was added to each coverslip. The cells in the humidity chamber were incubated for 60 min at 37°C. Sixty minutes later, the PLA probes were removed, the coverslips were returned to the 24-well plate and cells were washed four times with Duolink *In Situ* Wash Buffer A for 10 min each while gently agitated. During the wash period, the ligation solution was prepared by diluting the 5X ligation stock (Sigma-Aldrich, ON) 1:5 in ddH$_2$O. Immediately before applying the ligation solution to the cells, the 1X ligase (1 U/µl; Sigma-Aldrich, ON) was added to the ligation mixture at a 1:40 dilution and the mixture was vortexed. The coverslips were returned to the humidity chamber and 30 µl of the ligation mixture was added to each coverslip. The coverslips were allowed to incubate for 60 min at 37 °C. After removing the ligation mixture, coverslips were placed in the 24-well plate and washed twice using Duolink In Situ Wash Buffer A for 2 min each while gently agitated. In a light protected area, the amplification solution was prepared by

diluting 5X Amplification Orange stock (Sigma-Aldrich, ON) 1:5 in ddH$_2$O. 1X

Figure 2.5: In situ Proximity Ligation Assay (PLA). **(A)** *In situ* PLA involves the use of two primary antibodies specific for two different GPCRs and two secondary antibodies conjugated to different oligonucleotides (PLA probes). When the two GPCRs are physically separated, the two PLA oligonucleotides cannot hybridize and undergo covalent ligation. As such no PLA signals were detected. **(B)** When the two GPCRs are in close proximity, the PLA probes will hybridize and ligate together forming a continuous circular DNA structures. The DNA-dependent polymerase will amplify these circular DNA structures through rolling circle amplification. The amplified circular DNA structures can be detected using a fluorescent label. The resulting distinct red spots (PLA signals) are indicative of protein-protein interaction and can be visualized using fluorescence microscopy. Figure 2.5 was modified from Söderberg *et al*., 2006.
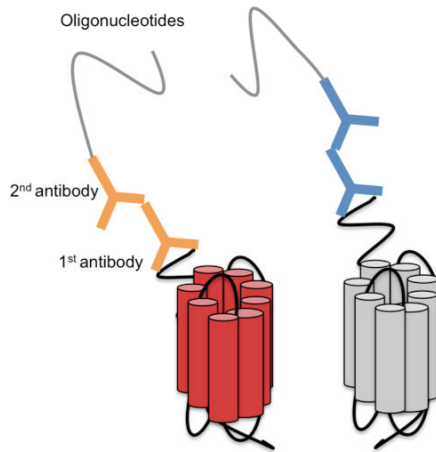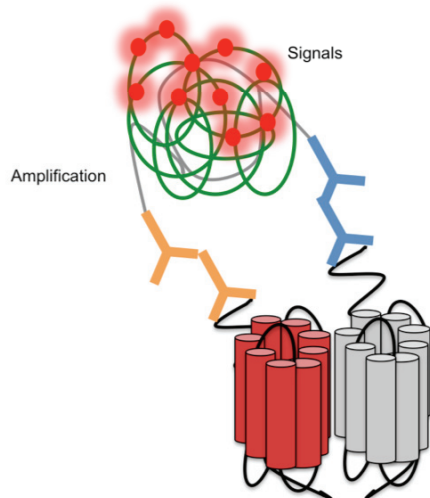
Polymerase (Sigma-Aldrich, ON) was then diluted in the amplification solution at a ratio of 1:80 and vortexed. The Amplification-Polymerase solution was added to the cells and incubated for 100 min at 37°C in the humidity chamber protected from light. Coverslips were placed in the 24-well plate and washed with 1X Wash Buffer B twice for 10 min each followed by a final wash with 0.01X Wash Buffer B for 1 min while gently agitated. Coverslips were allowed to air dry in the dark for 15 min before being mounted on slides using Duolink In Situ Mounting Medium with DAPI (Sigma-Aldrich, ON). Coverslips were edge sealed using clear nail polish and were allowed to air dry in the dark for another 15 min. Images were acquired using Zeiss Axiovert 200M-inverted fluorescence microscopes at 100X objectives and captured with the AxioVision 4.7 Multi Channel Fluorescence software. The following filter sets were used: Amplification Orange (546 nm excitation, 575-640 nm emission) and DAPI (365 nm excitation, 420 nm emission). Slides were stored at -20 in the dark. The same *in situ* PLA protocol was used to study the interaction between CB_1 and D_{2L} receptors in the *globus pallidus* of brain tissue slides from C57BL/6J mice *globus pallidus* following chronic ligand treatment.

High-resolution images were analyzed in ImageJ (NIH) to calculate the PLA signals (red spots) using a previously published protocol (Trifilieff *et al*., 2011). For all experiments, quantifications were performed from at least 9 images from 3 independent experiments per group. A threshold was selected manually to discriminate red PLA dots from background signals. Once selected, this threshold was applied uniformly to all images in the sample set. The built-in macro 'Analyze Particles' was then used to count and characterize all objects in an image. Objects larger than 5 μm^2, such as nuclei, were excluded from the count. The remaining objects were counted as PLA signals. The total number of cells in the field (blue nuclei) was counted manually and included ~ 10-20 cells per image analyzed. Finally, PLA signals (red spots) relative to cell number (nuclei) were calculated (dots/cell).

2.16 Animal Care and Handling

Six-week-old, male, wild-type (C57BL/6J) mice were purchased from Jackson Laboratory (Bar Harbor, ME). Animals were group housed (5 per cage) with *ad libitum*

access to food, water, and environmental enrichment and maintained on a 12 hr light/dark cycle. Mice were randomly assigned to receive volume-matched, daily intraperitoneal (i.p.) injection of vehicle (10% (v/v) DMSO, 0.1% (v/v) Tween-20 in saline) or 0.01 mg/kg CP 55,940, 0.3 mg/kg haloperidol, or 1.5 mg/kg olanzapine alone or in combination (n = 10 per group). Mice were weighed daily. All protocols were in accordance with the guidelines detailed by the Canadian Council on Animal Care (CCAC; Ottawa ON: Vol 1, 2nd Ed, 1993; Vol 2, 1984) and approved by the Carleton Animal Care Committee at Dalhousie University.

2.17 Open Field Test

An open field test was performed to assess locomotive activities in mice following drug administration according to previously published protocols (Seibenhener and Wooten 2015). Open field test measurements were performed 24 hr before the first drug injection and on day 1, 7, 14 and 21. The task was performed using an open-filed arena (60 cm width × 60 cm length × 20 cm height). The open-field arena was divided into a 6 × 6 grid of equally sized squares. The central region of the open-field arena was defined as the 4 squares in the middle of the box (i.e. 4 out of 36 squares), while the outer region of the open-field arena was defined as the sum of all the squares, excluding the 4 corner squares and the 4 center squares (i.e. 28 out of 36 squares). At the beginning of the test, each mouse was placed in the same quadrant in the outer section of the arena. The behavior of each mouse was recorded for 2 min using a digital video camera. At the end of each session, the mouse was removed from the open field arena, and the arena was thoroughly cleaned with 70% (v/v) ethanol. The video was scored afterward using The Ethovision® 5.0 software, a video tracking system that automatically records behavioural experiments (Noldus Information Technologie).

2.18 Brain Tissue Preparation

After completion of all drug treatments and behavioral analyses, brains were collected from mice the day after the last drug injection. Mice were deeply anesthetized by an i.p. injection of 100 mg/kg pentobarbital and then perfused intracardially with 1X PBS followed by ice-cold 4% (w/v) PFA solution. Mice brains were then collected and

fixed overnight in 4% (w/v) PFA solution. Next day, the brains were cryoprotected by placing them in 10% (w/v) sucrose (0.1 M PBS, pH 7.4) for several hours until the brain sank to the bottom of a 50 ml Falcon tube. The brains were transferred to 20% (w/v) sucrose for 1 day, then transferred to a 30% (w/v) sucrose solution for several days at 4°C. Brains were flash-frozen on dry ice for 1-2 min and stored at -80°C until use. Sections 20 μm thick were cut using a cryostat and mounted on Superfrost Plus microscopic slides (Fisher Scientific). The mounted brain sections on slides were stored at −20°C until use (Borroto-Escuela *et al*., 2016).

2.19 *Dual-Labeled Quantitative Fluorescence Immunohistochemistry (QF-IHC) Staining of Tissue Sections*

Dual-Labeled quantitative fluorescence immunohistochemistry (QF-IHC) staining was used to quantify CB_1 and D_2 protein levels in the in the *globus pallidus* of C57BL/6J mice following chronic ligand treatment. Tissue sections were exposed to IR-labeled antibodies and scanned using infrared-based tissue imaging, which allows for determination of relative protein levels in defined areas (Kearn, 2004; Eaton *et al.,* 2016). PFA-fixed frozen sections mounted on slides were taken out of storage at -80°C, equilibrated to room temperature, then rehydrated in 1X PBS for 10 min. The tissues were blocked using Odyssey Blocking Buffer (Li-Cor Biotechnology) containing 0.1% (v/v) Tween-20 for 90 min at room temperature. The primary monoclonal rabbit N-terminal CB_1 antibody (1:500; Cayman Chemical Company) and the primary monoclonal mouse N-terminal-D_2 antibody (1:200; Santa Cruz Biotechnology) were diluted in Odyssey Blocking Buffer containing 0.1% (v/v) Tween-20. Tissues were incubated with primary antibodies overnight at 4°C. The next day, slides were washed four times in 1X PBS containing 0.1% (v/v) Tween-20 each for 30 min. The tissues were then incubated for 2 hr with the IR800CW-conjugated anti-rabbit IgG secondary antibody (Rockland Immunochemical) and Alexa Fluor 680 conjugated anti-mouse secondary antibody (Invitrogen) diluted 1:10,000 in 20% (v/v) Odyssey Blocking Buffer in 1X PBS and containing 0.1% (v/v) Tween-20. During antibody exposure sections were protected from light. Slides were washed four times for 30 min in 1X PBS containing 0.1% (v/v) Tween-20 and allowed to air-dry overnight in the dark. Slides were scanned using the Odyssey

infrared imaging system (Li-Cor Biotechnology) with the resolution set at 21 μm, quality set at 'highest', focus offset set at 0 mm and the intensity set at 2.0 for both the 700 nm and 800 nm channel. Image quantification of the *globus pallidus* was carried out using ImageJ (NIH) software.

2.20 Statistical Analyses and Curve Fitting

Data are presented as the Mean ± standard error mean (SEM) or 95% confidence interval, as indicated. Statistical analysis and curve fitting of the data were performed using GraphPad version 6.0. Concentration-response curves were fit to non-linear regression model with variable slope (four parameters). Hill coefficients were calculated from the slope of curves and represent the cooperativity of oligomeric allosteric proteins (Edelstein and Le Novère, 2013). If the Hill coefficient is larger than 1, it is a positive cooperativity, whereas the Hill coefficient smaller than 1 indicates negative cooperatively. Statistical analyses were conducted by one-way analysis of variance (ANOVA), as indicated. *Post-hoc* analyses were performed using Tukey's honest significance test. The level of significance was set to $P < 0.05$.

CHAPTER 3

ANTAGONISM OF DOPAMINE RECEPTOR 2 LONG (D$_{2L}$) AFFECTS CANNABINOID RECEPTOR 1 (CB$_1$) SIGNALING IN A CELL CULTURE MODEL OF STRIATAL MEDIUM SPINY PROJECTION NEURONS

Copyright Statement

Contribution Statement

The manuscript used as the basis for this chapter was written with guidance from Dr. Eileen Denovan-Wright. Data were collected and analyzed by myself. Critical reagents were provided by Drs. Eileen Denovan-Wright and Melanie Kelly.

3.1 Abstract

Activation of dopamine receptor 2 long (D_{2L}) switches the signaling of type 1 cannabinoid receptor (CB_1) from $G\alpha_i$ to $G\alpha_s$, a process which is thought to be mediated through CB_1/D_{2L} heteromerization. Given the clinical importance of D_2 antagonists, the goal of this study was to determine if D_2 antagonists could modulate CB_1 signaling. Interactions between CB_1 and D_{2L}, $G\alpha_i$, $G\alpha_s$, and β-arrestin1, were studied using $BRET^2$ in ST$Hdh^{Q7/Q7}$ cells. CB_1-dependent ERK1/2, CREB phosphorylation and CB_1 internalization following co-treatment of CB_1 agonist and D_2 antagonist were quantified. Pre-assembled CB_1-$G\alpha_i$ complexes were detected by $BRET^2$. Arachidonyl-2'-chloroethylamide (ACEA), a selective CB_1 agonist, caused a rapid and transient increase in $BRET_{Eff}$ between $G\alpha_i$-Rluc and CB_1-GFP^2, and a $G\alpha_i$-dependent increase in ERK phosphorylation. Physical interactions between CB_1 and D_{2L} were observed using $BRET^2$. Co-treatment of ST$Hdh^{Q7/Q7}$ cells with ACEA and haloperidol, a D_2 antagonist, inhibited $BRET_{Eff}$ signals between $G\alpha_i$-Rluc and CB_1-GFP^2 and reduced the E_{Max} and pEC_{50} of ACEA-mediated $G\alpha_i$-dependent ERK phosphorylation. ACEA and haloperidol co-treatments produced a delayed and sustained increase in $BRET_{Eff}$ between $G\alpha_s$-Rluc and CB_1-GFP^2 and increased the E_{Max} and pEC_{50} of ACEA-induced $G\alpha_s$-dependent CREB phosphorylation. In cells expressing CB_1 and D_{2L} treated with ACEA, binding of haloperidol to D_2 receptors switched CB_1 coupling from $G\alpha_i$ to $G\alpha_s$. In addition, haloperidol treatment reduced ACEA-induced β-arrestin1 recruitment to CB_1 and CB_1 internalization. D_2 antagonists allosterically modulate cannabinoid-induced CB_1 coupling, signaling and β-arrestin1 recruitment through binding to CB_1/D_{2L} heteromers. These findings indicate that D_2 antagonism, like D_2 agonists, change agonist-mediated CB_1 coupling and signaling.

3.2 Introduction

The type 1 cannabinoid receptor (CB_1) is highly expressed in the central nervous system where it regulates neuromodulatory processes (Matsuda *et al*., 1990; Howlett *et al*., 2004; Bosier *et al*., 2010). The CB_1 is activated by endogenous lipid mediators, such as anandamide (AEA) and 2-arachidonoylglycerol (2-AG), and exogenous cannabinoids such as Δ^9-tetrahydrocannabinol (THC) (Mechoulam *et al*., 1995). CB_1 receptors signal

primarily through *Pertussis* toxin (PTx)-sensitive $G\alpha_{i/o}$ proteins (Demuth and Molleman, 2006). In addition, it has been demonstrated that different CB_1 agonists can promote CB_1 signaling through $G\alpha_s$, $G\alpha_{q/11}$, and β-arrestin1 (Maneuf and Brotchie, 1997; Lauckner *et al.*, 2005; Laprairie *et al.*, 2014).

CB_1 receptors can self-associate to form homomers and can also associate with other class-A GPCRs to form heteromers (Hudson *et al.*, 2010). Specifically, CB_1 is known to heteromerize with the dopamine receptor type 2 long (D_{2L}), the δ-, κ- and δ-opioid receptors, the orexin-1 receptor, the A_{2A} receptor, and $β_2AR$ (Wager-Miller *et al.,* 2002; Kearn *et al.,* 2005; Mackie, 2005; Ellis *et al.,* 2006; Rios *et al.*, 2006; Carriba *et al.,* 2007; Hudson *et al.,* 2010b). Heteromerization of CB_1 with the D_{2L} has received significant attention due to the fact that both receptors are co-localized in the GABA-ergic medium spiny neurons projecting from the striatum to the globus pallidus, as well as on the axon terminals at the globus pallidus (Hermann *et al.*, 2002; Pickel *et al.,* 2006). Medium spiny neurons play important roles in the coordination of movement, emotions and, cognition (Gerfen, 1992; Graybiel, 2005).

Co-localization of CB_1 and D_{2L} in the basal ganglia may allow for bidirectional functional interaction between the two receptors (reviewed in Fernández-Ruiz *et al.*, 2010). Activation of CB_1 leads to an increase in dopamine release in the nucleus accumbens (Tanda *et al.*, 1997; Solinas *et al.*, 2006). In addition, D_{2L} activation has been shown to increase endocannabinoid release in the dorsal striatum (Giuffrida *et al.,* 1999; Pan *et al.,* 2008). *In vitro* functional interactions between CB_1 and D_{2L} were first observed in striatal neurons by Glass and Felder (1997). Co-stimulation of both these receptors by their respective agonists in striatal neurons leads to an accumulation of cAMP, while stimulation of either receptor alone leads to an inhibition of cAMP (Glass and Felder, 1997). These authors hypothesized that this response was the result of a change in the coupling of CB_1 from $G\alpha_i$ to $G\alpha_s$ when the two receptors were co-activated by agonists (Glass and Felder, 1997). Subsequent work demonstrated that D_2 agonists altered CB_1-dependent signaling, CB_1 localization and receptor expression (Jarrahian *et al.,* 2004; Kearn *et al.*, 2005; Marcellino *et al.,* 2008; Przybyla and Watts, 2010; Khan and Lee, 2014). Functional interactions between CB_1 and D_{2L} receptors have been attributed to heteromerization between the two receptors as demonstrated using co-

immunoprecipitation, fluorescence resonance energy transfer (FRET), and bimolecular fluorescence complementation (BiFC) (Kearn *et al.,* 2005, Marcellino *et al.,* 2008, Przybyla and Watts, 2010). Suggesting allosteric interactions between CB_1 and D_{2L} receptors heteromers.

Allosteric ligands modulate orthosteric ligand binding by binding to a distinct allosteric receptor site. In doing so, allosteric modulators can change the potency and efficacy of the orthosteric ligands. In the context of GPCR heteromer, allosteric modulations can be envisioned between the protomers of the heteromer. Each protomer possesses an orthosteric-binding pocket (Kenakin, 2010). Binding of orthosteric ligand to one protomer of the receptor complex may exert allosteric effects on the response of the other protomer to ligand binding. Such allosteric modulation may result in positive or negative cooperatively across the heteromer pair (Kenakin, 2010; Wootten *et al*., 2013). A well-known example of allosteric interactions between GPCR heteromers is within the D_2 /A_{2A} receptor heteromer complex (reviewed in Ferré, 2015).

The purpose of the current study was to examine if the high-affinity D_2 antagonist haloperidol can allosterically modulate CB_1 pharmacology within the CB_1/D_{2L} heteromers. D_2 antagonists are widely used as antipsychotics and for the management of movement disorders. We measured the effects of the D_2 antagonist haloperidol on the coupling of CB_1 to $G\alpha_i$, $G\alpha_s$, and β-arrestin1 in the presence of the cannabinoid agonist arachidonyl-2'-chloroethylamide (ACEA). ACEA is a stable synthetic analogue of the endocannabinoid anandamide (Howlett *et al.,* 2004; Bosier *et al*., 2010). Bioluminescence resonance energy transfer 2 ($BRET^2$) was used in this study to monitor the coupling between CB_1 to $G\alpha_i$, $G\alpha_s$, and β-arrestin1 in STH$dh^{Q7/Q7}$ cells, a model of striatal medium spiny projection neurons. These cells endogenously express both CB_1 and D_{2L} receptors (Trettel *et al*., 2000; Laprairie *et al*., 2013, 2014).

3.3 Results

3.3.1 CB_1 and D_{2L} Receptors Form Heteromers in STHdh$^{Q7/Q7}$ Cells

STH$dh^{Q7/Q7}$ cells endogenously express CB_1 and D_2 receptors and other proteins associated with signaling *via* these receptors (Trettel *et al*., 2000; Lee *et al*., 2007; Laprairie *et al*., 2013). We confirmed *via* PCR, qRT-PCR, In-cell western™ and

immunofluorescence that ST*Hdh*$^{Q7/Q7}$ cells express CB$_1$ and D$_2$ receptors (Supplementary Fig. 3.1). Our immunocytochemistry experiments show co-localization of CB$_1$ and D$_2$ in ST*Hdh*$^{Q7/Q7}$ cells. CB$_1$ immunofluorescence was not confined to the plasma membrane, but those intracellular reactions were also seen, as previously reported (Leterrier *et al.,* 2006; McDonald *et al.*, 2007; Scavone *et al.,* 2010). Using PCR primers that span the alternatively spliced exon that distinguished the D$_2$ long (D$_{2L}$) and D$_2$ short (D$_{2S}$) isoforms (Coronas *et al.,* 1997), we found that ST*Hdh*$^{Q7/Q7}$ cells only express the D$_{2L}$ isoform (data not shown). The D$_{2L}$ isoform was cloned and used for all BRET^2 analyses.

BRET^2 was used to determine whether CB$_1$ and D$_{2L}$ receptors heteromerize when expressed in ST*Hdh*$^{Q7/Q7}$ cells. Cells were co-transfected with CB$_1$-Rluc and D$_{2L}$-GFP^2 constructs. Negative control included the human *ether-a-go-go*-related gene (HERG), HERG-GFP^2, which is a membrane-localized K$^+$ channel that does not interact with GPCRs or G-proteins (Hudson *et al.*, 2010b). The combination of CB$_1$-Rluc and D$_{2L}$-GFP^2 resulted in greater BRET$_{Eff}$ compared to negative controls obtained from cells expressing CB$_1$-Rluc and HERG-GFP^2 (Fig. 3.1A), indicating that CB$_1$ and D$_{2L}$ form heteromers when co-expressed in ST*Hdh*$^{Q7/Q7}$ cells. The interaction between CB$_1$ and D$_{2L}$ is mediated by the C-terminus of CB$_1$ and the third intracellular loop of D$_{2L}$ (Khan and Lee, 2014). To disrupt the formation of CB$_1$ and D$_{2L}$ complexes, a CB$_1$ blocking peptide (CB$_1$-BP) that binds to the CB$_1$ receptor C-terminal region (C417-S431) was cloned (Khan and Lee, 2014). The CB$_1$-BP inhibits the heteromerization of CB$_1$ and D$_{2L}$ by competing with CB$_1$ for binding with D$_{2L}$ (Khan and Lee*,* 2014). The co-expression of CB$_1$-Rluc and D$_{2L}$-GFP^2 together with the CB$_1$-BP reduced BRET$_{Eff}$ relative to cells transfected with CB$_1$-Rluc and D$_{2L}$-GFP^2 (Fig. 3.1A). CB$_1$-BP did not alter BRET$_{Eff}$ in cells expressing CB$_1$-Rluc and CB$_1$-GFP^2 (Fig. 3.1A). These differences in BRET^2 signals were not due to the difference in the expression level of BRET^2 partners quantified by luminescence and fluorescence measurements (Supplementary Fig. 3.2). These data indicate that CB$_1$-BP blocks the formation of CB$_1$/D$_{2L}$ heteromers, but not CB$_1$ homomers, suggesting that the protein regions crucial for CB$_1$ homomerization are different than those involved in CB$_1$/D$_{2L}$ heteromerization.

Figure 3.1: CB₁ and D₂ₗ Receptors Formed Heteromers When Expressed in STHdh^{Q7/Q7}
Cells Demonstrated Using BRET². **(A)** $BRET_{Eff}$ was measured in cells expressing CB_1-Rluc
and D_{2L}-GFP^2, or CB_1-GFP^2 constructs and the CB_1-BP or pcDNA vector. As a negative
control, cells were co-transfected with CB_1-Rluc and HERG-GFP^2. * $P < 0.01$ compared
to cells expressing CB_1-Rluc and HERG-GFP^2, ~ $P < 0.01$ compared to cells expressing
CB_1-Rluc, D_{2L}-GFP^2, and pcDNA. **(B)** $BRET^2$ saturation curves of cells transiently
transfected with a constant amount of CB_1-Rluc and an increasing amount of D_{2L}-GFP^2. * P
< 0.01 compared to cells expressing CB_1-Rluc and HERG-GFP^2. **(C)** $BRET_{Max}$ and $BRET_{50}$
parameters derived from $BRET^2$ saturation curves of cells transiently transfected with a
constant amount of CB_1-Rluc and an increasing amount of D_{2L}-GFP^2 and treated for 30 min
with the vehicle, 1 μM ACEA, 10 μM haloperidol (HALO) alone or treated with ACEA. * P
< 0.01 compared to cells treated with vehicle. Data are presented as mean ± SEM of 4
independent experiments. Significance was determined *via* one-way ANOVA followed
by Tukey's *post-hoc* test.

A

B

- ● CB$_1$-Rluc + D$_{2L}$-GFP^2
- ○ CB$_1$-Rluc + HERG-GFP^2
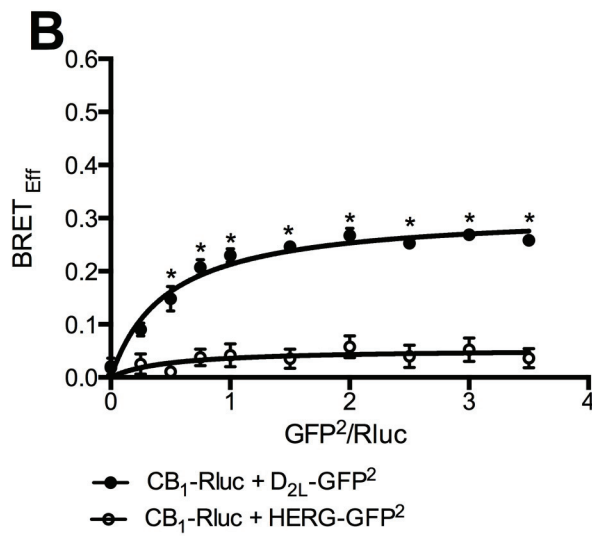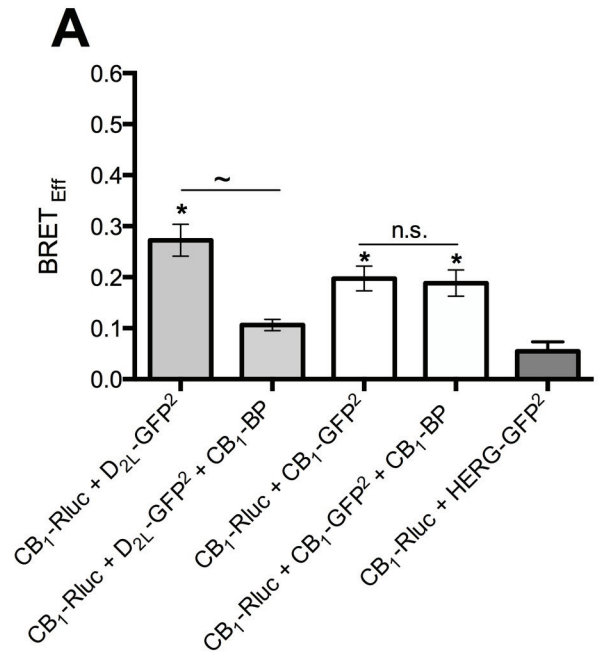
C

Ligand	BRET$_{Max}$	BTRET$_{50}$
Vehicle	0.28 ± 0.01	0.41 ± 0.03
1 µM ACEA	0.35 ± 0.01*	0.43 ± 0.03
10 µM HALO	0.25 ± 0.01	0.41 ± 0.02
1 µM ACEA + 10 µM HALO	0.33 ± 0.01*	0.37 ± 0.05

82

A BRET^2 saturation curve was generated to demonstrate the ability of CB_1 and D_{2L} receptors to form heteromers at constant donor expression levels and increasing acceptor expression levels. For the BRET^2 saturation curve, cells were co-transfected with a constant amount of CB_1-Rluc with increasing amounts of D_{2L}-GFP^2 or HERG-GFP^2 (Fig. 3.1B). The combination of CB_1-Rluc with D_2-GFP^2 resulted in a significantly different saturation curve than the control curve, which was generated with the co-expression of CB_1-Rluc with HERG-GFP^2 (Fig. 3.1B). The BRET^2 saturation curve resulted in a $BRET_{Max}$ of 0.28 ± 0.01 and a $BRET_{50}$ of 0.41 ± 0.03. Treating cells co-expressing CB_1-Rluc and D_{2L}-GFP^2 for 30 min with 1 μM ACEA +/- 10 μM haloperidol resulted in higher $BRET_{Max}$, but not $BRET_{50}$, compared to the $BRET_{Max}$ observed in vehicle-treated cells. Haloperidol treatment alone did not alter $BRET_{Max}$ or $BRET_{50}$ compared to vehicle-treated cells (Fig. 3.1C). The change in $BRET_{Max}$, but not $BRET_{50}$, following treatment with cannabinoid alone or in combination with the D_2 antagonist, suggests that ligand binding stabilized the conformation of this heteromer, which enhanced the energy transfer between CB_1 and D_{2L} without increasing the number of receptors involved in heteromerization.

3.3.2 D_2 Antagonism Can Allosterically Inhibit The Association of CB_1 Receptor and $G\alpha_i$ Protein

Different CB_1 agonists can activate different G proteins including $G\alpha_i$ and $G\alpha_s$ proteins (Bosier *et al.,* 2010; Laprairie*, et al.,* 2014). To study coupling of CB_1 to $G\alpha_i$ and $G\alpha_s$ proteins, we used BRET^2 for real-time assessment of receptor-G protein interaction in living STH*dh*$^{Q7/Q7}$ cells transiently transfected with G-protein-Rluc and CB_1-GFP^2. Our first aim was to investigate the coupling of CB_1 to $G\alpha_i$ protein in the absence of agonist. STH*dh*$^{Q7/Q7}$ cells were transiently transfected with $G\alpha_i$-Rluc and CB_1-GFP^2. Co-expression of $G\alpha_i$-Rluc and CB_1-GFP^2 resulted in $BRET_{Eff}$ equal to 0.23 ± 0.08, which was higher than cells expressing $G\alpha_i$-Rluc and HERG-GFP^2 (Fig. 3.2A). We found basal $BRET_{Eff}$ was insensitive to 24 h PTx treatment (Fig. 3.2A). Chronic PTx treatment inactivates $G\alpha_i$ protein. This finding confirms that CB_1 receptors are pre-assembled with $G\alpha_i$ prior to the addition of exogenous ligand and does not result from constitutive activation of $G\alpha_i$ (Ayoub *et al*., 2007). Next, the influence of CB_1 agonist treatment on CB_1-$G\alpha_i$ coupling

was tested. Treating cells with 1 μM ACEA resulted in an increase in $BRET_{Eff}$ (Fig. 3.2A). Inactivating $G\alpha_i$ with PTx suppressed ACEA-induced $BRET_{Eff}$ to the basal level (Fig 2A). The agonist-induced $BRET_{Eff}$ increase clearly demonstrates a functional coupling of CB_1 and $G\alpha_i$ protein.

We measured the effect of D_2 antagonism on CB_1 agonist-induced CB_1- and $G\alpha_i$-dependent $BRET_{Eff}$ in cells co-transfected with $G\alpha_i$-Rluc and CB_1-GFP^2 and un-tagged D_{2L}-pcDNA. An ACEA concentration-response curve was generated. Increasing ACEA concentration resulted in an increase in $BRET_{Eff}$ between $G\alpha_i$ and CB_1 (EC_{50} = 0.22 (0.19 - 0.28), E_{Max} = 0.45 (0.41-0.48), Hill coefficient= 1.15 (0.91-1.4) (Fig. 3.2B). Treating the cells with different concentrations of haloperidol alone did not alter $BRET_{Eff}$ between $G\alpha_i$ and CB_1 (data not shown). However, pre-treating the cells with haloperidol 25 s prior the addition of ACEA reduced ACEA-induced $BRET_{Eff}$ signal between $G\alpha_i$ and CB_1 in a haloperidol concentration-dependent manner (Fig. 3.2B). Haloperidol produced a concentration-dependent rightward and downward shift in the ACEA concentration-response curves. Both the efficacy and the potency of ACEA dependent $G\alpha_i$-CB_1 interaction were diminished by D_2 antagonism. The rightward shift in EC_{50} for ACEA concentration-response curves was significant at 0.1, 1 and 10 μM haloperidol for ACEA-treated cells (Table 3.1). The decrease in E_{max} was significant at all concentrations of haloperidol tested (Table 3.1). The Hill coefficient was significantly less than 1 at 0.1, 1 and 10 μM haloperidol for ACEA-concentration-response curves (Table 3.1). The observed effects of haloperidol on ACEA-dependent $G\alpha_i$-CB_1 interaction indicate the presence of negative cooperatively; the Hill coefficient is less than one.

To confirm that the observed allosteric effect of haloperidol was mediated through CB_1/D_{2L} heteromers and not mediated through the direct effect of haloperidol on the CB_1 receptor, cells were co-transfected with $G\alpha_i$-Rluc and CB_1-GFP^2 and treated with 10 μM haloperidol prior to 1 μM ACEA application. No change in $BRET_{Eff}$ between $G\alpha_i$-Rluc and CB_1-GFP^2 was observed (Fig. 3.2C). These data demonstrate that CB_1/D_{2L} heteromerization was required for effect of haloperidol, as haloperidol had no effect on CB_1-$G\alpha_i$ interactions in the absence of D_{2L} (Fig. 3.2C). In addition, the expression of equimolar D_{2L}-pcDNA and CB_1-GFP^2 in the presence of excess pool of $G\alpha_i$-Rluc did not alter CB_1 coupling to $G\alpha_i$-Rluc protein in the presence of vehicle or ACEA, compared to

Figure 3.2: Haloperidol Treatment Inhibited Interactions Between CB$_1$ and Gα_i in The Presence of ACEA in STHdh$^{Q7/Q7}$ Cells. (A) BRET$_{Eff}$ was measured at 2 min following the addition of vehicle or 1 μM ACEA +/- 24 h pre-treatment with 50 ng/ml PTx in cells expressing Gα_i-Rluc and CB$_1$-GFP^2. * $P < 0.01$ relative to cells expressing Gα_i-Rluc and HERG-GFP^2; ~ $P < 0.01$ compared to cells expressing Gα_i-Rluc and CB$_1$-GFP^2 treated with PTx for 24 hr. **(B)** Concentration-response curves of ACEA- induced BRET$_{Eff}$ between Gα_i-Rluc and CB$_1$-GFP^2 in the absence or presence of HALO measured at 2 min following ACEA application. **(C)** BRET$_{Eff}$ was measured at 2 min following the addition of vehicle, 10 μM HALO, 1 μM ACEA +/- with 10 μM HALO and pre-treated for 30 min with 0.5 μM O-2050 in cells expressing Gα_i-Rluc and CB$_1$-GFP^2 +/- D$_{2L}$-pcDNA. *n.s.* $P > 0.05$ compared with cells expressing Gα_i-Rluc and CB$_1$-GFP^2 only; ~ $P < 0.01$ relative to cells expressing Gα_i-Rluc and CB$_1$-GFP^2 and treated with 1 μM ACEA and 10 μM HALO; * $P < 0.01$ compared to cells treated with vehicle. **(D)** Cells were transfected with Gα_i-Rluc, CB$_1$-GFP^2, D$_2$-pcDNA, and CB$_1$-BP or pcDNA, and BRET$_{Eff}$ was measured at 2 min following the addition of vehicle, 10 μM HALO, 1 μM ACEA +/- 10 μM HALO. * $P < 0.01$ relative to cells expressing Gα_i-Rluc, CB$_1$-GFP^2 and CB$_1$-BP and treated with 1 μM ACEA and 10 μM HALO. **(E)** BRET^2 saturation curves were generated by co-transfecting constant amounts of Gα_i-Rluc and increasing amounts of CB$_1$-GFP^2 alone or with D$_{2L}$-pcDNA or HERG GFP^2, and BRET$_{Eff}$ was measured following the addition of vehicle, 1 μM ACEA alone or in combination with 10 μM HALO. * $P < 0.01$ compared with cells expressing Gα_i-Rluc and HERG-GFP^2. **(F)** BRET$_{Eff}$ was measured over 9 min (540 s) in cells expressing Gα_i-Rluc and CB$_1$-GFP^2 alone or together with D$_{2L}$-pcDNA and treated with vehicle, 1 μM ACEA +/- 10 μM HALO. As a negative control, cells were co-transfected with Gα_i-Rluc and HERG-GFP^2. * $P < 0.01$ compared to cells expressing Gα_i-Rluc and CB$_1$-GFP^2 and treated with vehicle; ~ $P < 0.01$ compared to cells expressing Gα_i-Rluc and CB$_1$-GFP^2 and treated with 1 μM ACEA. Data are presented as mean ± SEM of 4 independent experiments; significance was determined via one-way ANOVA followed by Tukey's *post-hoc* test.

A

Vehicle	+	+	+	-	-
1 μM ACEA	-	-	-	+	+
50 ng/mL PTx	-	-	+	-	+

☐ Gαi -Rluc + CB₁-GFP²
■ Gαi -Rluc + HERG-GFP²

B

[HALO] μM
- ▲ 0.00
- ▲ 0.01
- ▲ 0.10
- ▲ 1.00
- ▲ 10.0

C

Vehicle	+	+	-	-	-	-	-	-	-	-
1 μM ACEA	-	-	+	+	-	-	+	+	+	+
10 μM HALO	-	-	-	-	+	+	+	+	+	+
0.5 μM O-2050	-	-	-	-	-	-	-	-	+	+

☐ Gαi -Rluc + CB₁-GFP²
■ Gαi -Rluc + CB₁-GFP² + D₂L-pcDNA

D

Vehicle	+	+	-	-	-	-
1 μM ACEA	-	-	+	+	+	+
10 μM HALO	-	-	-	-	+	+

☐ Gαi -Rluc + CB₁-GFP² + D₂L-pcDNA
■ Gαi -Rluc + CB₁-GFP² + D₂L-pcDNA + CB₁-BP

E

- ● Gαi -Rluc + CB₁-GFP²
- △ Gαi -Rluc + CB₁-GFP² + 1 μM ACEA
- ▲ Gαi -Rluc + CB₁-GFP² + D₂L-pcDNA + 10 μM HALO + 1 μM ACEA
- ○ Gαi -Rluc + HERG-GFP²

F

- ● Gαi -Rluc + CB₁-GFP²
- △ Gαi -Rluc + CB₁-GFP² + 1 μM ACEA
- ▲ Gαi -Rluc + CB₁-GFP² + D₂L-pcDNA + 10 μM HALO + 1 μM ACEA
- ○ Gαi -Rluc + HERG-GFP²

86
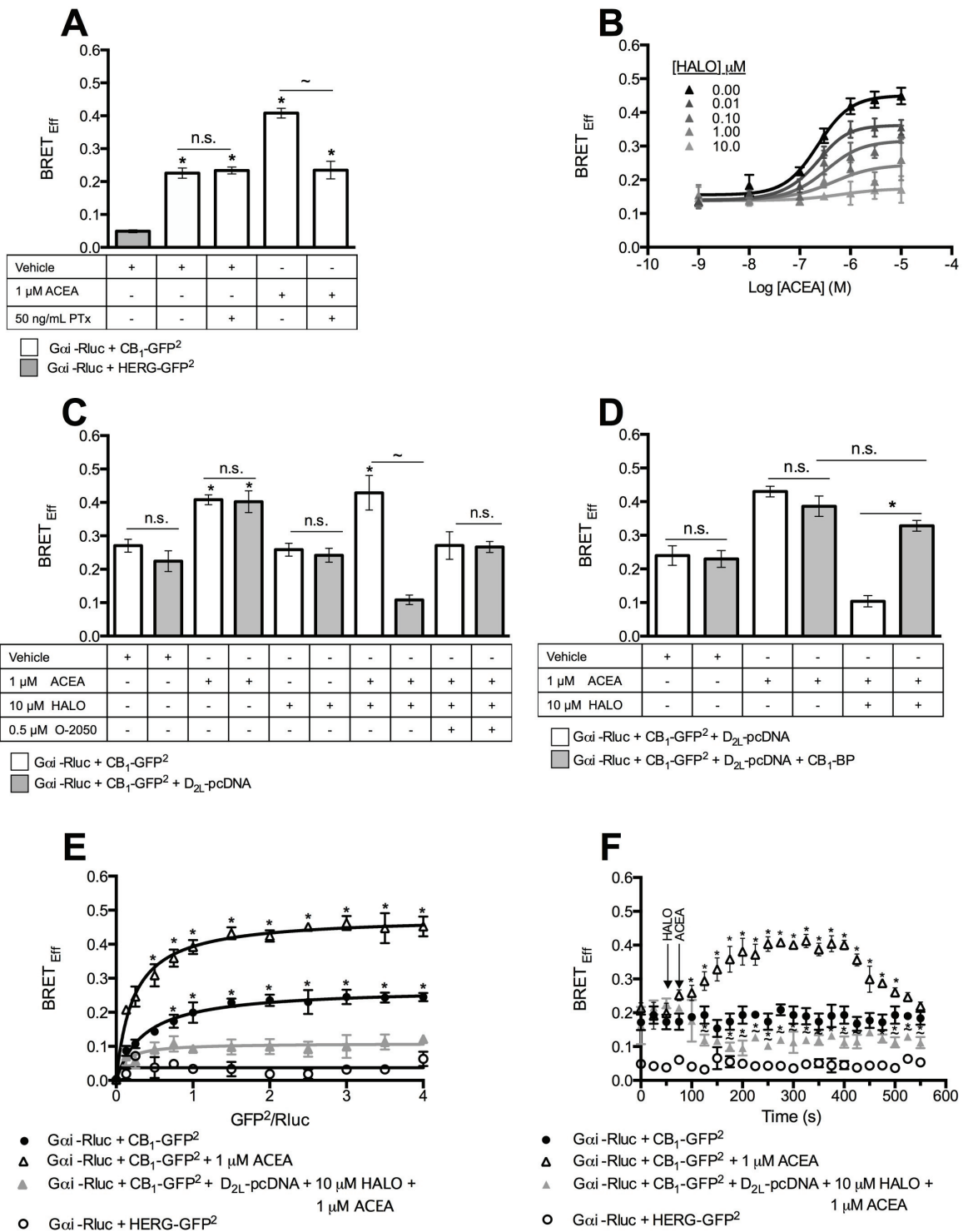
Table 3.1: The Effects of Haloperidol on BRET^2 (Gα_i- Rluc + CB$_1$-GFP^2), Gα_i - Dependent ERK Phosphorylation, BRET^2 (Gα_s- Rluc + CB$_1$-GFP^2), Gα_s-Dependent CREB Phosphorylation and BRET^2 (β-arrestin1-Rluc + CB$_1$-GFP^2). Determined using nonlinear regression with variable slope (four parameters) in GraphPad (version 6.0). Data are presented as the mean and 95% confidence interval (CI) from four independent experiments. N.C. not converged. *$P < 0.01$, compared with ACEA-treated cells; one-way ANOVA with Tukey's Post-hoc test.

Agonist	HALO (μM)	EC_{50} μM (95% CI)	E_{Max} (95% CI)	Hill coefficient (95% CI)
BRET^2 (Gα_i- Rluc + CB$_1$- GFP^2)				
ACEA	0	0.22 (0.19 -0.28)	0.45 (0.41-0.48)	1.15 (0.91-1.40)
	0.01	0.25 (0.21-0.32)	0.36 (0.33-0.38)*	0.90 (0.86-0.94)
	0.1	0.38 (0.32-0.43)*	0.33 (0.26-0.39)*	0.82 (0.76-0.89)*
	1	0.68 (0.33-0.92)*	0.23 (0.21-0.25)*	0.71 (0.67-0.75)*
	10	0.98 (0.94-1.41)*	0.17 (0.14-0.20)*	0.57 (0.60-0.54)*
Gα_i-dependent ERK phosphorylation				
ACEA	0	0.27 (0.25-0.29)	0.76 (0.71-0.80)	1.11 (0.89-1.23)
	0.01	0.31 (0.26-0.36)	0.69 (0.64-0.75)	0.93 (0.84-1.03)
	0.1	0.41 (0.37-0.45)*	0.52 (0.48-0.57)*	0.84 (0.78-0.89)
	1	0.72 (0.67-0.78)*	0.39 (0.37-0.42)*	0.79 (0.69-0.79)*
	10	1.01 (0.82-1.21)*	0.32 (0.29-0.34)*	0.74 (0.67-0.81)*
BRET^2 (Gα_s-Rluc + CB$_1$- GFP^2)				
ACEA	0	N.C.	N.C.	N.C.
	0.01	0.49 (0.36-0.62)*	0.18 (0.16-0.19)*	1.12 (0.92-1.32)*
	0.1	0.35 (0.29-0.42)*	0.26 (0.24-0.27)*	1.28 (1.21-1.36)*
	1	0.29 (0.24-0.35)*	0.31 (0.28-0.33)*	1.43 (1.36-1.51)*
	10	0.23 (0.18-0.31)*	0.36 (0.32-0.40)*	1.53 (1.43-1.63)*
Gα_s-dependent CREB phosphorylation				
ACEA	0	0.35 (0.31-0.40)	0.26 (0.23-0.28)	1.02 (0.90-1.14)
	0.01	0.31 (0.29-0.35)	0.42 (0.40-0.45)*	1.11 (0.98-1.31)
	0.1	0.29 (0.23-0.48)*	0.56 (0.53-0.59)*	1.26 (1.10-1.42)*
	1	0.23 (0.19-0.27)*	0.65 (0.62-0.68)*	1.56 (1.17-1.86)*
	10	0.21 (0.17-0.25)*	0.70 (0.67-0.74)*	1.67 (1.42-1.91)*
BRET^2 (β-arrestin1-Rluc + CB$_1$- GFP^2)				
ACEA	0	0.25 (0.19-0.35)	0.56 (0.52-0.60)	1.21 (0.11-1.23)
	0.01	0.27 (0.21-0.37)	0.53 (0.49-0.56)	1.12 (0.98-1.10)
	0.1	0.33 (0.28-0.51)*	0.48 (0.45-0.52)	1.01 (0.95-1.21)
	1	0.36 (0.29-0.44)*	0.38 (0.36-0.41)*	1.12 (0.90-1.12)
	10	0.45 (0.34-0.57)*	0.32 (0.29-0.34)*	1.04 (0.85-1.11)

cells expressing CB_1-GFP^2 and $G\alpha_i$-Rluc alone (Fig. 3.2C). The co-application of the CB_1 orthosteric antagonist, O-2050, prior to the application of ACEA and haloperidol, returned $BRET_{Eff}$ to basal levels, which confirms that the observed increase in $BRET_{Eff}$ between CB_1 and $G\alpha_i$ is due to the binding of ACEA to the orthosteric site of the CB_1 (Fig. 3.2C). Therefore, expression of D_{2L} receptors did not alter CB_1 coupling to $G\alpha_i$, but co-treatment of cells with haloperidol and ACEA resulted in reduced $BRET_{Eff}$ signals between $G\alpha_i$ and CB_1.

Next, we confirmed that the inhibition of $BRET_{Eff}$ between $G\alpha_i$ and CB_1 following haloperidol and ACEA application was mediated through the binding of haloperidol to CB_1/D_{2L} complexes. To confirm this we blocked the heteromerization between CB_1 and D_{2L} receptors by the co-expression of CB_1-BP. Cells co-transfected with $G\alpha_i$-Rluc, CB_1-GFP^2, D_{2L}-pcDNA and CB_1-BP treated with ACEA and haloperidol had higher $BRET_{Eff}$ compared to cells transfected with $G\alpha_i$-Rluc, CB_1-GFP^2, D_{2L}-pcDNA, and no CB_1-BP (Fig. 3.2D). Thus, haloperidol inhibited ACEA-enhanced CB_1-$G\alpha_i$ induced $BRET^2$ through binding to CB_1/D_{2L} complexes.

$BRET^2$ saturation curves were generated between $G\alpha_i$-Rluc and CB_1-GFP^2 in the presence and absence of ACEA to validate the specificity of the interaction between $G\alpha_i$ and CB_1 (Fig. 3.2E). Cells were co-transfected with constant amounts of $G\alpha_i$-Rluc and increasing amounts of CB_1-GFP^2 or HERG-GFP^2 (Fig. 3.2E). The combination of $G\alpha_i$-Rluc and CB_1-GFP^2 resulted in a $BRET_{Max}$ of 0.26 ± 0.04 and a $BRET_{50}$ of 0.37 ± 0.05. The $BRET_{Max}$ and $BRET_{50}$ values were higher compared to cells expressing $G\alpha_i$-Rluc and HERG-GFP^2 (Fig. 3.2E). Therefore, the interaction between $G\alpha_i$ and CB_1 was specific and saturable. To test whether ACEA treatment resulted in conformational changes within the pre-assembled CB_1-$G\alpha_i$ complexes (observed as changes in $BRET_{Max}$), rather than the recruitment of more $G\alpha_i$ to CB_1 (observed as changes in $BRET_{50}$) (Ayoub *et al.,* 2012), a $BRET^2$ saturation curve was created following ACEA (1 μM) treatment (Fig. 3.2E). The $BRET^2$ saturation curve displayed $BRET_{Max}$ of 0.40 ± 0.03 and $BRET_{50}$ of 0.39 ± 0.04. The $BRET_{Max}$ obtained from treatment with ACEA was significantly higher compared to cells treated with vehicle ($BRET_{Max}$ of 0.26 ± 0.04). No significant change in $BRET_{50}$ values was observed (Fig. 3.2E). Therefore, ACEA treatment only induced conformational changes with the CB_1-$G\alpha_i$ complexes. To test whether haloperidol treatment induces conformational changes with the $CB_1/D_{2L}/G\alpha_i$ complexes or it promotes the

dissociation of CB_1 and $G\alpha_i$, a $BRET^2$ saturation curve was generated in cells expressing $G\alpha_i$-Rluc, CB_1-GFP^2, and D_{2L}-pcDNA (Fig. 3.2E). Co-treating the cells with 10 μM haloperidol and 1 μM ACEA significantly reduced $BRET_{Max}$ (0.11 ± 0.04) and $BRET_{50}$ (0.11± 0.07) compared to vehicle-treated cells. Reduction in both $BRET_{Max}$ and $BRET_{50}$ following haloperidol and ACEA treatment suggested that haloperidol induced dissociation of $G\alpha_i$ and CB_1 and induced conformational changes between $G\alpha_i$-Rluc and CB_1-GFP^2.

A kinetic analysis of ACEA-induced $BRET^2$ between $G\alpha_i$ and CB_1 was carried out. Cells were co-transfected with $G\alpha_i$-Rluc and CB_1-GFP^2 and signals were recorded as repeated measures in vehicle-treated cells for over 9 min (540 s). Treating cells with 1 μM ACEA 75 s after the addition of coelenterazine 400a resulted in a rapid increase in $BRET_{Eff}$ (Fig. 3.2F). $BRET_{Eff}$ peaked at ~125 s and remained significantly higher for ~ 400 s before declining (Fig. 3.2F). By ~ 450 s following ACEA application (Fig. 3.2F), the $BRET_{Eff}$ returned to pre-ACEA levels and remained at this level for 30 min (data not shown). However, in cells co-expressing $G\alpha_i$-Rluc, CB_1-GFP^2 and D_{2L}-pcDNA, treating the cells with 10 μM haloperidol added [50 s following the initiation of the reaction and 25 s prior to the application of 1 μM ACEA] resulted in a rapid reduction in $BRET_{Eff}$ compared to vehicle-treated cells and compared to ACEA-treated cells (Fig. 3.2F). The reduction in $BRET_{Eff}$ was sustained for the remaining 480 s (Fig. 3.2F). Reduction of $BRET_{Eff}$ below the basal level was observed at 10, 20 and 30 min following ACEA application ($P < 0.01$) (data not shown).

3.3.3 D_2 Antagonism Reduced the Efficacy and Potency of CB_1-Dependent $G\alpha_i$ - Mediated ERK Phosphorylation

We had observed a reduction in $BRET_{Eff}$ between $G\alpha_i$ and CB_1 in STH$dh^{Q7/Q7}$ cells co-expressing D_{2L} following ACEA and haloperidol treatment, which might suggested that CB_1 receptors are dissociated from $G\alpha_i$ proteins. Thus, we measured whether ACEA-induced and $G\alpha_i$-mediated ERK phosphorylation was also inhibited by haloperidol treatment. A concentration-response curve of ACEA-induced ERK phosphorylation was generated following 5 min treatment (EC_{50} = 0.27 (0.25-0.29), E_{Max} 0.76 (0.71-0.80), Hill coefficient =1.11 (0.89-1.23) (Fig. 3.3A; Table 3.1). Haloperidol (0.01- 10 μM) treatment alone did

Figure 3.3: Haloperidol Reduced ACEA-Induced ERK Phosphorylation. **(A)** pERK concentration-response curve from STH*dh*$^{Q7/Q7}$ cells treated with ACEA alone or in the presence of HALO measured at 5 min. **(B)** STH*dh*$^{Q7/Q7}$ cells were treated with 1 μM ACEA alone for 5 min or in combination with 10 μM HALO +/- 24 h pre-treatment with 50 ng/ml PTx or CTx. * $P < 0.01$ compared to vehicle treatment; ~ < 0.01 compared to cells treated with 1 μM ACEA. **(C)** STH*dh*$^{Q7/Q7}$ cells were transfected with the pcDNA or CB$_1$-BP and treated with 1 μM ACEA alone for 5 min or in combination with 10 μM HALO. * $P < 0.01$ compared to vehicle treatment; ~ < 0.01 compared to cells transfected with empty pcDNA vector and treated with 1 μM ACEA and 10 μM HALO. Data are presented as mean ± SEM of 4 independent experiments, one-way ANOVA followed by Tukey's *post-hoc* test.

A

B

C

92
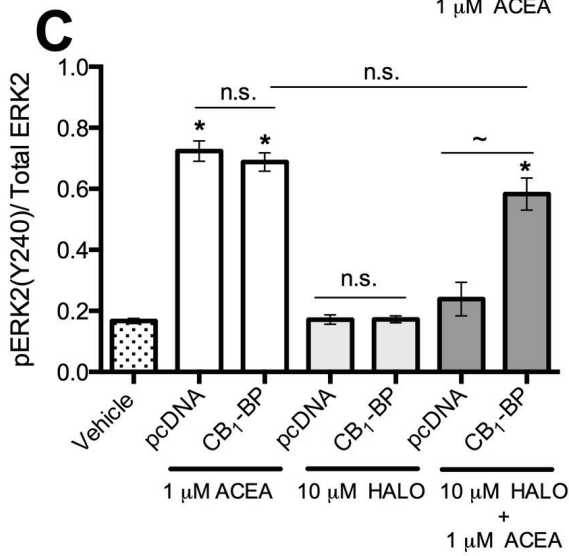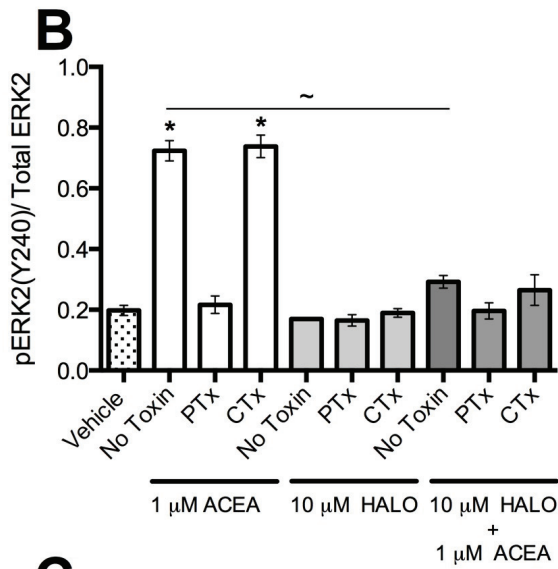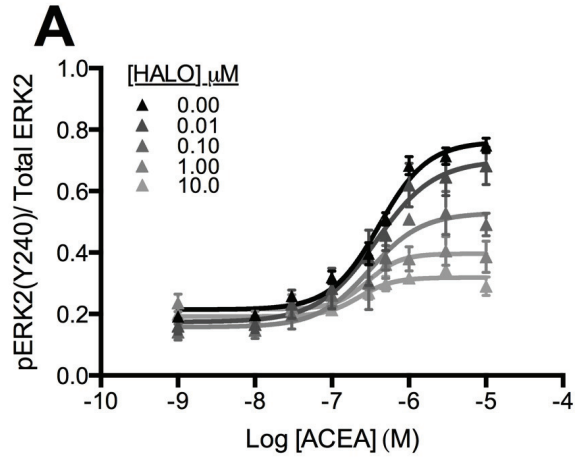
not increase ERK phosphorylation (data not shown). Co-treating the cells with increasing concentrations of haloperidol 25 s prior the addition of ACEA, produced a concentration-dependent reduction in ACEA E_{Max} and EC_{50}. The reduction in EC_{50} and E_{Max} was significant at 0.1, 1 and 10 μM haloperidol (Table 3.1). The Hill coefficient was less than 1 in cells treated with 1 and 10 μM haloperidol, indicating a negative cooperativity effect (Table 3.1). To confirm that the CB_1-mediated ERK phosphorylation was mediated through $G\alpha_{i/o}$ protein, STH$dh^{Q7/Q7}$ cells were pre-treated with PTx for 24 hr, prior to ACEA +/- haloperidol application (Fig. 3.3B). PTx pre-treatment inhibited ERK phosphorylation induced by 1 μM ACEA. However, pre-treating the cells with CTx for 24 hr, which suppresses $G\alpha_s$ expression, did not alter ACEA-mediated ERK phosphorylation. These results demonstrated that ACEA treatment induced a PTx-sensitive, $G\alpha_{i/o}$- mediated increase in ERK phosphorylation. O-2050 pre-treatment inhibited ACEA-mediated ERK phosphorylation (data not shown). The co-application of 10 μM haloperidol and ACEA prevented ACEA-induced $G\alpha_{i/o}$-dependent ERK phosphorylation (Fig. 3.3B). Transfecting STH$dh^{Q7/Q7}$ cells with CB_1-BP did not alter ACEA-induced ERK phosphorylation (Fig. 3.3C). The expression of CB_1-BP restored ACEA-induced ERK phosphorylation in haloperidol-treated cells (Fig. 3.3C). Haloperidol inhibited CB_1-dependent and $G\alpha_{i/o}$-mediated ERK signaling through binding to CB_1/D_{2L} complexes.

3.3.4 Combined D_2 antagonism and CB_1 agonism enhanced $BRET_{Eff}$ Between CB_1 and $G\alpha_s$

Next, we studied the coupling of CB_1 to $G\alpha_s$ protein in the absence and in the presence of cannabinoid CB_1 agonist. $BRET_{Eff}$ between $G\alpha_s$-Rluc and CB_1-GFP^2 was similar to that observed in cells co-expressing $G\alpha_s$-Rluc and HERG-GFP^2 (Fig. 4A). Twenty-four-hour CTx pre-treatment did not affect $BRET_{Eff}$ compared to vehicle-treated cells (Fig. 3.4A). The higher basal $BRET_{Eff}$ between cells expressing $G\alpha_i$-Rluc and CB_1-GFP^2 (Fig. 3.2A) compared to cells expressing $G\alpha_s$-Rluc and CB_1-GFP^2 (Fig. 3.4A) was not a result of different levels in the expression of $G\alpha_i$-Rluc, $G\alpha_s$-Rluc or CB_1-GFP^2 proteins in the cells because luminescence and fluorescence intensities measured from cells transfected with these constructs were not different (data not shown). In addition, 1 μM ACEA treatment did not alter $BRET_{Eff}$ between $G\alpha_s$-Rluc and CB_1-GFP^2 (Fig. 3.4A).

Figure 3.4: Co-treatment With ACEA and Haloperidol Promoted Interactions Between CB$_1$ and Gα$_s$ in STHdh$^{Q7/Q7}$ Cells. **(A)** BRET$_{Eff}$ was measured 5 min following the addition of vehicle or 1 μM ACEA or with 500 nM CTx pre-treated for 24 h in cells expressing Gα$_s$-Rluc and CB$_1$-GFP^2. *n.s. P* > 0.05 relative to cells expressing Gα$_s$-Rluc and HERG-GFP^2. **(B)** Concentration-response curves of ACEA-induced BRET$_{Eff}$ between Gα$_s$-Rluc and CB$_1$-GFP^2 in the absence or presence of HALO measured at 5 min following ACEA application. **(C)** BRET$_{Eff}$ was measured at 5 min following the addition of vehicle, 10 μM HALO or 1 μM ACEA +/- 10 μM HALO and pre-treated for 30 min with 0.5 μM O-2050 in cells expressing Gα$_s$-Rluc and CB$_1$-GFP^2 alone or together with D$_{2L}$-pcDNA. *n.s. P* > 0.05 compared with cells expressing Gα$_s$-Rluc and CB$_1$-GFP^2 only; ~ *P* < 0.01 relative to cells expressing Gα$_s$-Rluc and CB$_1$-GFP^2 and treated with 1 μM ACEA and 10 μM HALO; * *P* < 0.01 compared to cells treated with vehicle. **(D)** Cells were transfected with Gα$_s$-Rluc, CB$_1$-GFP2, and D$_2$ together with CB$_1$-BP or pcDNA, and BRET$_{Eff}$ was measured at 5 min following the addition of vehicle, 10 μM HALO, 1 μM ACEA alone or together with 10 μM HALO. * *P* < 0.01 relative to cells expressing Gα$_s$-Rluc, CB$_1$-GFP^2 and CB$_1$-BP and treated with 1 μM ACEA and 10 μM HALO. **(E)** BRET^2 saturation curves were generated by co-transfected constant amounts of Gα$_s$- Rluc and increasing amounts of CB$_1$-GFP^2 alone or with D$_{2L}$-pcDNA or HERG GFP^2, and BRET$_{Eff}$ was measured following the addition of vehicle, 1 μM ACEA +/- 10 μM HALO. * *P* < 0.01 compared with cells expressing Gα$_s$-Rluc and HERG-GFP^2. **(F)** BRET$_{Eff}$ was measured over 9 min in cells expressing Gα$_s$-Rluc and CB$_1$-GFP^2 alone or together with D$_{2L}$-pcDNA and treated with vehicle, 1 μM ACEA alone or together with 10 μM HALO. As a negative control, cells were co-transfected with Gα$_s$-Rluc and HERG-GFP^2. Cells co-transfected with Gα$_s$-Rluc and β$_2$AR-GFP^2 were used as a positive control. .* *P* < 0.01 compared to cells expressing Gα$_s$-Rluc and CB$_1$-GFP^2 and treated with vehicle; ~ *P* < 0.01 compared to cells expressing Gα$_i$-Rluc and CB$_1$-GFP^2 and treated with 1 μM ACEA. Data are presented as mean ± SEM of 4 independent experiments, significance was determined via one-way ANOVA followed by Tukey's *post-hoc* test.
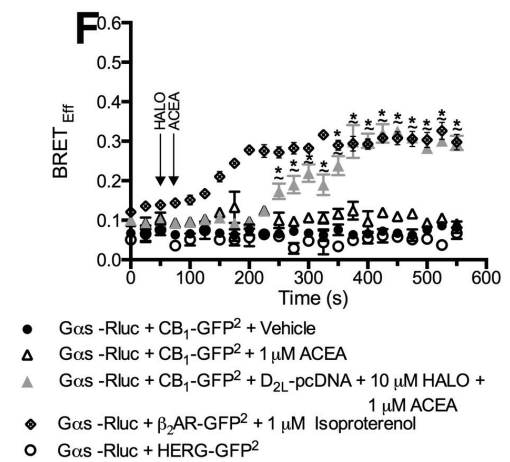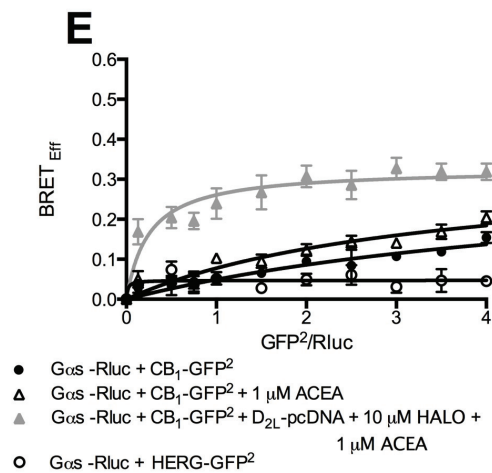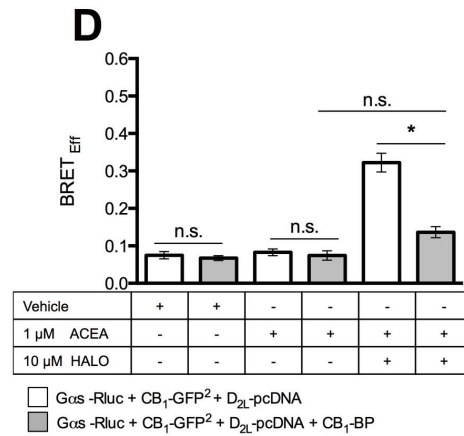
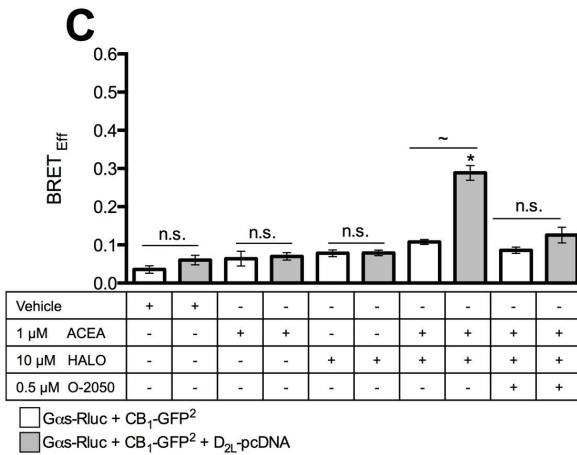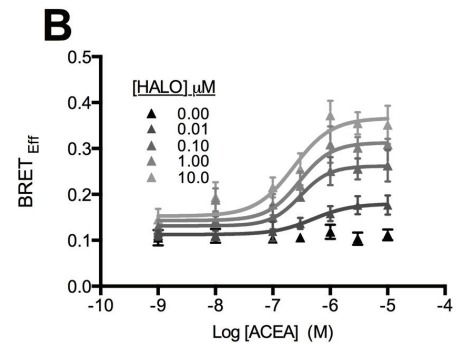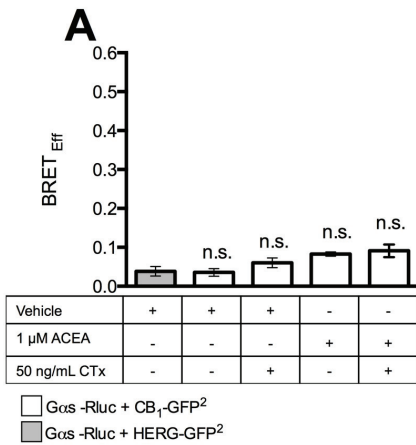In the absence or presence of CB_1 agonist, no energy transfer was detected between $G\alpha_s$-Rluc and CB_1-GFP^2 proteins.

Since we have observed an inhibition in $BRET^2$ signals between $G\alpha_i$-Rluc and CB_1-GFP^2 proteins and inhibition of CB_1-dependent and $G\alpha_{i/o}$- mediated ERK signaling following ACEA and haloperidol co-application, we tested if the co-application of both ligands promoted CB_1 coupling to $G\alpha_s$ protein. An ACEA concentration-response curve was generated to determine the concentration-dependent increase in $G\alpha_s$-Rluc and CB_1-GFP^2 association in the presence of D_{2L}-pcDNA and increasing concentrations of haloperidol (0.01-10 µM), added 25 s prior the application of ACEA (Fig. 3.4B). Increasing ACEA concentration in the presence of increasing concentrations of haloperidol (0.01-10 µM) resulted in an increase in $BRET_{Eff}$ between $G\alpha_s$-Rluc and CB_1-GFP^2 in a concentration-dependent manner, shifting the ACEA concentration-response curves to the left and upward. The reduction in EC_{50} and the increase in E_{max} were significant at all haloperidol concentrations tested (0.01-10.0 µM) (Table 3.1). Similarly, the Hill coefficient was significantly more than 1 at all haloperidol concentrations tested (Table 3.1) suggesting that haloperidol exerts a positive cooperative effect on CB_1 to $G\alpha_s$ interaction.

Previous studies have shown that co-expression of D_{2L} and CB_1 in HEK 293 cells is sufficient to change the signaling of CB_1 from $G\alpha_i$ to $G\alpha_s$ (Jarrahian *et al.,* 2004). In our study, we found that the co-expression of equimolar of D_{2L}-pcDNA and CB_1-GFP^2 in the presence of $G\alpha_s$-Rluc did not change $BRET_{Eff}$ between $G\alpha_s$-Rluc and CB_1-GFP^2 in the presence of vehicle or ACEA (Fig. 3.4C). The application of haloperidol alone did not alter $BRET_{Eff}$ between $G\alpha_s$-Rluc and CB_1-GFP^2 in the absence or presence of D_{2L} (Fig. 3.4C). Haloperidol promoted $BRET^2$ signals between $G\alpha_s$-Rluc and CB_1-GFP^2 only in ACEA treated cells in the presence of D_{2L}, suggesting that the observed effect of haloperidol and ACEA is mediated through CB_1/D_{2L} heteromers. Furthermore, inhibiting the heteromerization between CB_1 and D_{2L}, by the expression of CB_1-BP together with $G\alpha_s$-Rluc, CB_1-GFP^2, and D_{2L}-pcDNA, blocked haloperidol-induced $BRET^2$ signals between $G\alpha_s$-Rluc and CB_1-GFP^2 in the presence of ACEA (Fig. 3.4D). Co-treatment with ACEA and haloperidol, therefore, promoted $BRET^2$ signals between $G\alpha_s$-Rluc and CB_1-GFP^2 through binding to D_{2L} receptors in CB_1/D_{2L} complexes.

BRET^2 saturation curves were generated to determine the specificity of the interaction between CB$_1$ and Gα_s in the presence and absence of ACEA and/or haloperidol. In cells expressing constant amounts of Gα_s-Rluc increasing the concentration of transfected CB$_1$-GFP^2 resulted in a gradual linear increase in BRET$_{Eff}$ in vehicle- or ACEA- treated cells, indicating that the interaction between Gα_s-Rluc and CB$_1$-GFP^2 was non-specific (Fig. 3.4E). However, treating cells expressing Gα_s-Rluc, CB$_1$-GFP^2 and D$_{2L}$-pcDNA with 10 μM haloperidol prior to 1 μM ACEA application resulted in a hyperbolic increase in BRET$_{Eff}$ between Gα_s-Rluc and CB$_1$-GFP^2, with BRET$_{Max}$ of 0.33 ± 0.01 and BRET$_{Min}$ of 0.25 ± 0.01 (Fig. 3.4E). The interaction between Gα_s and CB$_1$ was specific and saturable in cells co-treated with ACEA and haloperidol.

Ligand-induced BRET$_{Eff}$ between Gα_s-Rluc and CB$_1$-GFP^2 was recorded for 9 min. No BRET$_{Eff}$ signals were observed following the application of 1 μM ACEA over the 9 min (540 s) observation period (Fig. 3.4F). Interestingly, treating cells with 10 μM haloperidol 50 s post-coelenterazine addition and 25 s prior to 1 μM ACEA application resulted in a delayed increase in BRET$_{Eff}$ between Gα_s -Rluc and CB$_1$-GFP^2 (225 s after the application of ACEA) (Fig. 3.4F). The signal peaked at 5 min (300 s) following the addition of ACEA (375 s post-coelenterazine addition) (Fig. 3.4F). BRET$_{Eff}$ signal was still observed at 5, 10 and 20, but not at 30 min following ACEA (data not shown). As a positive control, we used β$_2$AR, which has been demonstrated to pre-assemble with Gα_s (Lachance *et al.*, 1999; Galés *et al.*, 2005). We measured BRET$_{Eff}$ between Gα_s-Rluc and β$_2$AR -GFP^2 before and following the application of the β$_2$AR agonist isoproterenol (1 μM). High BRET$_{Eff}$ was observed between Gα_s-Rluc and β$_2$AR-GFP^2 in the absence of exogenous ligand. Isoproterenol led to a rapid and sustained elevation in BRET$_{Eff}$ (Fig. 3.4F). Therefore, the delayed BRET$_{Eff}$ between Gα_s and CB$_1$ following ACEA and haloperidol application could be due to the recruitment of Gα_s to CB$_1$ and its activation instead of the activation of pre-assembled GPCR-G protein complexes.

3.3.5 Combined D$_2$ Antagonism and CB$_1$ Agonism Induced CREB Phosphorylation

We observed that haloperidol treatment increased BRET$_{Eff}$ between Gα_s-Rluc and CB$_1$-GFP^2 in the presence of ACEA (Fig. 3.4). To confirm that haloperidol treatment induced functional coupling of Gα_s to CB$_1$ following ACEA treatment, we measured

Figure 3.5: Co-Treatment with Haloperidol and ACEA Induced CREB phosphorylation.
(A) pCREB concentration-response curve from STH$dh^{Q7/Q7}$ cells treated with ACEA +/-
HALO measured at 30 min. **(B)** STH$dh^{Q7/Q7}$ cells were treated with 1 μM ACEA +/- 10 μM
HALO for 30 min with or without 24 h pre-treatment with 50 ng/ml PTx or CTx. * $P < 0.01$
compared to vehicle treatment; ~ $P < 0.01$ compared to cells treated with 1 μM ACEA. **(C)**
STH$dh^{Q7/Q7}$ cells were transfected with pcDNA or the CB$_1$-BP and treated with 1 μM ACEA
+/- 10 μM HALO for 30 min. * $P < 0.01$ compared to vehicle treatment; ~ < 0.01 compared
to cells transfected with empty pcDNA and treated with 1 μM ACEA and 10 μM HALO .
CREB phosphorylation was quantified via In-Cell™ Western Data are presented as mean ±
SEM of 4 independent experiments, one-way ANOVA followed by Tukey's *post-hoc* test.
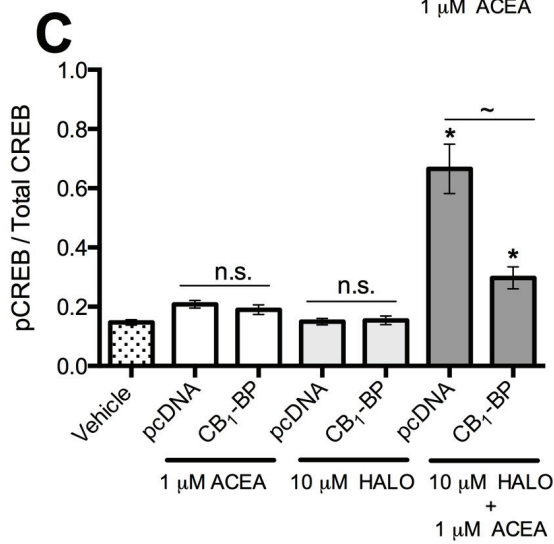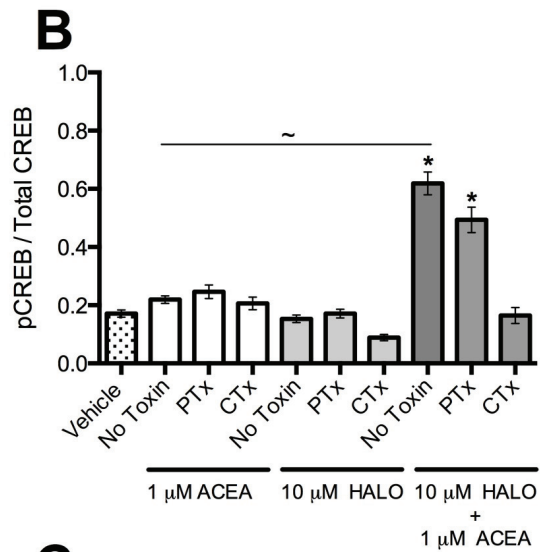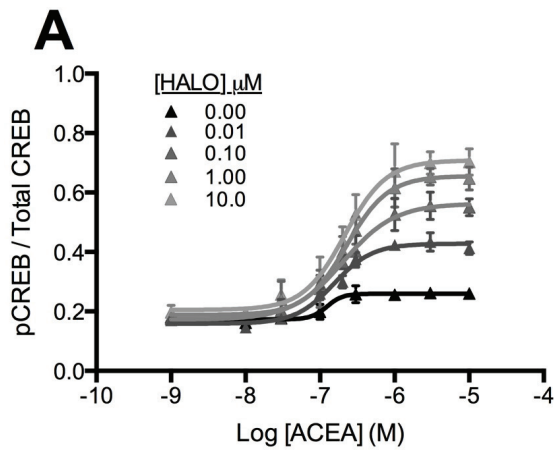
CTx-sensitive, $G\alpha_s$-dependent CREB phosphorylation (Fig. 3.5). A concentration-response curve of ACEA-induced CREB phosphorylation was generated following 30 min treatment (Fig. 3.5A). Treating ST*Hdh*$^{Q7/Q7}$ cells with different concentrations of ACEA did not change CREB phosphorylation compared to vehicle-treated cells (Fig. 3.5A,B). Similarly, haloperidol (0.01- 10 μM) treatment did not increase CREB phosphorylation (data not shown). Pre-treating the cells with haloperidol 25 s prior to the application of ACEA significantly increased CREB phosphorylation. The co-application of increasing concentrations of haloperidol reduced the EC_{50} and increased E_{max} for ACEA-induced CREB phosphorylation (Table 3.1). The Hill coefficient values were greater than 1, suggesting a positive cooperatively effects on CB_1-dependent CREB phosphorylation (Fig. 3.5A). To confirm that the observed CREB phosphorylation following the application of haloperidol and ACEA was $G\alpha_s$-dependent, cells were pre-treated with CTx for 24 hr. Pre-treating the cells with CTx blocked $G\alpha_s$-dependent CREB phosphorylation in cells co-treated with 1 μM ACEA and 10 μM haloperidol (Fig. 3.5B). CB_1-BP reduced ACEA induced CREB phosphorylation in haloperidol-treated cells (Fig. 3.5C). Therefore, co-treatment with haloperidol and ACEA induced $G\alpha_s$-mediated CREB phosphorylation through binding of haloperidol to CB_1/D_{2L}.

To determine whether the observed effects of haloperidol on CB_1 signaling was specific to haloperidol or common to other high-affinity D_2 antagonists, we tested the influence of the high-affinity D_2 antagonist, sulpiride, on the coupling of CB_1 to G-proteins and downstream signaling. A reduction in ACEA-enhanced $BRET^2$ between $G\alpha_i$ and CB_1 (Supplementary Fig. 3.3A) and $G\alpha_i$ -dependent ERK phosphorylation (Suppl. Fig. 3.3B) was observed when ST*Hdh*$^{Q7/Q7}$ cells were treated with 10 μM sulpiride and 1 μM ACEA. In addition, an increase in $BRET^2$ signaling between $G\alpha_s$ and CB_1 (Supplementary Fig. 3.3C) and $G\alpha_s$-dependent CREB signaling (Supplementary Fig. 3.3D) was detected in ST*Hdh*$^{Q7/Q7}$ cells were treated with 10 μM sulpiride and 1 μM ACEA. Our findings demonstrated that high affinity orthosteric D_2 antagonists switch CB_1 coupling and signaling from $G\alpha_i$ to $G\alpha_s$ in response to CB_1 agonist when both CB_1 and D_{2L} receptors are expressed.

3.3.6 CB₁ Agonism Resulted in Slow and Sustained β-arrestin1 Recruitment to CB₁ Receptor, Which Was Inhibited by D₂ Antagonism

CB_1 activation is followed by C-terminal tail phosphorylation and β-arrestin1 (Laprairie *et al*., 2014) or β-arrestin2 (Jin *et al*., 1999; van der Lee *et al.,* 2009) recruitment to CB_1 leading to receptor internalization. β-arrestin1 recruitment to CB_1 following ligand application was measured over 30 min using $BRET^2$. $STHdh^{Q7/Q7}$ cells endogenously express β-arrestin1 (Laprairie *et al.,* 2014). $BRET_{Eff}$ signals observed from cells expressing β-arrestin1-Rluc and CB_1-GFP^2 treated with the vehicle was higher than $BRET_{Eff}$ between β-arrestin1-Rluc and HERG-GFP^2 (Fig. 3.6A). ACEA (1 μM) treatment increased $BRET_{Eff}$ between β-arrestin1-Rluc and CB_1-GFP^2 starting at 5 min compared to vehicle-treated cells and reached a plateau at 15 min. The signal was sustained for 30 min (Fig. 3.6A). However, treating the cells co-expressing β-arrestin1-Rluc, CB_1-GFP^2 and D_{2L}-pcDNA with 10 μM haloperidol 25 s prior to the application of 1 μM ACEA decreased $BRET_{Eff}$ between β-arrestin1-Rluc and CB_1-GFP^2 over the 30 min ($P < 0.01$) compared to cells treated with 1 μM ACEA (Fig. 3.6A). $BRET_{Eff}$ signals between β-arrestin1-Rluc and CB_1-GFP^2 occurred in an ACEA concentration-dependent manner (Fig. 3.6B). The addition of increasing concentrations of (0.1, 1 and 10 μM) haloperidol prior to ACEA application resulted in a lower E_{Max} and EC_{50} (Table 3.1). The reduction in ACEA-induced β-arrestin1-recruitment to CB_1 mediated by haloperidol is consistent with the interpretation that haloperidol acts as a negative allosteric modulator of CB_1-β-arrestin1 interactions. Treating the cells expressing β-arrestin1-Rluc, CB_1-GFP^2 and D_{2L}-pcDNA with 10 μM haloperidol or 0.5 μM O-2050 alone did not alter $BRET_{Eff}$ between β-arrestin1-Rluc and CB_1-GFP^2 compared to vehicle-treated cells (Fig. 3.6C). Our results demonstrated that D_2 antagonism reduced β-arrestin1 recruitment to CB_1 receptors in the presence of CB_1 agonist. CB_1 internalization was measured in ST$Hdh^{Q7/Q7}$ cells transfected with CB_1-GFP^2 and β-arrestin1. CB_1 internalization was measured over 30 min following ligand treatment (Fig. 3.7A,B). Treating STH$dh^{Q7/Q7}$ cells with 1 μM ACEA resulted in CB_1 internalization starting at 10 min compared to vehicle-treated cells (Fig. 3.7A, B). Treating the cells with 10 uM haloperidol alone or 0.5 μM O-2050 did not alter CB_1 localization compared to vehicle-treated cells (Fig. 3.7B). Pre-treating the cells with 0.5 μM O-2050 before the application of 1 μM ACEA inhibited CB_1 internalization over 30 min (Fig. 3.7A,B). Haloperidol pre- **Figure**

3.6: *ACEA Treatment Resulted in Slow and Sustained β-arrestin1 Recruitment to CB$_1$ Receptors, Which Was Inhibited With Haloperidol.* **(A)** BRET$_{Eff}$ was measured over 30-min in cells expressing β-arrestin1-Rluc and CB$_1$-GFP^2 +/- D$_{2L}$-pcDNA and treated with vehicle, 1 μM ACEA alone or together with 10 +/-HALO. As a control, cells were co-transfected with β-arrestin1-Rluc and HERG-GFP^2. * $P < 0.01$ compared to vehicle-treated cells; ~ $P < 0.01$ compared to cells treated with 1 μM ACEA. **(B)** Concentration-response curves of ACEA- induced BRET$_{Eff}$ between β-arrestin1-Rluc and CB$_1$-GFP^2 in the absence or presence of increasing concentrations of HALO. **(C)** BRET$_{Eff}$ was measured at 30 min following the addition of vehicle, 1 μM ACEA +/- 10 μM HALO or with 30 min pre-treatment with 0.5 μM O-2050 in cells expressing β-arrestin1-Rluc and CB$_1$-GFP^2 alone or together with D$_{2L}$-pcDNA. *n.s.* $P > 0.05$ compared with cells expressing β-arrestin1-Rluc and CB$_1$-GFP^2 only; ~ $P < 0.01$ relative to cells expressing β-arrestin1-Rluc and CB$_1$-GFP^2 and treated with 1 μM ACEA and 10 μM HALO; * $P < 0.01$ compared to cells treated with vehicle. Data are presented as mean ± SEM of 4 independent experiments, as determined via one-way ANOVA followed by Tukey's *post-hoc* test.

A

- ● β-arrestin1-Rluc + CB$_1$-GFP^2 + Vehicle
- △ β-arrestin1-Rluc + CB$_1$-GFP^2 + 1 μM ACEA
- ▲ β-arrestin1-Rluc + CB$_1$-GFP^2 + D$_{2L}$- pcDNA + 10 μM HALO + 1 μM ACEA
- ○ β-arrestin1-Rluc + HERG-GFP^2

B

[HALO] μM
0.00
0.01
0.10
1.00
10.0

C

Vehicle	+	+	-	-	-	-	-	-	-	-
1 μM ACEA	-	-	+	+	-	-	+	+	+	+
10 μM HALO	-	-	-	-	+	+	+	+	+	+
0.5 μM O-2050	-	-	-	-	-	-	-	-	+	+

□ β-arrestin1-Rluc + CB$_1$-GFP^2
▨ β-arrestin1-Rluc + CB$_1$-GFP^2 + D$_{2L}$-pcDNA

103
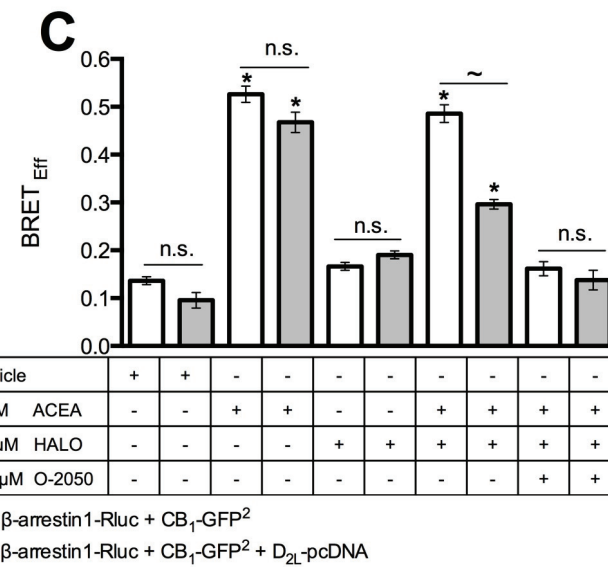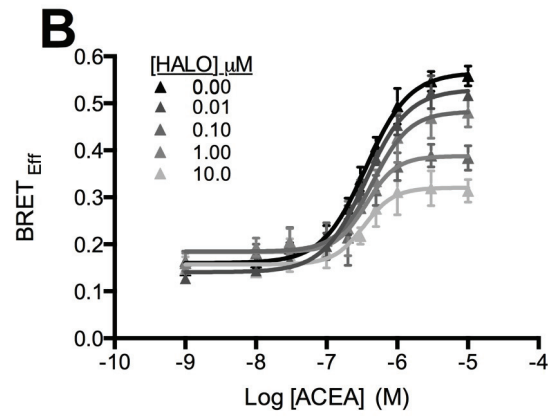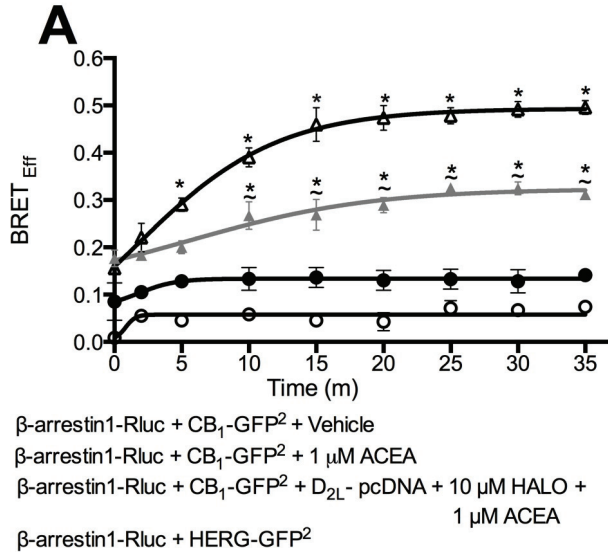
Figure 3.7: Haloperidol Inhibited CB$_1$ Internalization Following ACEA Treatment. **(A)** Time-course analysis of CB$_1$ cell surface expression and total protein levels over 30 min in cells expressing β-arrestin1-Rluc and CB$_1$-GFP^2 + D$_{2L}$-pcDNA measured using On-Cell Western™ and In-Cell Western™ in cells treated with vehicle, 1 μM ACEA +/- 10 μM HALO 0.5 μM O-2050. * $P < 0.01$ compared with vehicle. **(B)** CB$_1$ cell surface expression measured at 30 min following ligand treatment. * $P < 0.01$ compared with vehicle-treated cells. ~ $P < 0.01$ compared to ACEA-treated cells. Data are presented as mean ± SEM of 4 independent experiments, one-way ANOVA followed by Tukey's *post-hoc* test.

A

B

Legend (between panels A and B):
- △ 1 μM ACEA
- ▲ 10 μM HALO + 1 μM ACEA
- ◇ 0.5 μM O-2050 + 1 μM ACEA
- ● Vehicle
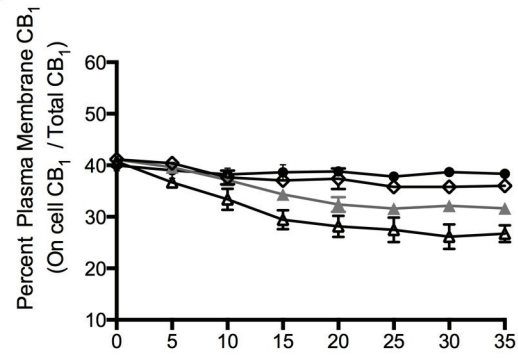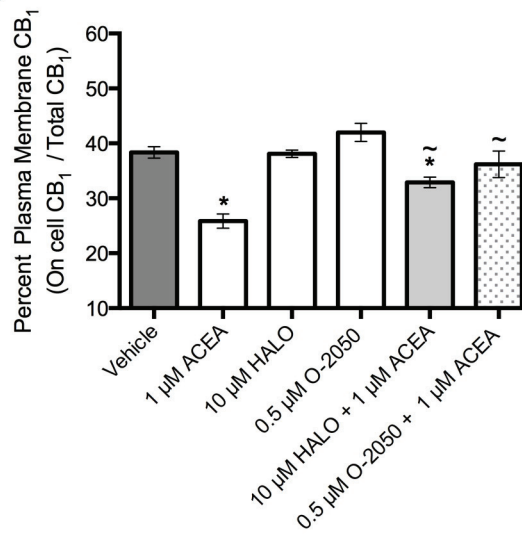
treatment significantly inhibited ACEA-induced CB_1 internalization compared to ACEA-treated cells. Endogenous CB_1 internalization was also measured in ST*Hdh*$^{Q7/Q7}$ cells (Supplementary Fig. 4). The reduction of BRET^2 between β-arrestin1-Rluc and CB_1-GFP^2 following transfection is consistent with the observation that endogenous CB_1 receptor internalization was reduced following haloperidol and ACEA treatment (Supplementary Fig. 3.4).

3.4 Discussion

3.4.1 Haloperidol Allosterically Alters CB_1-G-protein Coupling and Downstream Cellular Signaling

Given the clinical importance of D_2 antagonists and previous reports that D_2 agonists influence CB_1 signaling, the goal of this study was to determine if D_2 antagonists act as modulators of CB_1 signaling. Specifically, we wanted to investigate how D_2 antagonists and CB_1 agonists influence the activity of CB_1/D_{2L} heteromers. We investigated the influence of D_2 antagonism on CB_1 coupling to $G\alpha_i$ and $G\alpha_s$, as well as β-arrestin1 recruitment and internalization in a model of striatal medium spiny projection neurons (Summarized in Fig. 3.8). In this study, we were able to show that CB_1 and D_{2L} receptors heteromerize when co-expressed in ST*Hdh*$^{Q7/Q7}$ cells in the absence and presence of exogenous CB_1 ligand. CB_1 agonist treatment stabilized the conformation of the pre-assembled CB_1/D_{2L} heteromers but did not alter the number of receptors involved in forming CB_1/D_{2L} complexes. CB_1 was coupled to $G\alpha_i$ in the absence of CB_1 ligand. Agonist-dependent CB_1-activation led to a rapid and transient conformational rearrangement of the pre-assembled CB_1-$G\alpha_i$ complexes, rather than the recruitment of $G\alpha_i$-proteins to CB_1. Activation was observed as a rapid increase in ERK phosphorylation through the PTx-sensitive $G\alpha_i$ pathway (Galés *et al*., 2005, 2006; Levoye *et al.,* 2009). Sustained activation of CB_1 was followed by the return of CB_1-$G\alpha_i$ complexes to the inactive conformation rather than dissociation of CB_1 and $G\alpha_i$ protein (Bunemann *et al.,* 2003; Galés *et al.,* 2006). Interactions between $G\alpha_i$ and CB_1 were completely undetectable following CB_1 agonist and D_2 antagonist co-treatment. In contrast, the efficacy of ACEA-dependent ERK phosphorylation was reduced by only ~80% in the presence of haloperidol relative to ACEA-treated cells. The residual pERK signal (~20%) was retained in the,

Figure 3.8: Kinetic Interaction of CB$_1$ Receptor and CB$_1$/D$_2$ Heteromers With Gα_i, Gα_s, and β-arrestin1. **(A, C)** BRET^2 data demonstrated that CB$_1$ receptor is pre-assembled with Gα_i. CB$_1$ agonist induced fast and transient increases in BRET^2 indicating conformational changes within the pre-assembled CB$_1$-Gα_i complexes. The deactivation phase of the pre-assembled CB$_1$-Gα_i occurs parallel to the slow and stable recruitment of β-arrestin1. **(B, D)** CB$_1$/D$_{2L}$ pre-assembled complexes are coupled to Gα_i, CB$_1$ agonist and D$_2$ antagonist induced a delayed and sustained recruitment of Gα_s to CB$_1$/D$_2$ complexes. Reduced and sustained recruitment of β-arrestin1 to the CB$_1$/D$_{2L}$/Gα_s was observed.
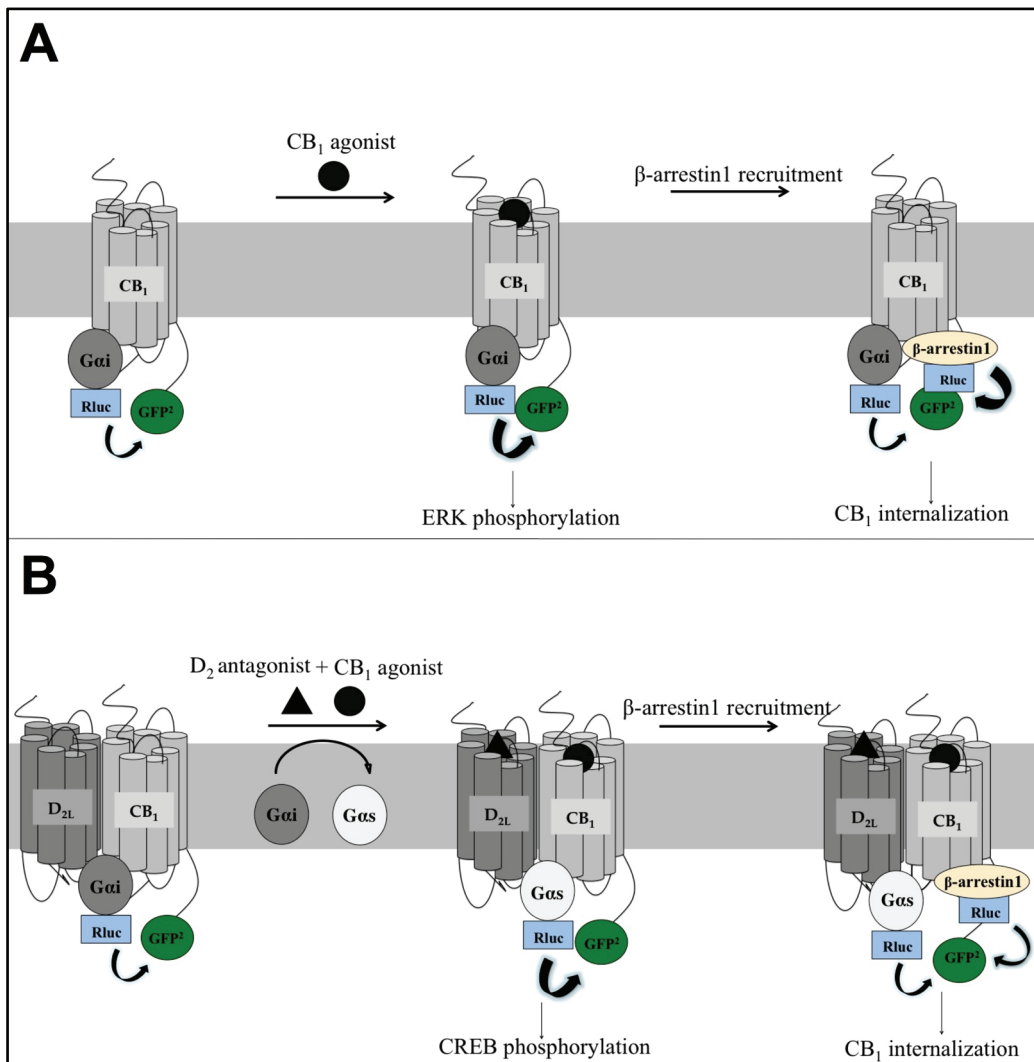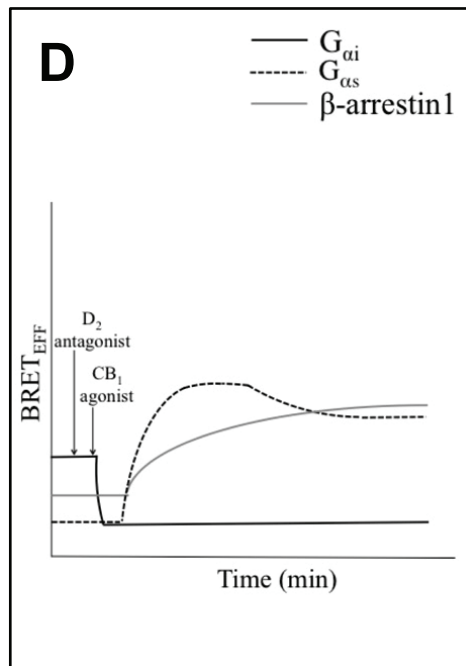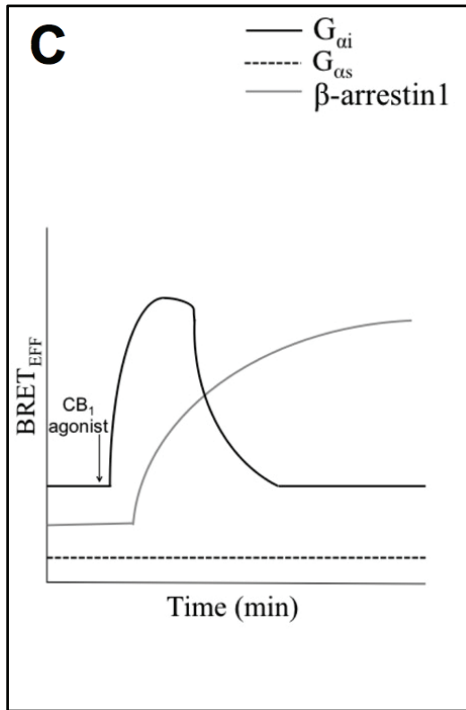
presence of haloperidol suggesting that a portion of ACEA-dependent ERK signaling occurred through CB_1 monomers, CB_1 homomers or CB_1-GPCR heteromers or CB_1-independent mechanisms. (Wager-Miller *et al.*, 2002; Rios *et al.*, 2006; Carriba *et al.*, 2007; Hudson *et al.*, 2010b). In the presence of ACEA, haloperidol switched the CB_1 coupling from $G\alpha_i$ to $G\alpha_s$ and induced $G\alpha_s$-dependent CREB phosphorylation. Previous studies have demonstrated that the co-expression and co-activation of both CB_1 and D_{2L} receptors are required to switch CB_1 signaling from $G\alpha_i$ to $G\alpha_s$ (Glass and Felder, 1997; Kearn *et al.*, 2005). In our study, we found that the co-expression of both receptors and the addition of a CB_1 agonist and D_2 antagonist was sufficient to induce conformational changes within the pre-assembled $CB_1/D_{2L}/G\alpha_i$ complexes and favor a higher proportion of CB_1 to dissociate from $G\alpha_i$ (Bunemann *et al.*, 2003; Galés *et al.,* 2006).

The delayed interaction between $G\alpha_s$ and CB_1 following CB_1 agonist and D_2 antagonist application cannot be considered as a general feature for $G\alpha_s$ coupling since fast activation of $G\alpha_s$ following ligand binding has been demonstrated for other GPCRs. For example, the β_2AR receptor is known to pre-assemble with $G\alpha_s$ (Lachance *et al.*, 1999), which we also observed as a fast increase in $BRET_{Eff}$ between $G\alpha_s$-Rluc and β_2AR-GFP[2]. The delayed interaction between $G\alpha_s$ and CB_1 could be due to the recruitment of $G\alpha_s$ to CB_1 and its activation instead of the activation of pre-assembled GPCR-G protein complexes (Ayoub *et al.*, 2010). The "pre-assembled model" between GPCRs and G proteins can explain the fast increase in $BRET_{Eff}$ signal between $G\alpha_i$-Rluc and CB_1-GFP[2] (Janetopoulos *et al.,* 2001; Galés *et al.*, 2006; Ayoub *et al.*, 2007, 2012). However, the interaction between $G\alpha_s$ and CB_1 is more compatible with the "free collision model". This model also proposes that GPCRs can interact and activate many G proteins depending on the ligand (reviewed in Oldham and Hamm, 2008). The "free collision model" may explain the ability of CB_1 receptor to activate different G protein pathways observed in previous studies (Laprairie *et al.*, 2014).

Sulpiride is less effective in promoting D_2 coupling to $G\alpha_s$ and inducing CREB phosphorylation in cells treated with ACEA, compared to haloperidol. Both haloperidol and sulpiride are D_2 antagonists, but the two drugs have different receptor dissociation properties from D_2 receptors, which result in different kinetics of D_2 blockade. Haloperidol binds with higher affinity to the D_2 receptor and displays slow dissociation

from D_2. Conversely, sulpiride displays a lower affinity and a much faster dissociation rate, which would produce rapidly reversible antagonism (Kapur and Seeman, 2001). In addition, highly lipophilic antagonists, such as haloperidol, can accumulate in cell membranes and can reach receptors in membrane folds more easily than hydrophilic D_2 antagonists, such as sulpiride (Rayport and Sulzer, 1995; Sahlholm *et al*., 2016). Therefore, lipophilic D_2 antagonists with slow dissociation rates, such as haloperidol, have higher E_{Max} for Gα_s- dependent CREB activation.

3.4.2 Haloperidol Reduced β-arrestin1 Recruitment to CB₁

Heteromerization is known to affect β-arrestin recruitment. β-arrestin2 (Jin *et al*., 1999; van der Lee *et al.,* 2009) and β-arrestin1 facilitate the internalization of CB_1 after activation (Laprairie *et al*., 2014). We demonstrated that D_2 antagonism inhibited CB_1 agonist-induced recruitment of β-arrestin1 to $CB_1/D_{2L}/G\alpha_s$ complexes and inhibited CB_1 receptor internalization in ST*Hdh*$^{Q7/Q7}$ cells in a dose-dependent manner. Therefore, antagonism of one receptor in a GPCR heteromer may allosterically inhibit agonist-induced β-arrestin1 recruitment of the other receptor. However, a fraction of the response was not antagonized by haloperidol, suggesting that some CB_1 functioned as monomers, homomers or heteromers (Wager-Miller *et al*., 2002; Rios *et al*., 2006; Carriba *et al*., 2007; Hudson *et al.,* 2010b). It is unknown at this time how repeated stimulation of CB_1 and D_{2L} would affect receptor desensitization.

3.4.3 Allosteric Interaction Between CB₁ and D₂L

Allosteric communications between GPCR heteromers resulting from orthosteric ligand binding have been reported for different GPCRs (reviewed in Ferré *et al*., 2014). While previous work has highlighted a functional interaction between CB_1 and D_{2L} following agonist-dependent co-activation of both receptors, the current work indicates that allosteric interactions are dependent on D_{2L} receptor ligand binding and are not limited to D_{2L} agonism. Cooperativity effects resulting from allosteric interactions between GPCR protomers have been analyzed using a number of different models (reviewed in Giraldo, 2013). In our study, cooperativity between protomers was assessed using the Hill coefficients obtained from fitting the data to a non-linear regression model

111

with variable slope (four parameters). Haloperidol treatment was associated with negative cooperativity between $G\alpha_i$ and CB_1 because treating the cells with haloperidol decreased both the E_{Max} and Hill coefficient of the ACEA-mediated $G\alpha_i$ and CB_1 interaction and ACEA-mediated pERK concentration–response. However, haloperidol treatment was associated with positive cooperativity between $G\alpha_S$ and CB_1 because haloperidol increased the E_{Max} and Hill coefficient of $G\alpha_s$ and CB_1 interaction and ACEA-mediated pCREB response. Whether haloperidol alters cannabinoid agonist affinity to the CB_1 receptor is still to be determined.

3.5 Conclusion

In addition to defining pharmacological interactions between CB_1 and D_{2L} receptors, this work may have clinical implications. Many central nervous system diseases, including schizophrenia, Huntington disease (HD) and Parkinson's disease, are treated with drugs that bind D_2 receptors either as antagonists or agonists. Patients who are prescribed such drugs might also be exposed to cannabinoids in the forms of medically prescribed cannabinoids or illicit agents. The dosing regimen for such cannabinoids might be chronic or intermittent. Based on our data, the combined effect of D_2 antagonists and CB_1 agonists are likely to differ from the predicted effect of either drug alone. Typical antipsychotics, including haloperidol, are commonly prescribed to Huntington patients to control chorea and psychosis (Ross and Tabrizi, 2011). In the context of HD where levels of CB_1 and D_2 decline with disease progression (Augood *et al.,* 1997; Denovan-Wright and Robertson, 2000) drug response and response to co-administration of CB_1 agonists and D_2 antagonists may be even more complex than that observed for non HD's patients (Sagredo *et al.,* 2012). A better understanding of the interaction between drugs acting on the dopaminergic and endocannabinoid systems are required for symptom management of HD and other disorders.

3.6 Supplementary Figures

Supplementary Figure 3.1: STHdh$^{Q7/Q7}$ Cells Endogenously Co-Express CB$_1$ and D$_2$ Receptors. STH*dh*$^{Q7/Q7}$ cells express CB$_1$ and D$_2$ mRNAs as demonstrated by RT-PCR **(A)** and qRT-PCR **(B)** using RNA extracted form STH*dh*$^{Q7/Q7}$ cells. **(C)** Total CB$_1$ and D$_2$ protein abundance was determined In-Cell™ Western normalized to β-actin levels. * $P < 0.01$, as determined *via* t-test. $n = 4$. **(D)** CB$_1$ and D$_2$ proteins are co-localized as confirmed by confocal images of a representative STH*dh*$^{Q7/Q7}$ cells stained by immunofluorescence for CB$_1$ using a Cys^2-conjugated secondary antibody (left panel) and for D$_2$ using a Cy^3 conjugated secondary antibody (middle panel); and the merged image (right panel).

A

+ RT

CB$_1$ D$_2$

− RT

CB$_1$ D$_2$

B

Relative mRNA Level
(Receptor mRNA/β Actin)

*

CB$_1$ D$_2$

C

Relative Protein Expression
(Protein / β III tubulin)

*

CB$_1$ D$_2$

D

CB$_1$ D$_2$ Merge
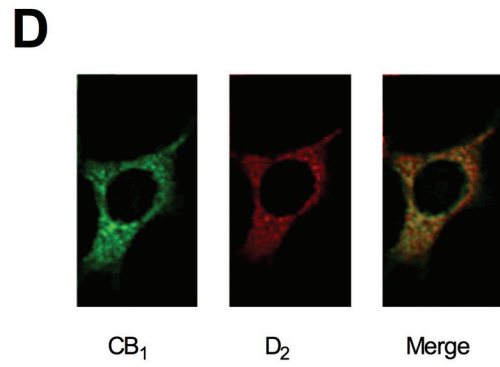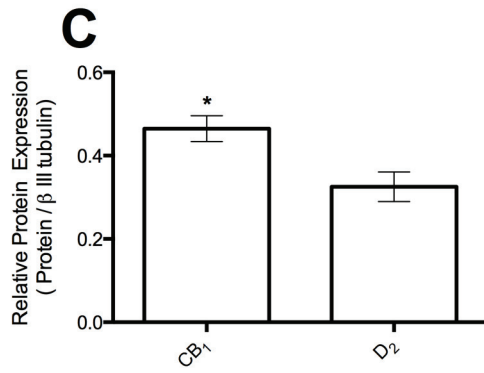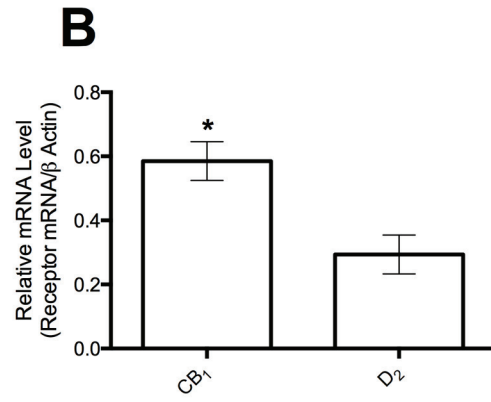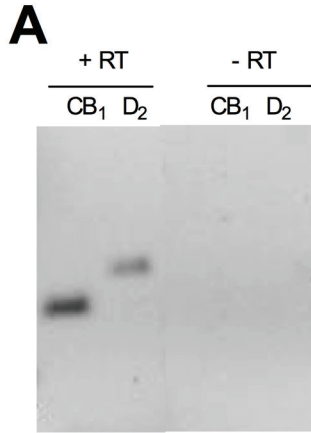
Supplementary Figure 3.2: The Expression of The CB$_1$ blocking peptide (CB$_1$-BP) Did Not Alter the Expression of Rluc and GFP^2 Tagged Receptors. Quantification of the Rluc activity and GFP^2 fluorescence measured in cells expressing of CB$_1$-Rluc and D$_{2L}$-GFP^2 (1:2 ratios) or CB$_1$-Rluc and CB$_1$-GFP^2 (1:2 ratios) together with CB$_1$-BP or pcDNA vector. *n.s.* > 0.05 relative to cells expressing CB$_1$-Rluc, D$_{2L}$-GFP^2 and pcDNA or CB$_1$-Rluc, CB$_1$-GFP^2 and pcDNA. Data are presented as mean ± SEM of four independent experiments, one-way ANOVA followed by Tukey's *post-hoc* test.
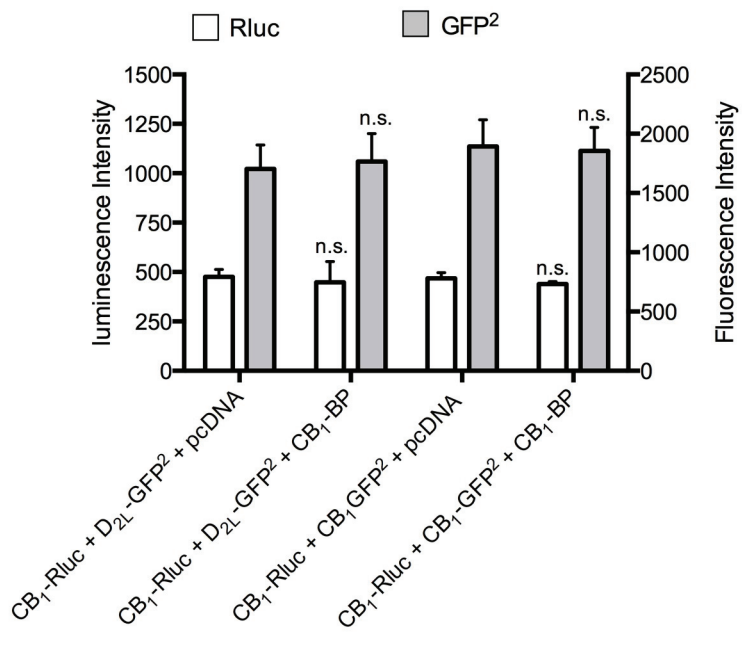
Supplementary Figure 3.3: Similarly to Haloperidol, Sulpiride Reduced ACEA- Induced ERK Phosphorylation. BRET_{Eff} was measured in cells expressing $G\alpha_i$-Rluc and CB_1-GFP^2 +/- with D_{2L}-pcDNA **(A)** or $G\alpha_s$-Rluc and CB_1-GFP^2 +/- with D_{2L}-pcDNA **(C)** and treated with vehicle, 10 µM sulpiride (SULP), 1 µM ACEA +/- 1 µM SULP and pre-treated for 30 min with 0.5 µM O-2050. *n.s.* $P > 0.05$ relative to cells expressing $G\alpha_i$-Rluc and CB_1-GFP^2; $\sim P < 0.01$ relative to cells expressing $G\alpha_i$-Rluc and CB_1-GFP^2 and treated with 1 µM ACEA and 10 µM SULP; * $P < 0.01$ compared to cells treated with vehicle. STH*dh*$^{Q7/Q7}$ cells were treated with 1 µM ACEA +/- 10 µM SULP +/- 24 h pretreatment with 50 ng/ml PTx or CTx and ERK phosphorylation was measured following 5 min treatment **(B),** while CREB phosphorylation was measured following 30 min treatment **(D)**. * $P < 0.01$ compared to vehicle treatment; $\sim P < 0.01$ compared to cells treated with 1 µM ACEA. Data are presented as mean ± SEM of four independent experiments, one-way ANOVA followed by Tukey's *post-hoc* test.

A

Gαi-Rluc + CB$_1$-GFP^2
Gαi-Rluc + CB$_1$-GFP^2 + D$_{2L}$-pcDNA

Vehicle	+	+	-	-	-	-	-	-	-	-
1 μM ACEA	-	-	+	+	-	-	+	+	+	+
10 μM SULP	-	-	-	-	+	+	+	+	+	+
0.5 μM O-2050	-	-	-	-	-	-	-	-	+	+

B

C

Gαs -Rluc + CB$_1$-GFP^2
Gαs -Rluc + CB$_1$-GFP^2 + D$_{2L}$-pcDNA

Vehicle	+	+	-	-	-	-	-	-	-	-
1 μM ACEA	-	-	+	+	-	-	+	+	+	+
10 μM SULP	-	-	-	-	+	+	+	+	+	+
0.5 μM O-2050	-	-	-	-	-	-	-	-	+	+

D

118
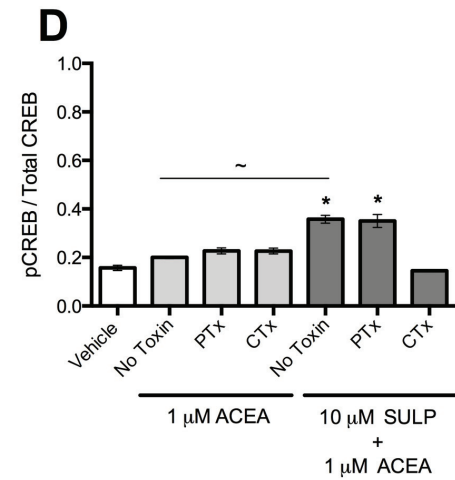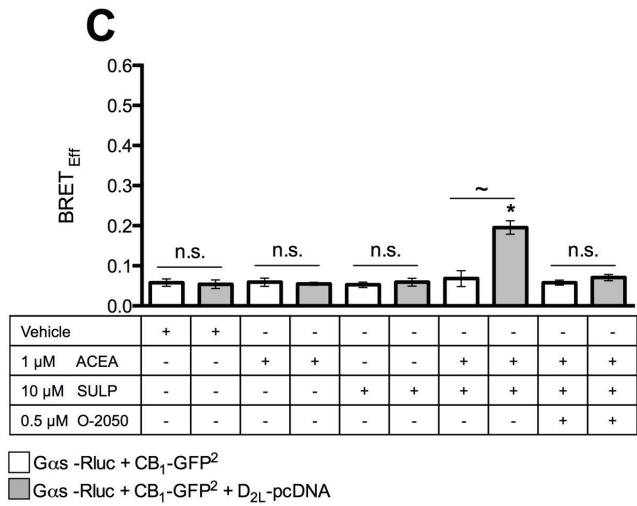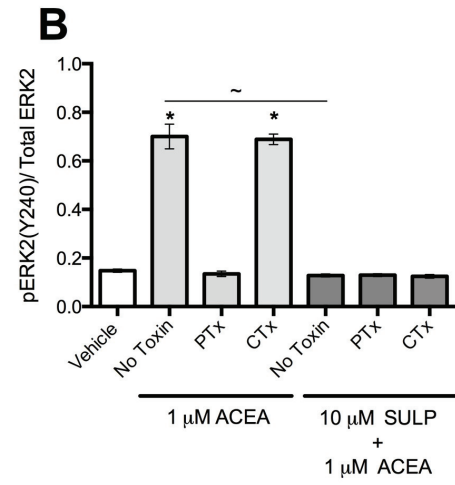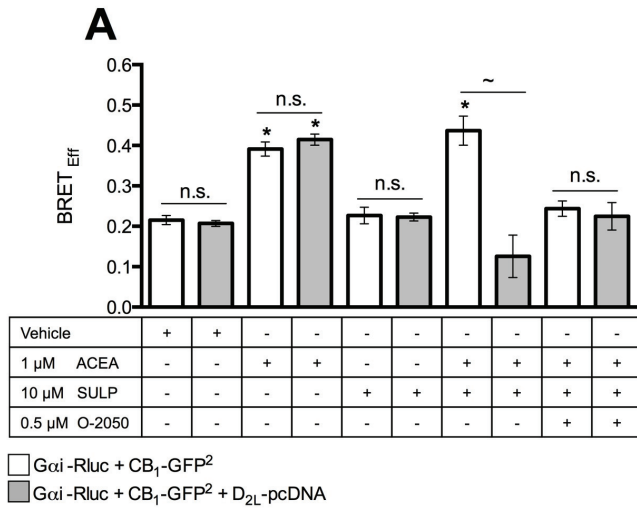
Supplementary Figure 3.4: Haloperidol Inhibited Endogenous CB$_1$ Internalization Following ACEA Treatment. *(**A**)* Time-course analysis of CB$_1$ cell surface expression and total protein levels over 30 min measured using On-Cell Western™ and In-Cell Western™ in cells treated with vehicle, 10 µM HALO, 0.5 µM O-2050 1 µM ACEA +/- 10 µM HALO or 0.5 µM O-2050. * $P < 0.01$ compared with vehicle. **(B)** CB$_1$ cell surface expression measured at 30 min following ligand treatment. * $P < 0.01$ compared with vehicle-treated cells. ~ $P < 0.01$ compared to ACEA-treated cells. Data are presented as mean ± SEM of 4 independent experiments, one-way ANOVA followed by Tukey's *post-hoc* test.

A

B

CHAPTER 4

BIDIRECTIONAL ALLOSTERIC INTERACTIONS BETWEEN CANNABINOID RECEPTOR 1 (CB$_1$) AND DOPAMINE RECEPTOR 2 L (D$_{2L}$) HETEROTETRAMERS

Copyright Statement

Contribution Statement

The manuscript used as the basis for this chapter was written with guidance from Dr. Eileen Denovan-Wright. Data were collected and analyzed by myself. Critical reagents were provided by Drs. Eileen Denovan-Wright and Melanie Kelly.

4.1 Abstract

Type 1 cannabinoid (CB_1) and dopamine 2 long form (D_{2L}) receptors can physically interact to form heteromers that display unique pharmacology *in vitro* compared to homomeric complexes. Co-expression of CB_1 and D_{2L} and co-application of CB_1 and D_2 agonists increases cAMP levels while administration of either agonist alone decreases cAMP levels. To understand the observed co-agonist response, our first goal of the current study was to define the stoichiometry of $CB_1/D_{2L}/G\alpha$ protein complexes. Using bioluminescence resonance energy transfer 2 ($BRET^2$), we confirmed that, CB_1 homodimers, D_{2L} homodimers, and CB_1/D_{2L} heteromers are formed. By using sequential energy transfer 2 ($SRET^2$) combined with bimolecular fluorescence complementation (BiFC), we were able to demonstrate that CB_1/D_{2L} form heterotetramers consisting of CB_1 and D_{2L} homodimers. We demonstrated that CB_1/D_{2L} heterotetramers are coupled to at least two $G\alpha$ proteins. The second aim of the study was to investigate allosteric effects of a D_{2L} agonist (quinpirole) on CB_1 receptor function and to investigate the effects of a CB_1 agonist [arachidonyl-2-chloroethylamide (ACEA)] on D_{2L} receptor function within CB_1/D_{2L} heterotetramers. Treating cells co-expressing CB_1 and D_{2L} with both ACEA and quinpirole switched CB_1 and D_{2L} receptor coupling and signaling from $G\alpha_i$ to $G\alpha_s$ proteins, enhanced β-arrestin1 recruitment and receptor co-internalization. The concept of bidirectional allosteric interaction within CB_1/D_2 heterotetramers has important implications for understanding the activity of receptor complexes in native tissues and under pathological conditions.

4.2 Introduction

It is well established that family A G protein-coupled receptors (GPCRs) can physically associate to form both homo- and hetero-oligomeric complexes (reviewed in Milligan, 2013; Bouvier and Hébert, 2014; Ferré *et al*., 2014, 2015; Gomes *et al.,* 2016; Franco *et al.,* 2016). To date, the evidence suggests that a minimum of two GPCR homodimers interact to form hetero-oligomeric complexes and each GPCR homodimer associates with one G protein within hetero-oligomeric complexes (Han *et al*., 2009; Jastrazebka *et al.,* 2013; Guitart *et al*., 2014; Bonaventura *et al*., 2015; Navarro *et al*., 2016). GPCR oligomerization allosterically induces conformational changes in each

receptor within the complex (Vilardaga *et al.,* 2008; Maier-Peuschel *et al.,* 2010; Bourque *et al.,* 2017; Sleno *et al.,* 2017). Allosteric interactions within hetero-oligomeric complexes result in unique pharmacology compared to homo-oligomeric complexes. Binding of a ligand to one of the GPCR homodimeric partners can modify the affinity or efficacy of ligands for the other GPCR homodimeric unit. Such allosteric modulation may result in positive or negative cooperativity across the heteromeric pairs and alter signaling bias (Kanakin and Christopoulos, 2013; Wootten *et al.,* 2013).

The type 1 cannabinoid receptor (CB_1) and the dopamine receptor 2 long (D_{2L}) can physically interact to form CB_1 and D_{2L} homomers as well as with each other to form CB_1/D_{2L} heteromers (Wager-Miller *et al.,* 2002; Kearn *et al.,* 2005; Guo *et al.,* 2008; Marcellino *et al.,* 2008; Przybyla and Watts 2010; Bagher *et al.,* 2016). Heteromerization between CB_1 and D_{2L} is associated with altered function of hetero- compared to homo-oligomeric complexes. Stimulation of either CB_1 or D_{2L} leads to an inhibition of cAMP *via Pertussis* toxin (PTx)-sensitive $G\alpha_{i/o}$ proteins (Felder *et al.,* 1992; Sibley and Monsma 1992; Demuth and Molleman, 2006). In contrast, co-stimulation of both receptors by their respective agonists leads to an accumulation of cAMP (Glass and Felder, 1997; Kearn *et al.,* 2005; Marcellino *et al.,* 2008; Khan and Lee, 2014; Bagher *et al.,* 2016). Switching in coupling from $G\alpha_i$ to $G\alpha_s$ proteins has been proposed to contribute to the observed increase in cAMP following co-activation of both receptors (Glass and Felder, 1997; Kearn *et al.,* 2005). To date, there is no evidence of a physical association between CB_1/D_{2L} heteromers and $G\alpha_s$ proteins following agonist co-treatment. Similar to other GPCRs, CB_1 and D_{2L} also signal *via* β-arrestins. Both β-arrestin1 (Kim *et al.,* 2001; Bakshi *et al.,* 2007; Amar *et al.,* 2008; Laprairie *et al.,* 2014) and β-arrestin2 (Jin *et al.,* 1999; Kim *et al.,* 2001; Masri *et al.,* 2008; van der Lee *et al.,* 2009; Huang *et al.,* 2013) are recruited to agonist-activated CB_1 and D_{2L} and facilitate receptor internalization and G protein-independent extracellular signal-regulated kinase (ERK) activation (Laprairie *et al.,* 2014). Whether simultaneous treatment with CB_1 and D_{2L} agonists also alters β-arrestin1 recruitment to CB_1/D_{2L} receptor complexes and leads to receptor co-internalization has not been studied.

Given that CB_1/D_{2L} dimerize and that higher order hetero-oligomers are minimally composed of homodimeric pairs, we hypothesized that CB_1 homodimers

selectively dimerize with D_{2L} homodimers and that one $G\alpha_i$ protein couples to the CB_1-homodimer while another $G\alpha_i$ protein couples to D_{2L}-homodimer within CB_1/D_{2L} heterotetramers. We further hypothesized that CB_1/D_{2L} complexes respond differentially to combinations of CB_1- and D_2-selective agonists compared to either agonist alone.

4.3 Results

4.3.1 CB_1 and D_{2L} Form Higher order Heteromers

The first objective of our study was to measure the relative affinities of CB_1 and D_{2L} homomers compared to CB_1/D_{2L} heteromers. $BRET^2$ saturation curves of CB_1 homomers, D_{2L} homomers and CB_1/D_{2L} heteromers were generated. For $BRET^2$ saturation curves, HEK 293A cells were transfected with a constant amount of one Rluc-tagged receptor and increasing amounts of a second GFP^2-tagged receptors. $BRET_{50}$ values obtained from $BRET^2$ saturation curves are indicative of the affinity of receptors to form complexes when they are co-expressed (Guan *et al.,* 2009). The negative control included human mGLuR6, mGLuR6-GFP^2, a family A GPCR that does not interact with CB_1 (Hudson *et al.*, 2010; Bagher *et al.,* 2013). The combination of CB_1-Rluc and mGLuR6-GFP^2 resulted in $BRET_{Eff}$ of 0.08 ± 0.03, which is significantly lower compared to the $BRET_{Eff}$ observed for CB_1 homomers, D_{2L} homomers and CB_1/D_{2L} heteromers (Fig. 4.1A). The CB_1 homomer saturation curve obtained from cells transfected with CB_1-Rluc and CB_1-GFP^2 yielded a $BRET_{50}$ of 0.31 ± 0.05 (Fig. 4.1A, 1B). The D_{2L} homomer saturation curve obtained from cells expressing D_{2L}-Rluc and D_{2L}-GFP^2 resulted in $BRET_{50}$ value of 0.28 ± 0.04 (Fig. 4.1A,B). The CB_1-Rluc and D_{2L}-GFP^2 heteromer saturation curve yielded a $BRET_{50}$ value of 0.27 ± 0.03 (Fig. 4.1A,B). There were no significant differences in $BRET_{50}$ values among CB_1 homomers, D_{2L} homomers and CB_1/D_{2L} heteromers. These findings demonstrated CB_1 and D_{2L} receptors have similar affinities to form both homo and heteromers when expressed in HEK 293A cells.

The oligomerization state of CB_1 and D_{2L} homo- and heteromers were assessed by fitting $BRET^2$ saturation curve values to the mathematical model of Veatch and Stryer model (Eq. 1; Vrecl *et al*., 2006; Drinovec *et al.*, 2012). In our experiments, the *E* values

Figure 4.1: CB₁ and D₂L Receptors Formed Both Homomers and Heteromers When Expressed in HEK 293A Cells Demonstrated Using BRET². (A) BRET^2 saturation curves obtained from cells transiently transfected with CB$_1$-Rluc and CB$_1$-GFP^2, D$_{2L}$-Rluc and D$_{2L}$-GFP^2 or CB$_1$-Rluc and D$_{2L}$ -GFP^2. As a negative control, cells were co-transfected with CB$_1$-Rluc and mGLuR6-GFP^2. BRET$_{Eff}$ was plotted against the ratio of GFP^2 fluorescence and Rluc emission. The data were fit to a rectangular hyperbola. **(B)** BRET$_{Max}$ and BRET$_{50}$ parameters derived from BRET^2 saturation curves. A model curve BRET= BRET$_{Max}$ $(1-1/(E +(1-E)(1+[A]/[D])^N))$ was used, where [D] and [A] are donor and acceptor concentrations, E is energy transfer efficiency and N is oligomerization state (1 = dimer, 2 = trimer, 3=tetramer). Data are presented as mean ± SEM of 4 independent experiments.

A
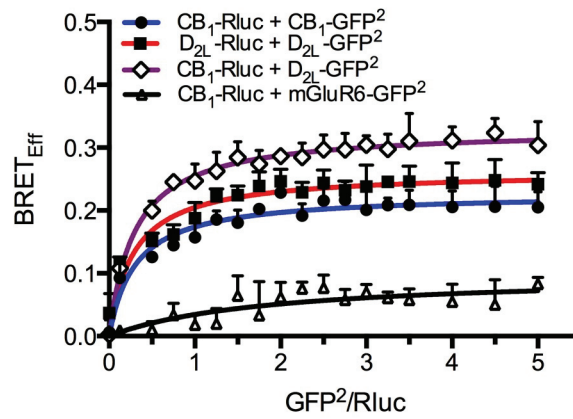
B

Constructs	BRET$_{Max}$	BRET$_{50}$	N	E
CB$_1$-Rluc + CB$_1$-GFP^2	0.23 ± 0.02	0.31 ± 0.05	1.0 ± 0.31	0.18
D$_{2L}$-Rluc + D$_{2L}$-GFP^2	0.26 ± 0.02	0.28 ± 0.04	1.0 ± 0.22	0.20
CB$_1$-Rluc + D$_{2L}$-GFP^2	0.32 ± 0.01	0.27 ± 0.03	2.6 ± 0.24	0.21

were low ($E < 0.2$) and not significantly different for the CB_1 and D_{2L} homo- and heteromers BRET[2] saturation curves (Vrecl *et al.,* 2006; Drinovec *et al.,* 2012). The calculated oligomerization state *(N)* suggested that CB_1 ($N = 1.00 \pm 0.31$) and D_{2L} ($N = 1.0 \pm 0.22$) form mainly homodimers as N is not different from 1 (Fig. 4.1B). In contrast, co-expression of CB_1 and D_{2L} resulted in a calculated oligomerization state value of $N = 2.61 \pm 0.24$ (Fig. 4.1B), which implied that CB_1/D_{2L} heteromers were present as tetramers or higher-order oligomeric complexes.

To directly test the mathematical prediction that CB_1 and D_{2L} homodimers form a heterotetrameric structure, we utilized SRET[2] combined with BiFC (Fig. 4.2A). In this approach, the oxidation of the Rluc substrate coelenterazine 400a by the donor Rluc-fused protein (D_{2L}-Rluc) excites the BRET[2] acceptor GFP[2]-fused protein (D_{2L}-GFP[2]) and emission from GFP[2] then excites the FRET acceptor EYFP Venus. The EYFP Venus acceptor is composed of CB_1 fused to the EYFP Venus N-terminal hemiprotein (CB_1-VN), and CB_1 fused to the EYFP Venus C-terminal hemiprotein (CB_1-VC) (Carriba *et al.,* 2008; Navarro *et al.*, 2013) (Fig. 4.2A).

We first confirmed that EYFP Venus was reconstituted following CB_1 homodimerization using BiFC. An increase in fluorescence was observed when HEK 293A cells were transfected with CB_1-VN and CB_1-VC at 1:1 ratio (Supplementary Fig. 4.1A). In cells expressing only CB_1-VN or CB_1-VC no fluorescence was detected (Supplementary Fig. 4.1A). The reconstitution of functional EYFP in the presence of CB_1-VN and CB_1-VC confirmed that CB_1 forms homodimers when expressed in HEK 293A cells. Using fluorescence microscopy, we observed that the CB_1-VN and CB_1-VC were co-localized with CB_1-GFP[2] (data not shown). The ratio of CB_1-VN and CB_1-VC was kept constant at a ratio of 1:1 for all subsequent experiments.

To test the hypothesis that D_{2L} homodimers associate with CB_1 homodimers to form heterotetramers or higher-order oligomers we generated SRET[2] combined with BiFC saturation curve. We selected the D_{2L}-Rluc and D_{2L}-GFP[2] cDNA ratio that produced the BRET$_{50}$ value calculated from the D_{2L} homodimer saturation curve (Fig. 4.1B). The ratio used for all subsequent experiments was 1:0.5 ratio for D_{2L}-Rluc and D_{2L}-GFP[2]. Higher D_{2L}-Rluc and D_{2L}-GFP[2] ratios resulted in excessive emission and overlap and obscured EYFP Venus emission (data not shown). Cells were transfected

Figure 4.2: CB$_1$ and D$_{2L}$ Receptors Form Heterotetramers in HEK 293A Cells Demonstrated by SRET^2 Combined with BiFC. **(A)** Scheme of SRET^2 combined with BiFC, D$_{2L}$ was tagged with Rluc (D$_{2L}$-Rluc) and GFP^2 (D$_{2L}$-GFP^2), while CB$_1$ was tagged with EYFP Venus N-terminal hemiprotein (CB$_1$- VN) and the EYFP Venus C-terminal hemiprotein (CB$_1$-VC). The oxidation of coelenterazine 400a by Rluc triggers the acceptor GFP^2 excitation by BRET^2 and subsequent energy transfer to the FRET acceptor EYFP Venus. Numbers indicate the peak wavelength of the emitted light. **(B)** SRET^2 saturation curves were obtained using HEK 293A cells transfected with a constant amount of D$_{2L}$-Rluc and D$_{2L}$-GFP^2 (1:0.5) and increasing amounts of EYFP Venus-tagged CB$_1$ (CB$_1$- VN and CB$_1$- VC at 1:1 ratio). Net SRET^2 was plotted against the ratio of EYFP fluorescence and Rluc emission. As a negative control, cells were transfected with equivalent amounts of D$_{2L}$-Rluc + mGluR6-GFP^2, and increasing amounts of EYFP Venus-tagged CB$_1$ (CB$_1$- VN and CB$_1$- VC at 1:1 ratio). **(C)** SRET^2 assays in cells transfected with D$_{2L}$-Rluc, D$_{2L}$-GFP^2, CB$_1$-VN, and CB$_1$-VC or negative controls. * $P <$ 0.01 compared to cells expressing D$_{2L}$-Rluc + mGluR6-GFP^2 + CB$_1$-VN + CB$_1$-VC; ~$P <$ 0.01 compared to cells expressing D$_{2L}$-Rluc + D$_{2L}$-GFP^2 + CB$_1$-VN + CB$_1$-VC. # $P <$ 0.01 compared to cells expressing D$_{2L}$-Rluc, D$_{2L}$-GFP^2, β_2AR-VN, and β_2AR-VC. Data are presented as mean ± SEM of 3 independent experiments, one-way ANOVA followed by Tukey's *post-hoc* test.

A

B

- ● D$_{2L}$-Rluc + D$_{2L}$-GFP^2 + CB$_1$-VN + CB$_1$-VC
- △ D$_{2L}$-Rluc + mGluR6-GFP^2 + CB$_1$-VN + CB$_1$-VC

net SRET^2

EYFP/Rluc

C

net SRET^2
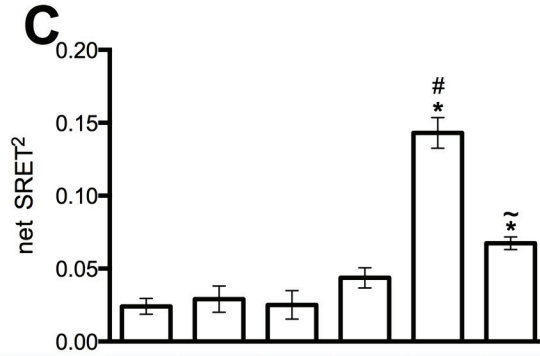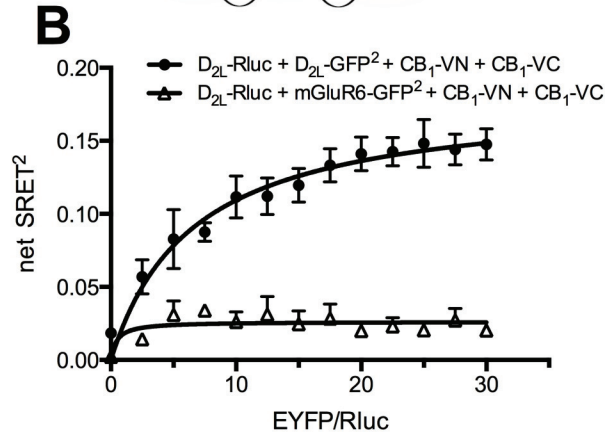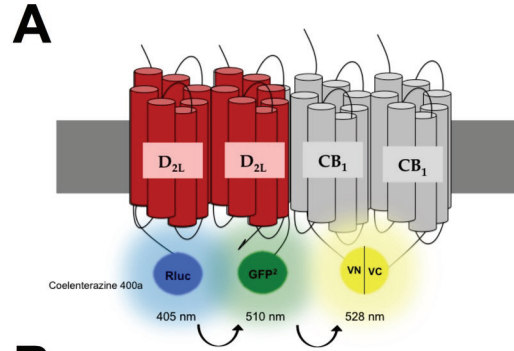
D$_{2L}$-Rluc	+	+	+	+	+	+
D$_{2L}$-GFP^2	-	+	-	+	+	+
CB$_1$-VN	+	-	+	-	+	+
CB$_1$-VC	+	-	+	-	+	+
β$_2$-VN	-	-	-	+	-	-
β$_2$-VC	-	-	-	+	-	-
mGluR6-GFP^2	-	-	+	-	-	-
GFP^2	+	-	-	-	-	-
EYFP	-	+	-	-	-	-
CB$_1$-BP	-	-	-	-	-	+

129

with a constant amount of the D_{2L}-Rluc and D_{2L}-GFP^2 constructs (1:0.5 ratio) and increasing amounts of the constructs encoding the EYFP Venus protein (CB$_1$-VN + CB$_1$-VC, 1:1 ratio) (Fig. 4.2B). Increasing the concentration of EYFP Venus protein (CB$_1$-VN+ CB$_1$-VC) resulted in a hyperbolic increase in net SRET^2. From the saturation curve, we calculated that the SRET$_{Max}$ value for hetero-oligomerization was 0.18 $\pm$ 0.01 and the SRET$_{50}$ value was 6.5 $\pm$ 0.84. As a negative control, cells were transfected with a constant amount of the D_{2L}-Rluc and mGLuR6-GFP^2 (1:0.5 ratio) and increasing concentration of EYFP Venus protein construct (CB$_1$-VN + CB$_1$-VC, 1:1 ratio). Cells expressing the negative controls yielded a weak and non-saturating SRET^2 signal (Fig. 4.2B) demonstrating the lack of specific interaction when mGLuR6 was present. Based on these experiments, we selected the optimal cDNA ratio of 1:0.5:4:4 for D_{2L}-Rluc: D_{2L}-GFP^2: CB$_1$-VN: CB$_1$-VC for subsequent SRET^2 determinations. The SRET^2 efficiency was minimal or negligible when we expressed constructs encoding GFP^2 instead of D_{2L}-GFP^2 or EYFP instead of CB$_1$-VC + CB$_1$-VN (Fig. 4.2C). As a control for the specificity of the interaction between D_{2L} homodimer and CB$_1$ homodimer, we performed SRET^2 combined with BiFC in cells expressing D_{2L} and β_2AR, which do not interact with the D_{2L}. We confirmed, using BiFC, that EYFP Venus can be reconstituted when the β_2AR fused to the EYFP Venus N-terminal hemiprotein (β_2AR-VN) and β_2AR fused to the EYFP Venus C-terminal hemiprotein (β_2AR-VC) were co-expressed in HEK 293A cells (Supplementary Fig. 4.1B). Significant fluorescence was observed in HEK 293A cells transfected with β_2AR-VN and β_2AR-VN, confirming that β_2AR-VN and β_2AR-VN formed β_2AR homodimers in HEK 293A cells (Supplementary Fig. 4.1B) as demonstrated previously (Hammad and Dupré, 2010). Net SRET^2 values were significantly higher between D_{2L} and CB$_1$ compared to D_{2L} and β_2AR indicating that the interaction between D_{2L} and CB$_1$ was selective (Fig. 4.2C). Taken together, our results demonstrate a selective interaction between D_{2L} and CB$_1$ homodimers into oligomeric complexes composed of at least two D_{2L} and two CB$_1$ receptors.

The CB$_1$/D_{2L} hetero-oligomer blocking peptide (CB$_1$-BP) binds to the C-terminal tail of CB$_1$ and blocks the interaction between CB$_1$ and D_{2L}, but not the interactions between CB$_1$ homomers (Khan and Lee, 2014; Bagher *et al.,* 2016). Co-expression of CB$_1$-BP with CB$_1$-VN and CB$_1$-VC did not change EYFP fluorescence observed when

CB$_1$-VN and CB$_1$-VC were expressed alone (Supplementary Fig. 4.1A). In contrast, co-expression of CB$_1$-BP with D$_{2L}$-Rluc + D$_{2L}$-GFP^2 + CB$_1$-VN and CB$_1$-VC interrupting the energy transfer from D$_2$-GFP^2 to EYFP Venus and resulted in significantly lower SRET^2 value compared to cells transfected only with D$_{2L}$-Rluc + D$_{2L}$-GFP^2 + CB$_1$-VN and CB$_1$-VC (Fig. 4.2C). Selective inhibitions of the energy transfer between D$_{2L}$ and CB$_1$ constructs demonstrated that CB$_1$-BP interferes with the formation of CB$_1$/D$_{2L}$ hetero-oligomers without interrupting the formation of CB$_1$ homodimers. Although we acknowledge that higher order structures are possible, these experiments define the minimum complex of D$_{2L}$ and CB$_1$ receptors as being a heterotetramer composed at least one D$_{2L}$ and one CB$_1$ homodimer.

4.3.2 CB$_1$/D$_{2L}$ Receptors Form Heterotetramers Consisting of CB$_1$ and D$_{2L}$ Homomers in Complex with at Least Two Gα Proteins

Based on our finding that CB$_1$/D$_{2L}$ minimally form heterotetramers and recent studies that suggested that GPCRs form heterotetramers in complex with two Gα proteins (Navarro *et al.,* 2016), we hypothesized that one Gα$_i$ protein couples to a CB$_1$ homodimer while another Gα$_i$ protein couples to a D$_{2L}$-homodimer within CB$_1$/D$_{2L}$ heterotetramers. The interaction between Gα$_i$ and CB$_1$ was studied using BRET^2. Higher BRET$_{Eff}$ signals were observed between Gα$_i$-Rluc and CB$_1$-GFP^2 compared to BRET$_{Eff}$ obtained from cells transfected with Gα$_i$-Rluc and β$_2$AR (Fig. 4.3A). The β$_2$AR receptor is known to pre-assemble with Gα$_s$ (Lachance *et al.*, 1999; Galés *et al.*, 2005). Such an increase in BRET$_{Eff}$ was insensitive to 24 hr PTx treatment. PTx inhibits the activity and dissociation of Gα$_i$ following ligand-dependent activation or constitutive activity of GPCRs (Ayoub *et al.,* 2007). PTx does not inhibit the physical association of Gα$_i$ with GPCRs (Ayoub *et al.,* 2010). As PTx did not inhibit the association between Gα$_i$-Rluc and CB$_1$-GFP^2, the increase in BRET$_{Eff}$ was not due to constitutive activation of CB$_1$ receptors (Fig. 4.3A). This data confirmed that CB$_1$ receptors are pre-assembled with Gα$_i$ protein (Demuth and Molleman, 2006). BRET^2 saturation curve was generated to determine that the interaction between Gα$_i$-Rluc and CB$_1$-GFP^2 (data not shown). The CB$_1$ agonist ACEA (1 μM) increased the observed BRET$_{Eff}$ between Gα$_i$-Rluc and CB$_1$-GFP^2 compared to the BRET$_{Eff}$ observed in vehicle-treated cells (Fig. 4.3A). The increase

Figure 4.3 CB₁/D₂ₗ Heterotetramers are Pre-Coupled to Gαᵢ Proteins. **(A)** BRET$_{Eff}$ was measured in cells expressing with CB_1-GFP^2 and $G\alpha_i$-Rluc +/- un-tagged D_{2L}-pcDNA following the addition of vehicle, 1 μM ACEA, 1 μM quinpirole and pre-treated for 24 hr min with 50 ng/ml PTx.; * $P < 0.01$ compared to cells expressing only $G\alpha_i$-Rluc and HERG- GFP^2; ~ $P < 0.01$ relative to cells expressing only $G\alpha_i$-Rluc and CB_1-GFP^2 and treated with 1μM quinpirole; *n.s.* $P > 0.05$ compared to cells expressing $G\alpha i$-Rluc and CB_1-GFP^2 only. **(B)** Scheme of $BRET^2$. A more efficient energy transfer was observed between $G\alpha_i$-Rluc and CB_1-GFP^2 in the presence of un-tagged D_{2L} following CB_1 agonist treatment compared to D_{2L} agonist treatment. **(C)** BRET$_{Eff}$ was measured in cells expressing $G\alpha_i$-Rluc and D_{2L}-GFP^2 +/- un-tagged CB_1-pcDNA following the addition of vehicle, 1 μM quinpirole, 1 μM ACEA and pre-treated for 24 hr min 50 ng/ml PTx. * $P < 0.01$ compared to cells expressing $G\alpha_i$-Rluc and β_2-GFP^2; ~ $P < 0.01$ relative to cells expressing $G\alpha_i$-Rluc and D_{2L}-GFP^2 only and treated with 1μM ACEA; *n.s.* $P > 0.05$ compared to cells expressing only $G\alpha_i$-Rluc and D_{2L}-GFP^2. **(D)** Scheme of $BRET^2$. A more efficient energy transfer was observed between $G\alpha_i$-Rluc and D_{2L}-GFP^2 in the presence of un-tagged CB_1 following D_{2L} agonist treatment compared to CB_1 agonist treatment. Data are presented as mean ± SEM of 3 independent experiments, one-way ANOVA followed by Tukey's *post-hoc* test.

A CB$_1$-GFP^2 + Gαi-Rluc +/- D$_{2L}$-pcDNA

Vehicle	+	+	+	+	+	-	-	-	-	-	-	-	-	-
1 μM ACEA	-	-	-	-	-	+	+	+	+	-	-	-	-	-
1 μM Quinpirole	-	-	-	-	-	-	-	-	-	+	+	+	+
50 ng/mL PTx	-	-	-	+	+	-	-	+	+	-	-	+	+

■ Gαi -Rluc + β$_2$-GFP^2
□ Gαi -Rluc + CB$_1$-GFP^2
▨ Gαi -Rluc + CB$_1$-GFP^2 + D$_{2L}$-pcDNA

C D$_{2L}$-GFP^2 + Gαi-Rluc +/- CB$_1$-pcDNA

Vehicle	+	+	+	+	+	-	-	-	-	-	-	-	-	-
1 μM ACEA	-	-	-	-	-	-	-	-	-	+	+	+	+
1 μM Quinpirole	-	-	-	-	-	+	+	+	+	-	-	-	-
50 ng/mL PTx	-	-	-	+	+	-	-	+	+	-	-	+	+

■ Gαi -Rluc + β$_2$-GFP^2
□ Gαi -Rluc + D$_{2L}$-GFP^2
▨ Gαi -Rluc + D$_{2L}$-GFP^2 + CB$_1$-pcDNA

B

D

133
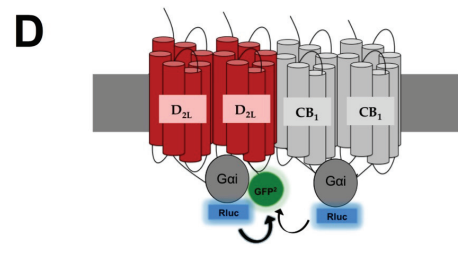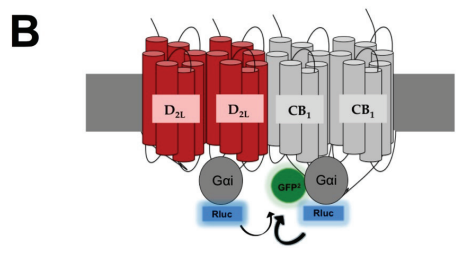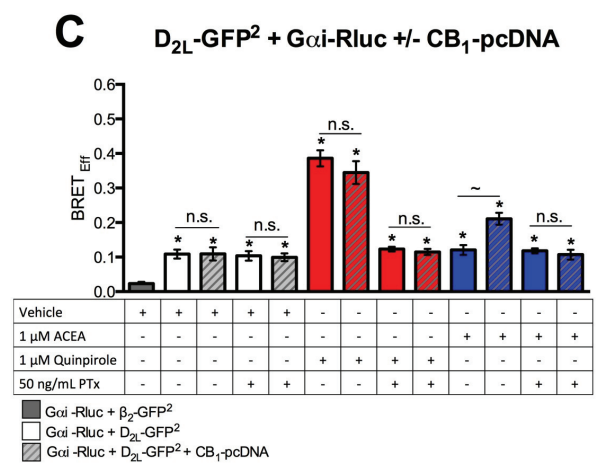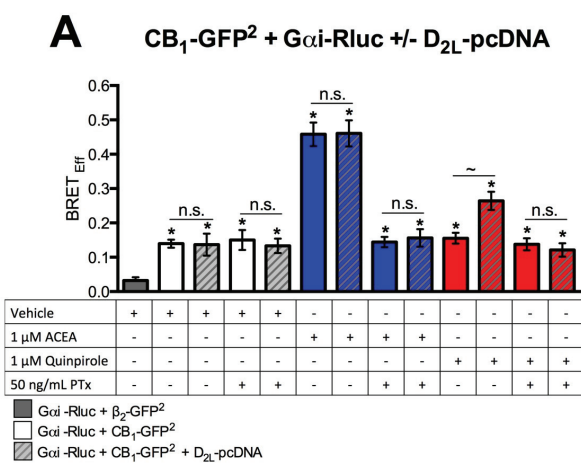
in $BRET_{Eff}$ following ACEA application was rapid and transient; $BRET_{Eff}$ peaked at ~125 sec following ACEA application and remained significantly elevated for ~ 400 sec before declining (Supplementary Fig. 4.2A) (Bagher *et al.,* 2016). Therefore, all $BRET_{Eff}$ measured between $G\alpha_i$-Rluc and CB_1-GFP^2 was performed ~125 sec following ligand application. CB_1 agonism stabilized the conformation of CB_1/$G\alpha_i$ increasing maximal energy transfer in the $BRET^2$ assay. The co-expression of un-tagged D_{2L}-pcDNA receptors did not alter the interaction between CB_1 and $G\alpha_i$ in the presence of vehicle or ACEA (Fig. 4.3A). Regardless of the presence of un-tagged D_{2L}-pcDNA, PTx blocked ACEA-dependent increases in $BRET_{Eff}$ demonstrating that ACEA was acting on the $G\alpha_i$-coupled CB_1 receptor (Fig. 4.3A). A more efficient energy transfer was observed between $G\alpha_i$-Rluc and CB_1-GFP^2 only in the presence of un-tagged D_{2L} and the D_2 agonist (quinpirole 1 μM) treatment (Fig. 4.3A,B); this increase in $BRET_{Eff}$ was PTx-sensitive. Together these observations indicate that CB_1 was pre-assembled with $G\alpha_i$ proteins and that treating cells expressing both CB_1 and D_{2L} receptors with either CB_1 or D_2 agonists increased $BRET_{Eff}$ signals between $G\alpha_i$ protein and CB_1 (Fig. 4.3B).

Next, the interaction between $G\alpha_i$-Rluc and D_{2L}-GFP^2 was studied using $BRET^2$ (Fig. 4.3C). Co-expression of $G\alpha_i$-Rluc and D_{2L}-GFP^2 resulted in an increase in $BRET_{Eff}$, which was insensitive to PTx treatment (Fig. 3.3C) indicating that D_{2L} was pre-assembled with $G\alpha_i$ proteins. Treating the cells with the D_2 agonist quinpirole (1 μM) resulted in a rapid and transient increase in $BRET_{Eff}$, which was indicative of D_{2L} receptors activation (Fig. 4.3C; Supplementary Fig. 4.2C) Therefore, all $BRET_{Eff}$ measured between $G\alpha_i$-Rluc and D_{2L}-GFP^2 was performed ~120 sec following ligand application. Co-expression of un-tagged CB_1-pcDNA receptors did not alter $BRET_{Eff}$ between $G\alpha_i$-Rluc and D_{2L}-GFP^2 in the presence of vehicle or quinpirole (Fig. 4.3C). A more efficient energy transfer was observed between $G\alpha_i$-Rluc and D_{2L}-GFP^2 in the presence of un-tagged CB_1 and with D_{2L} agonist treatment compared to CB_1 agonist treatment (Fig. 4.3C,D). These data indicate that CB_1/D_{2L}/$G\alpha_i$ proteins formed functional complexes composed of at least two homodimers each associated with a $G\alpha_i$ protein. Agonists of either homodimer activated the $G\alpha_i$ protein associated with the cognate receptor pair and the $G\alpha_i$ protein associated with the complexed heterodimer (Fig. 4.3D).

To determine the number of $G\alpha_i$ proteins a CB_1/D_{2L} complex, we cloned a

blocking peptide that specifically binds to the CB_1 third intracellular loop, CB_1 amino acids 316-344 (CB_1-$G\alpha_i$-BP), and compete for the association between CB_1 with $G\alpha_i$, but not the association between D_{2L} and CB_1 receptors (Mukhopadhyay and Howlett, 2001) (Fig. 4.4A). Co-expression of CB_1-$G\alpha_i$-BP together with $G\alpha_i$-Rluc, CB_1-GFP^2, un-tagged D_{2L}-pcDNA significantly reduced $BRET_{Eff}$ between $G\alpha_i$-Rluc and CB_1-GFP^2 in vehicle- and ACEA-treated cells compared to cells co-expressing $G\alpha_i$-Rluc, CB_1-GFP^2, un-tagged D_{2L}-pcDNA and empty pcDNA instead of the CB_1-$G\alpha_i$-BP (Fig. 4.4B). The reduction in $BRET_{Eff}$ indicated that the CB_1-$G\alpha_i$-BP inhibited the binding of $G\alpha_i$ to CB_1 receptors (Fig. 4.4A). There was no difference in the energy transfer between $G\alpha_i$-Rluc and CB_1-GFP^2 in quinpirole-treated cells in the presence or absence of CB_1-$G\alpha_i$-BP (Fig. 4.4B). Because quinpirole increased the $BRET_{Eff}$ between $G\alpha_i$-Rluc and CB_1-GFP^2 compared to vehicle treatment, we concluded that weak energy transfer was occurring between $G\alpha_i$-Rluc bound to the un-tagged D_{2L} receptors to the CB_1-GFP^2 within CB_1/D_{2L}/$G\alpha_i$ complexes (Fig. 4.4B). When $BRET^2$ was measured between $G\alpha_i$-Rluc and D_{2L}-GFP^2 in the presence of un-tagged CB_1 receptors (Fig. 4.4C), energy transfer between $G\alpha_i$-Rluc and D_{2L}-GFP^2 was unaffected by the co-expression CB_1-$G\alpha_i$-BP in vehicle- or quinpirole- treated cells compared to cells not expressing CB_1-$G\alpha_i$-BP (Fig. 4.4D). A weak energy transfer from $G\alpha_i$-Rluc and D_{2L}-GFP^2 in ACEA treated cells was detected; however, the expression of CB_1-$G\alpha_i$-BP significantly reduced $BRET_{Eff}$ to level that was the same as the level of vehicle-treated cells (Fig. 4.4D). Therefore, limited energy transfer was occurring between $G\alpha_i$-Rluc bound to un-tagged CB_1 receptors and D_{2L}-GFP^2 within CB_1/D_{2L}/$G\alpha_i$ complexes (Fig. 4.4D). To confirm that the expression of the CB_1-$G\alpha_i$-BP did not alter the ability of the CB_1 and D_{2L} receptors to form heterotetramers, we performed $SRET^2$ combined with BiFC in the presence of CB_1-$G\alpha_i$-BP. We found that blocking the interaction between CB_1 and $G\alpha_i$ using the CB_1-$G\alpha_i$-BP did not alter net $SRET^2$ values (Supplementary Fig. 4.3A). Overall, these results are consistent with the hypothesis that CB_1/D_{2L} formed functional heterotetramers that are coupled to at least two $G\alpha_i$ proteins. Application of CB_1 or D_2 agonists activated the $G\alpha_i$ protein associated with the cognate homodimer and weakly activated the $G\alpha_i$ protein associated with the associated heteromer within the CB_1/D_{2L}/$G\alpha_i$ complex (Fig. 4.4A,B).

Figure 4.4: CB₁/D₂L Heterotetramers are Coupled to Two Gαᵢ Proteins. **(A)** Scheme of BRET^2, CB$_1$ was tagged with GFP^2 (CB$_1$-GFP^2), Gα$_i$ was tagged with Rluc (Gα$_i$-Rluc) while D$_{2L}$ was un-tagged (D$_{2L}$-pcDNA) expressed together with CB$_1$-Gα$_i$-BP. **(B)** HEK 293A cells expressing CB$_1$-GFP^2, Gα$_i$-Rluc and un-tagged D$_{2L}$-pcDNA with an empty pcDNA vector or CB$_1$-Gα$_i$-BP. BRET$_{Eff}$ was measured following treatment with vehicle, 1 μM ACEA or 1 μM quinpirole. * $P < 0.01$ compared to cells expressing Gα$_i$-Rluc, CB$_1$-GFP^2, D$_{2L}$-pcDNA and an empty pcDNA vector and treated with vehicle. ~$P < 0.01$ compared to cells expressing Gα$_i$-Rluc, CB$_1$-GFP^2, D$_{2L}$-pcDNA and an empty pcDNA vector within the vehicle and ACEA treatment group. **(C)** Scheme of BRET^2, D$_{2L}$ was tagged with GFP^2 (D$_{2L}$ -GFP^2), Gα$_i$ was tagged with Rluc (Gα$_i$-Rluc) while CB$_1$ was un-tagged (CB$_1$-pcDNA**)** together with CB$_1$-Gα$_i$-BP. **(D)** HEK 293A cells expressing D$_{2L}$-GFP^2, Gα$_i$-Rluc and un-tagged CB$_1$-pcDNA with an empty pcDNA vector or CB$_1$-Gα$_i$-BP. BRET$_{Eff}$ was measured following treatment with vehicle, 1 μM ACEA or 1 μM quinpirole. * $P < 0.01$ compared to cells expressing Gα$_i$-Rluc, D$_{2L}$-GFP^2, CB$_1$-pcDNA and an empty pcDNA vector and treated with vehicle. ~$P < 0.01$ compared to cells expressing Gα$_i$-Rluc, D$_{2L}$-GFP^2, CB$_1$-pcDNA and an empty pcDNA vector and treated with ACEA. *n.s.* > 0.05 compared to cells expressing Gα$_i$-Rluc, D$_{2L}$-GFP^2, CB$_1$-pcDNA and an empty pcDNA vector within the vehicle and quinpirole treatment group. Data are presented as mean ± SEM of 3 independent experiments, one-way ANOVA followed by Tukey's *post-hoc* test.

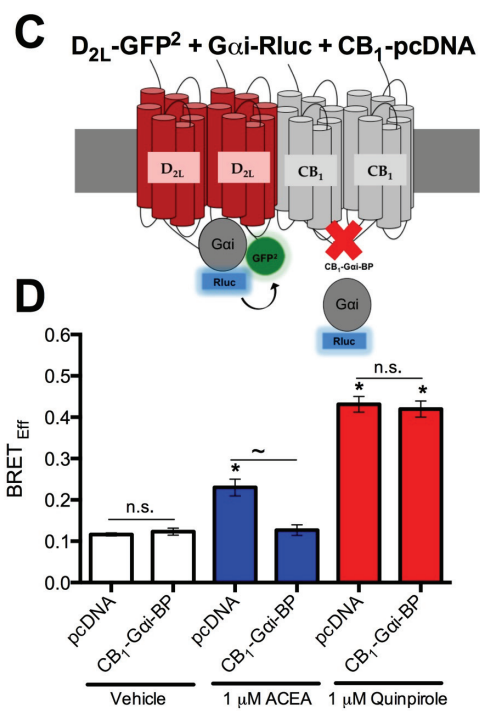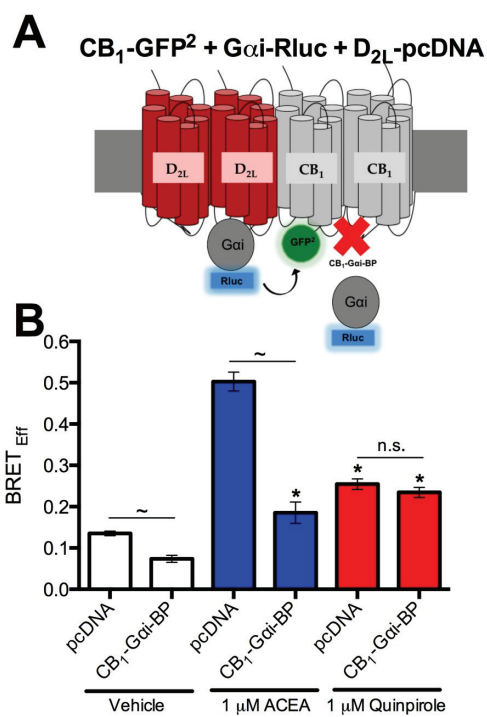**A** CB$_1$-GFP^2 + Gαi-Rluc + D$_{2L}$-pcDNA

C D$_{2L}$-GFP^2 + Gαi-Rluc + CB$_1$-pcDNA

137

4.3.3 CB$_1$ and D$_2$ Receptor Agonists Allosterically Modulate Interaction Between CB$_1$/D$_{2L}$/Gα Proteins

Co-activation of CB$_1$ and D$_2$ receptors with CB$_1$ and D$_2$ agonists resulted in an increase in cAMP production while activation of either receptor leads to a decrease in cAMP production. Given that we observed pre-association of CB$_1$/D$_{2L}$/Gα$_i$ complexes, we hypothesized that co-activation of both CB$_1$ and D$_2$ receptor complexes would either uncouple Gα$_i$ from the complex or switch coupling of CB$_1$/D$_{2L}$ complexes from Gα$_i$ to Gα$_s$. Our next objective was to determine if CB$_1$/D$_{2L}$/Gα$_i$ receptor complexes are involved in agonist-dependent Gα protein uncoupling or switching. In cells co-expressing Gα$_i$-Rluc, CB$_1$-GFP^2 and un-tagged D$_{2L}$ (Fig. 4.5A), increasing concentrations of the CB$_1$ agonist ACEA resulted in concentration-dependent Gα$_i$ activation and an increase in BRET$_{Eff}$ signals between Gα$_i$-Rluc and CB$_1$-GFP^2 [EC$_{50}$ = 0.15 μM (0.11-0.23), E_{Max} = 0.51 (0.45-0.56), Hill coefficient= 1.00 (0.88-1.37] (Fig 4.5.B). This suggests that ACEA promoted conformational changes within the Gα$_i$-Rluc/CB$_1$-GFP^2/D$_{2L}$ complexes leading to Gα$_i$ protein activation. Treating the cells with quinpirole resulted in a concentration-dependent increase in BRET$_{Eff}$ signals between Gα$_i$-Rluc and CB$_1$-GFP^2 (Fig. 4.5B) [EC$_{50}$ = 0.016 μM (0.014-0.019)] as expected given that we had observed energy transfer from the heterodimer partner (Fig. 4.4B). However, quinpirole treatment resulted in significantly lower E_{Max} [0.22 (0.21-0.24)], compared to ACEA treated cells (Fig. 4.5B). Treating the cells with 1 μM ACEA and increasing concentrations of the quinpirole resulted in concentration-dependent inhibition in BRET$_{Eff}$ between Gα$_i$-Rluc and CB$_1$-GFP^2 (Fig. 4.5B). This observation suggested that quinpirole binding to D$_{2L}$ inhibited the interaction between Gα$_i$ and CB$_1$. Quinpirole inhibition of this interaction was concentration-dependent (Fig. 4.5B). Higher quinpirole concentrations led to lower BRET$_{Eff}$ signals between Gα$_i$-Rluc and CB$_1$-GFP^2. In the absence of D$_{2L}$, increasing concentrations of quinpirole had no effect on BRET$_{Eff}$ between Gα$_i$-Rluc and CB$_1$-GFP^2 in the presence of 1 μM ACEA (data not shown). These findings indicate that quinpirole was not acting directly on CB$_1$ to mediate its effects but rather the effect was dependent on the presence of the D$_{2L}$ receptor. The influence of different concentrations of quinpirole (0.001-1 μM) on ACEA-induced BRET$_{Eff}$ between Gα$_i$-Rluc and CB$_1$-GFP^2 was then assessed (Fig. 4.5C; Table 4.1). Quinpirole produced a concentration-

Figure 4.5: Bidirectional Allosteric Inhibition of CB_1/D_{2L} Heterotetramer Interactions with $G\alpha_i$ Following CB_1 and D_{2L} Agonists Treatment. **(A)** Scheme of $BRET^2$, CB_1 was tagged with GFP^2 (CB_1-GFP^2), $G\alpha_i$ was tagged with Rluc ($G\alpha_i$-Rluc) while D_{2L} was un-tagged (D_{2L}-pcDNA). **(B)** Concentration-response curves of ACEA and quinpirole +/- 1 μM ACEA- induced $BRET_{Eff}$ between $G\alpha_i$-Rluc and CB_1-GFP^2 in the presence of D_{2L}-pcDNA. **(C)** Concentration-response curves of ACEA- induced $BRET_{Eff}$ between $G\alpha_i$-Rluc and CB_1-GFP^2 +/- different concentrations of quinpirole in the presence of D_{2L}-pcDNA. **(D)** Scheme of $BRET^2$, D_{2L} was tagged with GFP^2 (D_{2L}-GFP^2), $G\alpha_i$ was tagged with Rluc ($G\alpha_i$-Rluc) while CB_1 was un-tagged (CB_1-pcDNA). **(E)** Concentration-response curves of quinpirole and ACEA ± 1 μM quinpirole-induced $BRET_{Eff}$ between $G\alpha_i$-Rluc and D_{2L} -GFP^2 in the presence of CB_1-pcDNA. **(F)** Concentration-response curves of quinpirole- induced $BRET_{Eff}$ between $G\alpha_i$-Rluc and D_{2L} -GFP^2 ± different concentrations of ACEA in the presence of CB_1-pcDNA . Data are presented as mean ± SEM of 4 independent experiments.

A CB$_1$-GFP^2 + Gαi-Rluc + D$_{2L}$-pcDNA

B
ACEA
Quinpirole
Quinpirole + 1 μM ACEA
Vehicle

C
[Quinpirole] μM
0.000
0.001
0.010
0.100
1.000

D D$_{2L}$-GFP^2 + Gαi-Rluc + CB$_1$-pcDNA

E
ACEA
Quinpirole
ACEA + 1 μM Quinpirole
Vehicle

F
[ACEA] μM
0.000
0.001
0.010
0.100
1.000

dependent rightward and downward shift in the ACEA concentration-response curves (Fig. 4.5C). Both the efficacy and the potency of ACEA dependent $G\alpha_i$-CB_1 interaction were diminished by quinpirole. The increase in EC_{50} and the decrease in E_{Max} for ACEA concentration-response curves were significant at all concentrations of quinpirole tested (Fig. 4.5C; Table 4.1). The Hill coefficient was significantly less than 1 at 0.1 and 1 μM quinpirole for ACEA-concentration-response curves (Table 4.1), suggesting that quinpirole exerts negative cooperativity on CB_1 to $G\alpha_i$ interaction within CB_1/D_{2L} complexes.

Next, the effects of expression and activation of un-tagged CB_1 receptors (CB_1-pcDNA) on the interaction and activation of $G\alpha_i$ and D_{2L} was examined (Fig. 4.5D). Quinpirole treatment resulted in concentration-dependent increase in $BRET_{Eff}$ between $G\alpha_i$-Rluc and D_{2L}-GFP^2 [EC_{50} = 0.02 μM (0.01-0.03), E_{Max} = 0.39 (0.36-0.42), Hill coefficient= 1.16 (0.98-1.23)] (Fig. 4.5E). ACEA treatment alone resulted in an E_{Max} of 0.22 (0.19-0.25), which was significantly higher compared to vehicle-treated cells, but lower compared to quinpirole-treated cells. A reduction in $BRET_{Eff}$ signals between $G\alpha_i$-Rluc and D_{2L}-GFP^2 was observed in cells treated with 1 μM quinpirole and increasing concentrations of ACEA (Fig. 4.5E). The effects of different concentrations of ACEA on quipirole concentration-response curve were tested (Fig. 4.5F; Table 4.2). ACEA concentrations higher than 0.1 μM increased the EC_{50} and reduced both the E_{Max} and the Hill coefficient of quinpirole concentration-response curves (Fig. 4.5F; Table 4.2). This effect was dependent on the co-expression of CB_1 receptors (data not shown). ACEA allosterically inhibited the interaction between $G\alpha_i$ and D_{2L} through binding to CB_1 only in the presence of quinpirole.

The reduction in $BRET_{Eff}$ signals between CB_1 and $G\alpha_i$ protein or between D_{2L} and $G\alpha_i$ protein following co-treatment with both ACEA and quinpirole suggested that CB_1 and D_{2L} homodimers are dissociated from $G\alpha_i$ proteins within CB_1/D_{2L} heterotetramers. First, using $BRET^2$ we examined whether the CB_1 couples to $G\alpha_s$ protein (Supplementary Fig. 4.4A). No significant $BRET_{Eff}$ signals were observed between $G\alpha_s$-Rluc and CB_1-GFP^2 in vehicle-treated cells compared to the negative control obtained from cells transfected with $G\alpha_s$-Rluc and HERG-GFP^2, indicating that CB_1 does not interact with $G\alpha_s$ in the absence of ligand (Supplementary Fig. 4.4A). The negative

Table 4.1: The Effects of Quinpirole on BRET^2 (Gαi- Rluc and CB$_1$-GFP^2), Gαi-Dependent ERK Phosphorylation, BRET^2 (Gαs-Rluc and CB$_1$-GFP^2), Gα-Dependent CREB Phosphorylation, BRET^2 (β-arrestin1 - Rluc and CB$_1$-GFP^2). Data were determined using nonlinear regression with variable slope (four parameters) analysis. Data are presented as the mean and 95% confidence interval (CI) for four independent experiments. * $P < 0.01$, compared with vehicle; one-way ANOVA with Tukey's multiple comparison test.

Agonist	Quinpirole nM	EC_{50} nM (95% CI)	E_{max} (95% CI)	Hill coefficient (95% CI)
BRET² (Gαi-Rluc + CB₁-GFP²)				
ACEA	0	150 (110-230)	0.51 (0.45-0.56)	1.00 (0.88-1.37)
	1	250 (210-360)*	0.39 (0.37-0.41)*	0.93 (0.65-1.12)
	10	340 (300-410)*	0.26 (0.24-0.28)*	0.85 (0.65-0.95)
	100	640 (450-840)*	0.16 (0.14-0.19)*	0.61 (0.53-0.86)*
	1000	710 (680-923)*	0.12 (0.01-0.15)*	0.55 (0.30-0.74)*
BRET² (Gαs-Rluc + CB₁-GFP²)				
ACEA	0	380 (350-440)	0.10 (0.09-0.14)	0.68 (0.59-0.89)
	1	290 (234-320)*	0.13 (0.10-0.12)	1.13 (1.00-1.34)*
	10	200 (215-250)*	0.21 (0.18-0.23)*	1.14 (1.12-1.23)*
	100	180 (176-243)*	0.31 (0.28-0.32)*	1.34 (1.20-1.61)*
	1000	150 (155-223)*	0.39 (0.37-0.42)*	1.77 (1.68-2.13)*
Gαi-dependent ERK phosphorylation				
ACEA	0	160 (140-260)	0.81 (0.74-0.85)	1.01 (0.76-1.4)
	1	180 (160-201)	0.64 (0.61-0.67)*	1.02 (0.99-1.05)
	10	325 (298-356)*	0.45 (0.42-0.49)*	0.91 (0.65-0.90)
	100	540 (490-560)*	0.22 (0.16-0.27)*	0.69 (0.57-0.75)*
	1000	711 (590-743)*	0.17 (0.11-0.16)*	0.65 (0.51-0.71)*
Gαs-dependent CREB phosphorylation				
ACEA	0	390 (355-465)	0.19 (0.16-0.17)	0.81 (0.78-0.89)
	1	260 (246-304)*	0.37 (0.31-0.39)*	1.41 (1.11-1.90)*
	10	190 (108-177)*	0.52 (0.49-0.54)*	1.80 (1.34-2.13)*
	100	160 (154-203)*	0.74 (0.60-0.84)*	1.71 (1.53-2.3)*
	1000	150 (135-183)*	0.86 (0.97-0.79)*	1.77 (1.68-2.02)*
BRET² (β-arrestin1 – Rluc + CB₁-GFP²)				
ACEA	0	220 (190-258)	0.60 (0.58-0.64)	1.20 (0.91-1.41)
	1	200 (210-0.27)	0.67 (0.65-0.69)*	1.40 (1.03-1.79)
	10	180 (148-200)	0.72 (0.69-0.75)*	1.43 (1.21-1.96)
	100	153 (120-181)*	0.76 (0.73-0.79)*	1.65 (1.32-2.07)
	1000	112 (100-160)*	0.78 (0.75-0.82)*	1.75 (1.32-2.18)

Table 4.2: The Effects of ACEA on BRET^2 (Gα_i- Rluc and D$_{2L}$-GFP^2), Gα_i-Dependent ERK Phosphorylation, BRET^2 (Gα_s-Rluc and D$_{2L}$-GFP^2), Gα_s-Dependent CREB Phosphorylation, BRET^2 (D$_{2L}$-Rluc and β-arrestin1 -GFP^2). Data were determined using nonlinear regression with variable slope (four parameters) analysis. Data are presented as the mean and 95% confidence interval (CI) for four independent experiments. * $P < 0.01$, compared with vehicle; one-way ANOVA followed by a Tukey's with *post-hoc* test.

Agonist	ACEA nM	EC_{50} nM (95% CI)	Emax (95% CI)	Hill coefficient (95% CI)
BRET^2 (Gαi-Rluc + D$_{2L}$-GFP^2)				
Quinpirole	0	19 (14-26)	0.39 (0.36-0.42)	1.16 (0.98-1.23)
	1	21 (19-32)	0.36 (0.33-0.39)	1.13 (0.99-1.05)
	10	28 (23-38)	0.27 (0.25-0.30)*	0.78 (0.65-0.90)*
	100	75 (65-81)*	0.20 (0.18-0.23)*	0.73 (0.70-0.78)*
	1000	98 (79-112)*	0.14 (0.12-0.16)*	0.69 (0.58-0.79)*
BRET^2 (Gαs-Rluc + D$_{2L}$-GFP^2)				
Quinpirole	0	99 (90-135)	0.11 (0.09-0.12)	0.58 (0.51-0.64)
	1	92 (81-98)	0.15 (0.13-0.18)*	0.83 (0.71-0.98)*
	10	57 (50-65)*	0.25 (0.22-0.27)*	1.23 (1.00-1.42)*
	100	26 (24-32)*	0.30 (0.28-0.33)*	1.64 (1.23-1.85)*
	1000	21 (12-23)*	0.35 (0.32-0.37)*	1.81 (1.92-2.12)*
Gαi-dependent ERK phosphorylation				
Quinpirole	0	22 (15-23)	0.82 (0.79-0.85)	1.01 (0.98-1.23)
	1	25 (15-28)*	0.75 (0.72-0.79)	0.95 (0.99-1.05)
	10	26 (24-32)*	0.58 (0.56-0.60)*	0.90 (0.65-0.90)
	100	78 (56-82)*	0.43 (0.41-0.46)*	0.82 (0.73-0.90)*
	1000	92 (98-89)*	0.21 (0.19-0.23)*	0.78 (0.62-0.79)*
Gαs-dependent CREB phosphorylation				
Quinpirole	0	81 (76-89)	0.19 (0.18-0.21)	0.58 (0.51-0.63)
	1	71 (57-78)	0.26 (0.25-0.27)	0.69 (0.64-0.79)
	10	50 (35-61)*	0.45 (0.43-0.48)*	0.91 (1.02-0.98)*
	100	19 (15-23)*	0.67 (0.63-0.72)*	1.36 (1.12-1.65)*
	1000	14 (9-18)*	0.76 (0.72-0.82)*	1.62 (1.53-2.11)*
BRET^2 (D$_{2L}$-Rluc + β-arrestin1-GFP^2)				
Quinpirole	0	15 (13-17)	0.13 (0.12-0.14)	1.01 (0.98-1.12)
	1	16 (12-17)	0.14 (0.13-0.15)	1.11 (0.10-1.12)
	10	13 (11-15)	0.15 (0.14-0.15)	1.18 (0.11-0.13)
	100	11 (10-12)	0.16 (0.15-0.16)*	1.23 (1.21-1.42)*
	1000	10 (9-11)	0.16 (0.16-0.17)*	1.34 (1.24-1.45)*

control included HERG, a membrane-localized K^+ channel that does not interact with GPCRs or G proteins (Hudson *et al.*, 2010; Bagher *et al.*, 2016). Consistent with a previous study using BRET (Galés *et al.*, 2005), cells transfected with $G\alpha_s$-Rluc and β_2AR-GFP^2 resulted in a significantly higher BRET$_{Eff}$ compared to the negative control (Supplementary Fig. 4.4A).

Next, we examined whether CB$_1$ and D$_{2L}$ homodimers couple to $G\alpha_s$ proteins following the activation of both receptors within CB$_1$/D$_{2L}$ heterotetramer complexes. The interaction between $G\alpha_s$-Rluc and CB$_1$-GFP^2 in the presence of un-tagged D$_{2L}$ receptors was studied (Fig. 4.6A). Treating the cells with increasing doses of ACEA did not significantly increase BRET$_{EFF}$ between CB$_1$ and $G\alpha_s$ compared to vehicle treatment [E_{Max} = 0.10 (0.09-0.14), EC$_{50}$ = 0.38 μM (0.350-0.44) and Hill coefficient = 0.68 (0.59-0.89)]. Similarly, quinpirole treatment did not alter BRET$_{Eff}$ between CB$_1$ and $G\alpha_s$ compared to vehicle treatment [E_{Max} = 0.07 (0.05-0.08), EC$_{50}$=0.03 μM (0.02-0.04), Hill coefficient = 1.5 (1.7-1.0)] (Fig. 4.6B). The co-application of 1 μM ACEA and 1 μM quinpirole increased BRET$_{Eff}$ between $G\alpha_s$-Rluc and CB$_1$-GFP^2 in the presence of un-tagged D$_{2L}$ receptors (Supplementary Fig. 4.2B). The increase in BRET$_{Eff}$ following ACEA and quinpirole co-application was delayed and sustained. BRET$_{Eff}$ peaked at ~240 sec (4 min) following ligand application and remained significantly elevated for ~ 400 sec (Supplementary Fig. 4.2B; Bagher *et al.*, 2016). Therefore, all BRET$_{Eff}$ measured between $G\alpha_s$-Rluc and CB$_1$-GFP^2 was performed ~240 sec (4 min) following ligand application (Supplementary Fig. 4.2B). Treating the cells with 1 μM ACEA and increasing concentrations of quinpirole caused a concentration-dependent elevation in BRET$_{Eff}$ where E_{Max} = 0.40 (0.37-0.44), EC$_{50}$ = 0.03 (0.02-0.04) and Hill coefficient = 1.0 (0.71-1.3) (Fig. 4.6B). We also examined the effects of increasing concentrations of quinpirole on ACEA-induced BRET$_{Eff}$ between $G\alpha_s$-Rluc and CB$_1$-GFP^2 (Fig. 4.6C). Quinpirole produced a concentration-dependent leftward and upward shift in the ACEA concentration-response curves. Increasing the concentrations of quinpirole increased the efficacy and the potency of ACEA dependent $G\alpha_s$-CB$_1$ interaction (Fig. 4.6C; Table 4.2) where the Hill coefficient was greater than 1 suggesting that co-treatment with both ACEA and quinpirole exerted positive cooperatively effects on $G\alpha_s$-Rluc and CB$_1$-GFP^2 interactions within CB$_1$/D$_{2L}$ heterotetramers.

Figure 4.6 Bidirectional Allosteric Induction of CB_1/D_{2L} Heterotetramer Interactions with $G\alpha_s$ Following Agonists Treatment. **(A)** Scheme of $BRET^2$, CB_1 was tagged with GFP^2 (CB_1-GFP^2), $G\alpha_s$ was tagged with Rluc ($G\alpha_s$-Rluc) while D_{2L} was un-tagged (D_{2L}-pcDNA). **(B)** Concentration-response curves of ACEA and quinpirole +/- 1 μM ACEA-induced $BRET_{Eff}$ between $G\alpha_i$-Rluc and CB_1-GFP^2 in the presence of D_{2L}-pcDNA. **(C)** Concentration-response curves of ACEA- induced $BRET_{Eff}$ between $G\alpha_i$-Rluc and CB_1-GFP^2 +/- different concentrations of quinpirole in the presence of D_{2L}-pcDNA. **(D)** Scheme of $BRET^2$, D_{2L} was tagged with GFP^2 (D_{2L}-GFP^2), $G\alpha_s$ was tagged with Rluc ($G\alpha_s$-Rluc) while CB_1 was un-tagged (CB_1-pcDNA). **(E)** Concentration-response curves of quinpirole and ACEA +/- 1 μM quinpirole-induced $BRET_{Eff}$ between $G\alpha_s$-Rluc and D_{2L}-GFP^2 in the presence of CB_1-pcDNA. **(F)** Concentration-response curves of quinpirole- induced $BRET_{Eff}$ between $G\alpha_s$-Rluc and D_{2L} -GFP^2 +/- different concentrations of ACEA in the presence of CB_1-pcDNA. Data are presented as mean ± SEM of 4 independent experiments.

A CB$_1$-GFP^2 + Gαs-Rluc + D$_{2L}$-pcDNA

D D$_{2L}$-GFP^2 + Gαs-Rluc + CB$_1$-pcDNA

B

BRET$_{Eff}$

- ● ACEA
- ■ Quinpirole
- ◇ Quinpirole + 1 μM ACEA
- □ Vehicle

Log [Ligand] (M)

E

BRET$_{Eff}$

- ● ACEA
- ■ Quinpirole
- ◇ ACEA + 1 μM Quinpirole
- □ Vehicle

Log [Ligand] (M)

C

BRET$_{Eff}$

[Quinpirole] μM
- 0.000
- 0.001
- 0.010
- 0.100
- 1.000

Log [ACEA] (M)

F

BRET$_{Eff}$

[ACEA] μM
- 0.000
- 0.001
- 0.010
- 0.100
- 1.000

Log [Quinpirole] (M)

148
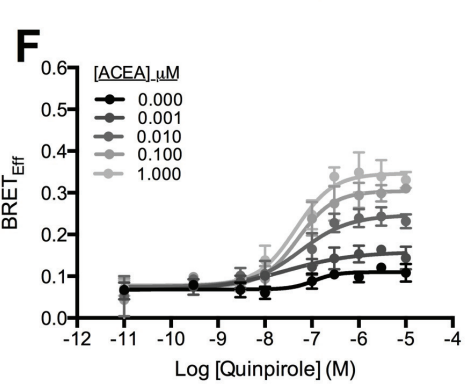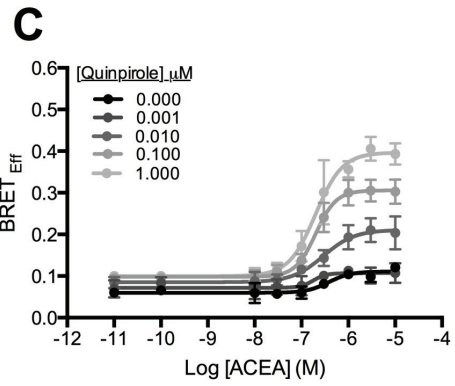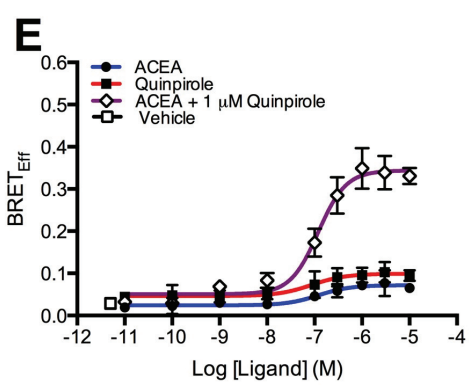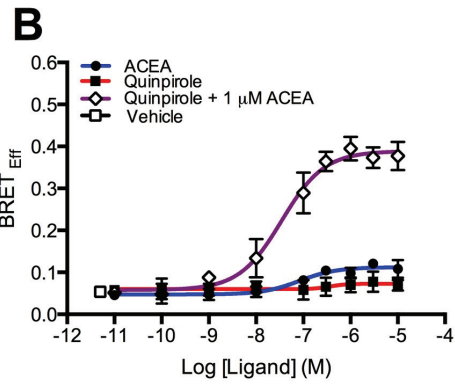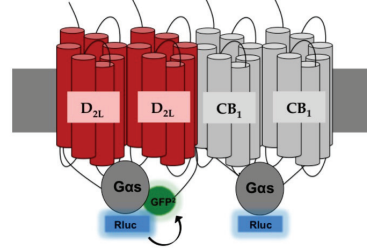
The interaction between D_{2L} and $G\alpha_s$ protein was also examined using $BRET^2$. In cells expressing $G\alpha_s$-Rluc and D_{2L}-GFP^2, no significant $BRET_{Eff}$ signals were detected in the vehicle- or quinpirole-treated cells, compared to cells expressing $G\alpha_s$-Rluc and β_2AR-GFP^2 (Supplementary Fig. 4.4B). These observations indicate that, similarly to CB_1, D_{2L} did not interact with $G\alpha_s$ proteins in the absence or presence of D_2 agonists.

In order to study the influence of ACEA treatment on $G\alpha_s$-Rluc and D_{2L}-GFP^2 interactions, cells were co- transfected with un-tagged CB_1 receptors (Fig. 4.6D). Increasing the concentrations of quinpirole or ACEA did not alter $BRET_{Eff}$ values compared to vehicle treatment (Fig. 4.6E). The co-application of 1 μM ACEA and 1 μM quinpirole increased $BRET_{Eff}$ between $G\alpha_s$-Rluc and D_{2L}-GFP^2 in the presence of un-tagged CB_1 receptors (Supplementary Fig. 4.2D). Similarly to CB_1, the increase in $BRET_{Eff}$ following ACEA and quinpirole co-application was delayed and sustained. $BRET_{Eff}$ peaked at ~240 sec (4 min) following co-application of both agonists and remained significantly elevated for ~ 400 sec (Supplementary Fig. 2D). Therefore, all $BRET_{Eff}$ measured between $G\alpha_s$-Rluc and D_{2L}-GFP^2 was performed ~240 sec (4 min) following ligand application (Supplementary Fig. 4.2D). Significantly higher $BRET_{Eff}$ values were observed in cells treated with 1 μM quinpirole and increasing concentrations of ACEA [E_{Max} = 0.34 (0.32-0.37), EC_{50} = 0.19 (0.21-0.31), Hill coefficient = 1.4 (0.82-2.35)] (Fig. 4.6E). Increasing ACEA concentrations resulted in a leftward and upward shift in quinpirole concentration-response curves (Fig. 4.6F; Table 4.2), indicating a positive cooperatively effects of ACEA on $G\alpha_s$ and D_{2L} interactions. The co-expression of CB_1/D_{2L} hetero-oligomer blocking peptide (CB_1-BP), which inhibited the physical interaction between CB_1 and D_2 (Fig. 4.2C), inhibited the switch of CB_1 and D_{2L} coupling from $G\alpha_i$ to $G\alpha_s$ proteins following co-activation of both receptors (Supplementary Fig. 4.5A,B). These findings demonstrate that co-activation of CB_1 and D_{2L} with CB_1 and D_2 agonists allosterically enhanced the association of CB_1 and D_{2L} receptors with $G\alpha_s$ proteins within CB_1/D_{2L} heterotetramer complexes. Altogether, co-treatment of CB_1/D_{2L} heterotetramer complexes led to physical uncoupling of $G\alpha_i$ followed by physical coupling of $G\alpha_s$. All $BRET^2$ experiments conducted to measure $G\alpha$ protein interaction with CB_1 or D_{2L} were performed in the present of excessive $G\alpha$ protein, which exclude the possibility that competition for a common pool of G protein is the reason for the

observed alteration in Gα protein coupling.

To confirm that the observed changes in coupling between Gα proteins and CB_1/D_{2L} complexes following the co-application of both receptor agonists were specific to CB_1/D_{2L} heterotetramers, we studied the effect of concurrent activation of CB_1 and $β_2AR$ receptors by their agonists on the interaction between CB_1 and Gα proteins. The CB_1 and $β_2AR$ can heteromerize when expressed in HEK 293A cells (Hudson *et al.,* 2010). The expression of $Gα_i$-Rluc and $ß_2$-GFP^2 resulted in low $BRET^2$ signal similar to cells expressing $Gα_i$-Rluc and the negative control HERG-GFP^2. In addition, treating the cells with the $β_2AR$ agonist isoproterenol (1 μM) did not alter $BRET_{Eff}$ signal between $Gα_i$-Rluc and $β_2AR$-GFP^2 (Supplementary Fig. 4.6A). Treating cells co-expressing $Gα_i$-Rluc, CB_1-GFP^2 and un-tagged $β_2AR$ with 1 μM ACEA alone or with 1 μM isoprenaline resulted in $BRET_{Eff}$ similar to cells treated with 1 μM ACEA and expressing $Gα_i$-Rluc, CB_1-GFP^2 (*n.s. P* > 0.05) relative to cells expressing empty pcDNA within treatment group (Supplementary Fig. 4.6A). Therefore, the co-expression and co-activation of both CB_1 and $β_2AR$ receptors by their agonists did not alter the interaction between CB_1 and $Gα_i$ protein (Supplementary Fig. 4.6A). The interaction between CB_1 and $Gα_s$ protein in cells co-expressing un-tagged $β_2AR$ was also studied following the co-application of both agonists. Treating cells expressing $Gα_s$-Rluc, CB_1-GFP^2 and un-tagged $β_2AR$ and treated with 1 μM ACEA alone or with 1 μM isoprenaline resulted in similar $BRET_{Eff}$ signals compared to cells treated with only 1 μM ACEA and expressing $Gα_i$-Rluc, CB_1-GFP^2 and un-tagged $β_2AR$ (Supplementary Fig. 4.6B). These results demonstrate that the co-activation of CB_1 and $β_2AR$ do not switch CB_1 coupling to either $Gα_i$ or $Gα_s$ proteins. Similarly, the co-expression and co-activation of D_{2L} and $β_2AR$ receptors did not alter the interaction between D_{2L} and $Gα_i$ protein (Supplementary Fig. 4.5C) or the interaction between D_{2L} and $Gα_s$ proteins (Supplementary Fig. 4.6D).

4.3.4 Activation of CB_1 and D_2 Receptors Allosterically Alter Their Downstream Signaling

To test whether physical uncoupling of CB_1 and D_{2L} from $Gα_i$ following treatment with both CB_1 and D_{2L} agonists is associated with functional un-coupling from $Gα_i$ proteins, we measured $Gα_i$-dependent ERK phosphorylation 5 min following drug

application because ERK phosphorylation is transient (Laprairie *et al.,* 2014). Treating cells co-expressing CB_1-pcDNA and D_{2L}-pcDNA with increasing concentration of ACEA resulted in concentration-dependent increase in ERK phosphorylation [E_{Max} = 0.81 (0.74-0.85), EC_{50} = 0.16 μM (0.14-0.26) and Hill coefficient = 1.01 (0.79-1.4)] (Fig. 4.7A). Treating the cells with 1 μM ACEA and increasing concentrations of quinpirole, resulted in an inhibition of ACEA-induced ERK phosphorylation (Fig. 4.7A). Similarly, treating the cells with an increasing concentration of quinpirole led to an increase in ERK phosphorylation [E_{Max} = 0.82 (0.79-0.85), EC_{50} = 0.022 (0.015-0.028) and Hill coefficient = 1.01 (0.98-1.23)] (Fig. 7D). Increasing ACEA concentrations inhibited ERK phosphorylation induced by 1 μM quinpirole (Fig. 4.7D). Increasing quinpirole concentrations shifted ACEA concentration-response curves rightward and downward (Fig. 7B; Table 4.1). Similarly, increasing ACEA concentrations shifted quinpirole concentration-response curves rightward and downward (Fig. 4.7E; Table 4.2). These data demonstrate bidirectional negative allosteric effects of ACEA and quinpirole on ERK phosphorylation .The observed ERK phosphorylation following the application of 1 μM ACEA or 1 μM quinpirole was mediated through activation of the PTx-sensitive $G\alpha_i$-dependent pathway (Fig. 4.7C). The inhibition of ERK phosphorylation following the activation of both CB_1 and D_{2L} receptors is mediated through CB_1/D_{2L} heteromers, as the expression of the CB_1/D_{2L} hetero-oligomer blocking peptide (CB_1-BP) restored PTx-sensitive ACEA- and quinpirole-dependent ERK activation (Fig. 4.7F).

As co-activation of both CB_1 and D_{2L} was associated with CB_1 and D_{2L} physical coupling to $G\alpha_s$ proteins at the expense of coupling to $G\alpha_i$, we next evaluated the effects of co-activation of both CB_1 and D_{2L} on $G\alpha_s$-dependent CREB phosphorylation. Cells transfected with un-tagged CB_1 and D_{2L} receptors, ACEA (Fig. 4.8A) or quinpirole (Fig. 4.8D) treatment did not alter CREB phosphorylation compared to vehicle-treated cells. Treating the cells with 1 μM ACEA and increasing concentrations of quinpirole led to a concentration-dependent elevation in CREB phosphorylation [E_{Max} = 0.76 (0.71-0.82), EC_{50} = 0.04 (0.01-0.04) and Hill coefficient= 1.7 (1.1-2.3)] (Fig. 4.8B). Likewise, treating cells with 1 μM quinpirole and increasing concentrations of ACEA led to an increase in CREB phosphorylation [E_{Max} = 0.72 (0.71-0.82), EC_{50} = 0.04 μM (0.01-0.04) and Hill coefficient = 1.8 (1.2 2.5)] (Fig. 4.8D). Quinpirole allosterically modulated ACEA-mediated CREB

Figure 4.7: The Co-activation of CB$_1$/D$_{2L}$ Heterotetramer Allosterically Inhibited Gα$_i$-Mediated ERK Phosphorylation. ERK phosphorylation (pERK1/2(Tyr-205/Tyr-185)/total ERK) concentration-response curves measured at 5 min obtained from HEK 293A expressing un-tagged CB$_1$ and D$_{2L}$ receptors and **(A)** treated with increasing concentration ACEA or with 1 µM ACEA and increasing concentration of quinpirole, or **(D)** or treated with increasing concentrations of quinpirole or with 1 µM quinpirole and increasing concentration of ACEA. **(B)** pERK concentration-response curve obtained from cells treated with ACEA alone or in the presence of increasing concentrations of quinpirole, or **(E)** from cells treated with quinpirole alone or in the presence of increasing concentrations of ACEA. **(C)** HEK 293A cells expressing un-tagged CB$_1$ and D$_{2L}$ receptors and treated with 1 µM ACEA or 1 µM quinpirole or in combination +/- 24 h pre-treatment with 50 ng/ml PTx or CTx. * $P < 0.01$ compared to vehicle treatment; ~$P < 0.01$ compared to cells treated with 1 µM ACEA; *n.s.* $P > 0.05$ compared to vehicle treated cells. **(F)** HEK 293A cells expressing un-tagged CB$_1$ and D$_{2L}$ receptors together with empty pcDNA vector or CB$_1$/D$_{2L}$ hetero-oligomer blocking peptide (CB$_1$-BP) and treated with 1 µM ACEA or 1 µM quinpirole or in combination for 5 min +/- 24 h pre-treatment with 50 ng/ml PTx. * $P < 0.01$ compared to vehicle treatment; ~ $P < 0.01$ compared to cells transfected with empty pcDNA vector and treated with 1 µM ACEA and 1 µM quinpirole; *n.s.* $P > 0.05$ compared to vehicle treated cells. Data are presented as mean ± SEM of 4 independent experiments, one-way ANOVA followed by Tukey's *post-hoc* test.
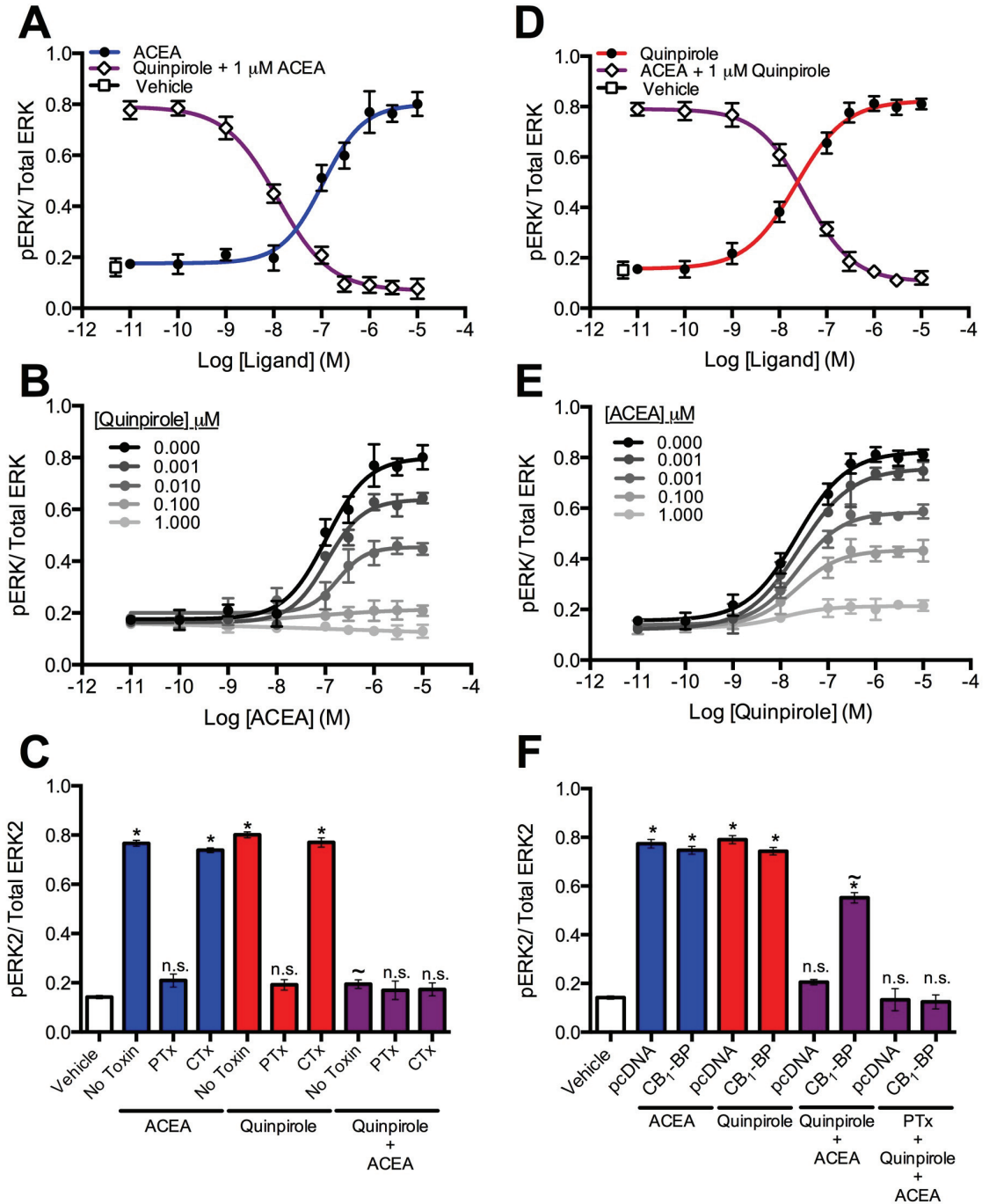
phosphorylation in a concentration-dependent manner, shifting ACEA concentration-response curves leftward and upward (Fig. 4.8B; Table 4.1). The same allosteric modulatory effects were also exerted by ACEA on quinpirole-mediated CREB phosphorylation (Fig. 4.8C; Table 4.2). The observed CREB-phosphorylation following the co-application of 1 μM ACEA and 1 μM quinpirole was mediated through the activation of the CTx-sensitive $G\alpha_s$-dependent pathway, as pre-treating the cells with CTx for 24 hr, which suppresses $G\alpha_s$ expression (Milligan *et al.,* 1989), inhibited $G\alpha_s$-dependent CREB-phosphorylation (Fig. 4.8C). The induced CREB phosphorylation was mediated through CB_1/D_{2L} heteromers, as the expression of the CB_1/D_{2L} hetero-oligomer blocking peptide (CB$_1$-BP) blocked CREB activation observed following ACEA and quinpirole co-application (Fig. 4.8F).

To confirm that the switch in CB_1 and D_{2L} coupling and signaling from $G\alpha_i$ to $G\alpha_s$ proteins following the application of ACEA and quinpirole was not an artifact observed only in HEK cells or only following of receptor overexpression, we tested the influence of quinpirole on coupling of CB_1 to $G\alpha_i$ and $G\alpha_s$ proteins and downstream signaling using STH$dh^{Q7/Q7}$ cells, a model of striatal medium spiny projection neurons that endogenously express CB_1 and D_{2L} receptors (Trettel *et al.,* 2000; Laprairie *et al.,* 2013) (Supplementary Fig. 4.7). We observed a reduction in ACEA-dependent BRET^2 signaling between $G\alpha_i$ and CB_1 (Supplementary Fig. 4.5A), followed by an increase in BRET^2 signaling between $G\alpha_s$ and CB_1 (Supplementary Fig. 4.7B) when STH$dh^{Q7/Q7}$ cells were treated with 1 μM ACEA and 1 μM quinpirole. In addition, we measured the effects of co-application of 1 μM ACEA and/or 1 μM quinpirole on endogenous CB_1 and D_{2L} receptor signaling. Similar to our results using HEK 293A cells, the co-application of 1 μM ACEA and 1 μM quinpirole inhibited ACEA- and quinpirole-induced $G\alpha_i$-dependent ERK phosphorylation (Supplementary Fig. 4.7C), followed by induced $G\alpha_s$-dependent CREB phosphorylation (Supplementary Fig. 4.7D) in STH$dh^{Q7/Q7}$ cells. Our findings demonstrated that the observed effects of quinpirole on CB_1 coupling and signaling in HEK 293A could also be replicated in a model of striatal medium spiny projection neurons that endogenously express both receptors.

154

Figure 4.8: The Co-Activation of CB_1/D_{2L} Heterotetramer Allosterically Induced $G\alpha_s$-Mediated CREB Phosphorylation. CREB phosphorylation concentration-response curves measured at 30 min obtained from HEK 293A expressing un-tagged CB_1 and D_{2L} receptors and **(A)** treated with increasing concentrations of ACEA or with 1 μM ACEA and increasing concentration of quinpirole, or **(D)** treated with increasing concentrations of quinpirole or with 1 μM quinpirole and increasing concentration of ACEA. pCREB concentration-response curve obtained from cells **(B)** treated with ACEA alone or in the presence of increasing concentrations of quinpirole**,** or **(E)** treated with quinpirole alone or in the presence of increasing concentrations of ACEA. **(C)** HEK 293A cells were treated with 1 μM ACEA or 1 μM quinpirole alone or in combination for 30 min +/- 24 h pre-treatment with 50 ng/ml PTx or CTx. * $P < 0.01$ compared to vehicle treatment; $\sim P < 0.01$ compared to cells treated with 1 μM ACEA; *n.s.* $P > 0.05$ compared to vehicle treated cells. **(F)** HEK 293A cells expressing un-tagged CB_1 and D_{2L} receptors together with empty pcDNA vector or CB_1-BP and treated with 1 μM ACEA or 1 μM quinpirole alone for 30 min or in combination. * $P < 0.01$ compared to vehicle treatment; $\sim P < 0.01$ compared to cells transfected with empty pcDNA vector and treated with 1 μM ACEA and 1 μM quinpirole for 30 min +/- 24 h pre-treatment with 50 ng/ml CTx; *n.s.* $P > 0.05$ compared to vehicle treated cells. Data are presented as mean ± SEM of 4 independent experiments, one-way ANOVA followed by Tukey's *post-hoc* test.
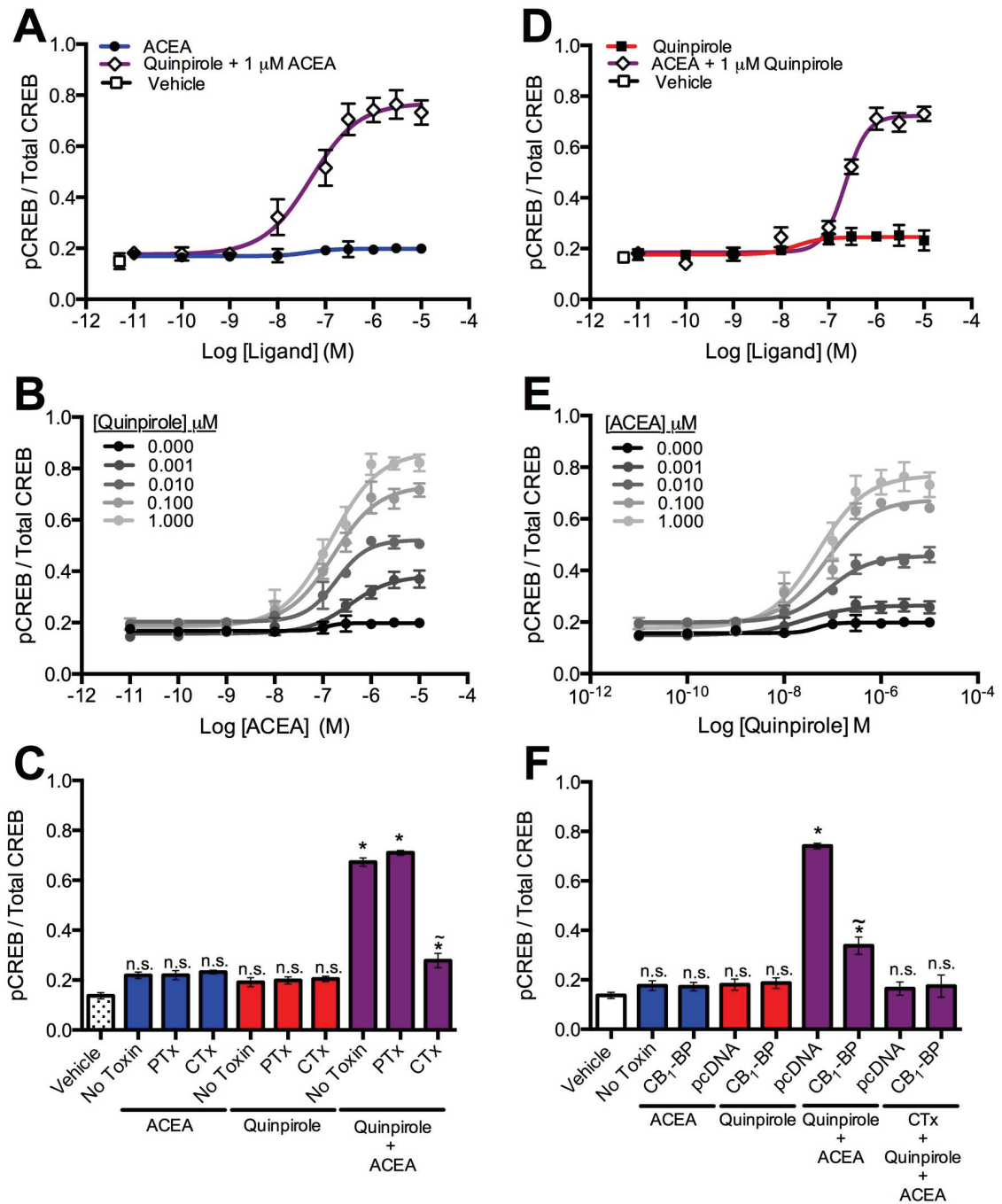
4.3.5 Quinpirole and ACEA Allosterically Potentiate β-arrestin1 Recruitment to CB$_1$ and D$_{2L}$ Receptors, Receptor Co-Internalization and β-arrestin1-Dependent ERK Phosphorylation

CB$_1$ and D$_{2L}$ are known to interact with β-arrestin1, which mediates receptor internalization, β-arrestin1-mediated signaling, receptor recycling and degradation (Sim-Selley and Martin, 2003; Laprairie *et al*., 2014). The effect of simultaneous treatment with CB$_1$ and D$_{2L}$ agonists on β-arrestin1 recruitment to CB$_1$/D$_{2L}$ receptor complexes and receptors co-internalization was tested. HEK 293A cells were transfected with β-arrestin1-Rluc, CB$_1$-GFP^2 and un-tagged D$_{2L}$ (Fig. 4.9A). β-arrestin1 recruitment to the CB$_1$ receptors within CB$_1$/D$_{2L}$ heterotetramers was measured over 30 min following drug application (Fig. 4.9B). BRET$_{Eff}$ signals observed from cells expressing β-arrestin1-Rluc and CB$_1$-GFP^2 treated with vehicle were higher than BRET$_{Eff}$ between β-arrestin1-Rluc and HERG-GFP^2 (Fig. 4.9B). Treating the cells with 1 μM ACEA enhanced β-arrestin1 recruitment to CB$_1$ as demonstrated by increased BRET$_{Eff}$ signals compared to vehicle-treated cells starting 5 min post-ACEA application and reaching a plateau at 15 min. The signal was sustained for 30 min (Fig. 4.9B). Treating cells with 1 μM quinpirole increased BRET$_{Eff}$ between β-arrestin1-Rluc and CB$_1$-GFP^2 compared to vehicle-treated cells. These findings suggest that D$_2$ agonists induced β-arrestin1-Rluc recruitment to the activated D$_{2L}$ within D$_{2L}$/CB$_1$-GFP^2/β-arrestin1-Rluc complexes. The co-application of both 1 μM ACEA and quinpirole significantly potentiated BRET$_{Eff}$ signal between β-arrestin1-Rluc and CB$_1$-GFP^2 compared to ACEA-treated cells (Fig. 4.9B). Such an increase in BRET$_{Eff}$ signals was not detected in cells co-treated with 1 μM ACEA and quinpirole in the absence of D$_{2L}$ receptors (data not shown), confirming that the observed induction in BRET$_{Eff}$ signals was mediated through the binding of quinpirole to D$_{2L}$ receptors and not due to its direct effect on CB$_1$ receptors. Increasing the concentration of ACEA led to a concentration-dependent increase in BRET$_{Eff}$ [E_{Max} = 0.60 (0.58-0.64), EC$_{50}$ = 0.22 μM (0.12-0.25) and Hill coefficient = 1.20 (0.91-1.41)] (Fig. 4.9C). Quinpirole treatment resulted in an increase in BRET$_{Eff}$ [E_{Max} = 0.38 (0.36-0.41), EC$_{50}$ = 0.013 μM (0.008-.02) and Hill coefficient = 1.00 (0.71-1.29)] (Fig. 4.9C). The E_{Max} between β-arrestin1-Rluc and CB$_1$-GFP^2 was lower compared to E_{Max} obtained from ACEA-treated cells. The effect of increasing quinpirole concentrations on ACEA-

Figure 4.9: ACEA Treatment Resulted in Slow and Sustained β-arrestin1 Recruitment to CB₁, Which was Allosterically Potentiated with Quinpirole Co-Application. **(A)** HEK 293A cells expressing β-arrestin1-Rluc CB$_1$-GFP^2, and un-tagged D$_{2L}$-pcDNA. **(B)** BRET$_{Eff}$ was measured over 30 min in cells expressing β-arrestin1-Rluc, CB$_1$-GFP^2 and un-tagged D$_{2L}$-pcDNA and treated with vehicle, 1 µM ACEA, 1 µM quinpirole +/- 1 µM ACEA. As a control, cells were co-transfected with β-arrestin1-Rluc and HERG-GFP^2. * $P < 0.01$ compared to vehicle-treated cells; ~ $P < 0.01$ compared to cells treated with 1 µM ACEA. **(C)** BRET$_{Eff}$ measured between β-arrestin1-Rluc and CB$_1$-GFP^2 in cells treated with increasing concentrations of ACEA or increasing concentrations of quinpirole in the presence of un-tagged D$_{2L}$-pcDNA. **(D)** Concentration-response curves of ACEA- induced BRET$_{Eff}$ between β-arrestin1-Rluc and CB$_1$-GFP^2 +/- increasing concentrations of quinpirole. Data are presented as mean ± SEM of 4 independent experiments, one-way ANOVA followed by Tukey's *post-hoc* test.

A

B

- ● β-arrestin1-Rluc + CB$_1$-GFP^2 + D$_{2L}$-pcDNA+ 1 μM ACEA
- ■ β-arrestin1-Rluc + CB$_1$-GFP^2 + D$_{2L}$-pcDNA+ 1 μM Quinpirole
- ◆ β-arrestin1-Rluc + CB$_1$-GFP^2 + D$_{2L}$-pcDNA+ 1 μM ACEA + 1 μM Quinpirole
- △ β-arrestin1-Rluc + CB$_1$-GFP^2 + D$_{2L}$-pcDNA+ Vehicle
- ▼ β-arrestin1-Rluc + HERG-GFP^2

C

D

159
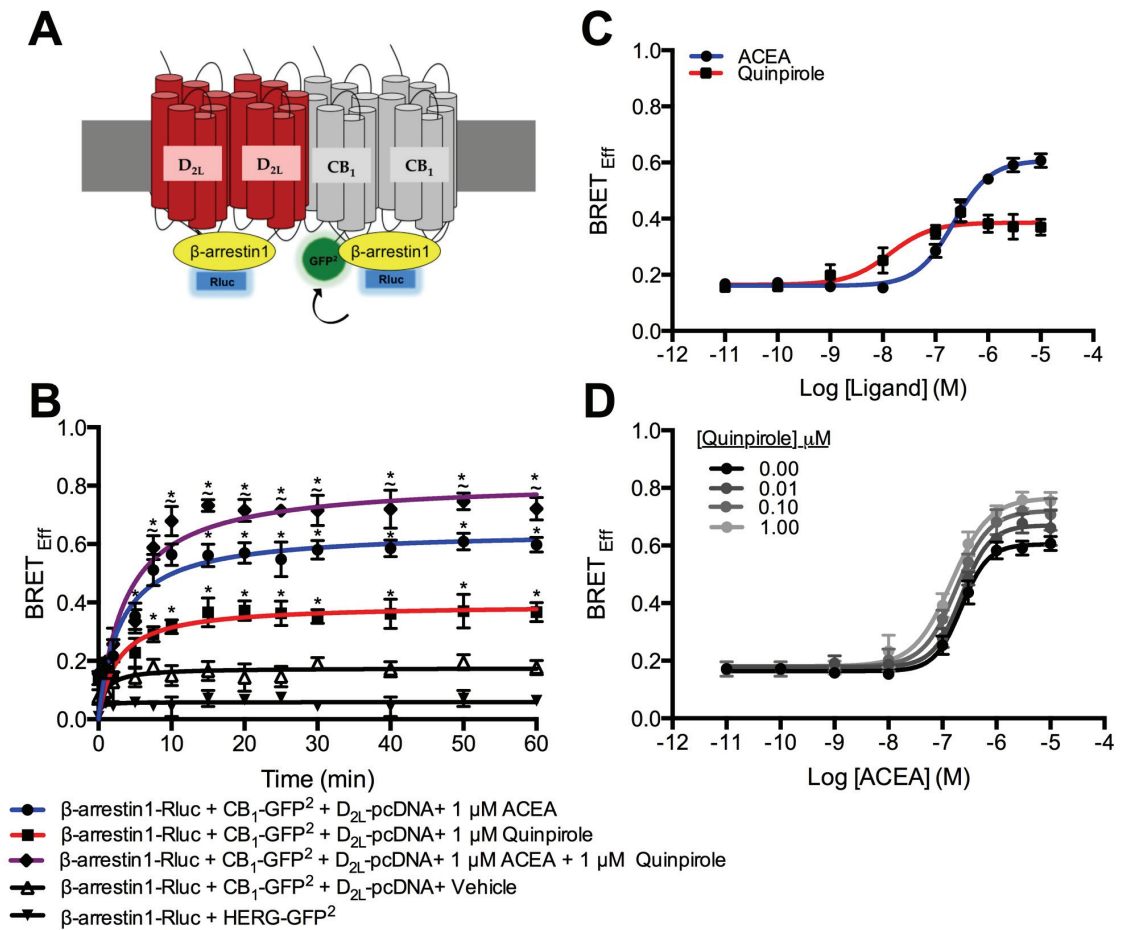
induced $BRET_{Eff}$ was evaluated. An increase in the concentration of quinpirole shifted ACEA-concentration-response curves leftward and upward (Fig. 4.9D; Table 4.1). Quinpirole acted as a positive allosteric modulator that potentiated β-arrestin1 requirement to the activated CB_1 receptors within CB_1/D_{2L} heterotetramers. To confirm that the potentiation of $BRET^2$ signals following co-application of both ACEA and quinpirole was specific to CB_1/D_{2L} heterotetramers we measured the effect of co-expression and co-activation of CB_1 and mGluR6 receptors on β-arrestin1 recruitment to CB_1 receptors (Supplementary Fig. 4.8A). The expression of β-arrestin1-Rluc and CB_1-GFP^2 together with un-tagged mGluR6 and treatment of the cells with 1 μM ACEA resulted in an increase in $BRET_{Eff}$ between β-arrestin1-Rluc and CB_1-GFP^2 compared to vehicle-treated cells (Supplementary Fig. 4.8A). Treating the cells with the selective mGluR6 agonist L-2-amino-4-phosphonobutyric acid (L-AP4, 1 μM) alone resulted in similar $BRET_{Eff}$ signals between β-arrestin1-Rluc and CB_1-GFP^2 compared to vehicle-treated cells. The co-application of both 1 μM ACEA and 1 μM L-AP4 resulted in similar $BRET_{Eff}$ signal between β-arrestin1-Rluc and CB_1-GFP^2 compared to cells treated with 1 μM ACEA (Supplementary Fig. 4.8A). Together these finding show that mGluR6, unlike D_{2L}, did not modulate β-arrestin1 recruitment to CB_1.

β-arrestin1 recruitment to D_{2L} receptors was also measured. HEK 293A cells were co-transfected with D_{2L}-Rluc, β-arrestin1-GFP^2, and un-tagged CB_1 receptors (Fig. 4.10A). $BRET_{Eff}$ was measured for 30 min following the addition of different ligands (Fig. 4.10B). Cells expressing D_{2L}-Rluc and β-arrestin1- GFP^2 resulted in higher $BRET_{Eff}$ signals compared to the negative control HERG (Fig. 4.10B). Treating the cells with 1 μM quinpirole significantly increased $BRET_{Eff}$ between D_{2L}-Rluc and β-arrestin1-GFP^2. ACEA (1 μM) treatment also resulted in higher $BRET_{Eff}$ compared to vehicle-treated cells (Fig. 4.10B). The co-application of both 1 μM quinpirole and ACEA potentiated $BRET_{Eff}$ between D_{2L}-Rluc and β-arrestin1-GFP^2 compared to $BRET_{Eff}$ obtained from cells treated with 1 μM quinpirole (Fig. 4.10B). Increasing the concentration of quinpirole resulted in a concentration-dependent increase in $BRET_{Eff}$ signals between D_{2L}-Rluc and β-arrestin1-GFP^2 [E_{Max} = 0.13 (0.12-0.14), EC_{50} = 0.02 μM (0.1-0.02) and Hill coefficient = 1.06 (0.90-1.21)] (Fig. 4.10C). Similarly, increasing the concentration of ACEA led to a concentration-dependent increase in $BRET_{Eff}$ signals between D_{2L}-Rluc

Figure 4.10: ACEA Co-Application Allosterically Potentiated Quinpirole- Induced β-arrestin1 Recruitment to D_{2L}. **(A)** HEK 293A cells expressing D_{2L}-Rluc and β-arrestin1-GFP^2 and un-tagged CB_1-pcDNA. **(B)** $BRET_{Eff}$ was measured over 30 min in cells expressing D_{2L}-Rluc and β-arrestin1-GFP^2 and un-tagged CB_1-pcDNA and treated with vehicle, 1 μM quinpirole, 1 μM ACEA alone or with 1 μM quinpirole. As a control, cells were co-transfected with HERG-Rluc and β-arrestin1-GFP^2. * $P < 0.01$ compared to vehicle-treated cells; ~ $P < 0.01$ compared to cells treated with 1 μM quinpirole. **(C)** $BRET_{Eff}$ measured between D_{2L}-Rluc and β-arrestin1-GFP^2 in cells treated with increasing concentrations of quinpirole or increasing concentrations of ACEA in the presence of un-tagged CB_1-pcDNA. **(D)** Concentration-response curves of quinpirole-induced $BRET_{Eff}$ between D_{2L}-Rluc and β-arrestin1-GFP^2 with increasing concentrations of ACEA. Data are presented as mean ± S.E.M. of 4 independent experiments, one-way ANOVA followed by Tukey's post-hoc test.

A

D_{2L} D_{2L} CB_1 CB_1

β-arrestin1   β-arrestin1

Rluc   GFP²   GFP²

B

BRET_{Eff}

Time (min)

C

- ACEA
- Quinpirole

BRET_{Eff}

Log [Ligand] (M)

D

[ACEA] μM
- 0.00 μM
- 0.01 μM
- 0.10 μM
- 1.00 μM

BRET_{Eff}

Log [Quinpirole] (M)

- D_{2L}-Rluc + β-arrestin1-GFP² + CB_1-pcDNA+ 1 μM Quinpirole
- D_{2L}-Rluc + β-arrestin1-GFP² + CB_1-pcDNA+ 1 μM ACEA
- D_{2L}-Rluc + β-arrestin1-GFP² + CB_1-pcDNA+ 1 μM Quinpirole + 1 μM ACEA
- D_{2L}-Rluc + β-arrestin1-GFP² + CB_1-pcDNA+ Vehicle
- HERG-Rluc + β-arrestin1-GFP²

162
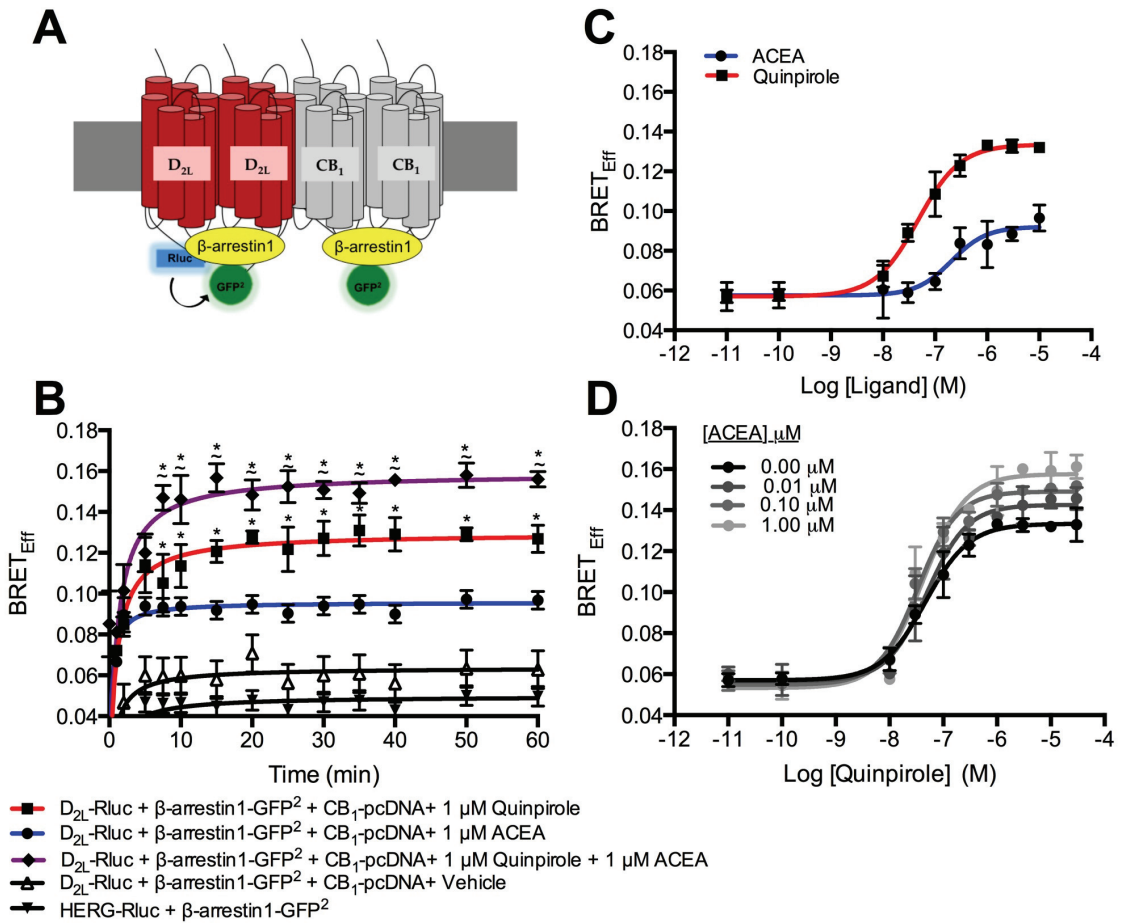
and β-arrestin1-GFP^2 [E_{Max} = 0.1 (0.09-0.12), EC$_{50}$ = 0.20 μM (0.12-0.25) and Hill coefficient = 1.20 (0.98-1.32)] (Fig. 4.10C). ACEA concentrations higher than 0.01 μM shifted quinpirole-concentration-response curves leftward and upward (Fig. 4.10D; Table 4.2). ACEA acted as a positive allosteric modulator that potentiated β-arrestin1 requirement to the activated D$_{2L}$ within CB$_1$/D$_{2L}$ heterotetramers. As a control, we measured the effect of the co-expression and co-activation of D$_{2L}$ and mGluR6 receptors on β-arrestin1 recruitment to D$_{2L}$ (Supplementary Fig. 4.6B). The co-expression of un-tagged mGluR6 together with D$_{2L}$-Rluc and β-arrestin1-GFP^2 did not alter quinpirole-induced β-arrestin1 recruitment to D$_{2L}$ receptors in the absence or presence of the mGluR6 agonist (L-AP4, 1 μM) (Supplementary Fig. 4.6B).

Next, we tested whether the observed potentiation in β-arrestin1 recruitment following co-activation of both CB$_1$ and D$_{2L}$ are mediated through CB$_1$/D$_{2L}$ heterotetramers binding to β-arrestin1. Our approach involved measuring the interaction between CB$_1$ and D$_{2L}$ with β-arrestin1 signaling in cells co-transfected with a blocking peptide (CB$_1$-BP), which interferes with CB$_1$ and D$_{2L}$ heterotetramer formation (Khan and Lee, 2014). Cells were transfected with β-arrestin1-Rluc, CB$_1$-GFP^2 and un-tagged D$_{2L}$-pcDNA together with empty pcDNA or pcDNA expressing CB$_1$-BP (Fig. 4.11A). BRET$_{\text{Eff}}$ was measured at 20 min following ligand application (Fig. 4.11B). A significantly lower energy transfer was observed between β-arrestin1-Rluc and CB$_1$-GFP^2 in cells expressing un-tagged D$_{2L}$-pcDNA and CB$_1$-BP treated with quinpirole alone or co-treated with quinpirole and ACEA compared to cells treated with the same agonist(s) expressing an empty pcDNA (Fig. 4.11B). In contrast, no change in the energy transfer between β-arrestin1-Rluc and CB$_1$-GFP^2 was observed in cells expressing the CB$_1$-BP following ACEA treatment compared to cells transfected with empty pcDNA (Fig. 4.11B). Our finding demonstrated that the increase in energy transfer between β-arrestin1-Rluc and CB$_1$-GFP^2 in the presence of quinpirole was due to the interaction between β-arrestin1-Rluc and D$_{2L}$ within CB$_1$/D$_{2L}$/β-arrestin1 complexes (Fig. 4.11B).

BRET$_{\text{Eff}}$ was also measured between D$_{2L}$-Rluc and β-arrestin1-GFP^2 in cells expressing CB$_1$-pcDNA together with empty pcDNA or CB$_1$-BP (Fig. 4.11C). A reduction in energy transfer between D$_{2L}$-Rluc and β-arrestin1-GFP^2 was observed in ACEA-treated cells and in cells co-treated with both ACEA and quinpirole when the CB$_1$-BP was expressed

Figure 4.11: Potentiation of β-arrestin1 Recruitment Following ACEA and Quinpirole Co-Application was Mediated Through CB₁/D₂L Heterotetramer. **(A)** Scheme of BRET^2, CB$_1$ was tagged with GFP^2 (CB$_1$-GFP^2), β-arrestin1was tagged with Rluc (β-arrestin1-Rluc) while D$_{2L}$ was un-tagged (D$_{2L}$-pcDNA). Cells were co-transfected with either empty pcDNA or CB$_1$-BP. **(B)** HEK 293A cells expressing β-arrestin1-Rluc, CB$_1$-GFP^2, un-tagged D$_{2L}$-pcDNA and either empty pcDNA or CB$_1$-BP. BRET$_{Eff}$ was measured 20 min following ligand treatment. * $P < 0.01$ compared cells expressing β-arrestin1-Rluc, CB$_1$-GFP^2, D$_{2L}$-pcDNA and empty pcDNA and treated with vehicle. # $P < 0.01$ compared to cells expressing β-arrestin1-Rluc, CB$_1$-GFP^2 and D$_{2L}$-pcDNA and empty pcDNA and treated with 1 μM ACEA and 1 μM quinpirole. ~ $P < 0.01$ compared to cells expressing β-arrestin1-Rluc, CB$_1$-GFP^2 and D$_{2L}$-pcDNA and empty pcDNA and treated with 1 μM quinpirole and ACEA. *n.s.* compared to cells expressing β-arrestin1-Rluc, CB$_1$-GFP^2, D$_{2L}$-pcDNA and empty pcDNA treated with 1 μM ACEA. **(C)** Scheme of BRET^2, D$_{2L}$ was tagged with Rluc (D$_{2L}$-Rluc), β-arrestin1was tagged with GFP^2 (β-arrestin1- GFP^2) while CB$_1$ was un-tagged (CB$_1$-pcDNA) and cells were co-transfected with CB$_1$-BP. **(D)** HEK 293A cells were transfected with D$_{2L}$-Rluc, β-arrestin1-GFP^2, CB$_1$-pcDNA and either empty pcDNA or CB$_1$-BP. BRET$_{Eff}$ was measured 20 min following ligand treatment. * $P < 0.01$ compared to cells expressing D$_{2L}$-Rluc, β-arrestin1-GFP^2, CB$_1$-pcDNA and empty pcDNA and treated with vehicle. # $P < 0.01$ compared to cells expressing D$_{2L}$-Rluc, β-arrestin1-GFP^2, CB$_1$-pcDNA and empty pcDNA and treated with 1 μM ACEA. ~ $P < 0.01$ compared to cells expressing D$_{2L}$-Rluc, β-arrestin1-GFP^2, CB$_1$-pcDNA and empty pcDNA and treated with 1 μM ACEA and quinpirole. *n.s.* compared to cells expressing D$_{2L}$-Rluc, β-arrestin1-GFP^2, and CB$_1$-pcDNA and treated with 1 μM quinpirole.

A

B

BRET $_{Eff}$

Vehicle   1 μM ACEA   1 μM Quinpirole   1 μM Quinpirole + 1 μM ACEA

n.s.   #   ~

□ β-arrestin1-Rluc + CB$_1$-Rluc + + D$_{2L}$-pcDNA + pcDNA
⊡ β-arrestin1-Rluc + CB$_1$-Rluc + + D$_{2L}$-pcDNA + CB$_1$-BP

C

D

BRET $_{Eff}$

Vehicle   1 μM ACEA   1 μM Quinpirole   1 μM Quinpirole + 1 μM ACEA

n.s.   ~

□ D$_{2L}$-Rluc + β-arrestin1-GFP^2 + CB$_1$-pcDNA + pcDNA
⊡ D$_{2L}$-Rluc + β-arrestin1-GFP^2 + CB$_1$-pcDNA + CB$_1$-BP

165
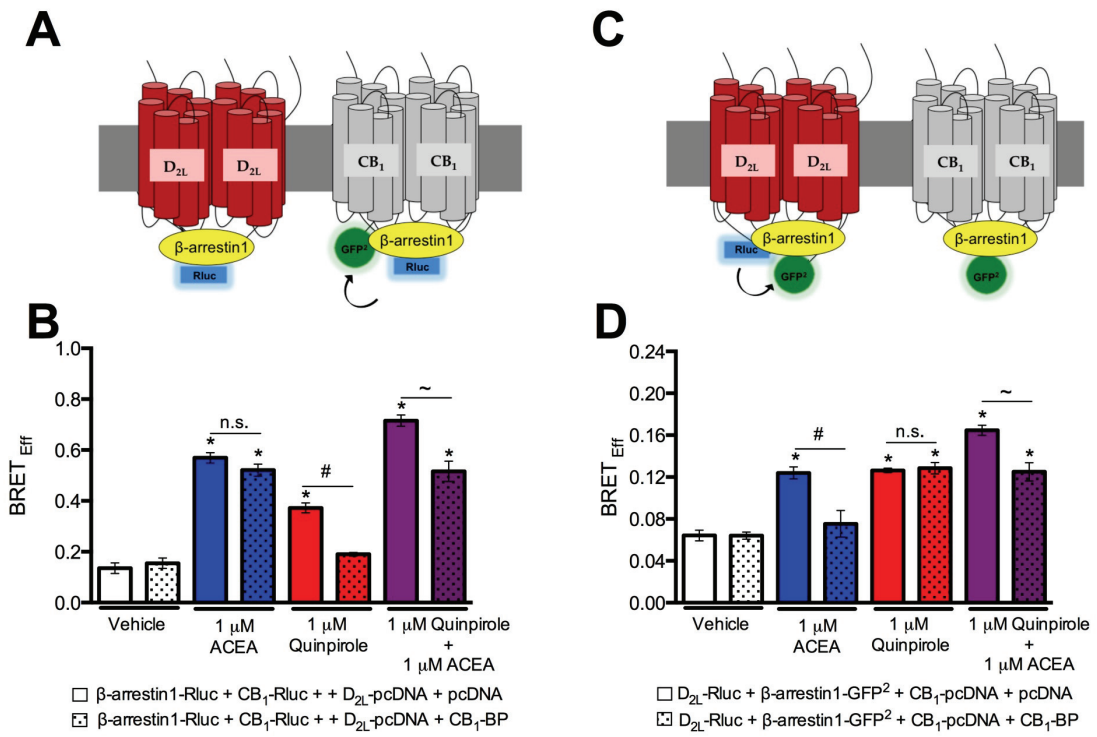
compared to cells expressing the empty pcDNA (Fig. 4.11D). Treating the cells with quinpirole did not alter $BRET_{Eff}$ in cells expressing CB_1-BP compared to those expressing empty pcDNA (Fig. 11D). Co-application of quinpirole and ACEA potentiated β-arrestin1 recruitment to CB_1/D_{2L} complexes, which is abolished when CB_1/D_{2L} interaction was blocked.

β-arrestin1 recruitment to CB_1/D_{2L} heterotetramers was followed by receptors internalization. CB_1 internalization was measured over 30 min following ligand treatment in cells co-transfected with CB_1-pcDNA and D_{2L}-pcDNA (Fig. 4.12A,B). Treating cells with 1 μM ACEA resulted in CB_1 internalization starting at 10 min compared to vehicle-treated cells (Fig. 4.12A,B). As predicted, treating cells with 1 uM quinpirole induced CB_1 internalization compared to vehicle-treated cells only in cells co-expressing both CB_1 and D_{2L} (Fig. 4.12B). Co-treating the cells with 1 μM ACEA and different concentrations of quinpirole dose-dependently increased CB_1 internalization over 30 min compared to ACEA-treated cells (Fig. 4.12A,B). We also measured D_{2L} internalization following ligand treatment (Fig. 4.12C,D). D_{2L} internalization was observed in cells treated with 1 μM quinpirole and 1 μM ACEA; however, ACEA was less efficacious in inducing D_{2L} internalization compared to quinpirole (Fig. 4.12C,D). Co-application of 1 μM quinpirole with 0.1 or 1 μM ACEA potentiated D_{2L} internalization compared to quinpirole-treated cells (Fig. 4.12D). Altogether, co-internalization of CB_1/D_{2L} complexes was observed following treatment with either ACEA or quinpirole treatment. Co-application of quinpirole and ACEA potentiated not only β-arrestin1 recruitment to CB_1/D_{2L} complexes but also complex co-internalization.

Next, we wanted to test the influence of co-application of CB_1 and D_2 agonists on β-arrestin1-dependent ERK phosphorylation. $Gα_i$-dependent PTx-sensitive ERK phosphorylation was observed at 5 min following treatment with either 1 μM ACEA or quinpirole (Fig. 4.7C, 4.13A). As expected based on earlier experiments, co-application of both 1 μM ACEA or quinpirole did not lead to $Gα_i$-dependent PTx-sensitive ERK phosphorylation (Fig. 4.7C, 4.13B). However, the co-application of both agonists resulted in a delayed and sustained potentiation in ERK phosphorylation, which peaked at 15 min (Fig. 4.13A). Such an elevation in pERK was mediated through $Gα_i$ -independent (PTx-insensitive) pathways (Fig. 4.13B). To test whether the observed increase in pERK was β-arrestin1-dependent, we co-transfected the cells with plasmid encoding β-arrestin1

Figure 4.12: Quinpirole and ACEA Co-Application Potentiated CB$_1$/D$_{2L}$ Heterotetramer Internalization. **(A)** Time-course analysis of CB$_1$ receptors cell surface expression and total protein levels over 30 min measured using On-Cell Western™ and In-Cell Western™ in cells treated with ligands. **(B)** Cell surface expression of CB$_1$ receptors measured at 30 min following ligand treatment. * $P < 0.01$ compared with vehicle-treated cells. ~ $P < 0.01$ compared to ACEA-treated cells **(C)** Time-course analysis of D$_{2L}$ receptors cell surface expression and total protein levels over 30 min measured using On-Cell Western™ and In-Cell Western™ in cells treated with ligands. **(D)** Cell surface expression of D$_{2L}$ receptors measured at 30 min following ligand treatment. * $P < 0.01$ compared with vehicle-treated cells. ~ $P < 0.01$ compared to quinpirole-treated cells. Data are presented as mean ± SEM of 4 independent experiments, one-way ANOVA followed by Tukey's *post-hoc* test.
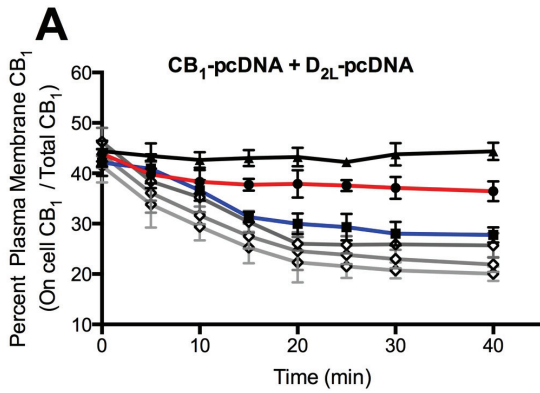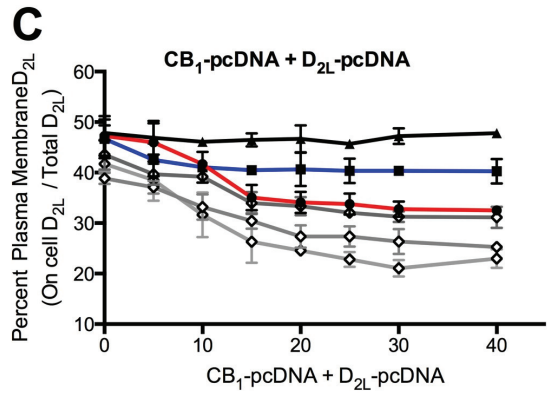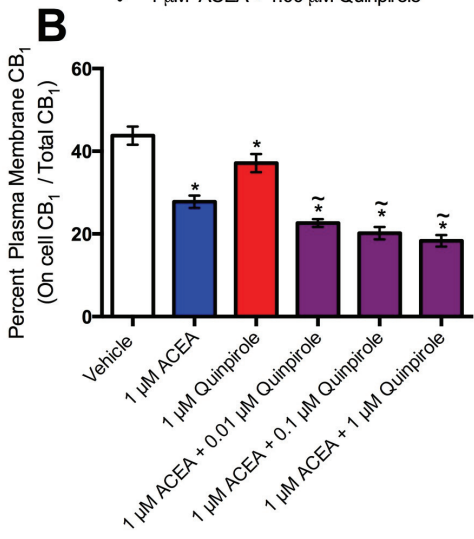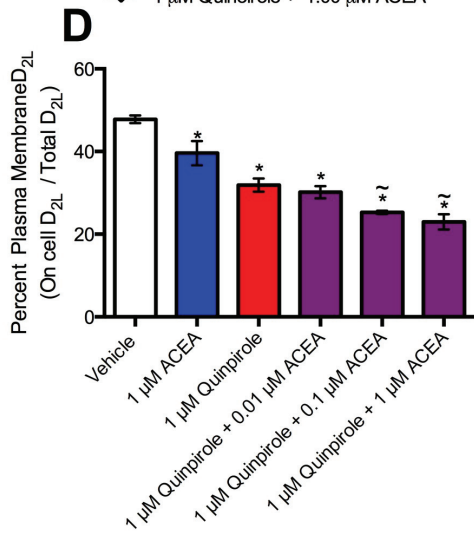
Figure 4.13: Quinpirole and ACEA Co-Application Resulted in β-arrestin1-Dependent Sustained ERK Phosphorylation. **(A)** ERK phosphorylation (pERK1/2(Tyr-205/Tyr-185)/total ERK) was measured over 60 min in cells treated with vehicle, 1 μM ACEA, 1 μM quinpirole or both agonists. Vehicle or drug was added to cells at time 0; * $P < 0.001$ compared to vehicle-treated cells; ~ $P < 0.001$ compared to ACEA-treated cells. **(B)** ERK phosphorylation was measured at 15 min in cells treated with 1 μM ACEA, 1 μM quinpirole or both agonists with or without pre-treatment with 50 ng/ml PTx, 50 ng/ml CTx or in the presence of a β-arrestin1 dominant negative mutant (β-arrestin1 V53D). * $P < 0.01$ compared to vehicle-treated cells. ~ $P < 0.001$ compared to No Toxin treatment within the treatment group. Data are presented as mean ± SEM of 4 independent experiments, one-way ANOVA followed by Tukey's *post-hoc* test.

A

B
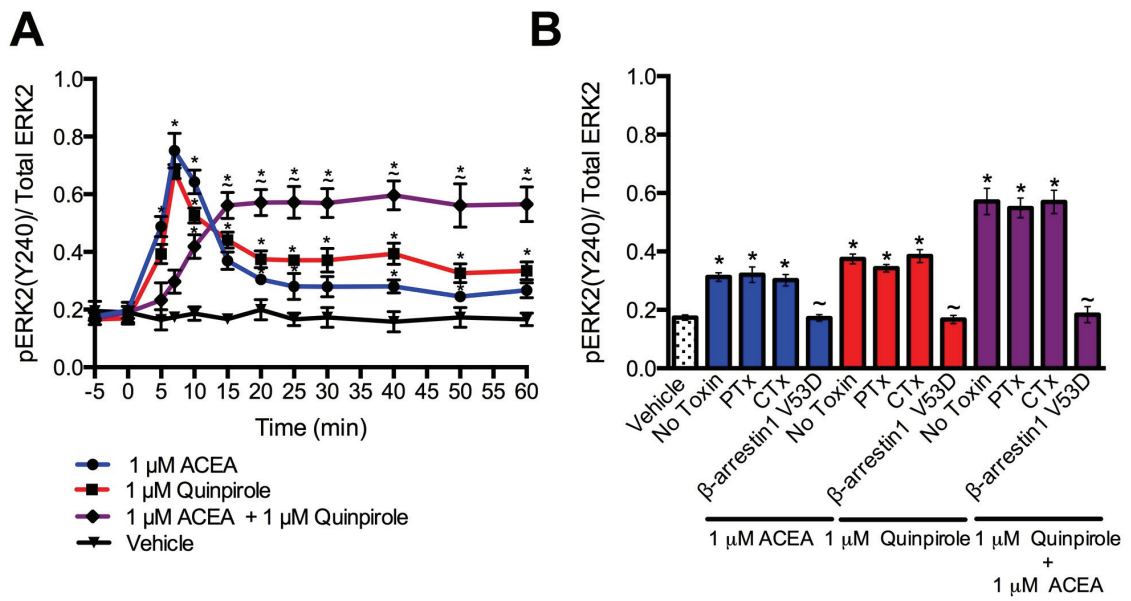
dominant negative mutant (β-arrestin1 V53D) that has previously been shown to block sustained pERK signaling (Daaka *et al.,* 1998). Co-expressing β-arrestin1 V53D with CB_1blocked ACEA and quinpirole mediated pERK at 15 min (Fig. 4.13B). Based on these data, ACEA and quinpirole co-application potentiated a delayed and a sustained ERK phosphorylation via β-arrestin1- mediated signaling

4.4 Discussion

The first objective of the current study was to understand the stoichiometry of $CB_1/D_{2L}/G\alpha$ protein complexes. The second objective was to understand the allosteric interactions among the components of the $CB_1/D_{2L}/G\alpha$ protein complex following the co-application of CB_1 and D_2 agonists. Our results from $SRET^2$ experiments combined with BiFC in addition to $BRET^2$ saturation experiments provide strong evidence that the basic functional unit is a CB_1/D_{2L} heterotetramer composed of CB_1 and D_{2L} homodimers coupled to a minimum of two $G\alpha$ proteins. While the minimum functional unit appears to be a heterotetramer plus at least two $G\alpha$ proteins, it is possible that multiple units associate to form higher order hetero-oligomers. The co-application of CB_1 and D_2 agonists led to changes in receptor- $G\alpha$ units association from $G\alpha_i$ to $G\alpha_s$, which influenced signaling and trafficking of CB_1/D_{2L} heterotetramer *via* bidirectional allosteric mechanism (Summarized in Fig. 4.14)

4.4.1 CB_1/D_{2L} Receptors Form Heterotetramers Consisting of CB_1 and D_{2L} Homodimers

Our current study and other studies provide evidence that supports the hypothesis that two GPCR homodimers associate to form a heterotetramer (Guitart *et al.,* 2014; Bonaventura *et al.,* 2015; Navarro *et al.,* 2016). Specifically, Guitart *et al.* (2014) reported that the dopamine receptor type 1 (D_1) and dopamine receptor type 3 (D_3) receptors form heterotetramers composed of D_1 and D_3 homodimers as demonstrated using BRET and BiFC and bimolecular luminescence complementation (BiLC) assays. The same approach has also been used to uncover the tetrameric structure of A_{2A} and D_2 heteromers (Bonaventura *et al.,* 2015). A more recent study, using microscope-based single-particle tracking and molecular modeling, reported that A_1 and A_{2A} form mainly

Figure 4.14: Allosteric Interactions Within CB₁/D₂L Heterotetramers. **(A)** CB_1/D_{2L} receptors form heterotetramers consisting of CB_1 and D_{2L} homodimers. CB_1/D_{2L} heterotetramers are coupled to at least two Gα proteins. Treating cells with the CB_1 agonist [arachidonyl-2-chloroethylamide (ACEA)] **(A),** or the D_2 agonist quinpirole **(B)** resulted in $G\alpha_i$-dependent ERK phosphorylation, β-arrestin1 recruitment, and receptor co-internalization. **(C)** Treating cells co-expressing CB_1 and D_{2L} with both ACEA and quinpirole, switched CB_1/D_{2L} heterotetramers coupling and signaling from $G\alpha_i$ to $G\alpha_s$ proteins, enhanced β-arrestin1 recruitment, and receptor co-internalization.
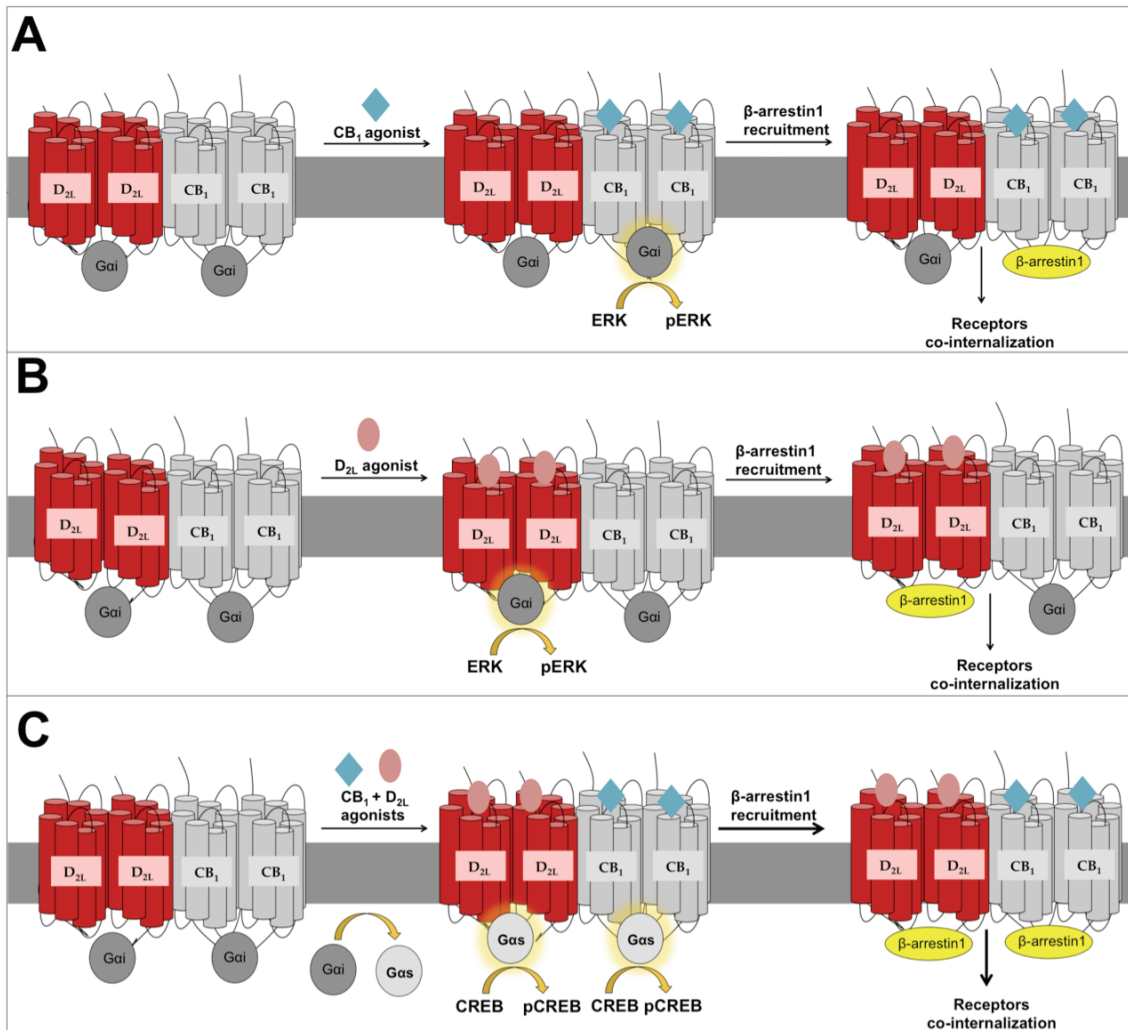
heterotetramers composed of two homodimers, while A_1 and A_{2A} homomers, homotrimers and homotetramers were scarce (Navarro *et al.*, 2016). The application of the Veatch and Stryer model (Vrecl *et al.*, 2006; Drinovec *et al.*, 2012) to the BRET[2] saturation data suggests that CB_1 and D_{2L} heterotetramers were the main species in cells that expressed CB_1 and D_{2L}. SRET[2] combined with BiFC further confirmed that CB_1 and D_{2L} heterotetramers were composed of CB_1 and D_{2L} homodimers. However, these findings do not rule out the possibility that a mixed population of CB_1 and D_{2L} homomers, heterodimers and higher oligomeric complex may simultaneously exist.

Even though monomeric GPCRs can activate G-proteins (Ernst *et al.*, 2007; Kuszak *et al.*, 2008), recent evidence suggests that a single protein binds to a GPCR homodimer (Navarro *et al.*, 2016). It follows then that hetero-oligomeric complexes would be composed of multimers of homodimers each with an associated protein (reviewed in Ferré, 2015). Using complemented donor-acceptor resonance energy transfer (CODA-RET), Guitart *et al.*, (2014) found that D_1 and D_3 heterotetramers are composed of two interacting D_1 and D_3 homodimers coupled to one $G\alpha_s$ and one $G\alpha_i$ protein, respectively. The same scheme has also been reported for A_1/A_{2A} heterotetramers (Navarro *et al.*, 2016). BRET and computer modeling was used to demonstrate that A_1 and A_{2A} homodimers form a heterotetrameric complex with two G proteins. $G\alpha_i$ couples with an A_1 homodimer and $G\alpha_s$ couples with an A_{2A} homodimer (Navarro *et al.*, 2016). Our result using BRET[2] experiments fit with the proposed model of receptor heterotetramers/G protein stoichiometry where CB_1 and D_{2L} homodimers each associate with one $G\alpha_i$ protein. Even in the presence of a peptide that specifically blocks the interaction between CB_1 receptors and $G\alpha_i$, we were able to detect energy transfer from $G\alpha_i$-Rluc to CB_1-GFP[2] following D_2 agonist treatment. This energy transfer would be observed only if another $G\alpha_i$ protein was bound to the D_{2L} homodimer within the CB_1/D_{2L}/$G\alpha_i$ protein complex. There was no energy transfer in the presence of the $G\alpha_i$ blocking peptide when only CB_1 was expressed. However, our experimental design does not exclude the possibility that CB_1 and D_{2L} monomers interact with the $G\alpha_i$ protein. Although several powerful tools are available and have been used to identify GPCR heteromerization in recombinant heterologous systems, it remains a challenge to detect and quantify the stoichiometry and distribution of GPCR complexes in native cells.

4.4.2 Bidirectional Allosteric Interactions Within CB$_1$/D$_{2L}$ Heterotetramers Modulate G Protein Coupling

CB$_1$/D$_{2L}$ heterotetramers elicit distinct signaling properties compared with receptor homodimers (Kearn *et al.*, 2005; Glass and Felder, 1997; Khan and Lee, 2014). Activation of either CB$_1$ or D$_{2L}$ homodimers by their respective selective agonists, within the CB$_1$/D$_{2L}$ heterotetramers, activated Gα_i proteins and resulted in Gα_i-dependent signaling. Simultaneous co-activation of CB$_1$ and D$_{2L}$ altered the coupling of each homodimer within the CB$_1$/D$_{2L}$/Gα heterotetrameric complex. This effect was specific to CB$_1$/D$_{2L}$ heterotetramers as the effect was not observed when the interaction between CB$_1$ and D$_{2L}$ was blocked. In addition, the co-expression CB$_1$ and β_2 in HEK 293A cells, which are known to form heteromers, and the co-application of both receptor agonists did not alter the interaction between Gα_i and CB$_1$. We speculate that binding of both CB$_1$ and D$_2$ agonists to CB$_1$ and D$_{2L}$, respectively, leads to agonist dose-dependent conformational changes within CB$_1$/D$_{2L}$/Gα_i complexes. This conformational change induces bidirectional allosteric modulation to reduce coupling of both receptors to Gα_i protein, while inducing each CB$_1$ and D$_{2L}$ homodimer within the CB$_1$/D$_{2L}$ complex to couple to Gα_s. In such a situation, D$_2$-selective agonists, through D$_{2L}$ receptor binding within CB$_1$/D$_{2L}$/Gα_i complexes, acted as allosteric modulators that altered the efficacy and potency of CB$_1$ to couple and activate different Gα protein pathways only in the presence of CB$_1$ agonist. At the same time, CB$_1$-selective agonists, binding to CB$_1$, acted as allosteric modulators that altered the efficacy and potency of D$_{2L}$ receptors to couple and activate different G proteins in the presence of D$_2$ agonist. The allosteric mechanisms exert negative and positive cooperatively with respect to Gα_i and Gα_s. Changes in GPCR and G-protein coupling following ligand application was also observed by Rashid *et al.*, (2007). D$_1$ and D$_2$ homomers are coupled to Gα_s and Gα_i, respectively. Heterodimerization between D$_1$ and D$_2$ results to a drastic shift of G protein coupling, where D$_1$/D$_2$ heterodimer is mainly coupled to a G$\alpha_{q/11}$ protein (Rashid *et al.,* 2007).

4.4.3 Co-Activation of Both CB$_1$ and D$_{2L}$ Potentiated CB$_1$/D$_{2L}$ Heterotetramers β-Arrestin Recruitment

CB$_1$ and D$_{2L}$ are known to interact with β-arrestin1, which mediates receptor

internalization, β-arrestin1-mediated signaling, receptor recycling and degradation (Laprairie *et al*., 2014; Sim-Selley and Martin, 2003; Wu *et al.,* 2008). Within CB_1/D_{2L} heterotetramers, the D_2 agonist acted as a positive allosteric modulator that potentiated the efficacy and potency of β-arrestin1 interaction with CB_1 receptors following the application of the CB_1 agonist. Similarly, the CB_1 agonist potentiated the interactions between β-arrestin1 and D_{2L}. These finding suggest bidirectional allosteric interactions between CB_1 and D_{2L} within CB_1/D_{2L} heterotetrameric complexes positively modulate β-arrestin1 recruitment to CB_1/D_{2L} complexes paralleled CB_1/D_{2L} complex co-internalization. Unlike the D_2 agonist quinpirole used in the current experiments, the high-affinity D_2 antagonist haloperidol acts as a negative allosteric modulator that reduced β-arrestin1 recruitment to CB_1 receptors and subsequently inhibited CB_1 receptor internalization (Przybyla and Watts, 2010). Quinpirole did not alter β-arrestin1-CB_1 interaction in the absence of D_{2L}. Similarly, the CB_1 agonist ACEA did not alter β-arrestin1-D_{2L} interactions in the absence of CB_1. Therefore, expression and activation, and not simply ligand binding, of both CB_1 and D_{2L} is required for the potentiation β-arrestin1 recruitment to CB_1/D_{2L} complexes. As was observed for CB_1/D_{2L} heterotetramers,, agonist co-activation of other GPCR heteromers have been shown to alter agonist- induced β-arrestin recruitment to receptor complexes (Borroto-Escuela *et al.,* 2011). In A_{2A}/D_{2L} co-expressing cells, A_{2A}/D_{2L} form heterotetramers and the A_{2A} agonist CGS21680 was found to enhance the D_2 agonist-induced β-arrestin1 recruitment to D_{2L} receptors with subsequent co-internalization of $A_{2A}R/D_{2L}$ complexes (Borroto-Escuela *et al.,* 2011).

In addition to modulating β-arrestin1 binding and receptor internalization, co-treatment of CB_1/D_{2L} heterotetramers with CB_1 and D_2 agonists significantly augmented β-arrestin1-dependent ERK phosphorylation compared to cells treated with either CB_1 agonist or D_2 agonist alone. β-arrestin1-dependent ERK phosphorylation was insensitive to Ptx treatment, but was significantly reduced in cells expressing a β-arrestin1 dominant negative mutant. The potentiation of β-arrestin1-dependent ERK phosphorylation can be explained by the potentiation of β-arrestin1 binding to CB_1/D_{2L} complexes. Similarly, the co-activation of both D_1 and D_3 with their agonists, 7-OH-PIPAT and SKF 38393, respectively, increased recruitment of β-arrestin1 to D_1/D_3 heterotetramers and

176

potentiated β-arrestin1-dependent ERK phosphorylation compared to levels observed when single agonist was applied (Guitart *et al*., 2014).

4.5 Conclusion

Taken together, the results presented here demonstrated bidirectional allosteric interactions between CB_1 and D_{2L} within CB_1/D_{2L} heterotetramers, which modulate both G protein-coupling and G protein-dependent signaling as well as β-arrestin1 recruitment and G-protein-independent ERK signaling. The concept of bidirectional allosteric interaction between CB_1/D_{2L} heterotetramers has important implications for understanding the activity of receptor complexes in native tissues and the potential for altered drug response under pathological conditions. For example, patients with Parkinson's disease, which is characterized by the progressive loss of dopaminergic neurons in the substantia nigra *pars compacta* and dopaminergic denervation of the striatum (Pisani *et al*., 2011; El Khoury *et al.,* 2012), may have altered responses to their prescribed Parkinson's disease medication if they are prescribed cannabinoids or choose to expose themselves to cannabinoids. Treatment of Parkinson's disease frequently involves the administration of levodopa to increase striatal dopamine levels or administration of direct dopamine agonists. The half-life of levodopa is relatively short requiring multiple daily dosing leading to peak and trough values throughout the day (Brooks, 2008). The timing of exposure to cannabinoids in relation to levodopa or dopamine agonists could influence drug response and the pool of receptors at the membrane. In addition, the dose, potency, combination of cannabinoids (such as levels of THC relative to cannabidiol, and half-life of specific cannabinoids within marijuana may not be consistent such that the response to the combination of drugs may be variable. On the other hand, understanding the interaction within CB_1/D_{2L} heterotetramers may assist in the design, identification and use of novel combinations of ligands. Ligands specifically targeting CB_1/D_{2L} heterotetramers within restricted neuronal populations may be beneficial in central nervous disorders associated with dopaminergic and/or endocannabinoid signaling dysregulation.

4.6 Supplementary Figures

Supplementary Figure 4.1: CB₁ and β_2AR ***Receptors form Homodimers When Expressed in HEK 293A Cells Demonstrated Using BiFC.*** **(A)** HEK 293A cells were transfected with CB_1-VC, CB_1-VN, or CB_1-VC and, CB_1-VN with or without CB_1/D_{2L} hetero-oligomer blocking peptide (CB_1-BP). * $P < 0.01$ compared to cells expressing CB_1-VN. **(B)** HEK 293A cells were transfected with β_2AR-VC, β_2AR-VN or β_2AR-VC, and β_2AR-VN. Fluorescence was measured using an EnVision plate reader with excitation at 515 nm and emission at 528 nm. * $P < 0.01$ compared to cells expressing β_2AR-VN. Data are presented as mean ± SEM of 4 independent experiments, significance was determined *via* one-way ANOVA followed by Tukey's *post-hoc* test.
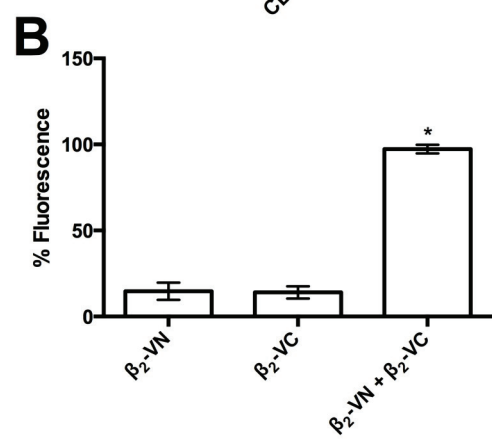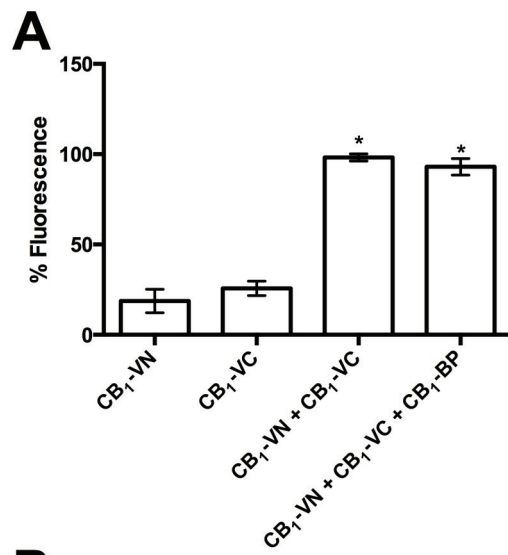
Supplementary Figure 4.2: Kinetic Interaction of CB₁ and D₂L with Gαᵢ and Gαₛ Proteins. BRET$_{Eff}$ was measured over 540 s in cells expressing Gα$_i$-Rluc, CB$_1$-GFP^2, and D$_{2L}$-pcDNA **(A)**, Gα$_s$-Rluc, CB$_1$-GFP^2, and D$_{2L}$-pcDNA **(B)**, Gα$_i$-Rluc, D$_{2L}$-GFP^2, and CB$_1$-pcDNA or **(C)** or Gα$_s$-Rluc, D$_{2L}$-GFP^2, and CB$_1$-pcDNA **(D)**. Cells were treated with vehicle, 1 μM ACEA, 1 μM quinpirole alone or in combination added at 50 sec after the addition of Coelenterazine 400a. Arrows indicate the times of drug(s) application. Data are presented as mean ± SEM of 4 independent experiments.

A   **Gαi-Rluc + CB$_1$-GFP^2 + D$_{2L}$-pcDNA**

- 1 μM ACEA
- 1 μM Quinpirole
- 1 μM ACEA + 1 μM Quinpirole
- Vehicle

B   **Gαs-Rluc + CB$_1$-GFP^2 + D$_{2L}$-pcDNA**

- 1 μM ACEA
- 1 μM Quinpirole
- 1 μM ACEA + 1 μM Quinpirole
- Vehicle

C   **Gαi-Rluc + D$_{2L}$-GFP^2 + CB$_1$-pcDNA**

- 1 μM ACEA
- 1 μM Quinpirole
- 1 μM ACEA + 1 μM Quinpirole
- Vehicle

D   **Gαs-Rluc + D$_{2L}$-GFP^2 + CB$_1$-pcDNA**

- 1 μM ACEA
- 1 μM Quinpirole
- 1 μM ACEA + 1 μM Quinpirole
- Vehicle

181
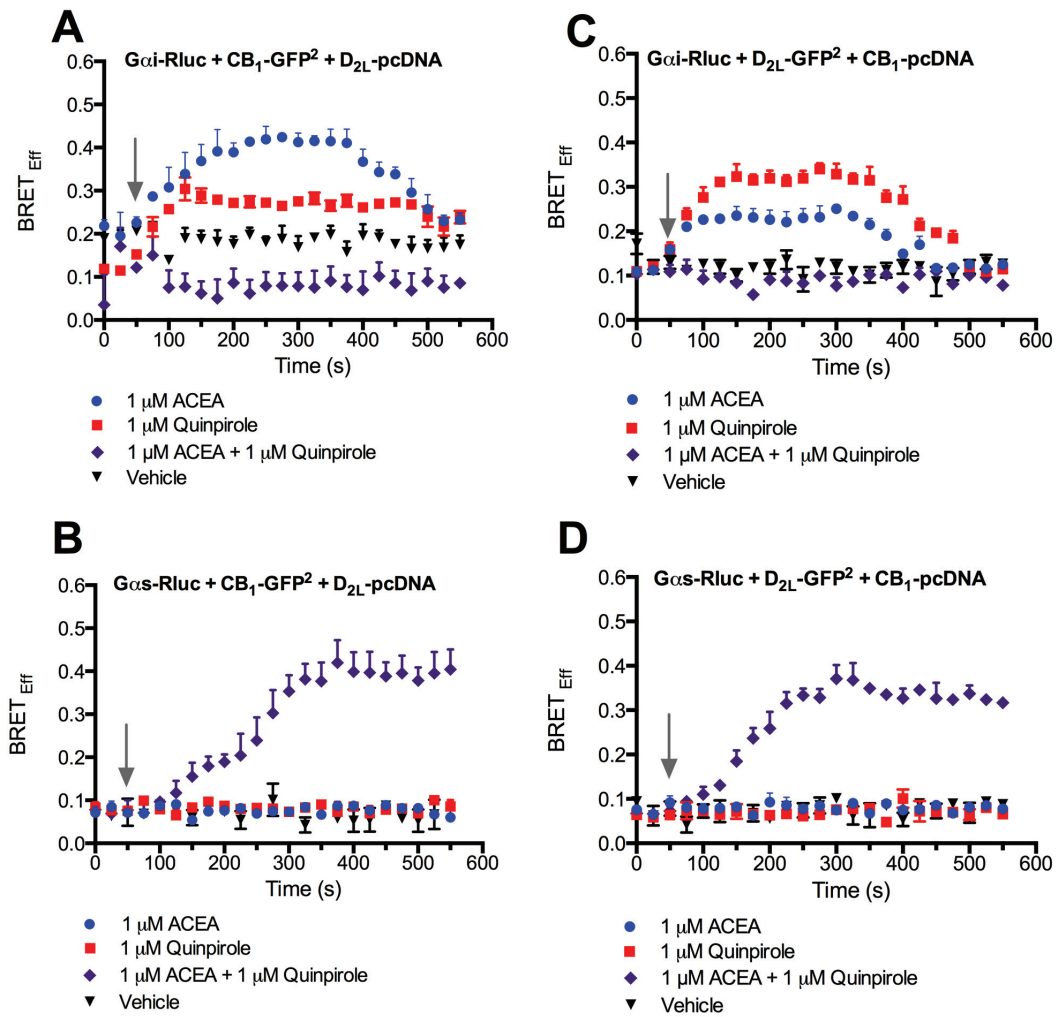
Supplementary Figure 4.3: The Expression of CB$_1$-Gα$_i$-BP Does Not Alter the Ability of the CB$_1$ and D$_{2L}$ to Form Heterotetramers. Cells were transfected with D$_2$ Rluc, D$_2$-GFP[2], CB$_1$-VN and CB$_1$-VC together with an empty pcDNA, CB$_1$-BP or CB$_1$- Gα$_i$-BP. SRET[2] combined with BiFC was performed. * *P* < 0.01 compared to cells expressing empty pcDNA; *n.s. P* > 0.05 relative to cells expressing empty pcDNA. Data are presented as mean ± SEM of 4 independent experiments, significance was determined *via* one-way ANOVA followed by Tukey's *post-hoc* test.

D_{2L}-Rluc + D_2-GFP^2 + CB$_1$-VN + CB$_1$-VC

net SRET^2

n.s

*

pcDNA   CB$_1$-BP   CB$_1$-Gα$_i$-BP
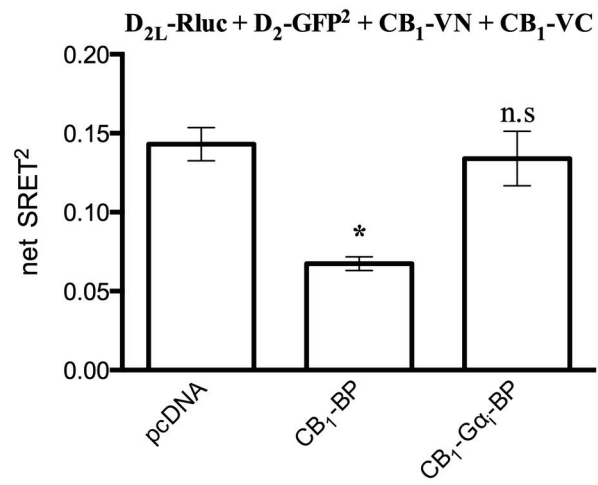
Supplementary Figure 4.4: CB₁ and D₂L Do Not Interact With Gα_s Proteins. BRET$_{Eff}$ was measured following the addition of vehicle or 1 µM ACEA +/- 24 h pre-treatment with 50 ng/ml CTx **(A)** in cells expressing Gα_s-Rluc and CB$_1$-GFP^2 or **(B)** cells expressing Gα_s-Rluc and D$_{2L}$-GFP^2. Controls included cell transfected with Gα_s-Rluc and β_2AR-GFP^2 (positive control) or HERG-GFP^2 (negative control) treated with vehicle or β_2AR agonist isoprenaline. * $P < 0.01$ compared to cells expressing Gα_s-Rluc and HERG-GFP^2; ~ $P < 0.01$ compared to cells expressing Gα_s-Rluc and β_2AR-GFP^2 and treated with vehicle; *n.s. P > 0.05* relative to cells expressing Gα_s-Rluc and HERG-GFP^2. Data are presented as mean ± SEM of 4 independent experiments; significance was determined *via* one-way ANOVA followed by Tukey's *post-hoc* test.

A

Vehicle	+	+	+	-	-	+	+	-	-
1 µM ACEA	-	-	-	-	-	-	-	+	+
1 µM Isoprenaline			-	+	+	-	-	-	-
50 ng/ml CTx	-	-	+	-	+	-	+	-	+

■ Gαs -Rluc + HERG-GFP^2

■ Gαs -Rluc + β$_2$-GFP^2

□ Gαs -Rluc + CB$_1$-GFP^2

B

Vehicle	+	+	+	-	-	+	+	-	-
1 µM Quinpirole	-	-	-	-	-	-	-	+	+
1 µM Isoprenaline			-	+	+	-	-	-	-
50 ng/ml CTx	-	-	+	-	+	-	+	-	+

■ Gαs -Rluc + D$_{2L}$-GFP^2

■ Gαs -Rluc + β$_2$-GFP^2

□ Gαs -Rluc + D$_{2L}$-GFP^2

Supplementary Figure 4.5: Blocking the Interaction Between CB₁ and D₂ₗ Inhibited ***the Switch of CB₁ and D₂ₗ Coupling from Gα_i to Gα_s Proteins Following Co-*** ***Application of Both Receptor Agonists***. $BRET_{Eff}$ was measured in cells treated with vehicle, 1 μM ACEA, 1 μM quinpirole alone or in combination. **(A)** Cells expressing $Gα_i$-Rluc, CB_1-GFP^2, D_{2L}-pcDNA together with an empty vector pcDNA or CB_1-B **(B)** Cells expressing $Gα_i$-Rluc, CB_1-GFP^2, D_{2L}-pcDNA together with an empty vector pcDNA or CB_1-BP. * $P < 0.01$ compared to cells expressing empty pcDNA and treated with quinpirole; ~ $P < 0.01$ compared to cells expressing empty pcDNA and treated with ACEA and quinpirole; # $P < 0.01$ compared to cells expressing empty pcDNA and treated with ACEA; *n.s.* $P > 0.05$ relative to cells expressing empty pcDNA within treatment group. Data are presented as mean ± SEM of 4 independent experiments, one-way ANOVA followed by Tukey's *post-hoc* test.
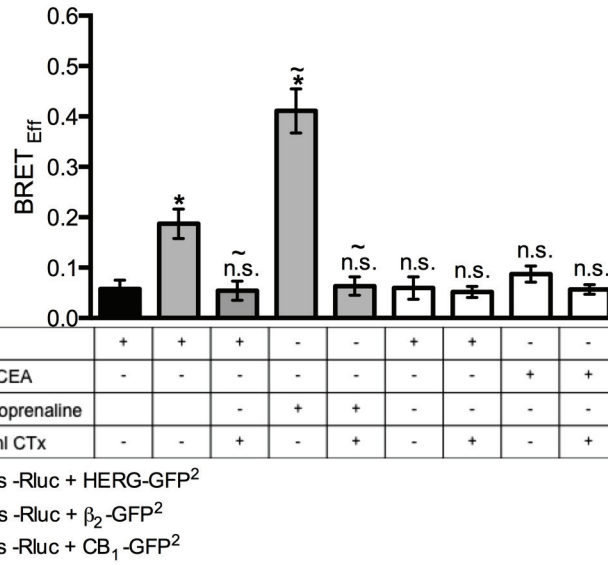
A

Gαi-Rluc + CB₁-GFP² + D₂L-pcDNA
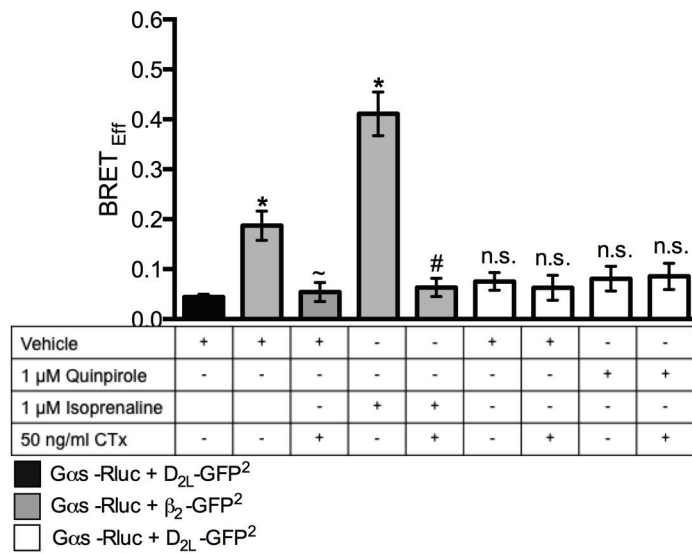
B

Gαi-Rluc + D₂L-GFP² + CB₁-pcDNA
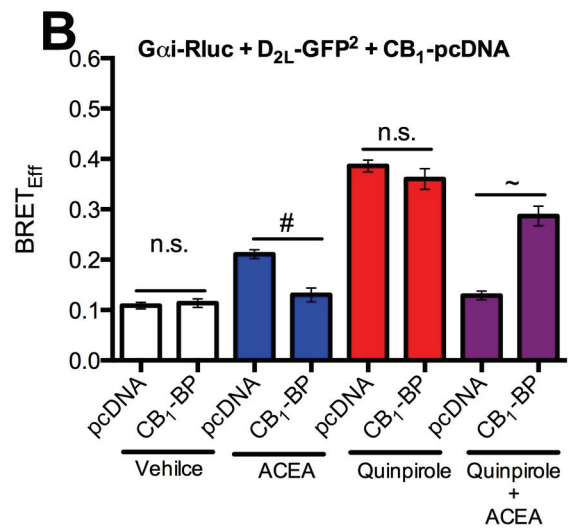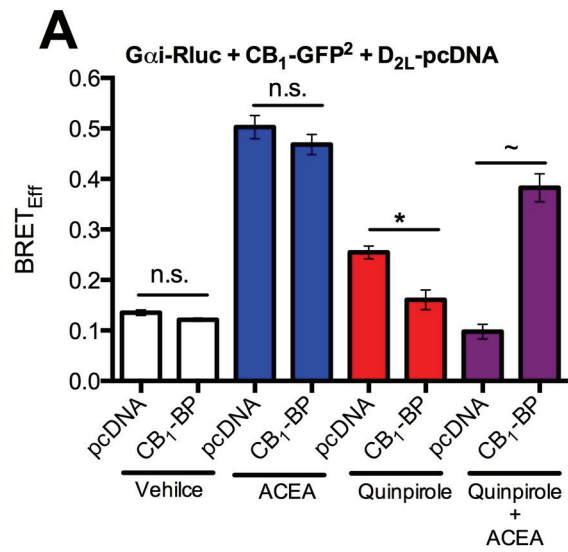
Supplementary Figure 4.6: The Co-Expression and Co-Activation of Either CB$_1$ and β$_2$AR or D$_{2L}$ and β$_2$AR Did Not Alter CB$_1$ or D$_2$ Coupling to G proteins. BRET$_{Eff}$ was measured in cells expressing Gα$_i$-Rluc **(A, C)** or Gα$_s$-Rluc **(B, D)** and either CB$_1$-GFP^2, D$_{2L}$-GFP^2, β$_2$-GFP^2 or the negative control HERG-GFP^2 and treated with vehicle, 1 μM ACEA, 1 μM quinpirole, 1 μM isoprenaline alone or in combination. * $P < 0.01$ compared to cells expressing Gα$_i$-Rluc or Gα$_s$-Rluc and HERG-GFP^2. Data are presented as mean ± SEM of 4 independent experiments, one-way ANOVA followed by Tukey's *post-hoc* test.

A

BRET $_{Eff}$

x-axis: Vehicle, Vehicle, Isoprenaline, ACEA, ACEA+Quinpirole, ACEA, ACEA+Isoprenaline

- ■ Gαi -Rluc + HERG-GFP^2
- ▨ Gαi -Rluc + β$_2$-GFP^2 + CB$_1$-pcDNA
- □ Gαi -Rluc + CB$_1$-GFP^2 + D$_{2L}$-pcDNA
- ▦ Gαi -Rluc + CB$_1$-GFP^2 + β$_2$-pcDNA
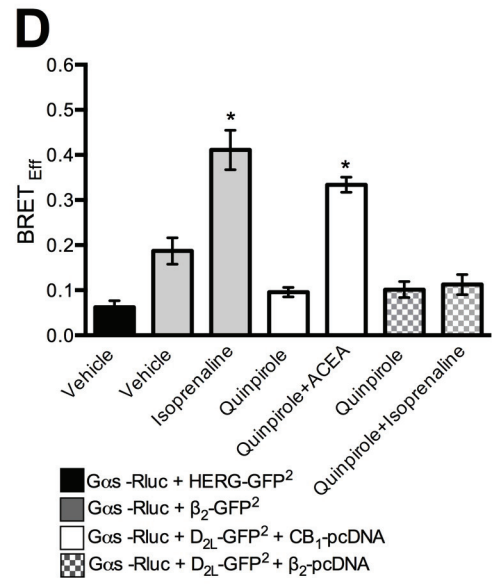
B

BRET $_{Eff}$

x-axis: Vehicle, Vehicle, Isoprenaline, ACEA, ACEA+Quinpirole, ACEA, ACEA+Isoprenaline

- ■ Gαs-Rluc + HERG-GFP^2
- ▨ Gαs -Rluc + β$_2$-GFP^2 + CB$_1$-pcDNA
- □ Gαs -Rluc + CB$_1$-GFP^2 + D$_{2L}$-pcDNA
- ▦ Gαs -Rluc + CB$_1$-GFP^2 + β$_2$-pcDNA

C

BRET $_{Eff}$

x-axis: Vehicle, Vehicle, Isoprenaline, Quinpirole, Quinpirole+ACEA, Quinpirole, Quinpirole+Isoprenaline

- ■ Gαi -Rluc + HERG-GFP^2
- ▨ Gαi -Rluc + β$_2$-GFP^2
- □ Gαi -Rluc + D$_{2L}$-GFP^2 + CB$_1$-pcDNA
- ▦ Gαi -Rluc + D$_{2L}$-GFP^2 + β$_2$-pcDNA

D

BRET $_{Eff}$

x-axis: Vehicle, Vehicle, Isoprenaline, Quinpirole, Quinpirole+ACEA, Quinpirole, Quinpirole+Isoprenaline

- ■ Gαs -Rluc + HERG-GFP^2
- ▨ Gαs -Rluc + β$_2$-GFP^2
- □ Gαs -Rluc + D$_{2L}$-GFP^2 + CB$_1$-pcDNA
- ▦ Gαs -Rluc + D$_{2L}$-GFP^2 + β$_2$-pcDNA

189

Supplementary Figure 4.7: The Co-Application of ACEA and Quinpirole Switched CB₁ *Coupling and Signaling From $G\alpha_i$ to $G\alpha_s$ Proteins in STHdh$^{Q7/Q7}$ Cells.* BRET$_{Eff}$ was measured in STH*dh*$^{Q7/Q7}$ cells expressing $G\alpha_i$-Rluc and CB₁-GFP² +/- D$_{2L}$-pcDNA **(A)** or $G\alpha_s$-Rluc and CB₁-GFP² +/- D$_{2L}$-pcDNA **(B)** and treated with vehicle, 1 μM ACEA, 1 μM quinpirole or both agonists. * $P < 0.01$ compared to cells treated with vehicle; ~ $P < 0.01$ relative to cells expressing $G\alpha_i$-Rluc and CB₁-GFP² and treated with 1 μM ACEA and 1 μM quinpirole; *n.s.* $P > 0.05$ relative to cells expressing $G\alpha_i$-Rluc and CB₁-GFP² or $G\alpha_i$-Rluc and CB₁-GFP². HEK 293A cells were treated with 1 μM ACEA, 1 μM quinpirole or both agonists +/- 24 h pretreatment with 50 ng/ml PTx or CTx; ERK phosphorylation was measured 5 min following ACEA, quinpirole or the combination **(C)**, while CREB phosphorylation was measured following 30 min treatment **(D)**. * $P < 0.01$ compared to vehicle treatment; ~ $P < 0.01$ compared to cells treated with 1 μM ACEA. Data are presented as mean ± SEM of 4 independent experiments, one-way ANOVA followed by Tukey's *post-hoc* test.
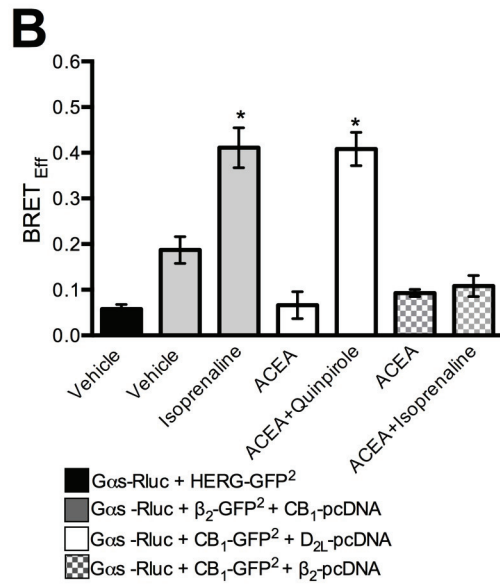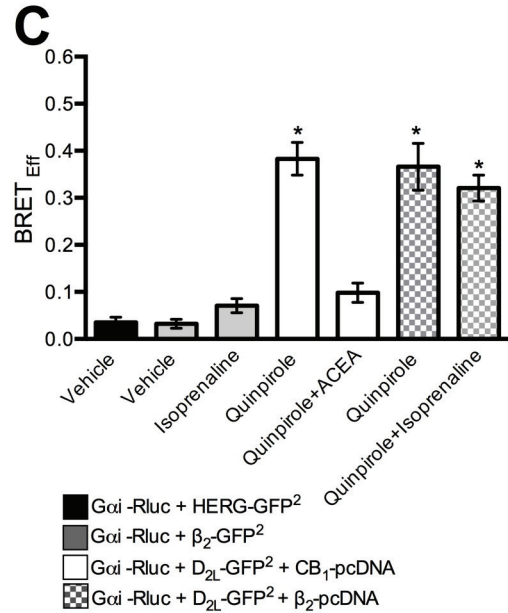
A
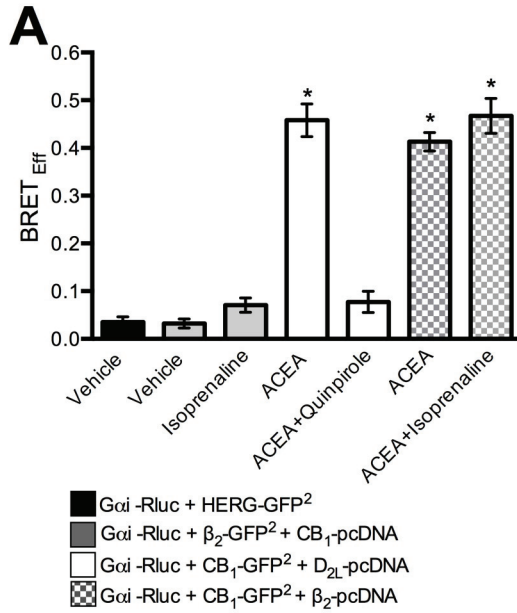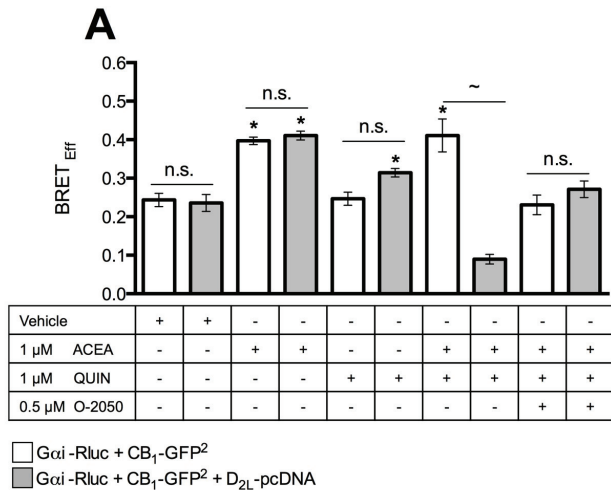
BRET$_{Eff}$

Vehicle	+	+	-	-	-	-	-	-	-	-
1 μM ACEA	-	-	+	+	-	-	+	+	+	+
1 μM QUIN	-	-	-	-	+	+	+	+	+	+
0.5 μM O-2050	-	-	-	-	-	-	-	-	+	+

☐ Gαi -Rluc + CB$_1$-GFP^2
▨ Gαi -Rluc + CB$_1$-GFP^2 + D$_{2L}$-pcDNA

B

BRET$_{Eff}$

Vehicle	+	+	-	-	-	-	-	-	-	-
1 μM ACEA	-	-	+	+	-	-	+	+	+	+
1 μM QUIN	-	-	-	-	+	+	+	+	+	+
0.5 μM O-2050	-	-	-	-	-	-	-	-	+	+

☐ Gαs -Rluc + CB$_1$-GFP^2
▨ Gαs -Rluc + CB$_1$-GFP^2 + D$_{2L}$-pcDNA

C

pERK/ Total ERK

Vehicle | No Toxin | PTx | CTx | No Toxin | PTx | Ctx | No Toxin | PTx | Ctx
1 μM ACEA | 1 μM Quinpirole | 1 μM Quinpirole + 1 μM ACEA

D

pCREB / Total CREB

Vehicle | No Toxin | PTx | CTx | No Toxin | PTx | CTx | No Toxin | PTx | CTx
1 μM ACEA | 1 μM Quinpirole | 1 μM Quinpirole + 1 μM ACEA
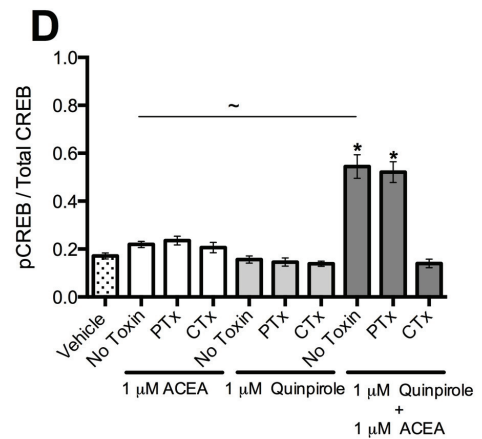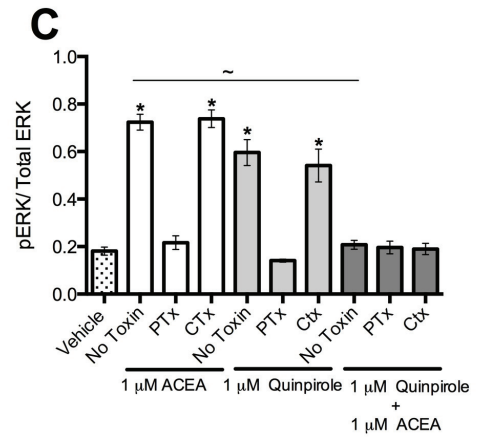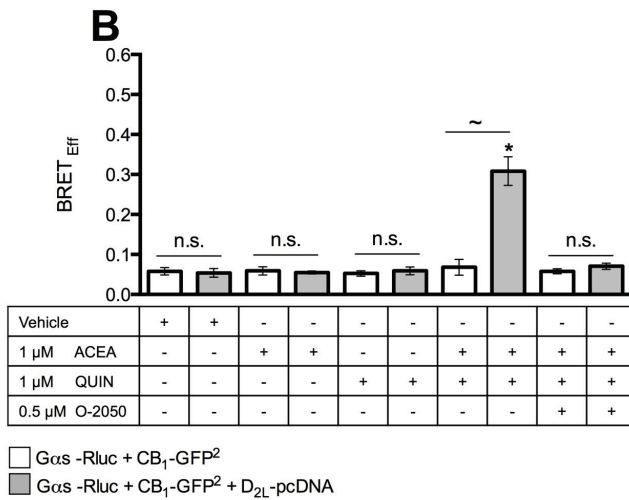
Supplementary Figure 4.8: The Potentiation of β-arrestin1 Recruitment to CB$_1$ and D$_{2L}$ Following ACEA and Quinpirole Co-Application is Specific to CB$_1$/D$_{2L}$ Heteromer. HEK 293A Cells were transfected with β-arrestin1-Rluc + CB$_1$-GFP^2 + mGluR6-pcDNA **(A)** or D$_{2L}$-Rluc + β-arrestin1-GFP^2 + mGluR6-pvDNA **(B)**. BRET$_{Eff}$ signals were measured over 60 min following the application of vehicle, 1 μM ACEA, 1 μM quinpirole or 1 μM L-AP4 alone or in combination. Data are presented as mean ± SEM of 4 independent experiments.
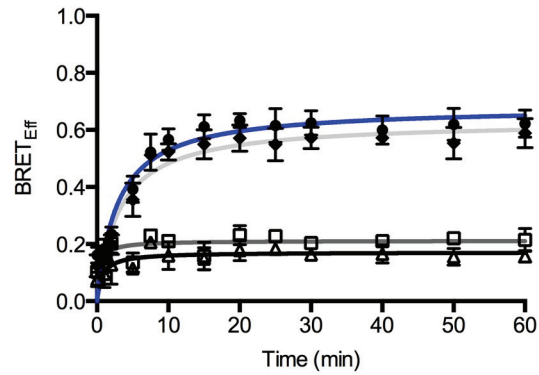
A

β-arrestin1-Rluc + CB$_1$-GFP^2 + mGluR6-pcDNA + 1 μM ACEA
β-arrestin1-Rluc + CB$_1$-GFP^2 + mGluR6-pcDNA + 1 μM L-AP4
β-arrestin1-Rluc + CB$_1$-GFP^2 + mGluR6-pcDNA + 1 μM ACEA + 1 μM L-AP4
β-arrestin1-Rluc + CB$_1$-GFP^2 + mGluR6-pcDNA + Vehicle

B
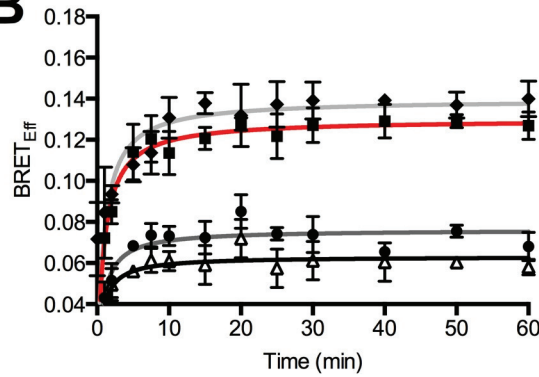
D$_{2L}$-Rluc + β-arrestin1-GFP^2 + CB$_1$-pcDNA + 1 μM Quinpirole
D$_{2L}$-Rluc + β-arrestin1-GFP^2 + mGluR6-pcDNA + 1 μM L-AP4
D$_{2L}$-Rluc + β-arrestin1-GFP^2 + mGluR6-pcDNA + 1 μM Quinpirole + 1 μM L-AP4
D$_{2L}$-Rluc + β-arrestin1-GFP^2 + mGluR6-pcDNA + Vehicle

193

CHAPTER 5

CHRONIC CANNABINOID AND TYPICAL ANTIPSYCHOTIC TREATMENT REDUCE CANNABINOID RECEPTOR TYPE 1 (CB$_1$) AND THE DOPAMINE RECEPTOR TYPE 2 (D$_2$) HETEROMER EXPRESSION IN THE GLOBUS PALLIDUS OF MICE

Copyright Statement

This chapter is being prepared for submission as Amina M. Bagher, James T. Toguri, Robert B. Laprairie, Adel Zrein, Melanie E.M. Kelly, and Eileen M. Denovan-Wright. Chronic cannabinoid and typical antipsychotic treatment reduce cannabinoid receptor type 1 (CB$_1$) and the dopamine receptor type 2 (D$_2$) heteromer expression in the globus pallidus of mice. *Journal of Neuroscience Research*. The manuscript is in preparation. The manuscript has been modified to meet formatting requirements.

Contribution Statement

The manuscript used as the basis for this chapter was written with guidance from Dr. Eileen Denovan-Wright. Data were collected and analyzed by myself. Data were collected by myself with assistance from Dr. Robert B. Laprairie, Dr. James T. Toguri, and Adel Zrein. Critical reagents were provided by Drs. Eileen Denovan-Wright and Melanie Kelly.

5.1 Abstract

The cannabinoid receptor type 1 (CB_1) and the dopamine receptor type (D_{2L}) are co-localized on medium spiny neuron terminals in the globus pallidus where they play an important role in modulating voluntary movement. Physical interactions between the two receptors (heteromerization) have been shown to alter receptor coupling and signaling in cell culture. The main objectives of the current study were to examine whether CB_1 and D_{2L} heteromers can be detected in the globus pallidus of C57BL/6J mice and to determine whether CB_1/D_{2L} heteromer levels are altered following chronic treatment with cannabinoids and antipsychotic alone or in combination. By using *in situ* proximity ligation assays, we observed CB_1 and D_{2L} heteromer-specific signals in the globus pallidus of C57BL/6J mice. An increase in CB_1/D_{2L} heteromer-specific signal was observed in the globus pallidus of C57BL/6J mice following chronic CP 55,940 treatment. In contrast, haloperidol treatment reduced CB_1/D_{2L} heteromer-specific signals. Olanzapine treatment did not affect CB_1/D_{2L} heteromer-specific signals relative to vehicle treatment. Chronic co-treatment with CP 55,940 and haloperidol resulted in CB_1/D_{2L} heteromer-specific signals similar to those observed in the haloperidol-treated group. Chronic co-treatment with CP 55,940 and olanzapine resulted in a similar distribution of heteromers as the CP 55,940-treated group. The alteration in CB_1/D_{2L} heteromer-specific signals following persistent ligand exposure was due to alteration in the mutual affinity of CB_1 and D_{2L} receptors and was not due to changes in CB_1/D_{2L} protein expression or receptor co-localization. Chronic exposure to cannabinoid and antipsychotics alone or in combination alters CB_1/D_{2L} heteromerization and affects movement.

5.2 Introduction

The endocannabinoid system (ECS) and dopaminergic system (DS) play important roles modulating voluntary movement under the control of the basal ganglia (reviewed in Fernández-Ruiz *et al.,* 2010; El Khoury *et al*., 2012; Bloomfield *et al.,* 2016; García *et al.,* 2016). Stimulating dopaminergic transmission in the basal ganglia results in hyperkinesia (Gershanik *et al.,* 1983; Kelly *et al.,* 1998; reviewed in Iversen and Iversen, 2007), whereas blocking normal dopamine function leads to hypolocomotion (Hauber and Lutz, 1999; Schindler and Carmona, 2002). In contrast, activation of the

195

ECS has been associated with motor inhibition, although effects on locomotion are dose-dependent (McGregor *et al.,* 1996, reviewed in Giuffrida and Piomelli, 2000; Fernández-Ruiz and Gonzáles 2005; Fernández-Ruiz, 2009; Kluger *et al.,* 2015). Interactions between the ECS and DS have been described. For example, cannabinoid agonists block both dopamine agonist-induced hyperlocomotion (Marcellino *et al.,* 2008) and amphetamine-induced hyperactivity (Gorriti *et al.,* 1999). Interactions between the ECS and DS may occur indirectly through the independent modulation of GABA- and/or glutamate release (reviewed in Fernández-Ruiz *et al.,* 2010; El Khoury *et al*., 2012; Bloomfield *et al.,* 2016; García *et al.,* 2016). The interactions can also occur at the synapse *via* depolarization-induced suppression of excitation (DSE) and inhibition (DSI) involving receptors located on both sides of the synaptic cleft (reviewed in Fernández-Ruiz *et al.,* 2010; El Khoury *et al*., 2012). In addition, recent evidence indicates that the cannabinoid receptor type 1 (CB_1) is able to physically interact with the dopamine receptor 2 long (D_{2L}) to form heteromers (Kearn *et al.,* 2005; Marcellino *et al.,* 2008; Przybyla and Watts, 2010; Bagher *et al*., 2016, 2017). Heteromers composed of CB_1 and D_{2L} might represent an additional pharmacological target for the combined effects of cannabinoids and dopaminergic ligands. Both receptors are co-localized in GABAergic medium spiny projection neuron (MSN) terminals located in the globus pallidus of rodents and primates (Herkenham *et al.,* 1991; Levey *et al*., 1993; Ong and Mackie, 1999; Pickel *et al*., 2006). Heteromerization between CB_1 and D_{2L} has been detected in the striatum of *Macaca fascicularis* using *in situ* proximity ligation assays (PLA), demonstrating that the association between CB_1/D_{2L} receptors occurs in native tissues (Bonaventura *et al*., 2014).

Physical and functional interactions between CB_1 and D_{2L} receptors have been observed in cell culture. Physical interactions between CB_1 and D_{2L} receptors have been observed using co-immunoprecipitation, Förster resonance energy transfer (FRET), bioluminescence resonance energy transfer (BRET) and bimolecular fluorescence complementation (BiFC) (Kearn *et al.,* 2005; Marcellino *et al.,* 2008; Przybyla and Watts 2010; Bagher *et al*., 2016). Functional interactions have been observed in cells co-expressing both CB_1 and D_{2L} receptors. Stimulation of either CB_1 or D_{2L} receptors by receptor-specific agonists resulted in the activation of the $G\alpha_i$ protein, while simultaneous

co-activation of both receptors switched coupling and signaling from $G\alpha_i$ to $G\alpha_s$ protein (Glass and Felder, 1997; Kearn *et al.,* 2005; Marcellino *et al.,* 2008; Bagher *et al.*, 2016). The co-ligand dependent switch in signaling is dependent on reciprocal allosteric modulation of G protein coupling, which results in CB_1 and D_{2L} heteromer-specific signaling and co-internalization that differs from independent CB_1 or D_2 receptor signaling (Bagher *et al.,* 2017). It has been suggested that ligands that bind CB_1 and/or D_{2L} might modulate receptor expression and the proportion of CB_1 and D_{2L} receptors existing in homo- versus heteromers (Bonaventura *et al.,* 2014). For example, CB_1/D_{2L} heteromer expression was lower in the striatum of *Macaca fascicularis* following chronic administration of the dopamine precursor levodopa (L-DOPA) (Bonaventura *et al.,* 2014).

Given the documented interactions between CB_1 and D_{2L} receptors in cultured cells and brain tissue, receptor-specific ligands must be considered in the context of their effects on the cognate receptor, and on interacting receptors within heteromeric complexes. Drugs that act on the D_2 receptors such as typical- and atypical-antipsychotics are prescribed for the management of movement disorders such as Tics, Tourette syndrome and Huntington's disease (Videnovic, 2013; Gilberta and Jankovicb, 2014; Wyant *et al.*, 2017). Typical and atypical antipsychotics, however, have been shown to have different clinical, biochemical and behavioral profiles (reviewed in Seeman and Ulpian, 1988; Lowe *et al.*, 1988; Blin, 1999; Rummel-Kluge *et al.*, 2012). Patients prescribed typical- or atypical- antipsychotics are sometimes exposed to cannabinoids for therapeutic or recreational purposes. Based on the co-localization of CB_1 and D_{2L} in MSN terminals in the globus pallidus, we hypothesized that chronic cannabinoid and antipsychotics administration alone or in combination differentially affects CB_1/D_2 heteromerization and protein expression, which in turn affects motor output. In the current study, *in situ* PLA was utilized to detect CB_1/D_2 heteromerization and to measure changes in CB_1/D_2 heteromer-specific PLA signals following chronic drug administration of either cannabinoid or antipsychotics alone or in combination. Heteromer distribution was measured in the globus pallidus of C57BL/6J mice and in a cell culture model of MSN that endogenously expresses both CB_1 and D_{2L} receptors. Haloperidol and olanzapine were chosen as representative typical and atypical

antipsychotics, respectively. Haloperidol acts primarily as a D_2 dopamine receptor antagonist. In contrast, olanzapine is an antagonist at many receptors, including 5-HT$_{2A}$, H_1, D_2, D_4, and M_5 receptors (reviewed in Murray *et al*., 2017). The CB$_1$ agonist CP 55,940 was used in the current study; this synthetic cannabinoid has similar tetrad effects and ligand bias compared to the phytocannabinoid delta-9-tetrahydrocannabinol (THC) found in *Cannabis* (Glass and Northup, 1999; Mukhopadhyay and Howlett 2005; Laprairie *et al*., 2016; reviewed in Laprairie *et al*., 2017).

5.3 Results

5.3.1 CB$_1$ and D$_2$ Heteromers are Found in the Globus Pallidus of C57BL/6J Mice, and Chronic Cannabinoid and/or Antipsychotic Treatment Alters CB$_1$/D$_2$ Heteromer-Specific PLA Signals

The first aim of the current study was to examine whether CB$_1$ and D_2 receptors physically associate in the globus pallidus of C57BL/6J mice. *In situ* PLA detects endogenous receptors that are in close proximity (< 16 nm). In PLA, closely associated receptors allow two different receptor-specific antibody-DNA probes to form a ligation complex resulting in a punctate fluorescent signal (PLA signal) that can be detected by fluorescence microscopy. By incubating mouse brain slices with two primary antibody-DNA probes directed against the N-terminal of CB$_1$ and D_{2L} receptors, we observed CB$_1$/D_{2L} heteromer-specific PLA signals in the globus pallidus (Fig. 5.1A, B). PLA signals were not observed when brain slices were incubated with CB$_1$ or D_2 antibody/probe alone (data not shown). These results indicate that CB$_1$ and D_{2L} can physically associate in the globus pallidus.

Our second aim was to investigate whether chronic exposure to cannabinoid or antipsychotic treatment alone or in combination alters the number of CB$_1$/D_{2L} heteromer-specific PLA signals in the globus pallidus of C57BL/6J mice. C57BL/6J mice were treated with vehicle or 0.01 mg/kg/d CP 55,940, 0.3 mg/kg/d haloperidol, 1.5 mg/kg/d olanzapine, or co-treated with 0.01 mg/kg/d CP 55,940 and 0.3 mg/kg/d haloperidol or 0.01 mg/kg/d CP 55,940 and 1.5 mg/kg/d olanzapine. Dosages used in this study were based on previous studies and were chosen for pharmacological and behavioral effects (Arjona *et al.,* 2004, Huang *et al.,* 2006; Han *et al.,* 2009). The dosages of haloperidol

Figure 5.1: Chronic Haloperidol Treatment Inhibited CB$_1$/D$_2$ Heteromer-Specific PLA Signals in the Globus Pallidus of C57BL/6J Mice, Unlike CP 55,940 Which Increased CB$_1$/D$_2$ Heteromer-Specific PLA Signals. **(A)** *In situ* PLA in the globus pallidus following treatment for 21 days with vehicle or 0.01 mg/kg/d CP 55,940, 0.3 mg/kg/d haloperidol or 1.5 mg/kg/d olanzapine i.p. alone or in combination and primary antibodies for CB$_1$ and D$_{2L}$ receptors. Microscopy images (superimposed sections) are shown in where heteromers appear as red dots, while cell nuclei were stained with DAPI (blue). Scale bars: 10 μm. **(B)** PLA signals were presented as the number of the red dot per 1000 μM^2 from three different fields within globus pallidus from five different animals per group. * $P < 0.01$ compared to vehicle-treated group. # $P < 0.01$ compared to CP 55,940-treated group. Data are presented as mean ± SEM of 15 different fields. Significance was determined *via* one-way ANOVA followed by Tukey's *post-hoc* test.

A)
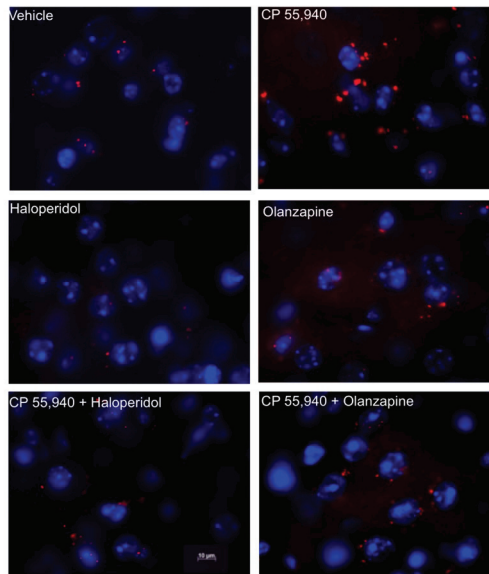
B)
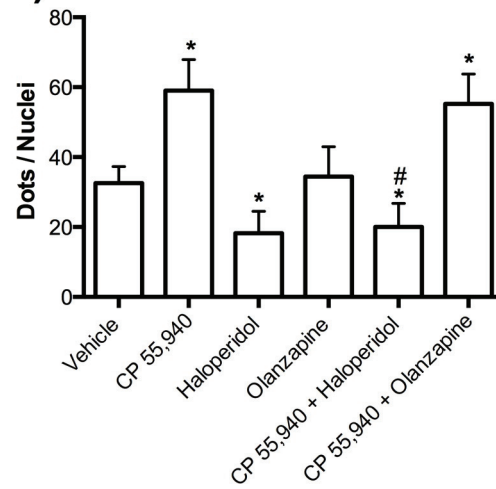
and olanzapine result in 70-80% D_2 receptor occupancy in rats (Kapur and Mamo, 2003, Natesan *et al.,* 2006). The dose of CP 55,940 was chosen based on the preliminary studies of Marcellino *et al*. (2008). Daily drug injection began when mice were 7 weeks of age and continued for 3 weeks (21 days). At the end of the study, mouse brains were collected and brain sections were prepared. *In situ* PLA assays were performed to detect changes in the number of CB_1/D_{2L} heteromers-specific PLA signals for each treatment. The numbers of CB_1/D_{2L} heteromer-specific PLA signals was reduced in the globus pallidus of haloperidol-treated mice compared with vehicle (Fig. 5.1A, B). CP 55,940 increased the number of 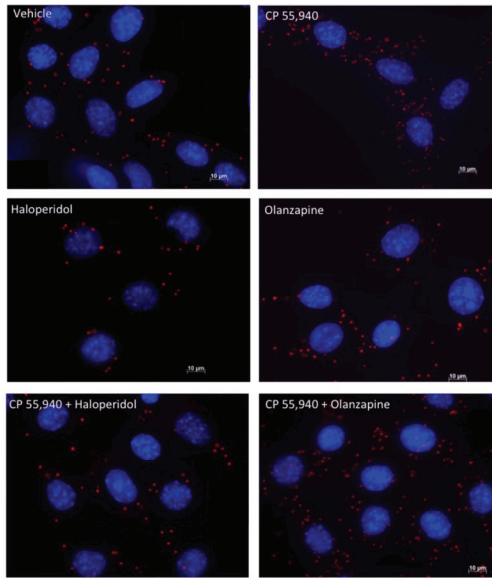CB_1/D_{2L} heteromer-specific PLA signals (Fig. 5.1A, B) in the globus pallidus compared to vehicle treatment. However, co-treatment with both CP 55,940 and haloperidol resulted in lower CB_1/D_{2L} heteromer-specific PLA signals compared to either CP 55, 940 or vehicle treatment suggesting that the haloperidol effect blocked CP 55, 940-dependent increases in heteromer formation (Fig. 5.1A, B). No alteration in CB_1/D_{2L} heteromer-specific PLA signals was observed in the globus pallidus of olanzapine-treated mice. Co-treatment of mice with CP 55, 940 and olanzapine resulted in CB_1/D_{2L} heteromer-specific PLA signals similar to that observed in CP 55, 940-treated mice (Fig. 5.1A, B). Taken together, these results indicate that chronic cannabinoid and typical, but not atypical, antipsychotics differentially altered the CB_1 and D_{2L} heteromer population in the globus pallidus of C57BL/6J mice**.**

5.3.2 Persistent Treatment with Cannabinoid and/or Antipsychotics Modulates CB_1 / D_{2L} Heteromerization in STHdh$^{Q7/Q7}$ Cells

We also tested whether the observed alteration in CB_1/D_{2L} heteromer-specific PLA signals in the globus pallidus of C57BL/6J mice following chronic drug treatment also occurred in STH*dh*$^{Q7/Q7}$ cells endogenously expressing CB_1 and D_{2L} receptors that model striatal MSN. Co-localization of CB_1 and D_{2L} receptors in STHdh$^{Q7/Q7}$ has been reported previously (Bagher *et al*., 2016) suggesting that the two endogenous receptors might form heteromers. STHdh$^{Q7/Q7}$ cells were subjected to *in situ* PLA. CB_1/D_{2L} heteromer-specific PLA signals were observed in cells when both CB_1 and D_{2L} primary antibodies were applied (Fig. 5.2A), whereas no PLA signal was detected if CB_1 or D_2-specific primary antibodies were applied alone (data not shown). These observations

Figure 5.2: Persistent Treatment with Cannabinoid and/or Antipsychotics Modulates Endogenous CB$_1$ and D$_{2L}$ Heteromers in STHdh$^{Q7/Q7}$ Cells Demonstrated Using PLA. **(A)** Cells were treated with vehicle or cannabinoid and/or antipsychotics for 20 hr, fixed, blocked and exposed to antibodies against CB$_1$ and D$_{2L}$. Interacting complexes were visualized following PLA. Immunofluorescence microscopy images (merged images) are shown in which CB$_1$/D$_{2L}$ heteromers appear as red dots and cell nuclei were stained with DAPI (blue). Scale bars 100 μm. **(B)** PLA signals are presented as the average number of red dots per cell. * $P < 0.01$ compared to cells treated with vehicle. # $P < 0.01$ compared to cells treated with CP 55, 940. Data are represented as mean ± SEM for 10-20 cells from three independent experiments. Significance was determined *via* one-way ANOVA followed by Tukey's *post-hoc* test.

A)

Vehicle | CP 55,940

Haloperidol | Olanzapine

CP 55,940 + Haloperidol | CP 55,940 + Olanzapine

B)
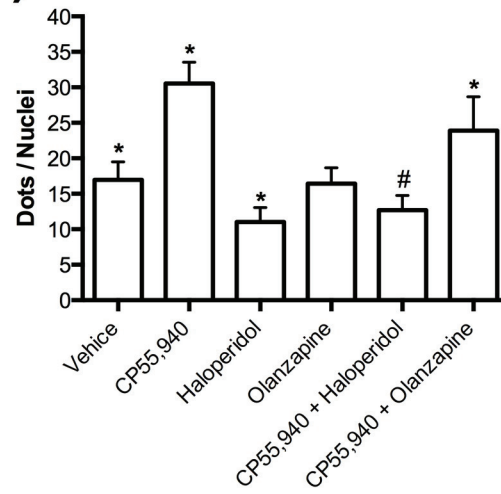
indicate that endogenous CB_1 and D_{2L} receptors form heteromers in STH$dh^{Q7/Q7}$ cells. The effect of persistent treatment with CB_1 and/or D_2 ligands on CB_1/D_{2L} heteromer-specific PLA signals in STH$dh^{Q7/Q7}$ cells was evaluated (Fig. 5.2A, B). STH$dh^{Q7/Q7}$ cells were treated with 1 μM CP 55,940, haloperidol, olanzapine or combinations of each antipsychotic with CP 55,940 for 20 hr followed by *in situ* PLA. Treating STH$dh^{Q7/Q7}$ cells with haloperidol alone or in combination with CP 55,940 decreased the number of CB_1/D_{2L} heteromer-specific PLA signals compared to vehicle-treated cells (Fig. 5.2A,B his finding might suggest that haloperidol alone or in the presence of CP 55,940 reduced the affinity of the two receptors, reduced expression of CB_1 and D_{2L}, or changed the cellular localization of the two receptors. Olanzapine treatment alone did not alter PLA signals (Fig. 5.2A, B). The application of CP 55,940 alone or in combination with olanzapine significantly increased CB_1/D_{2L} heteromer-specific PLA signals compared to vehicle-treated cells (Fig. 5.2A, B) indicating that CP 55,940 either increased the affinity of the two receptors, increased expression of the CB_1 and D_{2L} proteins, or altered the cellular localization of the two receptors.

5.3.3 Persistent Treatment with Cannabinoid and/or Antipsychotics Modulates Inter-Receptor CB_1/D_{2L} Affinity and the Probability of Heteromer Formation

$BRET^2$ saturation assays were generated to measure the interaction between C-terminally tagged CB_1 and D_{2L} receptors in HEK 293A cells. $BRET^2$ assays were conducted using HEK 293A cells, instead of STH$dh^{Q7/Q7}$ cells, because HEK 293A cells do not express endogenous CB_1 or D_{2L} receptors and therefore no endogenous CB_1 or D_{2L} receptors were available to interfere with the observed $BRET_{Eff}$ values generated by exogenous expression of each receptor. $BRET^2$ saturation assays provide information about the affinity of tagged receptors and provide information about conformational changes within tagged receptor complexes (Ramsay *et al.*, 2002; James *et al.*, 2006). HEK 293A cells were co-transfected with a constant amount of CB_1-Rluc with increasing amounts of D_{2L} -GFP^2 and ligands were added 5 hr following transfection. Cells were exposed to ligand treatment for 20 hours. The combination of CB_1-Rluc with D_2 -GFP^2 resulted in a hyperbolic increase in $BRET^2$ saturation curve as previously observed (Bagher *et al.,* 2016). The $BRET^2$ saturation curve in the presence of vehicle resulted in a

$BRET_{50}$ of 0.41 ± 0.03 and a $BRET_{Max}$ of 0.32 ± 0.01 (Fig. 5.3A,B). Negative controls included a plasmid expressing GFP^2-linked mGluR6 (mGluR6-GFP^2), a GPCR that is not known to have an affinity for CB_1 or D_{2L} (Hudson *et al.,* 2010). The $BRET^2$ saturation curve obtained from cells expressing CB_1-Rluc and mGluR6-GFP^2 (Fig. 5.3A) resulted in very weak $BRET^2$ signals. Consistent with earlier reports, the $BRET_{Eff}$ signal resulting from the interaction between CB_1 and D_{2L} was specific and saturable (Fig. 5.3A).

Treating cells co-expressing CB_1-Rluc and D_{2L}-GFP^2 for 20 h with 1 μM CP 55,940 resulted in a $BRET_{50}$ of 0.32 ± 0.02, which indicated that CP 55,940 increased the affinity between CB_1-Rluc and D_{2L}-GFP^2 (Fig. 5.3A,B). In contrast, 1 μM haloperidol-treatment resulted in a $BRET_{50}$ value of 0.51 ± 0.01, which indicated that haloperidol reduced the affinity of CB_1-Rluc and D_{2L}-GFP^2 relative to vehicle treatment (Fig. 5.3A,B). There was no difference in the $BRET_{50}$ values in cells treated with the vehicle or 1 μM olanzapine indicating that olanzapine did not alter the interaction between CB_1-Rluc and D_{2L}-GFP^2 (Fig. 5.3A,B).

The effect of co-treating cells with CP 55,940 together with haloperidol or olanzapine on the interaction between CB_1 and D_{2L} were also evaluated. Co-treating the cells with 1 μM CP 55,940 and haloperidol yielded a $BRET_{50}$ of 0.51 ± 0.01, which was similar to the value observed in the presence of haloperidol alone (Fig. 5.3A,B). Co-treating the cells with 1 μM CP 55,940 and olanzapine yielded a $BRET_{50}$ of 0.35 ± 0.02, which was similar to the value observed in the presence of CP 55,940 alone (Fig. 5.3A,B). When CP 55,940 was co-applied with haloperidol, the destabilizing influences of haloperidol on CB_1/D_{2L} heteromerization predominated. When CP 55,940 was co-applied with olanzapine, the stabilizing influences of CP 55,950 on CB_1 and D_2 was unopposed.

$BRET_{Max}$ reflects the relative orientations of the Rluc Donor and the GFP^2 acceptor (Guan *et al.,* 2009). Although $BRET_{Max}$ values can change if levels of the donor and acceptor are altered by ligand treatment, this is unlikely to have occurred in the current experiments; both donor and acceptor molecules were under the control of the CMV promoter within expression plasmids. Elevation in $BRET_{Max}$ values relative to vehicle treatment was observed in all treatment groups with the exception of olanzapine (Fig. 5.3B). The increase in $BRET_{Max}$ indicated that ligand binding altered and stabilized

Figure 5.3: Persistent Treatment with Cannabinoid and/or Antipsychotics Modulates CB$_1$ and D$_{2L}$ Receptors Heteromerization When Expressed in HEK 293A Cells Demonstrated Using BRET^2. (A) BRET^2 saturation curves obtained from cells transiently transfected with CB$_1$-Rluc and D$_{2L}$ -GFP^2. As a negative control, cells were co-transfected with CB$_1$-Rluc and mGluR6-GFP^2. BRET$_{Eff}$ is plotted against the ratio of GFP^2/ Rluc. Data were fit to a rectangular hyperbolic curve. Cells were treated for 20 hr with vehicle or 1 μM CP 55,940, haloperidol, olanzapine alone or in combination. **(B)** BRET$_{Max}$ and BRET$_{50}$ parameters derived from BRET^2 saturation curves. Data are presented as mean ± SEM of 4 independent experiments. Significance was determined *via* one-way ANOVA followed by Tukey's *post-hoc* test.

A)

- ●— CB_1-Rluc + D_{2L}-GFP^2 + Vehicle
- ▲— CB_1-Rluc + D_{2L}-GFP^2 + 1 μM CP 55,940
- □— CB_1-Rluc + D_{2L}-GFP^2 + 1 μM Haloperidol
- ◇— CB_1-Rluc + D_{2L}-GFP^2 + 1 μM Olanzapine
- ■— CB_1-Rluc + D_{2L}-GFP^2 + 1 μM CP 55,940 + 1 μM Haloperidol
- ◆— CB_1-Rluc + D_{2L}-GFP^2 + 1 μM CP 55,940 + 1 μM Olanzapine
- ✳— CB_1-Rluc + mGluR6-GFP^2
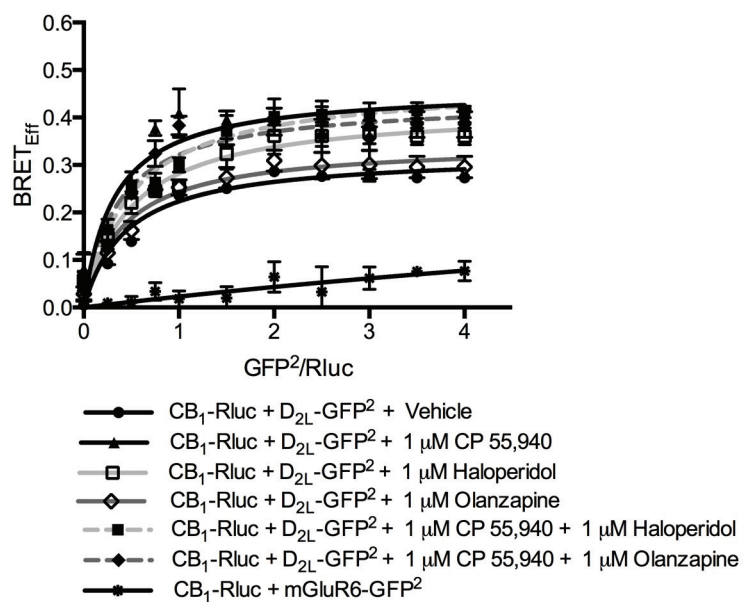
B)

Treatment	$BRET_{50}$	$BRET_{MAX}$
Vehicle	0.41 ± 0.03	0.32 ± 0.01
1 μM CP 55,940	0.32 ± 0.02*	0.46 ± 0.02*
1 μM Haloperidol	0.51 ± 0.01*	0.41 ± 0.01*
1 μM Olanzapine	0.42 ± 0.01	0.34 ± 0.01
1 μM CP 55,940 + 1 μM Haloperidol	0.50 ± 0.01*	0.47 ± 0.01*
1 μM CP 55,940 + 1 μM Olanzapine	0.35 ± 0.02*	0.44 ± 0.02*

207

the conformation of the CB_1 and D_{2L} heteromer, which enhanced the energy transfer between CB_1 and D_{2L}. Therefore, the observed changes in CB_1/D_{2L} heteromer-specific PLA signals following chronic exposure to ligand was most likely due to ligand-dependent changes in the affinity of the two receptors within the heteromeric complex.

5.3.4 Chronic Cannabinoid and/or Antipsychotic Treatment in C57BL/6J Mice Alters the Expression of CB_1 and D_2 in the Globus Pallidus

CB_1 and D_{2L} protein expression were measured in the globus pallidus to determine whether the ligand-dependent changes in CB_1/D_{2L} heteromer-specific PLA signals in the globus pallidus of C57BL/6J mice was due to alterations in the pool of receptors available to form heteromeric complexes. To measure the effects of chronic ligand treatment on CB_1 and D_2 protein expression in the globus pallidus of C57BL/6J mice, brain sections (Bregma - 0.82 mm) were subjected to dual-labeled QF-IHC and scanned using a LI-COR Odyssey IR scanner. The use of LI-COR Odyssey IR scanner allows for the determination of the relative CB_1 and D_2 protein-immunoreactivity in defined anatomic regions. Mice treated for 21 days with CP 55,940 had lower CB_1 levels compared to vehicle treatment (Fig. 5.4A, B). In contrast, mice treated with haloperidol showed higher CB_1 expression relative to vehicle treatment. Olanzapine-treated mice showed no change in CB_1 levels in the globus pallidus compared to vehicle-treated mice (Fig. 5.4A, B). CB_1 levels in the globus pallidus of C57BL/6J in mice co-treated with CP 55,940 and haloperidol were similar to vehicle treatment (Fig. 5.4A, B). CP 55,940 and olanzapine co-treatment resulted in CB_1 levels that were similar to CP 55,940-treated mice (Fig. 5.4A, B). We did not detect significant changes in D_{2L} protein levels following ligand treatment although there were similar trends in the patterns of drug-dependent protein changes compared to CB_1 (Fig. 5.4A, C).

5.3.5 Persistent Treatment with Haloperidol Increased the Steady-State Level of CB_1 and D_2 at the Plasma Membrane. CP 55, 940 Treatments Decreased the Level of Both Receptors at the Plasma Membrane

To confirm that the observed changes in CB_1/D_{2L} heteromer-specific PLA signals in STH$dh^{Q7/Q7}$ cells following chronic exposure to ligand might be due to changes in the

Figure 5.4: Chronic Haloperidol Treatment Increases CB$_1$ Expression in the Globus Pallidus of C57BL/6J Mice. **(A)** IR images showing CB$_1$ receptor (IRDye 800; green) and D$_2$ receptor (IRDye 700; red) labeling in C57BL/6J mice brain sections. Images were captured on the LI-COR Odyssey IR scanner at maximum quality, 21µm resolution. Graphical representation of the raw arbitrary abundance units of both CB$_1$ **(B)** and D$_2$ **(C)** expression. * $P < 0.01$ compared to vehicle-treatment group. ~ $P < 0.01$ compared to haloperidol-treated group. # $P < 0.01$ compared to CP 55,940 treatment. Data are presented as mean ± SEM of 5 independent experiments. Significance was determined *via* one-way ANOVA followed by Tukey's *post-hoc* test.
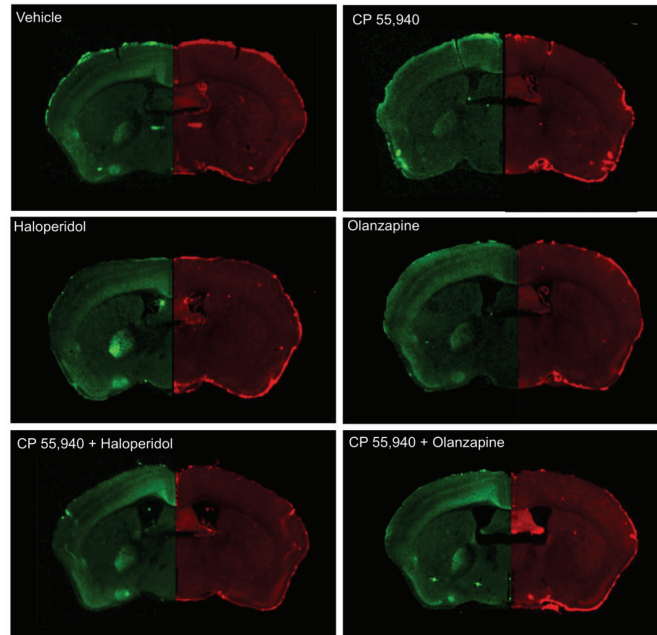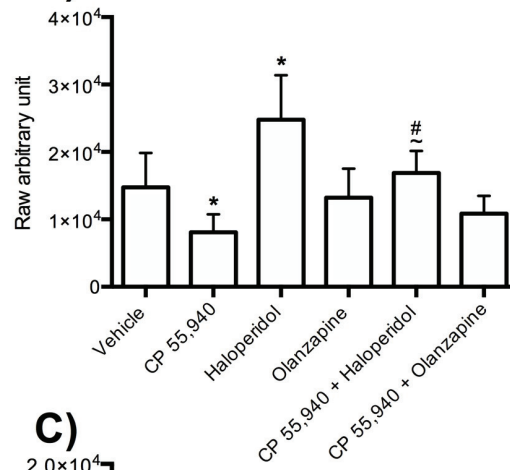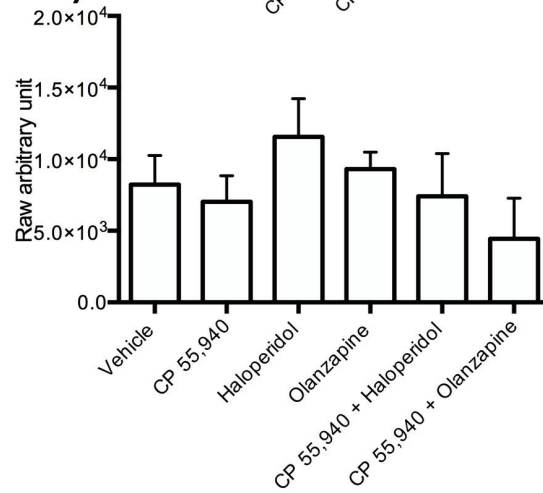
affinity of the two receptors to interact with each other rather than changes in the steady-state levels of protein or localization of the receptor. In- and On- Cell Western^{TM} analyses were used to estimate receptor densities and plasma membrane localization of CB_1 and D_{2L} in an effort to determine if changes in heteromer numbers were due to differential receptor expression and/or plasma localization. In- and On- Cell Western^{TM} analyses were performed after 20 hr persistent drug treatment in STH$dh^{Q7/Q7}$ cells. Treating STH$dh^{Q7/Q7}$ cells with 1 μM CP 55,940 resulted in decreased CB_1 levels compared with vehicle treatment (Fig. 5.5A). In contrast, 1 μM haloperidol increased CB_1 levels and 1 μM olanzapine did not change CB_1 protein levels (Fig. 5.5A). Co-treating cells with 1 μM CP 55,940 and 1 μM haloperidol resulted in CB_1 protein levels similar to vehicle-treated cells (Fig. 5.5A). In contrast, co-treatment with olanzapine and CP 55,940 reduced CB_1 levels similar to that observed when cells were treated with CP 55,940 alone (Fig. 5.5A).

The fraction of CB_1 receptors at the membrane following 20 hr ligand treatment was measured using On- Cell Western^{TM} analysis (plasma membrane) relative to In-Cell Western^{TM} (total protein) analysis. The fraction of CB_1 receptors at the cell membrane following 20 hr treatment with CP 55, 940 was significantly lower compared to vehicle-treated cells (Fig. 5.5B). An increase in the fraction of CB_1 receptors at the membrane was observed in haloperidol-treated cells compared to vehicle-treated cells (Fig. 5.5B). Treatment with olanzapine did not alter the fraction of CB_1 receptors at the membrane relative to vehicle-treated cells (Fig. 5.5B). Co-treatment with both CP 55,940 and haloperidol resulted in a lower fraction of CB_1 at the membrane compared to cell treated with haloperidol alone, but a higher fraction of CB_1 at the membrane compared to cells treated with CP 55,940 (Fig. 5.5B). However, CP 55,940 co-treatment with olanzapine yielded a similar fraction of CB_1 receptors as was observed when CP 55, 940 was applied alone. CP 55,940-induced CB_1 internalization, this effect was not opposed by olanzapine (Fig. 5.5B). Haloperidol stabilized CB_1 receptors at the plasma membrane. Haloperidol reduced but did not abolish CP 55,940-dependent CB_1 receptor internalization. Olanzapine did not affect the relative distribution of CB_1 receptor relative to vehicle treatment.

Figure 5.5: *Persistent Treatment with Cannabinoid and/or Antipsychotics Modulates Endogenous CB$_1$ and D$_{2L}$ Receptor Expression and Membrane Localization in STHdh$^{Q7/Q7}$ Cells.* **(A)** CB$_1$ and, **(C)** D$_{2L}$ receptor total protein levels measured at 20 hr measured using In-Cell Western™ in cells treated with vehicle or 1 µM CP 55,940, haloperidol, olanzapine alone or in combination. * $P < 0.01$ compared with vehicle-treated cells. ~ $P < 0.01$ compared to haloperidol-treated cells. **(B)** CB$_1$ and, **(D)** D$_{2L}$ cell surface expression at 20 hr measured using On-Cell Western™ and In-Cell Western™ in cells treated with vehicle or 1 µM CP 55,940, haloperidol, olanzapine alone. * $P < 0.01$ compared with vehicle-treated cells. ~ $P < 0.01$ compared to haloperidol-treated cells. Significance was determined *via* one-way ANOVA followed by Tukey's *post-hoc* test.
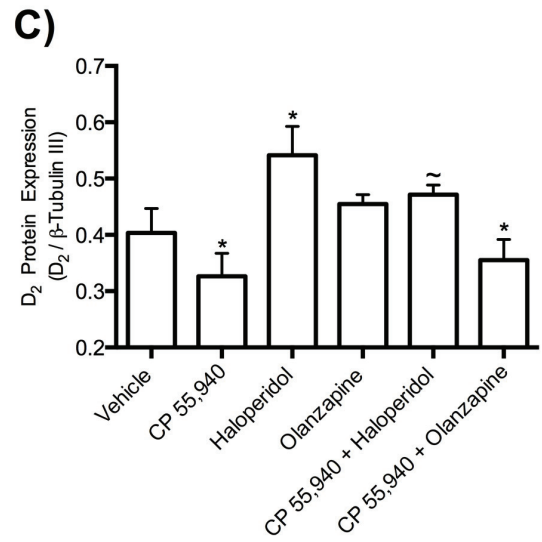
213
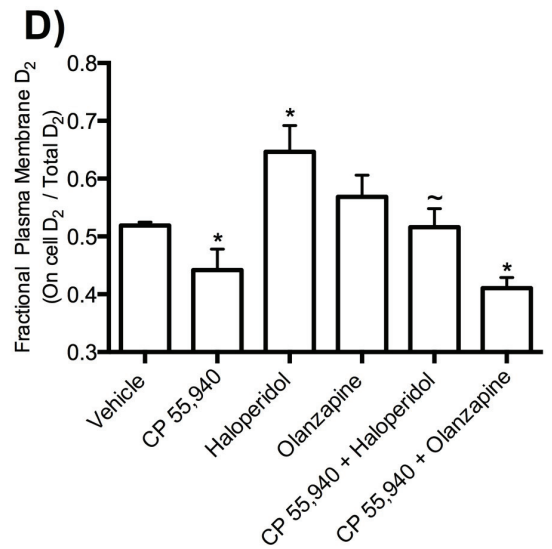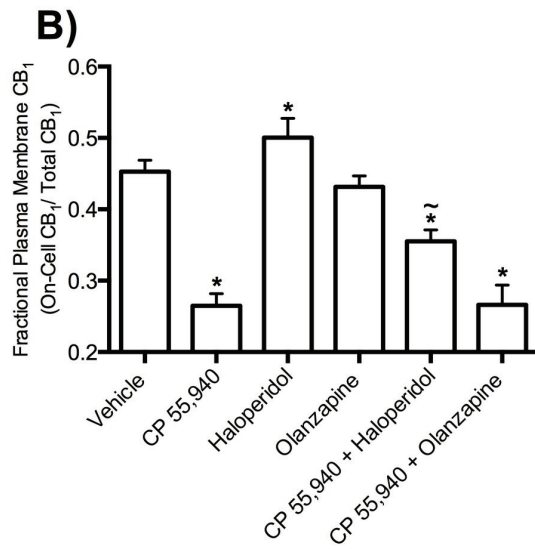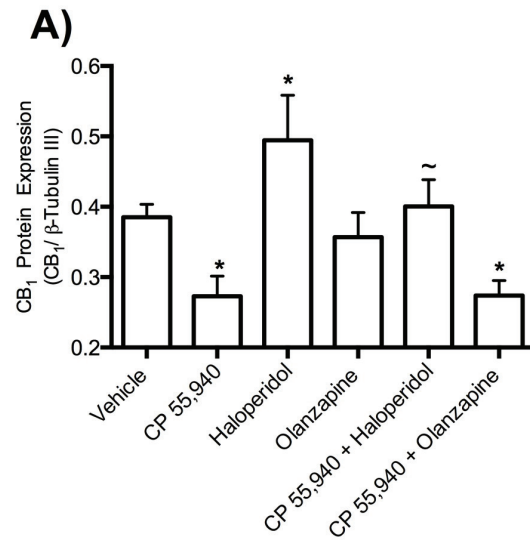
Overall, CP 55,940 treatments reduced both CB_1 protein expression and CB_1 membrane localization (Fig. 5.5A, B). Haloperidol treatment increased CB_1 expression and CB_1 membrane localization. CP 55,940 and haloperidol co-treatment resulted in CB_1 protein levels and CB_1 membrane distribution similar to that observed in vehicle-treated cells (Fig. 5.5A, B). In contrast, olanzapine treatment did not alter either CB_1 protein expression or CB_1 membrane localization; CP 55,940 co-treatment with olanzapine yielded both CB_1 protein expression and CB_1 membrane localization similar to CP 55,940 treated cells (Fig. 5.5A, B).

D_{2L} expression and membrane localization were also measured in STH$dh^{Q7/Q7}$ cells following 20 hr ligand treatment. CP 55, 940 treatment reduced D_{2L} levels compared with vehicle-treated cells (Fig. 5.5 C). Treatment with 1 μM haloperidol increased D_{2L} protein levels, while olanzapine treatment did not alter D_{2L} compared to vehicle-treated cells (Fig. 5.5C). Co-treatment with CP 55,940 together with haloperidol resulted in D_{2L} protein levels similar to vehicle-treated cells (Fig. 5.5C), unlike cells co-treated with CP 55,940 and olanzapine, which had lower D_{2L} protein levels compared with vehicle-treated cells (Fig. 5.5C).

D_{2L} membrane localization following ligand treatment for 20 hr was also analyzed. A decrease in the fraction of D_{2L} receptors at the membrane was observed in CP 55,940-treated cells compared with vehicle-treated cells (Fig. 5.5D). The fraction of D_{2L} at the membrane was increased following haloperidol treatment compared with vehicle-treated cells (Fig. 5.5D). Treatment with olanzapine did not alter the fraction of D_{2L} receptors at the membrane relative to vehicle-treated cells (Fig. 5.5D). Co-treatment with CP 55, 940 and haloperidol resulted in levels of D_{2L} at the membrane similar to vehicle-treated cells (Fig. 5.5D). Cells co-treated with CP 55, 940 and olanzapine showed similar D_{2L} receptors at the membrane compared to cells treated with CP 55,940 (Fig. 5.5D). Overall, haloperidol treatment increased D_{2L} at the plasma membrane, while CP 55,940 treatment alone or together with olanzapine reduced D_{2L} localization at the plasma membrane (Fig. 5.5D). CP 55,940 reduced the haloperidol-dependent increase in D_{2L} at the plasma membrane (Fig. 5.5D).

5.3.6 CP 55,940 Blocks GABA Release and This Effect is Not Altered by Co-Administration of Haloperidol or Olanzapine

GABA levels in the cell culture medium were measurde at 30 min and at 20 h following ligand treatment in STH*dh*$^{Q7/Q7}$ cells. GABA levels in the cell culture medium were determined using a GABA-specific enzyme-linked immunosorbent assay (Novatein Bio, Woburn MA). GABA release was inhibited by 1 μM CP 55,940 treatment for 30 min or 20 h compared to vehicle treatment (Fig 5.6A, B). No change in GABA levels was observed in both haloperidol- and olanzapine-treated cells at either 30 min or 20 hr relative to vehicle treatment (Fig. 5.6A, B). Co-treating STH*dh*$^{Q7/Q7}$ cells with CP 55,940 and haloperidol for 30 min resulted in GABA levels similar to vehicle-treated cells, however co-treating STH*dh*$^{Q7/Q7}$ cells with both drugs for 20 hr resulted in significantly lower GABA levels compared to vehicle-treated cells (Fig. 5.6A, B). Cells co-treated with CP 55,940 and olanzapine for 30 min or 20 hr yielded GABA levels similar to cells treated with CP 55,940 alone (Fig. 5.6A, B). Overall, acute treatment (30 min) with haloperidol inhibited CP 55,940-induced inhibition of GABA release; this effect was not observed following persistent treatment at 20 hr suggesting that over 20 hr the effect of CP 55, 940 over GABA release was unopposed by haloperidol. Neither typical nor atypical antipsychotics directly affected GABA levels and CP 55, 940-decreased GABA release even in the presence of haloperiodol or olanzapine.

5.3.7 CP 55,940 Attenuated Haloperidol-Induced Hypolocomotion and Catalepsy in C57BL/6J Mice

The effect of acute and chronic administration of CP 55,940, haloperidol and olanzapine alone or in combination on the locomotor activities of C57BL/6J mice was studied. Total distance travelled and time spent immobile in the open field were recorded for C57BL/6J mice treated with vehicle or 0.01 mg/kg/d CP 55,940, 0.3 mg/kg/d haloperidol, 1.5 mg/kg/d olanzapine, or co-treated with 0.01 mg/kg/d CP 55,940 and 0.3 mg/kg/d haloperidol and or 0.01 mg/kg/d CP 55,940 and 1.5 mg/kg/d olanzapine. Daily drug injection began when mice were 7 weeks of age and continued for 3 weeks (21 days). Twenty-four hours after the first injection, we observed that CP 55,940 did not have an effect on total distance traveled as expected for the low-dose of drug chosen (Marcellino

Figure 5.6: Changes in GABA Release in STHdh^{Q7/Q7} Cells Treated with Cannabinoids and/or Antipsychotics. STH*dh*^{Q7/Q7} cells were treated with ligands for 30 min **(A)** or 20 hr **(B)** and change in GABA release was measured from cell culture media using a GABA enzyme-linked immunosorbent assay. * $P < 0.01$ compared with vehicle-treated cells. ~ $P < 0.01$ compared to CP 55,940-treated cells. Data are presented as mean ± SEM of 4 independent experiments. Significance was determined *via* one-way ANOVA followed by Tukey's *post-hoc* test.

A)

30 min

B)

20 hr
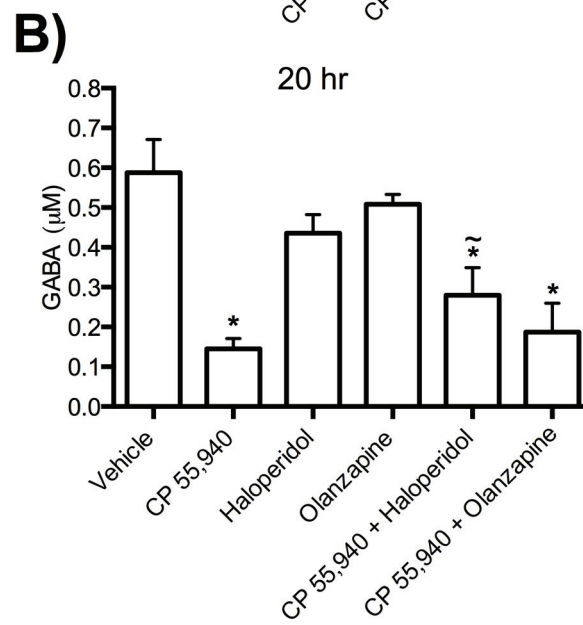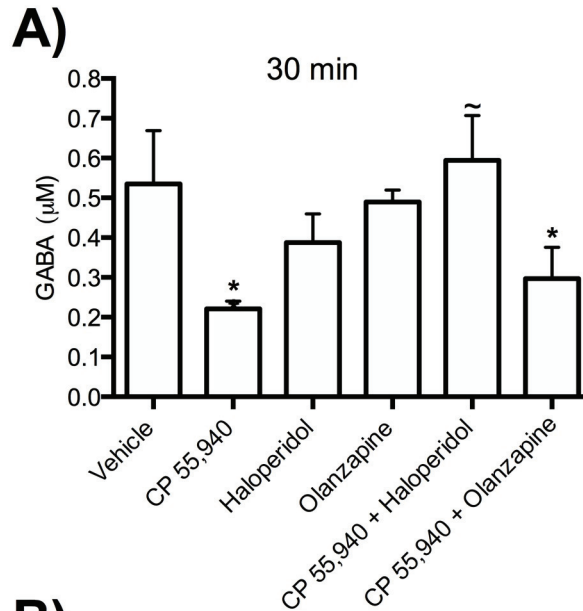
et al. 2008). Haloperidol- and olanzapine-treated mice showed reduced total distance traveled compared to vehicle-treated mice (Fig. 5.7A). The total distance traveled by C57BL/6J mice co-treated with both CP 55,940 and haloperidol was significantly higher compared to that observed for haloperidol-treated mice (Fig. 5.7A). C57BL/6J mice co-treated with CP 55,940 and olanzapine displayed similar total distance traveled compared to olanzapine-treated mice (Fig. 5.7A). Twenty-four hours after the first injection, we observed that CP 55,940 treatment did not affect immobility time, while haloperidol and olanzapine-treated mice showed increased immobility in the open field compared to vehicle treatment (Fig. 5.7B). Mice co-treated with CP 55,940 and haloperidol spent significantly less immobile time compared to haloperidol-treated mice; these mice had similar levels of immobility as vehicle-treated mice (Fig. 5.7B). In contrast, mice co-treated with CP 55,940 and olanzapine spent more time immobile compared to the vehicle-treated mice (Fig. 5.7B).

Open field tests were also performed after 21 daily drug treatments (Fig. 7C, D). C57BL/6J mice treated with CP 55,940 showed no change in either total distance traveled (Fig. 7C) nor time spent immobile compared to vehicle-treated mice (Fig. 5.7D). In contrast, mice treated with haloperidol or olanzapine alone or in combination with CP 55,940 showed a reduction in total distance traveled (Fig. 5.7C) and spent more time immobile (Fig. 5.7D). Therefore, acute co-treatment of CP 55,940 with haloperidol blocked reduced haloperidol-dependent decreases locomotor activities; such effect was not observed in mice following chronic exposure to both drugs or in mice treated with CP 55,940 together with olanzapine. This suggests that intermittent, but not chronic exposure, to low dose cannabinoids might alter locomotor effects of haloperidol.

5.4 Discussion

The main objective of this study was to examine whether the heteromeric CB_1/D_2 receptor population change following chronic exposure to cannabinoid alone or in combination with typical- or atypical- antipsychotics. We observed alterations in CB_1/D_{2L} heteromer-specific PLA signals both in the globus pallidus of C57BL/6J mice and ST*Hdh*$^{Q7/Q7}$ cells following chronic exposure to cannabinoid and/or antipsychotics (Summarized in Fig. 5.8).

Figure 5.7: CP 55,940 Attenuated Haloperidol-Induced Hypolocomotion in C57BL/6J Mice. Mice were treated with vehicle or 0.01 mg/kg/d CP 55,940, 0.3 mg/kg/d haloperidol or 1.5 mg/kg/d olanzapine i.p. alone or in combination for 3 weeks and total distance travelled (cm) and time spent immobile (s) was measured in the open field test. Total distance traveled was measured at Day 1 **(A)** and day 21 **(C)** and time spend immobile was measured at Day 1 **(B)** and Day 21 **(D)** post drug treatment. * $P < 0.01$ compared to vehicle-treatment. ~ $P < 0.01$ compared to haloperidol-treated group. Data are presented as mean ± SEM of 10 independent experiments. Significance was determined *via* one-way ANOVA followed by Tukey's *post-hoc* test.
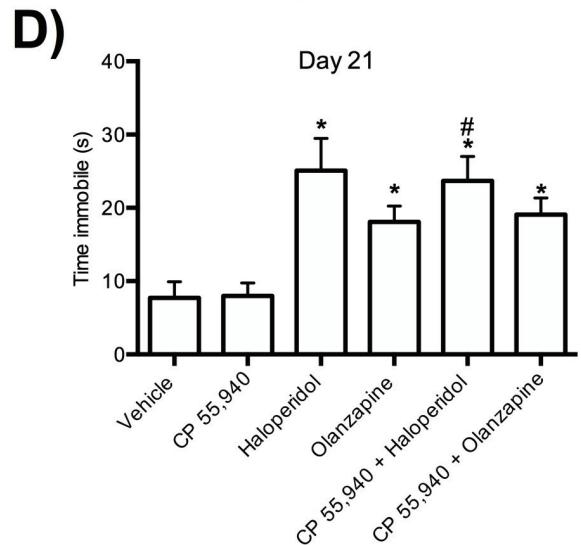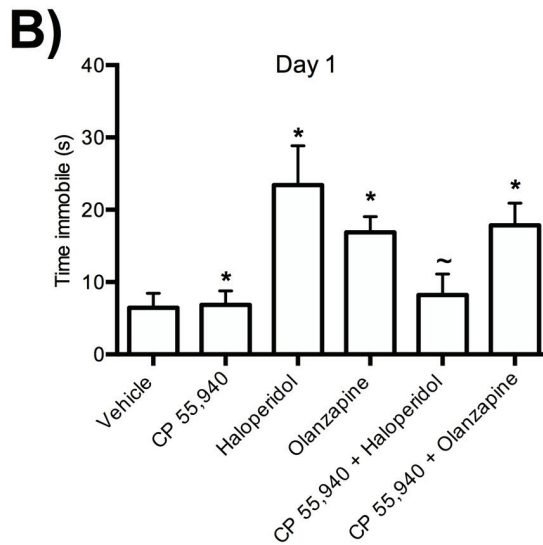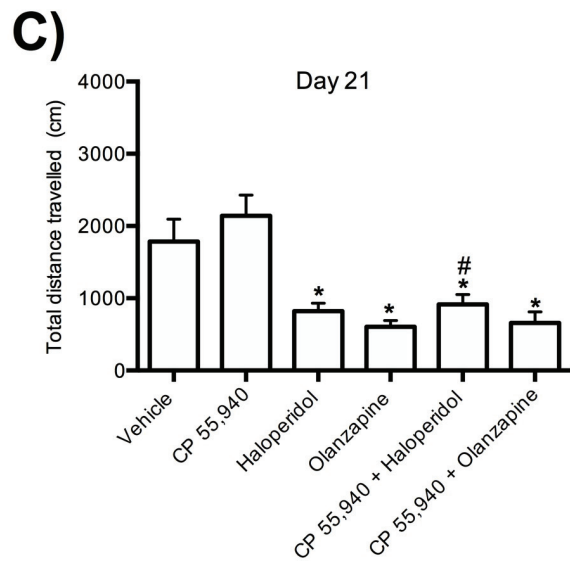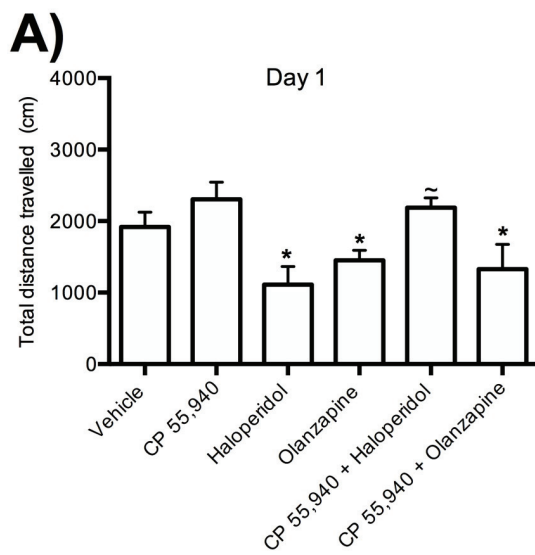
A)
Day 1

B)
Day 1

C)
Day 21

D)
Day 21

The cannabinoid, CP 55,940, increased the number of detectable CB_1/D_{2L} heteromeric complexes. The typical antipsychotic haloperidol reduced the population of CB_1/D_2 heteromeric complexes when administered alone or in combination with CP 55,940. The atypical antipsychotic, olanzapine, did not alter CB_1/D_2 heteromeric complexes population when administrated alone, whereas co-administration of CP 55,940 and olanzapine increased CB_1/D_{2L} heteromeric complexes population. The alteration in the CB_1/D_{2L} heteromer population observed in our study probably involves different mechanisms not reflected in shorter drug treatment or acute studies (Kearn *et al*., 2005; Marcellino *et al.,* 2008; Przybyla and Watts, 2010; Bagher *et al.,* 2016). The alteration in CB_1/D_{2L} heteromeric complexes population following ligand treatment could have been caused by alteration(s) in: (1) the affinity of CB_1 and D_2 receptors to form homo- versus heteromeric complexes, (2) the expression of either CB_1 and/or D_2 receptors, or (3) the localization of CB_1 and/or D_{2L} receptors.

Prolonged exposure to cannabinoids and/or antipsychotics, during the time of ongoing receptor biosynthesis and oligomerization, can alter the affinity of the receptors to form CB_1/D_{2L} heteromers (Przybyla and Watts, 2010). Changes in the relative affinity of CB_1 and D_{2L} receptors to interact was determined by comparing $BRET_{50}$ values obtained from $BRET^2$ saturation curves of cells co-expressing CB_1-Rluc and D_{2L}-GFP^2. CP 55,940 increased the affinity between CB_1 and D_{2L}, while haloperidol reduced the affinity of CB_1 and D_{2L} relative to vehicle treatment. CP 55,940 and haloperidol co-treatment reduced the affinity between CB_1 and D_{2L}. Olanzapine did not alter the affinity between CB_1 and D_{2L}. The changes in the affinity of CB_1- and D_{2L} receptors to each other following drug treatment was consistent with the observed changes in the number CB_1/D_2 heteromeric complexes *in vivo* and *in vitro*. Ligand-dependent changes in the relative affinity of receptors within the heteromeric complex population might shift the ratio of CB_1 and D_{2L} homomers versus heteromers. Consistent with our finding, multicolor BiFc was used to examine the regulation of CB_1 and D_{2L} homo- and heteromers in neuronal cells (Przybyla and Watts 2010). Persistent treatment for 20 hr with CP 55,940 increased the CB_1/D_2 heteromeric population relative to CB_1 and D_2 homomers. This effect was CB_1-dependent as pre-treating cells with the CB_1 receptor antagonist AM281 attenuated the CP55,940-induced increase in CB_1/D_2 heteromers

Figure 5.8: Chronic Cannabinoid and Typical Antipsychotic Alter CB$_1$ and D$_{2L}$ Localization, Expression and Heteromerization. **(A)** CB$_1$ and D$_{2L}$ receptors are localized at the plasma membrane and intracellular. CB$_1$ and D$_{2L}$ receptors form monomers, homomers and heteromers. Chronic treatment with olanzapine did not alter CB$_1$ and D$_{2L}$ protein levels, the fraction of the receptors at the membrane or CB$_1$/D$_{2L}$ heteromer expression. **(B)** The typical antipsychotic haloperidol increases CB$_1$ and D$_{2L}$ protein levels and the fraction of the receptors at the membrane, while reduces CB$_1$/D$_{2L}$ heteromer. **(C)** Chronic treatment with CP 55,940 alone or in combination with olanzapine reduces both CB$_1$ and D$_{2L}$ protein levels and the fraction of the receptors at the membrane, but increases CB$_1$/D$_{2L}$ heteromer expression. **(D)** Co-treatment with CP 55,940 and haloperidol results in CB$_1$ and D$_{2L}$ protein levels similar to vehicle treatment, the fraction of CB$_1$ and D$_{2L}$ receptors at the plasma memebrane and CB$_1$/D$_{2L}$ heteromer are reduced.

A Vehicle (or Olanzapine)

B Haloperidol

↑ CB$_1$ and D$_{2L}$ protein levels
↑ Fraction of CB$_1$ and D$_{2L}$ at plasma membrane
↓ CB$_1$/D$_{2L}$ heteromeric complexes

C CP 55,940 (+/- Olanzapine)

↓ CB$_1$ and D$_{2L}$ protein levels
↓↓ Fraction of CB$_1$ and D$_{2L}$ at plasma membrane
↑ CB$_1$/D$_{2L}$ heteromeric complexes

D CP 55,940 + Haloperidol

No change in CB$_1$ and D$_{2L}$ protein levels
↓ Fraction of CB$_1$ and D$_{2L}$ at plasma membrane
↓ CB$_1$/D$_{2L}$ heteromeric complexes

223

(Przybyla and Watts, 2010). There are no tools available to directly determine the proportion of monomeric versus heteromeric species that coexist *in vivo*. The current *in vivo* work can only determine the relative change in heteromeric complex number. While it is likely that there was a shift in the distribution of CB_1/D_{2L} hetero- versus homodimers, it is also possible that the reduction in the CB_1/D_{2L} heteromeric population might be due to CB_1 or D_{2L} interacting with other GPCRs expressed in the same cells as a result of ligand treatment. For example, In MSNs, CB_1 and D_{2L} are known to interact with adenosine A_{2A} receptors (Carriba *et al.*, 2007; Bonaventura *et al.,* 2015), which might compete with CB_1 and D_{2L} receptors.

Alteration in CB_1 and D_{2L} total protein expression following chronic cannabinoid and/or antipsychotic treatment is another possible mechanism by which these drugs might influence the relative CB_1/D_{2L} heteromeric population. Induction or suppression of either CB_1 or D_2 protein expression would alter the steady-state levels of receptors available for heteromeric receptor complex formation. Changes in CB_1 and D_2 expression following chronic exposure to exogenous cannabinoids and dopamine antagonists have been reported previously both *in vivo* and *in vitro*. Subchronic or chronic exposure to exogenous cannabinoids, such as THC, decreases CB_1 receptor binding in the mice caudate-putamen and the globus pallidus (Breivogel *et al.,* 1999; McKinney *et al., 2008*; Falenski *et al.,* 2010). Moreover, chronic exposure to marijuana decreases the expression of D_2 receptors in rat brain (Walter and Carr, 1986). Consistent with previous studies, we have observed a reduction in both CB_1 (Laprairie *et al.*, 2014) and D_{2L} protein expression following 20 h treatment with CP 55,940 in ST*Hdh*$^{Q7/Q7}$ cells. In addition, we observed a reduction in CB_1 expression in the globus pallidus of C57BL/6J mice following chronic CP 55,940 treatment. In the current study, we found that persistent haloperidol treatment, but not olanzapine, increased CB_1 and D_2 protein levels in cell culture model. Likewise, chronic treatment with haloperidol, but not olanzapine, increased CB_1 protein expression in the globus pallidus. Consistent with our findings, an increase in CB_1 protein expression following haloperidol treatment was previously reported by Andersson *et al*. (2005). Specifically, chronic treatment with haloperidol (1 mg/kg) for 14 days increased [^{3}H] CP 55,940 binding in the striatum of male Sprague-Dawley rats (Andersson *et al.*, 2005). Even though previous studies have found that chronic treatment with high dose

224

haloperidol (10 mg/kg/d) for 3 weeks increases D_2 receptor levels in the striatum (Muller and Seeman, 1977; Fox *et al*., 1994; Andersson *et al*., 2005), we did not observe a significant increase in D_2 protein expression in the globus pallidus following chronic haloperidol treatment, which could be due to the lower dose of haloperidol (0.3 mg/kg/d) used in the current study. The co-administration of CP 55,940 reduced haloperidol ability to increase CB_1 and D_2 protein expression ST*Hdh*$^{Q7/Q7}$ cells, and CB_1 in the globus pallidus. The endocannabinoids anandamide (AEA) and its synthetic analogues can alter CB_1 gene transcription by modulating CB_1 promoter activity, mRNA, and protein expression through Akt- and NF-κB-dependent mechanism (Laprairie *et al*., 2013). The mechanism by which haloperidol as an antagonist can alter CB_1 expression is still not known, but the additive effects of CP 55,940 and haloperidol co-administration on CB_1 protein expression suggest that both drugs might modulate gene transcription and/or mRNA translation(s). A previous study by Blume *et al.,* (2013) found that chronic reduction of CB_1 or D_2 expression in the rat globus pallidus using RNA interference resulted in deficits in gene and protein expression of the alternative receptor. Our study also indicates a reciprocal influence of the levels of CB_1 or D_2 receptors; together these data suggest that CB_1 and D_2 receptors are tightly coupled at the level of transcription and translation. Overall, alteration in CB_1/D_{2L} heteromer expression did not correlate with the observed alteration in CB_1 and D_2 protein expression following chronic ligand treatment. For example, even though haloperidol reduced the relative level of CB_1/D_{2L} heteromers, haloperidol induced both CB_1 and D_{2L} protein expression. Therefore, the observed loss of CB_1/D_{2L} receptor heteromers in both ST*Hdh*$^{Q7/Q7}$ cells and in the globus pallidus was unlikely to be caused by a reduction in the pool of available CB_1 and D_{2L} receptors.

We studied the influence of persistent ligand application on CB_1 and D_2 receptor localization in ST*Hdh*$^{Q7/Q7}$ cells to determine if chronic exposure to these agents affected the population of CB_1/D_{2L} heteromers by changing CB_1 and/or D_{2L} receptor localization. We observed similar distribution pattern of CB_1 and D_{2L} receptors following ligand treatment(s) in ST*Hdh*$^{Q7/Q7}$ cells. Treating cells with CP 55,940 induced CB_1 and D_{2L} receptor internalization suggesting that D_{2L} receptors were co-internalized with CB_1 receptor as heteromeric complexes in response to CP 55,940. In contrast, haloperidol

increased the ratio of CB_1 and D_{2L} receptors localized at the cell membrane and reduced CP 55,940-dependent CB_1 and D_{2L} receptor co-internalization. Olanzapine did not alter CB_1 nor D_{2L} receptors localization. Given the fact that persistent exposure to CB_1 agonists and the D_{2L} antagonist produced similar effects on the localization of both receptors, it is unlikely that these ligands differentially altered the location of CB_1 and D_{2L} receptors preventing or promoting association. The receptors appeared to respond to ligand binding as a complex. Co-internalization of GPCR heteromers has previously been reported for several GPCRs following ligand-receptor binding at both receptors of the GPCR heteromer. Additionally, ligand-receptor binding at one of the receptors in a GPCR heteromer can also induce receptor co-internalization (reviewed in Terrillon and Bouvier, 2004; Milligan, 2009; Ferré *et al.,* 2014; Franco *et al.,* 2016). Further studies will be required to determine whether both CB_1 and D_{2L} receptors are localized to the same subcellular compartments following ligand exposure.

The effects of chronic treatment with cannabinoid and/or antipsychotics on mice locomotor activities were examined in the current study. Both haloperidol and olanzapine reduced locomotor activities in mice on day 1 and day 21 after daily drug administration. No changes in locomotion activities were observed at day 1 and day 21 in mice treated with low dose of CP 55,940. Interestingly, co-administration of CP 55,940 and haloperidol blocked the haloperidol-dependent reduction in locomotor activities on day 1 after drug administration. An *in vitro* study showed that CP 55,940 reduces the affinity of D_2 receptor agonist binding to the D_2 receptors in both the dorsal and ventral striatum including the nucleus accumbens shell (Marcellino *et al*., 2008). Cannabinoid-dependent reduction on D_2 receptor agonist affinity might explain the observed change in locomotor activities in mice co-treated with both CP 55,940 and haloperidol compared to haloperidol-treated mice. Alternatively, concurrent activation of both CB_1 and D_2 within heteromeric complexes switched CB_1/D_2 heteromer coupling from $G\alpha_i$ to $G\alpha_s$ proteins, which could cause the observed disinhibition of movement (Glass and Felder, 1997; Bagher *et al*., 2016). In contrast to the effect observed 24 hours after a single dose of each drug, the ability of CP 55,940 to block haloperidol-dependent inhibition of locomotion was not observed in mice chronically co-treated with both CP 55,940 and haloperidol. The chronic treatment with CP 55,940 and haloperidol significantly reduced

the CB_1/D_{2L} heteromeric complexes population in the globus pallidus of C57BL/6J mice thereby removing the inhibitory effect exerted by CB_1 receptors on D_{2L} receptors. Variation in CB_1/D_{2L} heteromeric expression might influence GABA transmission in the globus pallidus. As expected, activation of the CB_1 receptor by CP 55,940 resulted in inhibition of GABA release (Manzoni and Bockaert, 2001; Szabo *et al.*, 2002; D'Amico *et al.*, 2004), while the D_2 antagonist haloperidol and olanzapine did not alter GABA release in ST*Hdh*$^{Q7/Q7}$ cells. Co-treating the cells for 30 min with CP 55,940 and haloperidol blocked CP 55,940-induced inhibition of GABA release, while persistent (20 h) co-treatment with CP 55,940 and haloperidol abolished the antagonistic effect of haloperidol on cannabinoid-induced inhibition of GABA release, which is consistent with the reduction in the expression of CB_1/D_2 heteromers.

5.5 Conclusion

This is the first study to our knowledge that reports alteration in CB_1 and D_2 heteromer expression *in vivo* following cannabinoid and/or antipsychotic exposure. The following conclusions may be drawn from our data. First, CB_1/D_{2L} receptor heteromers are expressed in in the globus pallidus of C57BL/6J mice and ST*Hdh*$^{Q7/Q7}$ cells, as demonstrated using *in situ* PLA. Second, the expression of CB_1/D_{2L} receptor heteromers is altered in both ST*Hdh*$^{Q7/Q7}$ cells and in mouse globus pallidus following chronic exposure to cannabinoids and/or typical antipsychotic. Third, alterations in CB_1/D_{2L} heteromer expression following chronic ligand treatment(s) might disturb the negative cross-talk between the CB_1 and D_{2L} receptor in the globus pallidus, which can affect movement. Typical and atypical antipsychotics differently altered CB_1/D_{2L} heteromer population, CB_1 and D_{2L} protein expression and localization when applied alone or in combination with cannabinoids. Overall, drugs that target CB_1 and D_2 receptors must be considered in the context of their interactions and effect on their cognate receptor and for their actions within allosteric heteromeric complexes. Pharmacodynamic drug-drug interactions are likely.

CHAPTER 6

GENERAL DISCUSSION

6.1. Objectives of the Research

The overall objective of my thesis was to understand the allosteric interactions within CB_1/D_{2L} heteromers. My hypothesis was that co-localization of CB_1 and D_{2L} receptors in the basal ganglia allows for bidirectional allosteric interactions within CB_1/D_{2L} heterotetramers following the applications of CB_1 and D_{2L} ligands, which may be physiologically and clinically relevant.

6.2. Summary of Research

Given that allosteric communication within heteromeric GPCR complexes is known to result in unique pharmacology (reviewed in Smith and Milligan, 2010; Ferré *et al.,* 2015; Jonas *et al*., 2016), the pharmacology of CB_1/D_{2L} heteromers was investigated in the current thesis. Using $BRET^2$ saturation curves, we confirmed that CB_1 and D_{2L} receptors physically interact to form homomeric and heteromeric complexes when these receptors were co-expressed in HEK 293A cells and $STHdh^{Q7/Q7}$ cells. The interaction was observed at low levels of expression and was specific and saturable. To improve the understanding of the functional consequences of the CB_1 and D_{2L} interaction and given the clinical importance of D_2 antagonists, the effects of D_2 antagonists on CB_1 pharmacology was investigated, and the finding was presented in chapter three and published in the Journal of Molecular of Pharmacology as *"Antagonism of dopamine receptor 2 long (D_{2L}) affects cannabinoid receptor 1 (CB_1) signaling in a cell culture model of striatal medium spiny projection neurons"*. In this study, the effects of a D_2 antagonist haloperidol on CB_1 coupling to $G\alpha_i$ and $G\alpha_s$ proteins and β-arrestin1 recruitment to CB_1 receptors were investigated using $STHdh^{Q7/Q7}$ cells. Also, CB_1-dependent ERK1/2, CREB phosphorylation and CB_1 internalization following co-applications of CB_1 agonist and D_2 antagonist were quantified. We confirmed that CB_1 was pre-assembled with $G\alpha_i$ protein in the absence of CB_1 agonist. The application of the selective CB_1 agonist ACEA resulted in a rapid and transient increase in $BRET_{Eff}$

between $G\alpha_i$-Rluc and CB_1-GFP^2 due to conformational changes within pre-assembled heteromeric complexes. The co-application of ACEA and haloperidol caused a rapid uncoupling of CB_1 from $G\alpha_i$ protein followed by a delayed and sustained interaction of the CB_1/D_{2L} with $G\alpha_s$ protein. In addition, haloperidol treatment reduced ACEA-induced β-arrestin1 recruitment to CB_1 receptor and receptor internalization. Overall, our first study suggested that a high-affinity D_2 antagonist allosterically modulated cannabinoid-induced CB_1 coupling, signaling and β-arrestin1 recruitment through binding to CB_1/D_{2L} heteromers.

Next, we tested whether a D_2 agonist could also modulate CB_1 pharmacology *via* allosteric interactions within CB_1/D_{2L} heteromeric complexes. D_2 agonists can modulate CB_1 coupling to $G\alpha$ protein, β-arrestin1 recruitment, and internalization when co-applied with the CB_1 agonist, but not if applied as single agents. Similarly, CB_1 agonists modulated D_{2L} coupling to $G\alpha$ protein, β-arrestin1 recruitment, and internalization in the presence of a D_2 agonist. The co-application of both CB_1 and D_{2L} agonists potentiated β-arrestin1 recruitment to CB_1/D_{2L} heteromeric complexes and resulted in CB_1/D_{2L} co-internalization. Since we observed bidirectional allosteric interactions within CB_1/D_{2L} heteromeric complexes, we aimed to define the stoichiometry of CB_1/D_{2L}/$G\alpha$ protein complexes. Using $BRET^2$ saturation curves, we observed that CB_1 and D_{2L} homodimers were the predominant species when either receptor was expressed alone; however heterotetramers were the predominant species when the receptors were co-expressed. Using mathematical models and $SRET^2$ combined with BiFC, we predicted that one CB_1 homodimer interacts with one D_{2L} homodimer to form a CB_1/D_{2L} heterotetrameric complex. Each homodimer, within a heterotetrameric complex, was coupled to at least one $G\alpha_i$ protein. Higher order oligomeric complexes might also form although our data suggested that the minimal functional unit was a heterotetramer. This work is presented in chapter four and was submitted to the European Journal of Pharmacology for publication with the title *"Bidirectional Allosteric Interactions Between Cannabinoid Receptor 1 (CB_1) and Dopamine Receptor 2 Long (D_{2L}) Heterotetramers"* (in press).

The main objective of the fifth chapter was to examine whether CB_1 and D_{2L} form heteromers in defined nuclei of the basal ganglia in C57BL/6J mice and to determine whether CB_1/D_{2L} heteromer levels were altered following chronic treatment with

cannabinoids and antipsychotic alone or in combination. By using *in situ* PLA, we observed CB_1 and D_{2L} heteromer-specific PLA signals in the globus pallidus, but not the striatum, of C57BL/6J mice. An increase in CB_1/D_{2L} heteromer-specific PLA signals was observed in the globus pallidus of C57BL/6J mice following chronic CP 55,940 treatment alone or in combination with olanzapine. In contrast, haloperidol treatment alone or in combination with CP 55,940 reduced CB_1/D_{2L} heteromer-specific PLA signals. Olanzapine treatment did not affect CB_1/D_{2L} heteromer-specific PLA signals relative to vehicle treatment. This finding demonstrated that typical and atypical antipsychotics differentially alter CB_1/D_{2L} heteromerization in the globus pallidus when applied alone or in combination with cannabinoid, which might have a different impact on the control of movement. Overall, the studies presented within this body of work improve understanding of allosteric interactions within GPCR heteromeric complexes and provide a better understanding of the effects of cannabinoids administration on the therapeutic effects of antipsychotics.

6.3 Allosteric Interactions Within CB_1/D_{2L} Heteromeric Complexes in Cell Culture

Bidirectional allosteric interactions within CB_1/D_{2L} heteromers were ligand-dependent as has been observed for other GPCR heteromers (Kenakin and Miller, 2010; Ferré *et al.,* 2015). In this model, CB_1/D_{2L} heteromeric complexes act as a conduit of the allosteric modulator. CB_1 agonists act as allosteric modulators influencing the efficacy of D_2 ligands. Conversely, D_2 ligands act as allosteric modulators of ligand efficacy of CB_1 agonists. The co-expression of D_2 receptors with CB_1 receptors, in the absence of D_2 ligands, did not alter G protein coupling to CB_1. In contrast to our finding, Jarrahian *et al*., (2004) reported that co-expression of the D_2 receptors with the CB_1 receptors in HEK 293 cells led to increased levels of cAMP instead of the expected decrease in levels of cAMP following CB_1 agonist treatment. Based on these finding, these authors suggested that the co-expression of the D_2 receptor was sufficient to change CB_1-dependent signaling from $G\alpha_i$ to $G\alpha_s$ proteins. In the same paper, they proposed that D_2 receptors sequester the available $G\alpha_i$ pool, preventing the binding of the CB_1 receptor to $G\alpha_i$, which promotes CB_1 to interact with the $G\alpha_s$ protein. Overexpression of $G\alpha_i$, but not $G\alpha_o$, restored coupling of the CB_1 with $G\alpha_i$ protein in the presence of D_{2L} (Jarrahian *et al*.,

2004). Our results strongly suggest that the coupling of CB_1/D_{2L} heteromeric complexes to $G\alpha_s$ proteins following the application of CB_1 agonist and D_2 ligands is a result of allosteric interactions within CB_1/D_{2L} heteromeric complexes and not due to the competition between CB_1 and D_{2L} receptors for the $G\alpha_i$-protein pool. This finding was confirmed by the fact that preventing the interaction between CB_1 and D_2 receptors using a blocking peptide was able to block the switching in G protein coupling following ligands CB_1/D_2 co-application. Importantly, we observed these effects in the presence of excess $G\alpha_i$ protein. Even though the expression of D_{2L} receptors did not alter $BRET_{Eff}$ between CB_1 and $G\alpha_i$ protein, in the absence of D_2 ligands, it is important to acknowledge that there is the possibility that the expression of D_{2L} receptor might induce conformational changes within $CB_1/G\alpha_i$ that may be undetectable using $BRET^2$.

Our data suggest that the overall functional receptor unit is composed of CB_1 and D_{2L} homodimers that interact to form heterotetramers coupled to at least two $G\alpha_i$ proteins. One might argue that the reduction in $BRET_{Eff}$ signals between $G\alpha_i$-Rluc and CB_1-GFP^2 or between $G\alpha_i$-Rluc and D_{2L}-GFP^2 following the co-application of both CB_1 and D_2 ligands is due to conformational changes within the complexes that resulted in a reduction in the energy transfer from Rluc to GFP^2 and not due to uncoupling of CB_1 and D_{2L} homodimers from $G\alpha_i$ proteins (Szalai *et al*., 2014; Lan *et al.,* 2015). Based on crystal structures of GPCR homodimers and computer modeling, the width of one G heterotrimer is larger than the width of one GPCR receptor (Han *et al.,* 2009: Wu *et al*., 2010; Manglik *et al.,* 2012, Wu *et al.,* 2012; Haung *et al.,* 2013; Jastrzebska *et al.,* 2013; Navarro *et al*., 2016). This observation suggests that it is not possible for CB_1/D_{2L} heterotetramers to couple simultaneously to two $G\alpha_i$ proteins and two $G\alpha_s$ proteins and uncoupling of CB_1/D_{2L} heterotetramers from $G\alpha_i$ proteins is required before coupling to $G\alpha_s$ proteins.

Previous studies have reported asymmetric structural arrangements within homo- or heterodimeric complexes, wherein individual protomers in a receptor dimer may interact with a shared heterotrimeric G protein through distinct interfaces. These studies suggest that structural asymmetries may result in asymmetric allosteric interactions (Damian *et al.,* 2006; Han *et al.,* 2009; Zylbergold and Hébert; 2009; Jonas *et al.,* 2015; Mishra *et al.,* 2016; Levitz *et al.,* 2016; Sleno *et al*., 2017). In our study, we have

observed that D_2 agonists can modulate CB_1 coupling to $G\alpha$ protein and β-arrestin1 recruitment when co-applied with the CB_1 agonist. Similarly, CB_1 agonists modulated D_{2L} coupling to $G\alpha$ protein and β-arrestin1 recruitment in the presence of a D_2 agonist. Based on our findings, we concluded that the allosteric communications between CB_1/D_{2L} heterotetramer are symmetrical and ligand-dependent. Asymmetric binding of G proteins may occur within CB_1 homodimers and D_2 homodimers and still produce symmetrical reciprocal allosteric interactions with the CB_1/D_{2L} heterotetramer. The precise conformational changes within of CB_1 homodimer induced by the co-expression and activation of D_{2L} receptors are yet to be determined. Alternative techniques such as GPCR conformation–sensitive biosensors might be useful to measure intramolecular conformational dynamics of CB_1/D_{2L} receptors within heteromeric complexes in response to agonist (Zurn *et al.,* 2009; Maier-Peuschel *et al.,* 2010; Ziegler *et al.,* 2011; Bourque *et al.*, 2017; Devost *et al.,* 2017; Sleno *et al.,* 2017).

6.4. Allosteric Interactions Within CB_1/D_2 Heteromic Complexs in the Basal Ganglia

While there is extensive *in vitro* evidence for heteromerization, there is currently considerably less evidence for allosteric interactions *in vivo* or an understanding of the functional consequences of heteromerization. In our studies, we observed that allosteric interactions within CB_1/D_2 heterooligomeric complexes occurred at relatively high concentrations of CB_1 and D_2 (chapters three and four). Endocannabinoids are released from depolarized postsynaptic neurons into the synapse. The levels of endogenous 2-AG in rat striatum ranges from 3 to10 nM, while AEA levels in rat striatum ranges from 0.5 to 5 nM (Giuffrida *et al.,* 1999; Walker *et al.*, 1999; Béquet *et al.,* 2007; Alvarez-Jaimes *et al.*, 2009; Orio *et al.,* 2009; reviewed in Buczynski and Parsons, 2010). The reported endogenous levels of both 2-AG and AEA are much lower than the concentrations that induced allosteric interactions within CB_1/D_2 heteromeric complexes *in vitro* although the local synaptic levels of endocannabinoids may be higher than those measured by microdialysis (reviewed in Buczynski and Parsons, 2010). On the other hand, the concentration of dopamine in the striatum varies during the tonic (baseline spike activity) and phasic (burst-spike firing pattern) dopamine release states. Dopamine concentrations measured locally in the vicinity of tonically firing neurons ranges from 10 to 20 nM,

while dopamine concentrations during phasic dopamine release are much higher and ranges from 100 μM to 1 mM (Ross and Jackson, 1989; Ross, 1991; Keef *et al.,* 1993; Floresco *et al.,* 2003). The phasic dopamine release state is transient as dopamine is immediately taken up *via* selective transporters into pre-synaptic terminals (Grace, 1991; Chergui *et al.,* 1994; Floresco *et al.,* 2003; Goto *et al*., 2007). We concluded that during phasic dopamine release, the levels of dopamine in the synapse would be transiently high while endocannabinoids levels would be relatively low; therefore bidirectional allosteric interactions between the two receptors might not occur *in vivo* in the absence of exogenous cannabinoids. It is possible that transient increases in dopamine could influence the production of endocannabinoids postsynaptically and influence presynaptic dopamine receptor function and indirectly affect cannabinoid signaling.

Direct and indirect dopamine agonists are used clinically to treat symptoms of Parkinson's disease (reviewed in Brooks, 2000; Stowe *et al*., 2008; Tomlinson *et al*., 2010; Stocchi *et al*., 2016), while D_2 antagonists are used to treat schizophrenia, Huntington's disease, and Tourette's syndrome (Seeman, 2010; Eddy and Rickards, 2011; Frank, 2014). Cannabinoid CB_1 orthosteric ligands have been proposed as pharmacotherapeutics for treating neurodegenerative diseases, spasticity, chronic pain, substance use disorders, and managing energy intake (Pacher *et al*., 2006; Vemuri *et al.,* 2008; Pertwee, 2012; Aizpurua-Olaizola, 2017). Also, patients might be exposed to drugs such as marijuana or stimulants that modulate the ECS and DS. Several clinical scenarios are likely for patients receiving combinations of drugs that target the CB_1 and D_2 receptors.

In the first scenario, patients taking drugs that lead to increased activation of dopamine receptors, such as D_2 agonists, levodopa (L-DOPA) or dopamine transporters reuptake inhibitors, such as cocaine, amphetamine, and methamphetamine. These patients would experience an increase in dopaminergic neurotransmission in the basal ganglia and an increase in locomotor activity (reviewed in Iversen and Iversen, 2007). In this case, an increase in endocannabinoids release in the dorsal striatum is predicted as a negative feedback mechanism to compensate for sustained over-activation of dopaminergic transmission (Giuffrida *et al*., 1999; Melis *et al*., 2004; Centonze *et al*., 2004; Pan *et al.,* 2008). Signaling through CB_1 and D_{2L} homodimers and heteromers could occur leading

to complex regulation of the ECS and DS pathways depending on the concentration of agents and duration of action.

In the second scenario, patients exposed to prescribed drugs that act as CB_1 agonists such as Sativex® (extract containing equimolar THC and cannabidiol), or the combination of cannabinoids in marijuana may influence dopaminergic transmission in addition to affecting the ECS. *In vivo* microdialysis showed that acute THC administration increases dopamine efflux in the striatum in rodents (Cheong *et al.,* 1988; Chen *et al*., 1990; Pistis *et al.,* 2002). Similarly, using positron emission tomography scanning, it was reported that THC causes an increase in dopamine release in the ventral striatum in the human brain (Bossong *et al.,* 2015). In such case, the concentrations of both cannabinoid and dopamine will be relatively high in the synapse and may induce allosteric interactions between CB_1/D_2 heteromers. Allosteric interactions will result in switching G protein coupling from $G\alpha_i$ to $G\alpha_s$ proteins. High concentrations of cannabinoid and dopamine are predicted to exert negative cooperativity on CB_1/D_{2L} and $G\alpha_i$ interaction within CB_1/D_{2L} complexes. The negative cooperativity effects on $G\alpha_i$ protein coupling could be a modulatory mechanism to protect the system from acute over elevation of endocannabinoids and dopamine resulting in hyperactivation of CB_1/D_{2L} receptors. Also, we might expect to see positive cooperativity effects on β-arrestin recruitment to CB_1/D_{2L} heteromer, which potentiates heteromer co-internalization and termination of signaling protecting the system from receptor over-activation. There is evidence that acute and chronic THC exposure have differing effects on the dopaminergic system. Chronic THC treatment reduces the expression of CB_1 in the striatum of both rodents and human, which is consistent with our finding presented in chapter 5 (Sim-Selley, 2002; Hirvonen *et* al., 2012). Moreover, chronic THC treatment increases the formation of CB_1/D_{2L} heteromers (chapter 5). Elevation in CB_1/D_2 heteromeric complexes will further potentiate those allosteric interactions within the two receptors and further increase the complexity of interactions between ECS and DS.

In the third scenario, patients taking drugs acting on D_2 receptors (agonist or antagonists) may be simultaneously exposed to CB_1 agonists. Acute administration of Δ^9-THC was reported to counteract the motor effect induced by ligands that increase synaptic dopamine concentration (Aulakh *et al.,* 1980; Moss *et al.,* 1981; Anderson *et al.*,

1996; Giuffrida *et al.,* 1999; Andersson *et al*., 2005; Marcelino *et al.,* 2008). For example, a single low-dose of the cannabinoid agonist CP 55940, which did not affect locomotor activity when administered alone, was able to reduce quinpirole-induced hyperactivity; this effect was counteracted by the CB_1 receptor antagonist rimonabant at a dose that did not change basal locomotor activity (Marcellino *et al.,* 2008). In our *in vitro* study, we found that application of high-affinity D_2 receptor antagonists as haloperidol-induced allosteric interactions within CB_1/D_{2L} heteromeric complexes (chapter three). Altogether, acute co-administration of cannabinoids along with D_2 agonists or antagonists might result in an allosteric interaction within CB_1/D_2 heteromers in the globus pallidus. Our study suggests that the administration of cannabinoid and/or antipsychotic can modulate the expression of CB_1/D_{2L} heteromeric complexes, which might can an effect on the control of movement and have clinical implications.

In addition to CB_1 and D_{2L}, GABAergic MSNs projecting to the globus pallidus express other GPCRs including the adenosine 2A (A_{2A}) receptor. $CB_1/D_{2L}/A_{2A}$ heteromerization has been confirmed both in rodent MSNs and cell cultures (Marcellino *et al.,* 2008; Carriba *et al.,* 2008; Navarro *et al.,* 2008; Pinna *et al*., 2014; Bonaventura *et al.,* 2014). Linking the observations available in the literature and the present study suggests a scenario where striatal neurons expressing $CB_1/D_2/A_{2A}$ heteromers would be subject to a very complicated receptor regulation scheme. For example, persistent exposure to CB_1 agonist would reduce CB_1 and D_{2L} receptor expression and promote the interaction between CB_1 and D_2 while the level of A_{2A} receptor would be lower resulting in the disturbance in the formation of the $CB_1/D_{2L}/A_{2A}$ heteromer. A more complicated scenario would be expected in patients being exposed to antipsychotic medications. As mentioned before, when CB_1 and D_2 receptors co-expressed in the same cells and co-stimulated by both agonists they couple to $G\alpha_s$ proteins (Glass and Felder, 1997; Jarrahian *et al*., 2004; Kearn *et al*., 2005; Bagher *et al.,* 2016). Whereas when A_{2A} and D_2 receptors are co-expressed in the same cells and co-activated by agonists, they couple to $G\alpha_q$ proteins (Ferré *et al.,* 1992; Bonaventura *et al*., 2015). It is still unknown whether $CB_1/D_2/A_{2A}$ heteromeric complexes coupled to $G\alpha_i$, $G\alpha_s$ and/or $G\alpha_q$ proteins. G protein coupling to the $CB_1/D_2/A_{2A}$ heteromeric complex might depend on which protomers are stimulated in the receptor heteromeric complexes.

6.5 CB₁/D₂L Allosteric Interactions in the Context of Huntington's Disease

CB_1/D_{2L} interactions may be of particular interest during the current drive to develop therapeutics for the management of HD. Despite the loss of CB_1 receptors early in Huntington's Disease (HD) progression, there is evidence that cannabinoids may reduce hyperkinetic movement, striatal atrophy, and peripheral inflammation in HD animal models (Sagredo *et al.,* 2007, 2011; Blázquez *et al*., 2011; Bari *et al*., 2013; Valdeolivas *et al*., 2012, 2015). In addition, cannabinoids can increase appetite and affect energy utilization, which has the potential to normalize weight loss that occurs during HD progression (Petersé *et al.,* 2005; van der Burg *et al.,* 2008; Casteels *et al.,* 2011; Chiarlione *et al*., 2014). Several clinical trials have been conducted to investigate cannabinoid-based medicines as a treatment for HD. In an early trial, cannabidiol was found to be safe and well tolerated in HD patients, but did not reduce abnormal choreic movement (Consroe *et al.,* 1991). Cesamet ® (nabilone), a synthetic THC analog, was evaluated in two clinical trials (Müller-Vahl *et al*., 1999; Curtis *et al.*, 2009). The *Unified Huntington's Disease Rating Scale* (UHDRS) was used to evaluate total motor score, chorea, cognition and neuropsychiatric outcomes (Müller-Vahl *et al.,*1999; Curtis *et al.,* 2009). In both trials, there was evidence of improvement in cognitive outcomes, but no reduction of chorea (Müller-Vahl *et al.,* 1999; Curtis *et al.,* 2009). In 2011, a double-blind, randomized, crossover, phase 2 clinical trial was conducted to assess the neuroprotective effects of Sativex® in HD. Although Sativex® in HD was found to be safe, no differences in motor, cognitive or, behavioral outcomes were detected during treatment with Sativex® compared to placebo (López-Sendón *et al.,* 2016). To date, all cannabinoid-based clinical trials have only enrolled symptomatic HD patients and trials had relatively short duration. For future trials, treatments with cannabinoid-based therapeutics might be administered earlier during HD progression and for a longer duration.

Tetrabenazine and deutetrabenazine, specifically approved as an antichoreic agent for HD, inhibit the vesicular monoamine transporter (VMAT), decrease levels of dopamine and act as indirect D_2 antagonists. Patients who do not tolerate tetrabenazine, or have other contraindications to its use such as depression, may be prescribed antipsychotics to control chorea, aggression, agitation, impulsivity, delirium, and

psychosis (Hayden *et al.,* 2009; Frank and Jankovic, 2010; Mestre and Ferreira, 2012; Frank *et al.,* 2016). There is no consensus based on evidence for selection of one antipsychotic over another for HD patients (Canadian Huntington's Physician Guide, Huntington Society of Canada, 2013). Patients prescribed tetrabenazine or antipsychotics may also be exposed to cannabinoids *via* prescribed cannabinoids or self-medication. The overall effects of these drugs on symptom management and disease progression are currently unknown.

Are typical- antipsychotics a favorable treatment strategy for HD or atypical- antipsychotics? Typical antipsychotics such as haloperidol have high affinity to block D_{2L} receptors; therefore the use of typical antipsychotics can result in extrapyramidal side effects (akathisia, dystonia and tardive dyskinesia). In a study of 10 patients with HD using haloperidol, oral doses of 1.5 to 10.0 mg/day resulted in at least a 30 % reduction in chorea compared with baseline (Barr *et al*., 1988). Other common side effects of typical antipsychotics are related to their potent antimuscarinic actions such as dry mouth, nervousness, urinary retention, and constipation. Atypical antipsychotic agents such as olanzapine are known to cause sedation (blocking the H1 histamine receptors), and weight gain (possibly due to blocking H1 histamine and 5-HT2 serotonin receptor) (reviewed in Gerlach, 1991; Kapur and Mamo, 2003; Meltzer, 2013; Murray *et al.,* 2017). HD patients suffer from severe weight loss and using olanzapine might be beneficial for them (Ross 2010; Ross and Tabrizi 2011; Labbadia and Morimoto, 2013). In two open-label studies of patients with HD, treatment with olanzapine (10 to 30 mg/day) resulted in significant improvement in anxiety, irritability, depression, and choreic movements (Paleacu *et al*., 2002, Bonelli *et al.,* 2002; reviewed in Adam *et al.,* 2008). The new atypical antipsychotic aripiprazole is a partial agonist at D_2 receptors and, thus, has a unique profile compared to other atypical antipsychotics (Leung *et al*., 2012). In one trial, aripiprazole was found to be as beneficial in reducing chorea having an equivalent effect to that of tetrabenazine (Ciammola *et al.,* 2009). Aripiprazole is associated with tardive dyskinesia (Ciammola *et al.,* 2009) therefore; particular attention has to be taken when prescribing antipsychotics to HD patients. The effects of partial agonists on CB_1/D_{2L} heteromer function have yet to be tested.

Based on studies presented in this thesis, I speculate that acute exposure to cannabinoid while taking typical or atypical- antipsychotics drugs will differentially affect CB_1/D_{2L} function. Exposure to exogenous cannabinoids and haloperidol, but not olanzapine, was able to allosterically modulated CB_1/D_{2L} functions and altered CB_1/D_2 heteromer expression in the basal ganglia. However, further studies are required to test whether typical- or atypical antipsychotics might be beneficial when co-administrated with cannabinoids. Since CB_1 and D_{2L} are co-expressed and co-localized selectively in the GABAergic MSNs, it may be possible to develop novel therapeutic compounds capable of recognizing and binding to the oligomeric arrangement of CB_1/D_{2L}, rather than individual receptors, thereby selectively regulating oligomer-related signaling and function and reducing unwanted side effects. Furthermore, it has been proposed that alterations in GPCR heteromer formation may be associated with neurological disorders such as schizophrenia and Parkinson's disease (reviewed in Borroto-Escuela *et al.,* 2017). Thus, being able to measure the relative population of CB_1/D_{2L} heteromers in HD using *in situ* PLA will increase understanding of normal and pathological states. Overall, a better understanding of the relationship between the ECS and DAS especially in respect to the pharmacology of heteromeric complexes is not only critical in and of itself, but it is also applicable to the design of therapies for HD.

REFERENCES

Abedi PM, Delaville C, De Deurwaerdere P, Benjelloun W, Benazzouz A (2013). Intrapallidal administration of 6-hydroxydopamine mimics in large part the electrophysiological and behavioral consequences of major dopamine depletion in the rat. *Neuroscience* **236**:289-97.

Abood ME, Martin BR (1992). Neurobiology of marijuana abuse. *Trends Pharmacol Sci* **13**: 201-6.

Adam OR, Jankovic J (2008). Symptomatic treatment of Huntington disease. *Neurotherapeutics* **5**:181-197.

Ahn K, McKinney MK, Cravatt BF (2008). Enzymatic pathways that regulate endocannabinoid signaling in the nervous system. Chem Rev **108**: 1687-707.

Ahn S, Shenoy SK, Wei H, Lefkowitz RJ (2004). Differential kinetic and spatial patterns of beta-arrestin and G protein-mediated ERK activation by the angiotensin II receptor. *J Biol Chem* **279**: 35518-25.

Aizpurua-Olaizola O, Elezgarai I, Rico-Barrio I, Zarandona I, Etxebarria N, Usobiaga A (2017). Targeting the endocannabinoid system: future therapeutic strategies. *Drug Discovery Today* **22**: 105.

Albizu L, Balestre MN, Breton C, Pin JP, Manning M, Mouillac B, Barberis C, and Durroux T (2006). Probing the existence of G protein-coupled receptor dimers by positive and negative ligand-dependent cooperative binding. *Mol Pharmacol* **70**:1783-1791.

Albizu L, Cottet M, Kralikova M, Stoev S, Seyer R, Brabet I, Roux T, Bazin H, Bourrier E, Lamarque L, Breton C, Rives ML, Newman A, Javitch J, Trinquet E, Manning M, Pin JP, Mouillac B, Durroux T (2010). Time-resolved FRET between GPCR ligands reveals oligomers in native tissues. *Nat Chem Biol* **6**:587-594.

Alvarez-Curto E, Ward RJ, Pediani JD, Milligan G (2010). Ligand regulation of the quaternary organization of cell surface M3 muscarinic acetylcholine receptors analyzed by fluorescence resonance energy transfer (FRET) imaging and homogeneous time-resolved FRET. *J Biol Chem* **285**: 23318-30.

Alvarez-Jaimes L, Polis I, Parsons LH (2009). Regional influence of CB1 receptor signaling on ethanol self-administration by rats. *The Open Neuropsychopharmacology* **2**: 77-85.

Anderson JJ, Kask AM, Chase TN (1996). Effects of cannabinoid receptor stimulation and blockade on catalepsy produced by dopamine receptor antagonists. *European Journal of Pharmacology* **295**:163-168.

Anderson RG. The caveolae membrane system (1998). *Annu Rev Biochem* **67**:199-225.

Andersson M, Terasmaa A, Fuxe K, Stromberg I (2005). Subchronic haloperidol increases CB(1) receptor binding and G protein coupling in discrete regions of the basal ganglia. *Journal of Neuroscience Research* **82**: 264-272.

Angers S, Salahpour A, Joly E, Hilairet S, Chelsky D, Dennis M, Bouvier M (2000). Detection of beta 2-adrenergic receptor dimerization in living cells using bioluminescence resonance energy transfer (BRET). *Proc Natl Acad Sci U S A* **97**: 3684-9.

Arjona AA, Zhang SX, Adamson B, Wurtman RJ (2004). An animal model of antipsychotic-induced weight gain. *Behavioural Brain Research* **152**: 121-127.

Armstrong D, Strange PG (2001). Dopamine D2 receptor dimer formation: evidence from ligand binding. *J Biol Chem* **276**: 22621-22629.

Atwal RS, Xia J, Pinchev D, Taylor J, Epand RM, Truant R (2007). Huntingtin has a membrane association signal that can modulate huntingtin aggregation, nuclear entry and toxicity. *Hum Mol Genet* **16**: 2600-2615.

Audet N, Gales C, Archer-Lahlou E, Vallieres M, Schiller PW, Bouvier M, Pineyro G (2008). Bioluminescence resonance energy transfer assays reveal ligand-specific Conformational changes within pre-formed signaling complexes containing delta-opioid receptors and heterotrimeric G proteins. *J Biol Chem* **283**: 15078-15088.

Augood SJ, Faull RL, Emson PC (1997). Dopamine D_1 and D_2 receptor gene expression in the striatum in Huntington's Disease. *Ann Neurol* **42**:215-221.

Aulakh CS, Bhattacharyya AK, Hossain MA, Pradhan SN (1980). Behavioral and neurochemical effects of repeated administration of Δ9-tetrahydrocannabinol in rats. *Neuropharmacology* **19**: 97-102.

Ayoub MA, Al-Senaidy A, Pin JP (2012). Receptor-G protein interaction studied by bioluminescence resonance energy transfer: lessons from protease-activated receptor 1. *Front Endocrinol* **22**:3-82.

Ayoub MA, Maurel D, Binet V, Fink M, Prezeau L, Ansanay H, Pin JP (2007). Real-time analysis of agonist-induced activation of protease-activated receptor 1/Galphai1 protein complex measured by bioluminescence resonance energy transfer in living cells. *Mol Pharmacol* **71**:1329-1340.

Ayoub MA, Trinquet E, Pfleger KD, Pin JP (2010). Differential association modes of the thrombin receptor PAR1 with G alphai1, G alpha12, and beta-arrestin1. *FASEBJ* **24**:3522-3535.

Azdad K, Gall D, Woods AS, Ledent C, Ferré S, and Schiffmann SN (2009). Dopamine D2 and adenosine A2A receptors regulate NMDA-mediated excitation in accumbens neurons through A2A-D2 receptor heteromerization. *Neuropsychopharmacology* **34**:972-986.

Azpiazu I, Gautam N (2004). A fluorescence resonance energy transfer-based sensor indicates that receptor access to a G protein is unrestricted in a living mammalian cell. *J Biol Chem* **279**: 27709-27718.

Bacci A, Huguenard JR, Prince DA (2004). Long-lasting self-inhibition of neocortical interneurons mediated by endocannabinoids. *Nature* **431**: 312-316.

Bagher AM, Laprairie RB, Kelly ME, Denovan-Wright EM (2013). Co-expression of the human cannabinoid receptor coding region splice variants (hCB1) affects the function of hCB$_1$ receptor complexes. *Eur J Pharmacol* **721**: 341-54.

Bagher AM, Laprairie RB, Kelly ME, Denovan-Wright EM (2016). Antagonism of Dopamine Receptor 2 Long Affects Cannabinoid Receptor 1 Signaling in a Cell Culture Model of Striatal Medium Spiny Projection Neurons. *Mol Pharmacol.* **89**: 652-66.

Bakshi K, Mercier RW, Pavlopoulos S (2007). Interaction of a Fragment of the Cannabinoid CB1 Receptor C-Terminus with Arrestin-2. *FEBS Lett* **581**: 5009-5016.

Banères JL, Parello J (2003). Structure-based analysis of GPCR function: evidence for a novel pentameric assembly between the dimeric leukotriene B4 receptor BLT1 and the G-protein. *J Mol Biol* **329**: 815-29.

Bari M, Spagnuolo P, Fezza F, Oddi S, Pasquariello N, Finazzi-Agro A, and Maccarrone M (2006). Effect of lipid rafts on CB2 receptor signaling and 2-arachidonoyl-glycerol metabolism in human immune cells. *J. Immunol* **177**: 4971-4980.

Beaulieu JM, Gainetdinov RR (2011). The physiology, signaling, and pharmacology of dopamine receptors. *Pharmacol Rev* **63**: 182-217.

Beaulieu JM, Sotnikova TD, Marion S, Lefkowitz RJ, Gainetdinov RR, Caron MG (2005). An Akt/beta-arrestin 2/PP2A signaling complex mediates dopaminergic neurotransmission and behavior. *Cell* **122**: 261-273.

Blankman JL, Simon GM, Cravatt BF (2007). A comprehensive profile of brain enzymes that hydrolyze the endocannabinoid 2-arachidonoylglycerol. *Chem Biol* **14**:1347-1356.

Benovic JL, Pike LJ, Cerione RA, Staniszewski C, Yoshimasa T, Codina J, Caron MG, Lefkowitz RJ. Phosphorylation of the mammalian beta-adrenergic receptor by cyclic AMP-dependent protein kinase (1985). Regulation of the rate of receptor phosphorylation

and dephosphorylation by agonist occupancy and effects on coupling of the receptor to the stimulatory guanine nucleotide regulatory protein. *J Biol Chem* **260**: 7094-7101.

Béquet F, Uzabiaga F, Desbazeille M, Ludwiczak P, Maftouh M, Picard C, Scatton B, Le Fur G (2007). CB1 receptor-mediated control of the release of endocannabinoids (as assessed by microdialysis coupled with LC/MS) in the rat hypothalamus. *Eur J Neurosci 26: 3458-64.*

Blázquez C, Chiarlone A, Bellocchio L, Resel E, Pruunsild P, García-Rincón D, Sendtner M, Timmusk T, Lutz B, Galve-Roperh I, Guzmán M (2015). The CB1 cannabinoid receptor signals striatal neuroprotection via a PI3K/Akt/mTORC1/BDNF pathway. *Cell Death Differ* **22**: 1618-1629.

Blázquez C, Chiarlone A, Sagredo O, Aguado T, Pazos MR, Resel E, Palazuelos J, Julien B, Salazar M, Borner C, Benito C, Carrasco C, Diez-Zaera M, Paoletti P, Diaz-Hernandez M, et al. (2011) Loss of striatal type 1 cannabinoid receptors is a key pathogenic factor in Huntington's disease. *Brain* **134**: 119-36.

Blin O (1999). A comparative review of new antipsychotics. *Can J Psychiatry* **44**: 235-44.
Bloomfield MA, Ashok AH, Volkow ND, Howes OD (2016). The effects of Δ9-tetrahydrocannabinol on the dopamine system. *Nature* **539**: 369-377.

Blume LC, Bass CE, Childers SR, Dalton GD, Roberts DC, Richardson JM, Xiao R, Selley DE, Howlett AC (2013). Striatal CB1 and D2 receptors regulate expression of each other, CRIP1A and δ opioid systems. *J Neurochem* **124**:808-820.

Bockaert J (1991). G proteins and G-protein-coupled receptors: structure, function and interactions. *Curr Opin Neurobiol* **1**:32-42.

Bonaventura J, Navarro G, Casadó-Anguera V, Azdad K, Rea W, Moreno E, Brugarolas M, Mallol J, Canela EI, Lluís C, Cortés A, Volkow ND, Schiffmann SN, Ferré S, Casadó V (2015). Allosteric interactions between agonists and antagonists within the adenosine A2A receptor-dopamine D2 receptor heterotetramer. *Proc Natl Acad Sci USA* **7**: 112(27).

Bonaventura J, Rico AJ, Moreno E, Sierra S, Sánchez M, Luquin N, Farré D, Müller CE, Martínez-Pinilla E, Cortés A, Mallol J, Armentero MT, Pinna A, Canela EI, Lluís C, McCormick PJ, Lanciego JL, Casadó V, Franco R. (2014). L-DOPA-treatment in primates disrupts the expression of A(2A) adenosine-CB(1) cannabinoid-D(2) dopamine receptor heteromers in the caudate nucleus. *Neuropharmacology* **79**: 90-100.

Bonelli RM, Niederwieser G, Tribl GG, Költringer P (2002). High-dose olanzapine in Huntington's disease. *Int Clin Psychopharmacol* **17**: 91-93.

Borroto Escuela DO, Hagman B, Woolfenden M, Pinton L, Jiménez-Beristain A, Oflijan J, Narvaez M, Palma MD, Feltmann K, Sartini S, Ambrogini P, Ciruela F, Cuppini R, Fuxe K (2016). In Situ Proximity Ligation Assay to Study and Understand the Distribution and Balance of GPCR Homo- and Heteroreceptor Complexes in the Brain. Receptor and Ion Channel Detection in the Brain. *Neuromethods* **110**: 109-124.

Borroto-Escuela DO, Carlsson J, Ambrogini P, Narváez M, Wydra K, Tarakanov AO, Li X, Millón C, Ferraro L8, Cuppini R, Tanganelli S, Liu F, Filip M, Diaz-Cabiale Z, Fuxe K (2017). Understanding the Role of GPCR Heteroreceptor Complexes in Modulating the Brain Networks in Health and Disease. *Front Cell Neurosci* **21**: 11-37.

Bosier B, Hermans E (2007). Versatility of GPCR recognition by drugs: from biological implications to therapeutic relevance. *Trends Pharmacol Sci* **28**: 438-46.

Bosier B, Muccioli GG, Hermans E, Lambert DM (2010). Functionally selective cannabinoid receptor signaling: therapeutic implications and opportunities. *Biochem Pharmacol* **80**:1-12.

Bossong MG, Mehta MA, van Berckel BN, Howes OD, Kahn RS, Stokes PR. Further human evidence for striatal dopamine release induced by administration of Δ9-tetrahydrocannabinol (THC): selectivity to limbic striatum. *Psychopharmacology* **232**: 2723-2729.

Bourque K, Pétrin D, Sleno R, Devost D, Zhang A, Hébert TE (2017). Distinct conformational dynamics of three G protein-coupled receptors measured using FlAsH-BRET biosensors. *Frontiers in Endocrinology* **8**: 61.doi:10.3389/fendo.2017.00061

Bouvier M, Hébert TE (2014). Cross Talk proposal: weighing the evidence for Class A GPCR dimers, the evidence favours dimers. *The Journal of Physiology* **592**:2439-2441.

Boveia V, Schutz-Geschwender A (2015). Quantitative analysis of signal transduction with in-cell western immunofluorescence assays. *Methods Mol Biol* **1314**: 115-30.

Brady AE, Limbird LE (2002). G protein-coupled receptor interacting proteins: emerging roles in localization and signal transduction. *Cell Signal* **14**:297-309.

Braun S, Levitzki A (1979) Adenosine receptor permanently coupled to turkey erythrocyte adenylate cyclase. *Biochemistry* **18**: 2134-2138.

Breivogel CS, Childers SR, Deadwyler SA, Hampson RE, Vogt LJ, Sim-Selley LJ (1999). Chronic delta9-tetrahydrocannabinol treatment produces a time-dependent loss of cannabinoid receptors and cannabinoid receptor-activated G proteins in rat brain. *J Neurochem* **73**: 2447-2459.

Brooks D (2000). Dopamine agonists: their role in the treatment of Parkinson's disease. *J Neurol Neurosurg Psychiatry* **68**: 685-689.

Buczynski MW, Parsons LH (2010). Quantification of brain endocannabinoid levels: methods, interpretations and pitfalls. *Br J Pharmacol* **160**: 423-442.

Bunemann M, Frank M, Lohse, MJ (2003). Gi protein activation in intact cells involves subunit rearrangement rather than dissociation. *Proc Natl Acad Sci USA* **100**: 16077-16082.

Bush CF, Jones SV, Lyle AN, Minneman KP, Ressler KJ, Hall RA (2007). Specificity of olfactory receptor interactions with other G protein-coupled receptors. *J Biol Chem* **282**: 19042-51.

Bushlin I, Gupta A, Stockton SD Jr, Miller LK, and Devi LA (2012). Dimerization with cannabinoid receptors allosterically modulates delta opioid receptor activity during neuropathic pain. *PLoS ONE* **7**:e49789.

Cadas H, Gaillet S, Beltramo M, Venance L, Piomelli D (1996). Biosynthesis of an endogenous cannabinoid precursor in neurons and its control by calcium and cAMP. *J Neurosci* **16**: 3934-42.

Calebiro D, Rieken F, Wagner J, Sungkaworn T, Zabel U, Borzi A, Cocucci E, Zürn A, Lohse MJ. (2013) Single-molecule analysis of fluorescently labeled G-protein-coupled receptors reveals complexes with distinct dynamics and organization. *Proc Natl Acad Sci U S A* **110**: 743-8.

Carriba P, Navarro G, Ciruela F, Ferré S, Casado V, Agnati LF, Cortes A, Mallol J, Fuxe K, Canela EI, Lluis C, Franco R (2008). Detection of heteromerization of more than two proteins by sequential BRET-FRET. *Nat Methods* **5**: 727-73310.

Carriba P, Ortiz O, Patkar K, Justinova Z, Stroik J, Themann A, Müller C, Woods AS, Hope BT, Ciruela F, Casadó V, Canela EI, Lluis C, Goldberg SR, Moratalla R, Franco R, Ferré S (2007). Striatal adenosine A2A and cannabinoid CB1 receptors form functional heteromeric complexes that mediate the motor effects of cannabinoids. *Neuropsychopharmacology* **32**: 2249-2259.

Carroll JB, Bates GP, Steffan J, Saft C, Tabrizi SJ (2015). Treating the whole body in Huntington's disease. *Lancet Neurol* **14**: 1135-1142.

Casadó V, Cortés A, Ciruela F, Mallol J, Ferré S, Lluis C, Canela EI, and Franco R (2007) Old and new ways to calculate the affinity of agonists and antagonists interacting with G-protein-coupled monomeric and dimeric receptors: the receptor dimer cooperativity index. *Pharmacol Ther* **116**:343-354.

Casadó V, Ferrada C, Bonaventura J, Gracia E, Mallol J, Canela EI, Lluís C, Cortés A, and Franco R (2009) Useful pharmacological parameters for G-protein-coupled receptor

homodimers obtained from competition experiments. Agonist-antagonist binding modulation. *Biochem Pharmacol* **78**:1456-1463.

Casadó-Anguera V, Bonaventura J, Moreno E, Navarro G, Cortés A, Ferré S, Casadó V (2016). Evidence for the heterotetrameric structure of the adenosine A2A-dopamine D2 receptor complex. *Biochem Soc Trans* **44**:595-600.

Casteels C, Vandeputte C, Rangarajan JR, Dresselaers T, Riess O, Bormans G, Maes F, Himmelreich U, Nguyen H, Van Laere K (2011). Metabolic and type 1 cannabinoid receptor imaging of a transgenic rat model in the early phase of Huntington disease. *Exp Neurol* **229**: 440-9.

Castillo PE, Younts TJ, Chávez AE, Hashimotodani Y (2012). Endocannabinoid signaling and synaptic function. *Neuron* **76**: 70-81.

Centonze D, Battista N, Rossi S, Mercuri NB, Finazzi-Agrò A, Bernardi G, Calabresi P, Maccarrone M (2004). A critical interaction between dopamine D2 receptors and endocannabinoids mediates the effects of cocaine on striatal gabaergic Transmission. *Neuropsychopharmacology* **29**: 1488-97.

Cepeda C, Murphy KPS, Parent M, Levine MS (2014). The Role of Dopamine in Huntington's Disease. *Progress in brain research*. **211**:235-254.

Chen JP, Paredes W, Li J, Smith D, Lowinson J, Gardner EL (1990). Delta 9-tetrahydrocannabinol produces naloxone-blockable enhancement of presynaptic basal dopamine efflux in nucleus accumbens of conscious, freely-moving rats as measured by intracerebral microdialysis. *Psychopharmacology* **102**: 156-62.

Chergui K, Suaud-Chagny MF, Gonon F (1994). Nonlinear relationship between impulse flow, dopamine release and dopamine elimination in the rat brain in vivo. *Neuroscience* **62**: 641-645.

Chiarlone A, Bellocchio L, Blázquez C, Resel E, Soria-Gómez E, Cannich A, Ferrero JJ, Sagredo O, Benito C, Romero J, Sánchez-Prieto J, Lutz B, Fernández-Ruiz J, Galve Roperh I, Guzmán M (2014). A restricted population of CB1 cannabinoid receptors with neuroprotective activity. *Proc Natl Acad Sci U S A* **111**: 8257-8262.

Chidiac P1, Green MA, Pawagi AB, Wells JW (1997). Cardiac muscarinic receptors. Cooperativity as the basis for multiple states of affinity. *Biochemistry* **36**: 7361-79.

Ciammola A, Sassone J, Colciago C, et al (2009). Aripiprazole in the treatment of Huntington's disease: a case series. *Neuropsychiatr Dis Treat* **5**: 1-4.

Consroe P, Laguna J, Allender J, Snider S, Stern L, Sandyk R, Kennedy K, Schram K (1991). Controlled clinical trial of cannabidiol in Huntington's disease. *Pharmacol Biochem Behav* **40**: 701-708.

Cordomí A, Navarro G, Aymerich MS, Franco R (2015). Structures for G-Protein Coupled Receptor Tetramers in Complex with G Proteins. *Trends Biochem Sci* **40**: 548-51.

Cornea A, Janovick JA, Maya-Nunez G, Conn PM (2001) Gonadotropin-releasing hormone receptor microaggregation rate monitored by fluorescence resonance energy transfer. *J Biol Chem* **276**: 2153-2158.

Coronas V, Srivastava LK, Liang JJ, Jourdan F, Moyse E (1997). Identification and localization of dopamine receptor subtypes in rat olfactory mucosa and bulb: a combined in situ hybridization and ligand binding radioautographic approach. *J Chem Neuroanat* **12**: 243-57.

Cravatt BF, Giang DK, Mayfield SP, Boger DL, Lerner RA, Gilula NB (1996). Molecular characterization of an enzyme that degrades neuromodulatory fatty-acid amides. *Nature* **384**: 83-7.

Curtis A, Mitchell I, Patel S, Ives N, Rickards H (2009). A pilot study using nabilone for symptomatic treatment in Huntington's disease. *Mov Disord* **24**: 2254-2259.

D'Amico M, Cannizzaro C, Preziosi P, Martire M (2004). Inhibition by anandamide and synthetic cannabimimetics of the release of [3H]D-aspartate and [3H]GABA from synaptosomes isolated from the rat hippocampus. *Neurochem Res* **29**: 1553-61.

Dal Toso R, Sommer B, Ewert M, Herb A, Pritchett DB, Bach A, Shivers BD, Seeburg PH (1989). The dopamine D2 receptor: two molecular forms generated by alternative splicing. *EMBO J* **8**: 4025-4034.

Damian M, Martin A, Mesnier D, Pin JP, and Bane`res JL (2006). Asymmetric conformational changes in a GPCR dimer controlled by G-proteins. *EMBO J* **25**:5693-5702.

Darren W. Engers and Craig W. Lindsley (2013). Allosteric Modulation of Class C GPCRs: A Novel Approach for the Treatment of CNS Disorders. *Drug Discov Today Technol* **2**: e269-e276.

de Lago E, de Miguel R, Lastres-Becker I, Ramos JA, Fernández-Ruiz JJ (2004). Involvement of vanilloid-like receptors in the effects of anandamide on motor behavior and nigrostriatal dopaminergic activity: in vivo and in vitro evidence. *Brain Res* **1007**: 152-159.

De Lean A, Stadel JM & Lefkowitz RJ (1980). A ternary complex model explains the agonist-specific binding properties of the adenylate cyclase-coupled β-adrenergic receptor. *J Biol Chem* **255**: 7108-7117.

De Mei C, Ramos M, Iitaka C, and Borrelli E (2009). Getting specialized: presynaptic and postsynaptic dopamine D2 receptors. *Curr Opin Pharmacol* **9**: 53-58.

DeGraff JL, Gurevich VV, Benovic JL (2002). The third intracellular loop of B2-adrenergic receptors determines subtype. *U S A* **84**: 8879-8882.

Demuth DG, Molleman A (2006). Cannabinoid signaling. *Life Sciences* **78**:549-563.
Denis C, Saulière A, Galandrin S, Sénard JM, Galés C (2012). Probing heterotrimeric G protein activation: applications to biased ligands. *Curr Pharm Des* **18**: 128-44.

Denovan-Wright EM, Robertson HA (2000) Cannabinoid receptor messenger RNA levels decrease in a subset of neurons of the lateral striatum, cortex and hippocampus of transgenic Huntington's disease mice. *Neuroscience* **98**:705-713.

Devane WA, Hanus L, Breuer A, Pertwee RG, Stevenson LA, Griffin G, Gibson D, Mandelbaum A, Etinger A, Mechoulam R (1992). Isolation and structure of a brain constituent that binds to the cannabinoid receptor. *Science* **258**: 1946-9.

Devost D, Sleno R, Pétrin D, Zhang A, Shinjo Y, Okde R, Aoki J, Inoue A, Hébert TE (2017) Conformational profiling of the AT1 angiotensin II receptor reflects biased agonism, G protein coupling and cellular context. *The Journal of Biological Chemistry* **292**: 5443-5456.

DeWire SM, Ahn S, Lefkowitz RJ, Shenoy SK (2007). Beta-arrestins and cell signaling. *Annu Rev Physiol* **69**:483-510.
Di Chiara G, Bassareo V (2007). Reward system and addiction: what dopamine does and doesn't do. *Curr Opin Pharmacol* **7**:69-76.

Di Marzo V, Bisogno T, De Petrocellis L, Melck, Martin BR (1999). Cannabimimetic fatty acid derivatives: the anandamide family and other endocannabinoids. *Curr Med Chem* **6**:721-44.

Di Marzo V, Lastres-Becker I, Bisogno T, De Petrocellis L, Milone A, Davis JB, Fernandez-Ruiz JJ (2001). Hypolocomotor effects in rats of capsaicin and two long chain capsaicin homologues. *Eur J Pharmacol* **420**:123-13.

Di Marzo V, Melck D, Bisogno T, De Petrocellis L (1998). Endocannabinoids: endogenous cannabinoid receptor ligands with neuromodulatory action. *Trends Neurosci* **21**: 521-8.

Drinovec L, Kubale V, Larsen JN, Vrecl M (2012). Mathematical models for quantitative qssessment of bioluminescence resonance energy transfer: application to seven transmembrane receptors oligomerization. *Front Endocrinol* **3**: 104.

247

Dupré DJ, Robitaille M, Ethier N, Villeneuve LR, Mamarbachi AM, Hébert TE (2006). Seven transmembrane receptor core signaling complexes are assembled prior to plasma membrane trafficking. *J Biol Chem* **281**: 34561-73.

Dupré DJ, Thompson C, Chen Z, Rollin S, Larrivée JF, Le Gouill C, Rola-Pleszczynski M, Stanková J (2007). Inverse agonist-induced signaling and down-regulation of the platelet-activating factor receptor. *Cell Signal* **19**: 2068-79.

Eaton SL, Cumyn E, King D, Kline RA, Carpanini SM, Del-Pozo J, Barron R, Wishart TM (2016). Quantitative imaging of tissue sections using infrared scanning technology. *J Anat* **228**: 203-13.

Eddy CM, Rickards HE (2011). Treatment strategies for tics in Tourette syndrome. *Ther Adv Neurol Disord* **4**: 25-45.

Edelstein SJ, Le Novère N (2013). Cooperativity of allosteric receptors. *J Mol Biol* **425**: 1424-32.

Egertová M, Giang DK, Cravatt BF, Elphick MR (1998). A new perspective on cannabinoid signalling: complementary localization of fatty acid amide hydrolase and the CB1 receptor in rat brain. *Proc Biol Sci* **265**: 2081-2085.

El Khoury MA, Gorgievski V, Moutsimilli L, Giros B, Tzavara ET (2012). Interactions between the cannabinoid and dopaminergic systems: evidence from animal studies. Prog *Neuropsychopharmacol Biol Psychiatry* **38**: 36-50.

Elisa Alvarez-Curto, Richard J. Ward, John D. Pediani, and Graeme Milligan (2010). Ligand Regulation of the Quaternary Organization of Cell Surface M3 Muscarinic Acetylcholine Receptors Analyzed by Fluorescence Resonance Energy Transfer (FRET) Imaging and Homogeneous Time-resolved FRET. *J Biol Chem* **285**: 23318-23330.

Ellis J, Pediani JD, Canals M, Milasta S, Milligan G (2006). Orexin-1 receptor cannabinoid CB1 receptor heterodimerization results in both ligand-dependent and independent coordinated alterations of receptor localization and function. *J Biol Chem* **281**: 38812-24.

Eriksen J, Jorgensen TN, Gether U (2010). Regulation of dopamine transporter function by protein-protein interactions: new discoveries and methodological challenges. *J Neurochem* **113**:27-41.

Ernst OP, Gramse V, Kolbe M, Hofmann KP, Heck M (2007). Monomeric G protein-coupled receptor rhodopsin in solution activates its G protein transducin at the diffusion limit. *Proc Natl Acad Sci U S A* **104**: 10859-64.

Falenski KW, Thorpe AJ, Schlosburg JE, Cravatt BF, Abdullah RA, Smith TH, Selley

DE, Lichtman AH, Sim-Selley LJ (2010). FAAH−/− mice display differential tolerance, dependence, and cannabinoid receptor adaptation after Δ9-tetrahydrocannabinol and anandamide administration. *Neuropsychopharmacology* **35**: 1775-1787.

Felder CC, Veluz JS, Williams HL, Briley EM, Matsuda LA (1992). Cannabinoid agonists stimulate both receptor- and non-receptor-mediated signal transduction pathways in cells transfected with and expressing cannabinoid receptor clones. *Mol Pharmacol* **42**; 838-45.

Ferguson SS, Downey WE, Colapietro AM, Barak LS, Ménard L, Caron MG (1996). Role of B-arrestin in mediating agonist promoted G protein-coupled receptor internalization. *Science* **271**: 363-366.

Fernández-Ruiz (2009). The endocannabinoid system as a target for the treatment of motor dysfunction. *Br J Pharmacol* **156**: 1029-1040.

Fernández-Ruiz J, Gonzáles S (2005). Cannabinoid control of motor function at the basal ganglia. *Handb Exp Pharmacol* **168**: 479-507.

Fernández-Ruiz J, Hernández M, Ramos JA (2010). Cannabinoid-dopamine interaction in the pathophysiology and treatment of CNS disorders. *CNS Neurosci Ther* **16**: e72–e9.

Ferrada C, Moreno E, Casadó V, Bongers G, Cortés A, Mallol J, Canela EI, Leurs R, Ferré S, and Lluís C, et al. (2009) Marked changes in signal transduction upon heteromerization of dopamine D1 and histamine H3 receptors. *Br J Pharmacol* **157**:64-75.

Ferré S (2015). The GPCR heterotetramer: challenging classical pharmacology. *Trends Pharmacol Sci* **36**:145-52.

Ferré S, Bonaventura J, Tomasi D, Navarro G, Moreno E, Cortés A, Lluís C, Casadó V, Volkow ND (2015b). Allosteric mechanisms within the adenosine A2A-dopamine D2 receptor heterotetramer. *Neuropharmacology* **104**:154-60.

Ferré S, Casadó V, Devi LA, Filizola M, Jockers R, Lohse MJ, Milligan G, Pin JP, Guitart X (2014). G protein-coupled receptor oligomerization revisited: functional and pharmacological perspectives. *Pharmacol Rev* **66**: 413-34.

Ferré S, Fuxe K, von Euler G, Johansson B, Fredholm BB (1992). Adenosine-dopamine interactions in the brain. *Neuroscience* **3**: 501-12.
Ferré S, Goldberg SR, Lluis C, Franco R (2009). Looking for the role of cannabinoid receptor heteromers in striatal function. *Neuropharmacology* **56**: 226-34.

Ferreira SG, Lomaglio T, Avelino A, Cruz F, Oliveira CR, Cunha RA, Köfalvi A (2009). N-acyldopamines control striatal input terminals via novel ligand-gated cation channels. *Neuropharmacology* **56**: 676-683.

Fiorentini C, Busi C, Gorruso E, Gotti C, Spano P, Missale C (2008). Reciprocal regulation of dopamine D1 and D3 receptor function and trafficking by heterodimerization. *Mol Pharmacol* **74**: 59-69.

Floresco SB, West AR, Ash B, Moore H, Grace AA (2003). Afferent modulation of dopamine neuron firing differentially regulates tonic and phasic dopamine transmission. *Nat Neurosci* 2003 **6**: 968-73.

Floresco SB, West AR, Ash B, Moore H, Grace AA (2003). Afferent modulation of dopamine neuron firing differentially regulates tonic and phasic dopamine transmission. *Nat neurosci* **6**: 968-973.

Foroud T, Gray J, Ivashina J, Conneally PM (1999). Differences in duration of Huntington's disease based on age at onset. *J Neurol Neurosurg Psychiatry* **66**: 52-56.

Fotiadis D, Liang Y, Filipek S, Saperstein DA, Engel A & Palczewski K (2003). Atomic-force microscopy: Rhodopsin dimers in native disc membranes. *Nature* **421**: 127-128.
Fox CA, Mansour A, Watson SJ Jr (1994). The effects of haloperidol on dopamine receptor gene expression. *Exp Neurol* **130**: 288-303.

Franco R, Martínez-Pinilla E, Lanciego JL, Navarro G (2016). Basic Pharmacological and Structural Evidence for Class A G-Protein-Coupled Receptor Heteromerization. *Front Pharmacol* **7**:76.

Frank S (2014). Treatment of Huntington's Disease. *Neurotherapeutics* **11**: 153-160.

Frank S, Jankovic J (2010). Advances in the pharmacological management of Huntington's disease. *Drugs* **70**: 561-71.

Frank S, Testa CM, Stamler D, Kayson E, Davis C, Edmondson MC, Kinel S, Leavitt B, Oakes D, O'Neill C, Vaughan C et al. (2016). Effect of Deutetrabenazine on Chorea Among Patients With Huntington Disease: A Randomized Clinical Trial. *JAMA* **316**: 40-50.

Fredriksson S, Gullberg M, Jarvius J, Olsson C, Pietras K, Gústafsdóttir SM, Ostman A, Landegren U (2002). Protein detection using proximity-dependent DNA ligation assays. *Nat Biotechnol*. **20**:473-7.

Fung JJ, Deupi X, Pardo L, Yao XJ, Velez-Ruiz GA, Devree BT, Sunahara RK, Kobilka BK (2009). Ligand-regulated oligomerization of beta(2)-adrenoceptors in a model lipid bilayer. *EMBO J* **28**: 3315-28.

Gaitonde SA, González-Maeso J (2017). Contribution of heteromerization to G protein-coupled receptor function. *Curr Opin Pharmacol* **32**: 23-31.

Galés C, Rebois RV, Hogue M,Trieu P, Breit A, Hébert TE, Bouvier M (2005). Real-time monitoring of receptor and G-protein interactions in living cells. *Nat Methods* **2**: 177-184.

Galés C,VanDurm JJ, Schaak S, Pontier S, Percherancier Y, Audet M, Paris H, Bouvier M (2006). Probing the activation-promoted structural rearrangements in preassembled receptor-G protein complexes. *Nat Struct Mol Biol* **13**: 778-786.

García C, Palomo-Garo C, Gómez-Gálvez Y1, Fernández-Ruiz J (2016). Cannabinoid-dopamine interactions in the physiology and physiopathology of the basal ganglia. *Br J Pharmacol* **173**: 2069-79.

Gazi L, Lopez-Gimenez JF, Rudiger M, Strange PG (2003). Constitutive oligomerization of human D2 dopamine receptors expressed in Spodoptera frugiperda 9 (Sf9) and in HEK293 cells. Analysis using co-immunoprecipitation and time-resolved fluorescence resonance energy transfer. *EurJ Biochem* **270**: 3928-3938.

Gentry PR, Sexton PM, Christopoulos A (2015). Novel Allosteric Modulators of G Protein-coupled Receptors. *J Biol Chem* **290**: 19478-19488.

George SR, Kern A, Smith RG, Franco R (2014). Dopamine receptor heteromeric complexes and their emerging functions. *Prog Brain Res* **211**:183-200.

Gerfen CR (1992). The neostriatal mosaic: multiple levels of compartmental organization in the basal ganglia. *Annu Rev Neurosci* **15**: 285-320.

Gerfen CR (2000). Molecular effects of dopamine on striatal-projection pathways. *Trends Neurosci* 23: S64-S70.

Gerlach J (1991). New antipsychotics: classification, efficacy, and adverse effects. *Schizophr Bull* **17**: 289-309.

Gershanik O, Heikkila RE, Duvoisin RC (1983). Behavioral correlations of dopamine receptor activation. *Neurology* **33**: 1489-92.

Gether U (2000). Uncovering molecular mechanisms involved in activation of Gprotein-coupled receptors. *Endocr Rev* **21**: 90-113.

Gilberta DL, Jankovicb J (2014). Pharmacological treatment of Tourette syndrome. *Journal of Obsessive-Compulsive and Related Disorders* **3**: 407-414.

Gilman AG (1987). G proteins: transducers of receptor-generated signals. *Annu Rev Biochem* **56**: 615-649.

Giraldo J (2013). Modeling cooperativity effects in dimeric G protein-coupled receptors. *Prog Mol Biol Transl Sci* **115**:349-373.

Girault JA, Greengard P (2004). The Neurobiology of Dopamine Signaling. *Arch Neurol*. **61**: 641-644.

Giros B, Sokoloff P, Martres MP, Riou JF, Emorine LJ, Schwartz JC (1989). Alternative splicing directs the expression of two D2 dopamine receptor isoforms. *Nature* **342**: 923-926.

Giuffrida A, Parsons LH, Kerr TM, Rodrigues de Fonseca F, Navarro M, Piomelli D (1999). Dopamine activation of endogenous cannabinoid signaling in dorsal striatum. *Nat Neurosci* **2**: 358-363.

Giuffrida A, Piomelli D (2000). The endocannabinoid system: a physiological perspective on its role in psychomotor control. *Chemistry and Physics of Lipids* **108**:151-158.

Glass M, Felder CC (1997). Concurrent stimulation of cannabinoid CB1 and dopamine D2 receptors augments cAMP accumulation in striatal neurons: Evidence for a Gs linkage to the CB1 receptor. *J Neurosci* **17**: 5327-33.

Glass M, Dragunow M, Faull RL (2000). The pattern of neurodegeneration in Huntington's disease: a comparative study of cannabinoid, dopamine, adenosine and GABA(A) receptor alterations in the human basal ganglia in Huntington's disease. *Neuroscience* **97**: 505-519.

Glass M, Northup JK (1999). Agonist selective regulation of G proteins by cannabinoid CB1 and CB2 receptors. *Mol Pharmacol* **56**:1362-1369.

Gomes I, Ayoub MA, Fujita W, Jaeger WC, Pfleger KD, Devi LA (2016). G Protein-Coupled Receptor Heteromers. *Annu Rev Pharmacol Toxicol* **56**: 403-25.

Goricanec D, Stehle R, Egloff P, Grigoriu S, Plückthun A, Wagner G, Hagn F (2016). Conformational dynamics of a G-protein α subunit is tightly regulated by nucleotide binding. *Proc Natl Acad Sci U S A* **113**; E3629-38.

Gorriti MA, Rodriguez de Fonseca F, Navarro M, Palomo T (1999). Chronic (-)-Δ9-tetrahydrocannabinol treatment induces sensitization to the psychomotor effects of amphetamine in rats. *Eur J Pharmacol* **365**: 133–142.

Goto Y, Otani S, Grace AA (2007). The Yin and Yang of dopamine release: a new perspective. *Neuropharmacology* **53**: 583-7.

Grace AA (1991). Phasic versus tonic dopamine release and the modulation of dopamine system responsivity: a hypothesis for the etiology of schizophrenia. *Neuroscience* **41**:1-24.

Grandy DK, Litt M, Allen L, Bunzow JR, Marchionni M, Makam H, Reed L, Magenis RE, Civelli O (1989). The human dopamine D2 receptor gene is located on chromosome 11 at q22-q23 and identifies a TaqI RFLP. *Am J Hum Genet* **45**:778-85.

Grant M, Alturaihi H, Jaquet P, Collier B, Kumar U (2008). Cell growth inhibition and functioning of human somatostatin receptor type 2 are modulated by receptor heterodimerization. *Mol Endocrinol* **22**: 2278-2292.

Graybiel AM (2005). The basal ganglia: learning new tricks and loving it. Curr Opin Neurobiol **15**:638-644.

Guan R, Feng X, Wu X, Zhang M, Zhang X, Hébert TE, Segaloff DL (2009). Bioluminescence resonance energy transfer studies reveal constitutive dimerization of the human lutropin receptor and a Lack of correlation between receptor activation and the propensity for dimerization. *J Biol Chem* **284**:7483-7494.

Guiramand J, Montmayeur JP, Ceraline J, Bhatia M, Borrelli E (1995). Alternative splicing of the dopamine D2 receptor directs specificity of coupling to G-proteins. *J Biol Chem* **270**: 7354-7358.

Guitart X, Navarro G, Moreno E, Yano H, Cai NS, Sánchez-Soto M, Kumar-Barodia S, Naidu YT, Mallol J, Cortés A1, Lluís C1, Canela EI1, Casadó V1, McCormick PJ1, Ferré S (2014). Functional selectivity of allosteric interactions within G protein-coupled receptor oligomers: the dopamine D1-D3 receptor heterotetramer *Mol Pharmacol* **86**: 417-29.

Guo W, Urizar E, Kralikova M, Mobarec JC, Shi L, Filizola M, Javitch JA (2008). Dopamine D2 receptors form higher order oligomers at physiological expression levels. *EMBO J* **27**: 2293-304.

Gurevich EV, Tesmer JJ, Mushegian A, Gurevich VV (2012). G protein-coupled receptor kinases: more than just kinases and not only for GPCRs. *Pharmacol Ther* **133**: 40-69.

Gurevich VV, Gurevich EV (2008). How and why do GPCRs dimerize? *Trends Pharmacol Sci* **29**: 234-240.

Gustafsson K, Wang X, Severa D, Eriksson M, Kimby E, Merup M, Christensson B, Flygare J, Sander B (2008). Expression of cannabinoid receptors type 1 and type 2 in non-Hodgkin lymphoma: growth inhibition by receptor activation. *Int J Cancer* **123**: 1025-1033.

Hadjiconstantinou M, Wemlinger TA, Sylvia CP, Hubble JP, Neff NH (1993). Aromatic L-amino acid decarboxylase activity of mouse striatum is modulated via dopamine receptors. *J Neurochem* **60**: 2175-2180.

Hague C, Uberti MA, Chen Z, Bush CF, Jones SV, Ressler KJ, Hall RA, Minneman KP (2004). Olfactory receptor surface expression is driven by association with the β2 adrenergic receptor. *Proc Natl Acad Sci USA* **101**:13672-6.

Hall H, Sedvall G, Magnusson O, Kopp J, Halldin C, Farde L (1994). Distribution of D1- and D2-dopamine receptors, and dopamine and its metabolites in the human brain. *Neuropsychopharmacology* **11**: 245-256.

Hall RA (2009). Olfactory receptor interactions with other receptors. *Ann N Y Acad Sci* **1170**: 147-149.
Hamdan FF, Rochdi MD, Breton B, Fessart D, Michaud DE, Charest PG, Laporte SA, Bouvier M (2007). Unraveling G protein-coupled receptor endocytosis pathways using real-time monitoring of agonist-promoted interaction between ß-arrestins and AP-2. *J. Biol. Chem* **282**: 29089-29100.

Hammad MH, Dupré DJ (2010). Chaperones contribute to G protein coupled receptor oligomerization, but do not participate in assembly of the G protein with the receptor signaling complex. *J Mol Signal* **5**: 16.

Han M, Huang XF, du Bois TM, Deng C (2009). The effects of antipsychotic drugs administration on 5-HT1A receptor expression in the limbic system of the rat brain. *Neuroscience* **164**: 1754-1763.

Han Y, Moreira IS, Urizar E, Weinstein H, Javitch JA (2009). Allosteric communication between protomers of dopamine class A GPCR dimers modulates activation. *Nat Chem Biol* **5**:688-95.

Hauber W, Lutz S (1999). Dopamine D1 or D2 receptor blockade in the globus pallidus produces akinesia in the rat. *Behav Brain Res* **106**: 143-50.

Hayden MR, Leavitt BR, Yasothan U, Kirkpatrick P (2009). Tetrabenazine. *Nat Rev Drug Discov* **8**: 17-8.

Hébert TE, Moffett S, Morello JP, Loisel TP, Bichet DG, Barret C, Bouvier M (1996). A peptide derived from a beta2-adrenergic receptor transmembrane domain inhibits both receptor dimerization and activation. *J Biol Chem* **271**: 16384-92.

Herkenham M, Lynn AB, Johnson MR, Melvin LS, de Costa BR, Rice KC (1991). Characterization and localization of cannabinoid receptors in rat brain: a quantitative in vitro autoradiographic study. *J Neurosci* **11**: 563-83.

Herkenham M, Lynn AB, Little MD, Johnson MR, Melvin LS, de Costa BR, Rice KC (1990). Cannabinoid receptor localization in brain. *Proceedings of the National Academy of Sciences USA* **87**:1932-1936.

Hermann H, Marsicano G, Lutz B (2002). Coexpression of the cannabinoid receptor type 1 with dopamine and serotonin receptors in distinct neuronal subpopulations of the adult mouse forebrain. *Neuroscience* **109**:451-460.

Hern JA, Baig AH, Mashanov GI, Birdsall B, Corrie JE, Lazareno S, Molloy JE, Birdsall NJ (2010) Formation and dissociation of M1 muscarinic receptor dimers seen by total internal reflection fluorescence imaging of single molecules. *Proc Natl Acad Sci USA* **107**: 2693- 2698.

Herrick-Davis K, Grinde E, Cowan A, Mazurkiewicz JE. (2013) Fluorescence correlation spectroscopy analysis of serotonin, adrenergic, muscarinic, and dopamine receptor dimerization: the oligomer number puzzle. *Mol Pharmacol* **84**:630-642.

Herrick-Davis K, Grinde E, Harrigan TJ, Mazurkiewicz JE (2005). Inhibition of serotonin 5-hydroxytryptamine2c receptor function through heterodimerization: receptor dimers bind two molecules of ligand and one G-protein. *J Biol Chem* **48**: 40144-51.

Herrick-Davis K, Mazurkiewicz JE. Fluorescence correlation spectroscopy and photon-counting histogram analysis of receptor-receptor interactions (2013). *Methods Cell Biol* **117**:181-96.

Herrick-Davis, K, Weaver BA, Grinde E, Mazurkiewicz JE (2006). Serotonin 5-HT2C receptor homodimer biogenesis in the endoplasmic reticulum: Real-time visualization with confocal fluorescence resonance energy transfer. *J Biol Chem* **281**: 27109-16.

Hillion J, Canals M, Torvinen M, Casado V, Scott R, Terasmaa A, Hansson A, Watson S, Olah ME, Mallol J, Canela EI, Zoli M, Agnati LF, Ibanez CF, Lluis C, Franco R, Ferre S, Fuxe K (2002) Coaggregation, cointernalization, and codesensitization of adenosine A2A receptors and dopamine D2 receptors. *J Biol Chem* **277**: 18091-18097.

Hirvonen J, Goodwin RS, Li CT, Terry GE, Zoghbi SS, Morse C, Pike VW, Volkow ND, Huestis MA, Innis RB (2012). Reversible and regionally selective downregulation of brain cannabinoid CB1 receptors in chronic daily cannabis smokers. *Mol Psychiatry* **17**: 642-9.

Hlavackova V, Zabel U, Frankova D, Bätz J, Hoffmann C, Prezeau L, Pin JP, Blahos J, Lohse MJ (2012). Sequential inter- and intrasubunit rearrangements during activation of dimeric metabotropic glutamate receptor 1. *Science Signaling* **5**:e323.
Hogel M, Laprairie RB, Denovan-Wright EM (2012). Promoters Are Differentially Sensitive to N-Terminal Mutant Huntingtin-Mediated Transcriptional Repression. *PLoS One* **7**: e41152.

Hohmann AG, Briley EM, Herkenham M (1999) Pre- and postsynaptic distribution of cannabinoid and mu opioid receptors in rat spinal cord. *Brain Res* **822**: 17-25.

Hojo M, Sudo Y, Ando Y, Minami K, Takada M, Matsubara T, Kanaide M, Taniyama K, Sumikawa K, Uezono Y (2008). mu-Opioid receptor forms a functional heterodimer with cannabinoid CB1 receptor: electrophysiological and FRET assay analysis. *J Pharmacol Sci* **108**: 308-19.

Hosking RD, Zajicek JP (2008). Therapeutic potential of cannabis in pain medicine. *Br J Anaesth* **101**: 59-68.

Howlett AC, Breivogel CS, Childers SR, Deadwyler SA, Hampson RE, Porrino LJ (2004). Cannabinoid physiology and pharmacology: 30 years of progress. *Neuropharmacology* **47**:345-358.

Hu CD, Chinenov Y, Kerppola TK (2002). Visualization of interactions among bZIP and Rel family proteins in living cells using bimolecular fluorescence complementation. *Mol Cell.* **9**:789-98.

Huang J, Chen S, Zhang JJ, Huang XY (2013). Crystal structure of oligomeric β1-adrenergic G protein-coupled receptors in ligand-free basal state. *Nat Struct Mol Biol* **20**: 419-25.

Huang XF, Han M, Huang X, Zavitsanou K, Deng C (2006). Olanzapine differentially affects 5-HT2A and 2C receptor mRNA expression in the rat brain. *Behavioural Brain Research* **171**: 355-362.

Hudson BD, Hébert TE, Kelly ME (2010a). Ligand- and heterodimer-directed signaling of the CB(1) cannabinoid receptor. *Mol Pharmacol* **77**: 1-9.

Hudson BD, Hébert TE, Kelly ME (2010b). Physical and functional interaction between CB1 cannabinoid receptors and β2-adrenoceptors. *Br J Pharmacol* **160**:627-642.

Huntington's disease collaborative research group (HDCRG) (1993). A novel gene containing a trinucleotide repeat that is expanded and unstable on Huntington's disease chromosomes. The Huntington's Disease Collaborative Research Group. *Cell* **72**: 971-983.

Hyman SE, Malenka RC, and Nestler EJ (2006). Neural mechanisms of addiction: the role of reward-related learning and memory. *Annu Rev Neurosci* **29**:565-598.

Ibsen MS, Connor M , Glass M (2017). Cannabinoid CB_1 and CB_2 Receptor Signaling and Bias**. *Research* **2**: 48-60.

Ikegami M, Uemura T, Kishioka A, Sakimura K, Mishina M (2014). Striatal dopamine D1 receptor is essential for contextual fear conditioning. *Sci Rep* **5**: 4:3976.

Ittai Bushlin, Achla Gupta, Steven D. Stockton Jr, Lydia K. Miller, Lakshmi A. Devi (2012). Dimerization with Cannabinoid Receptors Allosterically Modulates Delta Opioid Receptor Activity during Neuropathic Pain. *PLoS One* **7**: e49789.

Iversen L (2003). Cannabis and the brain. *Brain* **126**: 1252-1270.

Iversen SD, Iversen LL (2007). Dopamine: 50 years in perspective. *Trends Neurosci* **30**: 188-193.

James JR, Oliveira MI, Carmo AM, Iaboni A, Davis SJ (2006) A rigorous experimental framework for detecting protein oligomerization using bioluminescence resonance energy transfer. *Nature Methods* **3**:1001-1006.

Janetopoulos C, Jin T, Devreotes P (2001). Receptor-mediated activation of heterotrimeric G-proteins in living cells. *Science* **291**: 2408-2411.

Jäntti MH, Mandrika I, Kukkonen JP (2014). Human orexin/hypocretin receptors form constitutive homo- and heteromeric complexes with each other and with human CB1 cannabinoid receptors. *Biochem Biophys Res Commun* **445** :486-90.

Jarrahian A, Watts VJ, Barker EL (2004). D2 dopamine receptors modulate Gα-subunit coupling of the CB1 cannabinoid receptor. *J Pharmacol Exp Ther* **284**:291-297.

Jastrzebska B (2013). GPCR -G protein complexes – the fundamental signaling assembly. *Amino Acids* **45**: 6.

Jastrzebska B, Orban T, Golczak M, Engel A, Palczewski K (2013). Asymmetry of the rhodopsin dimer in complex with transducing. *FASEB J* **27**: 1572-1584.

Jin W, Brown S, Roche JP, Hsieh C, Celver JP, Kovoor A, Chavkin C, Mackie K (1999). Distinct domains of the CB1 cannabinoid receptor mediate desensitization and internalization. *J Neurosci* **19**:3773-80.

Johnston JP (1968). Some observations upon a new inhibitor of monoamine oxidase in brain tissue. *Biochem Pharmacol* **17**: 1285-1297.

Jonas KC, Fanelli F, Huhtaniemi IT, Hanyaloglu AC (2015). Single molecule analysis of functionally asymmetric G protein-coupled receptor (GPCR) oligomers reveals diverse spatial and structural assemblies. *J Biol Chem* **290**: 3875-92.
Jonas KC, Huhtaniemi I, Hanyaloglu AC (2016). Single-molecule resolution of G protein-coupled receptor (GPCR) complexes. *Methods Cell Biol* **132**:55-72.

Julian MD, Martin AB, Cuellar B, Rodriguez De Fonseca F, Navarro M, Moratalla R, Garcia-Segura LM (2003). Neuroanatomical relationship between type 1 cannabinoid receptors and dopaminergic systems in the rat basal ganglia. *Neuroscience* **119**: 309-318.

Kapur S, Mamo D (2003). Half a century of antipsychotics and still a central role for dopamine D2 receptors. *Prog Neuropsychopharmacol Biol Psychiatry* **27**: 1081-90.

Kapur S, Seeman P (2001). Does fast dissociation from the dopamine d(2) receptor explain the action of atypical antipsychotics?: A new hypothesis. Am J Psychiatry **158**:360-9.

Kasai RS, Suzuki KG, Prossnitz ER, Koyama-Honda I, Nakada C, Fujiwara TK, Kusumi A (2011) Full characterization of GPCR monomer-dimer dynamic equilibrium by single molecule imaging. *J Cell Biol* **192**: 463-480.

Katritch V, Cherezov , Stevens RC (2013). Structure-function of the G protein-coupled receptor superfamily. *Annu Rev Pharmacol Toxicol*. **53**:531-56.

Kearn CS, Blake Palmer K, Daniel E, Mackie K, Glass M (2005). Concurrent stimulation of cannabinoid CB1 and dopamine D2 receptors enhances heterodimer formation: A mechanism for receptor cross talk? *Mol Pharmacol* **67**: 1697-704.

Kearn CS (2004). Immunofluorescent mapping of cannabinoid CB1 and dopamine D2 receptors in the mouse brain. LI-COR Biosci, Application Notes.

Kearn CS, Blake-Palmer K, Daniel E, Mackie K, Glass M (2005). Concurrent stimulation of cannabinoid CB1 and dopamine D2 receptors enhances heterodimer formation: a mechanism for receptor cross-talk? *Mol Pharmacol* **67**: 1697-1704.

Keefe KA, Zigmond MJ, Abercrombie ED (1993). In vivo regulation of extracellular dopamine in the neostriatum: influence of impulse activity and local excitatory amino acids. *J Neural Transm Gen Sect* **91**: 223-40.

Kelly MA, Rubinstein M, Phillips TJ, Lessov CN, Burkhart-Kasch S, Zhang G, Bunzow JR, Fang Y, Gerhardt GA, Grandy DK, Low MJ (1998). Locomotor activity in D2 dopamine receptor-deficient mice is determined by gene dosage, genetic background, and developmental adaptations. *J Neurosci* **18**: 3470-9.

Kenakin T (2010). Functional selectivity and biased receptor signaling (2010). *J Pharmacol Exp Ther* **336**, 296-302.

Kenakin T, Christopoulos A (2013). Signalling bias in new drug discovery: detection, quantification and therapeutic impact. *Nat Rev Drug Discov* **12**: 205-216.

Kenakin T, Miller LJ (2010). Seven transmembrane receptors as shapeshifting proteins: the impact of allosteric modulation and functional selectivity on new drug discovery. *Pharmacol Rev* **62**: 265-304.

Kern A, Albarran-Zeckler R, Walsh HE, and Smith RG (2012). Apo-ghrelin receptor

forms heteromers with DRD2 in hypothalamic neurons and is essential for anorexigenic effects of DRD2 agonism. *Neuron* **73**:317-332.

Khan SS, Lee FJ (2014). Delineation of domains within the cannabinoid CB1 and dopamine D2 receptors that mediate the formation of the heterodimer complex. *J Mol Neurosci* **53**:10-21.

Khan ZU, Mrzljak L, Gutierrez A, de la Calle A, Goldman-Rakic PS (1998). Prominence of thedopamine D2 short isoform in dopaminergic pathways. *Proceedings of the National Academy of Sciences USA* **95**:7731-7736.

Kim KM, Valenzano KJ, Robinson SR, Yao WD, Barak LS, Caron MG (2001). Differential regulation of the dopamine D2 and D3 receptors by G protein-coupled receptor kinases and beta-arrestins. *J Biol Chem* **276**: 37409-37414.

Kirilly E, Gonda X, Bagdy G (2012). CB1 receptor antagonists: new discoveries leading to new perspectives. *Acta Physiol (Oxf)* **205**: 41-60.

Klein SH, Reuveni H, Levitzki A. Signal transduction by a nondissociable heterotrimeric yeast G protein (2000). *Proc Natl Acad Sci USA* **97**: 3219-3223.

Kluger B, Triolo P, Jones W, Jankovic J (2015). The Therapeutic Potential of Cannabinoids for Movement Disorders. *Mov Disord* **30**: 313-327.

Kobayashi H, Ogawa K, Yao R, Lichtarge O, Bouvier M (2009). Functional rescue of beta-adrenoceptor dimerization and trafficking by pharmacological chaperones. *Traffic* **10**:1019-33.

Köfalvi A, Rodrigues RJ, Ledent C, Mackie K, Vizi ES, Cunha RA, Sperlágh B (2005). Involvement of cannabinoid receptors in the regulation of neurotransmitter release in the rodent striatum: a combined immunochemical and pharmacological analysis. *J Neurosci* **25**: 2874-84.

Koob GF, Volkow ND (2010). Neurocircuitry of addiction. *Neuropsychopharmacology* **35**: 217-238.

Kuszak A. J., Pitchiaya S., Anand J. P., Mosberg H. I., Walter N. G., Sunahara R. K. (2008). Purification and functional reconstitution of monomeric μ-opioid receptors: allosteric modulation of agonist binding by Gi2. *J Biol Chem* **284**: 26732-26741.

Labbadia J, Morimoto RI (2013). Huntington's disease: underlying molecular mechanisms and emerging concepts. *Trends Biochem Sci* **38**: 378-85.

Lachance M, Ethier N, Wolbring G, Schnetkamp PP, Hébert TE (1999). Stable association of G proteins with beta 2AR is independent of the state of receptor activation. *Cell Signal* **11**: 523-53310.

Lan TH, Liu Q1, Li C, Wu G, Steyaert J, Lambert NA (2015). BRET evidence that β2 adrenergic receptors do not oligomerize in cells. *Sci Rep* **5**:10166.

Laprairie RB, Bagher AM, Denovan-Wright EM (2017). Cannabinoid receptor ligand bias: implications in the central nervous system. *Current Opinion in Pharmacology* **32**: 32-43.

Laprairie RB, Bagher AM, Kelly ME, Denovan-Wright EM (2016). Biased Type 1 Cannabinoid Receptor Signaling Influences Neuronal Viability in a Cell Culture Model of Huntington Disease. *Mol Pharmacol* **89**: 364-75.

Laprairie RB, Bagher AM, Kelly ME, Dupré DJ, Denovan-Wright EM (2014). Type 1 Cannabinoid Receptor Ligands Display Functional Selectivity in a Cell Culture Model of Striatal Medium Spiny Projection Neurons. *J Biol Chem* **289:** 24736-25392.

Laprairie RB, Bagher AM, Precious SV, Denovan-Wright EM (2015). Components of the endocannabinoid and dopamine systems are dysregulated in Huntington's disease: analysis of publicly available microarray datasets. *Pharmacol Res Perspect* *4*:e00104.

Laprairie RB, Kelly MEM, Denovan-Wright EM (2013). Cannabinoids increase type 1 cannabinoid receptor expression in a cell culture model of medium spiny projection neurons: Implications for Huntington's disease. *Neuropharmacology* **72**: 47-57.

Lauckner JE, Hille B, Mackie K (2005). The cannabinoid agonist WIN55,212-2 increases intracellular calcium via CB1 receptor coupling to Gq/11 G proteins. *Proc Natl Acad Sci USA* **102**:19144-19149.

Leach K, Sexton PM, Christopoulos A (2007). Allosteric GPCR modulators: taking advantage of permissive receptor pharmacology. *Trends Pharmacol Sci* **28**: 382-9.

Lee JM, Ivanova EV, Seong IS, Cashorali T, Kohane I, Gusella J, MacDonald ME (2007). Unbiased Gene Expression Analysis Implicates the huntingtin Polyglutamine Tract in Extra-mitochondrial Energy Metabolism. *PLoS Genet* **3**:8-135.

Lee SP, O'Dowd BF, Ng GY, Varghese G, Akil H, Mansour A, Nguyen T, George SR (2000). Inhibition of cell surface expression by mutant receptors demonstrates that D2 dopamine receptors exist as oligomers in the cell. *Mol Pharmacol* **58**: 120-128.

Lee SP, So CH, Rashid AJ, Varghese G, Cheng R, Lança AJ, O'Dowd BF, George SR (2004). Dopamine D1 and D2 receptor Co-activation generates a novel phospholipase C-mediated calcium signal. *J Biol Chem* **279**: 35671-8.

Lefkowitz RJ (1993). G protein-coupled receptor kinases. *Cell* **74**: 409-12.
Lefkowitz RJ, Shenoy SK (2005). Transduction of receptor signals by beta-arrestins.

Science **308**: 512-7.

Leterrier C, Laine J, Darmon M, Boudin H, Rossier J, Lenkei Z (2006) Constitutive activation drives compartment-selective endocytosis and axonal targeting of type 1 cannabinoid receptors. *J Neurosci* **26**:3141-3153.

Leung JY, Barr AM, Procyshyn RM, Honer WG, Pang CC (2012). Cardiovascular side-effects of antipsychotic drugs: the role of the autonomic nervous system. *Pharmacol Ther* **135**: 113-22.

Levey AI, Hersch SM, Rye DB, Sunahara RK, Niznik HB, Kitt CA, Price DL, Maggio R, Brann MR, Ciliax BJ (1993). Localization of D1 and D2 dopamine receptors in brain with subtype-specific antibodies. *Proc Natl Acad Sci U S A* **90**: 8861-5.

Levitzki A, Bar-Sinai A (1991). The regulation of adenylyl cyclase by receptor-operated G proteins. *Pharmacol Ther* **50**: 271-83.

Levoye A, Balabanian K, Baleux F, Bachelerie , Lagane B (2009). CXCR 7 heterodimerizes with CXCR4 and regulates CXCL12-mediated G protein signaling. *Blood* **113**: 6085-6093.

Liang Y, Fotiadis D, Filipek S, Saperstein DA, Palczewski K & Engel A (2003). Organization of the G protein-coupled receptors rhodopsin and opsin in native membranes. *J Biol Chem* **278**: 21655-21662.

Limbird LE (1983). Beta-adrenergic stimulation of adenylate cyclase and alpha adrenergic inhibition of adenylate cyclase: GTP-binding proteins as macro molecular messengers. *Adv Exp Med Biol* **161**:91-111.

Limbird LE, Meyts PD, Lefkowitz RJ (1975). Beta-adrenergic receptors: evidence for negative cooperativity. *Biochem Biophys Res Commun* **64**:1160-8.

Lohse MJ, Benovic JL, Codina J, Caron MG, Lefkowitz RJ (1990). Beta-Arrestin: a protein that regulates beta-adrenergic receptor function. *Science* **248**: 1547-50.

López-Sendón Moreno JL, García Caldentey J, Trigo Cubillo P, Ruiz Romero C, García Ribas G, Alonso Arias MA, García de Yébenes MJ, Tolón RM, Galve-Roperh I, Sagredo et al. (2016). A double-blind, randomized, cross-over, placebo-controlled, pilot trial with Sativex in Huntington's disease. *J Neurol* **263**: 1390-1400.

Lorenc-Koci E, Ossowska K, Wardas J, Wolfarth S (1995). Does reserpine induce parkinsonian rigidity? *Journal of Neural Transmission* **9**: 211-223.

Lowe JA, Seeger TF, Vinick FJ (1988). Atypical antipsychotics-recent findings and new perspectives. *Med Res Rev* **8**:475-497.

Luthi-Carter R, Strand AD, Hanson SA, Kooperberg C, Schilling G, La Spada AR, Merry DE, Young AB, Ross CA, Borchelt DR, Olson JM (2002). Polyglutamine and transcription: gene expression changes shared by DRPLA and Huntington's disease mouse models reveal contextindependent effects. *Hum Mol Genet* **15**: 1927-1937.

Luttrell LM, Lefkowitz RJ (2002). The role of β-arrestins in the termination and transduction of G-protein-coupled receptor signals. *Journal of cell science* **115**, 455-465.

Luttrell LM, Roudabush FL, Choy EW, Miller WE, Field ME, Pierce KL, Lefkowitz R J (2001). Activation and targeting of extracellular signal-regulated kinases by β-arrestin scaffolds. *Proceedings of the National Academy of Sciences* **98**: 2449-2454.

Mackie K (2005). Cannabinoid receptor homo- and heterodimerization. *Life Sci* **77**: 1667-1673.

Maier-Peuschel M, Frolich N, Dees C, Hommers LG, Hoffmann C, Nikolaev VO, Lohse, MJ (2010). A fluorescence resonance energy transfer-based M2 muscarinic receptor sensor reveals rapid kinetics of allosteric modulation. *The Journal of Biological Chemistry* **285**: 8793-8800.

Mailleux P, Vanderhaeghen JJ (1992). Distribution of neuronal cannabinoid receptor in the adult rat brain: a comparative receptor binding radioautography and in situ hybridization histochemistry. *Neuroscience* **48**3: 655-68.

Mamad O, Delaville C, Benjelloun W, Benazzouz A (2015). Dopaminergic Control of the Globus Pallidus through Activation of D2 Receptors and Its Impact on the Electrical Activity of Subthalamic Nucleus and Substantia Nigra Reticulata Neurons. *PLoS One* **10**: e0119152.

Maneuf YP, Brotchie JM (1997). Paradoxical action of the cannabinoid WIN55,212-2 in stimulated and basal cyclic AMP accumulation in rat globus pallidus slices. *Br J Pharmacol* **120**: 1397-8.

Manglik A, Kruse AC, Kobilka TS, Thian FS, Mathiesen JM, Sunahara RK, Pardo L, Weis WI, Kobilka BK, Granier S (2012). Crystal structure of the micro-opioid receptor bound to a morphinan antagonist. *Nature* **485**: 321-326.

Männistö PT, Ulmanen I, Lundström K, Taskinen J, Tenhunen J, Tilgmann C, Kaakkola S (1992). Characteristics of catechol O-methyl-transferase (COMT) and properties of selective COMT inhibitors. *Prog Drug Res* **39**: 291-350.

Manzoni OJ, Bockaert J (2001). Cannabinoids inhibit GABAergic synaptic transmission in mice nucleus accumbens. *Eur J Pharmacol* **412:** R3-R5.

Marcellino D, Carriba P, Filip M, Borgkvist A, Frankowska M, Bellido I, Tanganelli S, Muller CE, Fisone G, Lluis C, Agnati LF, Franco R, Fuxe K (2008). Antagonistic

cannabinoid CB1/dopamine D2 receptor interactions in striatal CB1/D2 heteromers. A combined neurochemical and behavioral analysis. *Neuropharmacology* **54**:815-23.

Marinelli S, Di Marzo V, Berretta N, Matias I, Maccarrone M, Bernardi G, Mercuri NB (2003). Presynaptic facilitation of glutamatergic synapses to dopaminergic neurons of the rat substantia nigra by endogenous stimulation of vanilloid receptors. *J Neurosci* **23**: 3136-3344.

Marinelli S, Pacioni S, Bisogno T, Di Marzo V, Prince DA, Huguenard JR, Bacci A (2008). The endocannabinoid 2-arachidonoylglycerol is responsible for the slow self-inhibition in neocortical interneurons. *J Neurosci* **28**: 13532-13541.

Marinelli S, Pacioni S, Cannich A, Marsicano G, Bacci A (2009). Self-modulation of neocortical pyramidal neurons by endocannabinoids. *Nat Neurosci* **12**: 1488-1490.

Marion S, Oakley RH, Kim KM, Caron MG, Barak LS (2006). A B-arrestin binding determinant common to the second intracellular loops of rhodopsin family G protein-coupled receptors. *J Biol Chem* 281: 2932-2938.

Martín AB, Fernandez-Espejo E, Ferrer B, Gorriti MA, Bilbao A, Navarro M, Rodriguez de Fonseca F, Moratalla R (2008). Expression and function of CB1 receptor in the rat striatum: localization and effects on D1 and D2 dopamine receptor-mediated motor behaviors. *Neuropsychopharmacology* **33**: 1667-79.

Mason SL, Barker RA (2016). Advancing pharmacotherapy for treating Huntington's disease: a review of the existing literature. *Expert Opin Pharmacother* **17**: 41-52.

Masri B, Salahpour A, Didriksen M, Ghisi V, Beaulieu JM, Gainetdinov RR, Caron MG (2008). Antagonism of dopamine D2 receptor/beta-arrestin 2 interaction is a common property of clinically effective antipsychotics. *Proc Natl Acad Sci U S A* **105**: 13656-61.

Matsuda LA, Lolait SJ, Brownstein MJ, Young AC, Bonner TI (1990). Structure of a cannabinoid receptor and functional expression of the cloned cDNA. *Nature* **346**: 561-4.

Mazurkiewicz JE, Herrick-Davis K, Barroso M, Ulloa-Aguirre A, Lindau-Shepard, B, Thomas RM et al. (2015). Single-molecule analyses of fully functional fluorescent protein-tagged follitropin receptor reveal homodimerization and specific heterodimerization with lutropin receptor. *Biology of Reproduction* **92**: 100.

McDonald NA, Henstridge CM, Connolly CN, Irving AJ (2007). An essential role for constitutive endocytosis, but not activity, in the axonal targeting of the CB1 cannabinoid receptor. *Mol Pharmacol* **71**: 976-984.

McKinney DL, Cassidy MP, Collier LM, Martin BR, Wiley JL, Selley DE, Sim-Selley LJ (2008). Dose-related differences in the regional pattern of cannabinoid receptor

adaptation and in vivo tolerance development to delta9-tetrahydrocannabinol. *J Pharmacol Exp Ther* **324**: 664-73.

McKinney MK, Cravatt BF (2005). Structure and function of Fatty acid amide hydrolase. *Annu Rev Biochem* **74**:411- 432.

Mechoulam R, Ben-Shabat S, Hanus L, Ligumsky M, Kaminski NE, Schatz AR, Gopher A, Almog S, Martin BR, Compton DR, et al (1995). Identification of an endogenous 2-monoglyceride, present in canine gut, that binds to cannabinoid receptors. *Biochemical pharmacology* **50**: 83-90.

Mechoulam R, Parker LA (2013). The endocannabinoid system and the brain. *Annu Rev Psychol* **64**:21-47.

Mehler-Wex C, Riederer P, Gerlach M (2006). Dopaminergic dysbalance in distinct basal ganglia neurocircuits: implications for the pathophysiology of Parkinson's disease, schizophrenia and attention deficit hyperactivity disorder. *Neurotox Res* **10**: 167-79.

Melis M, Pistis M, Perra S, Muntoni AL, Pillolla G, Gessa GL (2004). Endocannabinoids mediate presynaptic inhibition of glutamatergic transmission in rat ventral tegmental area dopamine neurons through activation of CB1 receptors. *J Neurosci* **24**: 53-62.

Meltzer HY (2013). Update on typical and atypical antipsychotic drugs. *Annu Rev Med* **64**: 393-406.

Meschler JP, Howlett AC (2001). Signal transduction interactions between CB1 cannabinoid and dopamine receptors in the rat and monkey striatum. *Neuropharmacology* **40**: 918-926.

Mestre TA, Ferreira JJ (2012). An evidence-based approach in the treatment of Huntington's disease. *Parkinsonism Relat Disord* **18**: 316-20.

Mezey E, Toth ZE, Cortright DN, Arzubi MK, Krause JE, Elde R et al. (2000). Distribution of mRNA for vanilloid receptor subtype 1 (VR1), and VR1-like immunoreactivity, in the central nervous system of the rat and human. *Proc Natl Acad Sci U S A* **97**: 3655-3660.

Mievis S, Blum D, Ledent C (2011). Worsening of Huntington disease phenotype in CB1 receptor knockout mice. Neurobiol Dis 42: 524-529.

Miller CA, Marshall JF (2005). Molecular substrates for retrieval and reconsolidation of cocaine-associated contextual memory. Neuron 47: 873-884.

Miller J. (2004) Tracking G protein-coupled receptor trafficking using Odyssey Imaging. http://www.licor.com/bio/PDF/Miller_GPCR.pdf (25 Jul. 2006).

Milligan G (2004). G protein-coupled receptor dimerization: function and ligand pharmacology. *Mol Pharmacol* **66**: 1-7.

Milligan G (2009). G protein-coupled receptor hetero-dimerization: contribution to pharmacology and function. *Br J Pharmacol* **158**: 5-14.

Milligan G, Bouvier M (2005). Methods to monitor the quaternary structure of G protein-coupled receptors. *FEBS J* **272**: 2914-25.

Mishra AK, Gragg M, Stoneman MR, Biener G, Oliver JA, Miszta P, Filipek S, Raicu V, Park PS (2016). Quaternary structures of opsin in live cells revealed by FRET spectrometry. *The Biochemical Journal* **473**: 3819-3836.

Missale C, Nash SR, Robinson SW, Jaber M, Caron MG (1998). Dopamine receptors: from structure to function. *Physiol Rev* **78**: 189-225.

Monsma FJ Jr, McVittie LD, Gerfen CR, Mahan LC, Sibley DR (1989). Multiple D2 dopamine receptors produced by alternative RNA splicing. *Nature* **342**: 926-9. *Nature* **485**: 327-32.

Morales P, Goya P, Jagerovic N, Hernandez-Folgado L (2016). Allosteric Modulators of the CB1 Cannabinoid Receptor: A Structural Update Review. *Cannabis and Cannabinoid Research* **1**: 22-30.

Moss DE, McMaster SB, Rogers J (1981). Tetrahydrocannabinol potentiates reserpine-induced hypokinesia. *Pharmacol Biochem Behav* **15**: 779-83.
Mukhopadhyay S, Howlett AC (2005). Chemically distinct ligands promote differential CB1 cannabinoid receptor-Gi protein interactions. *Mol Pharmacol* **67**: pp. 2016-2024.

Muller P, Seeman P (1977). Brain neurotransmitter receptors after long-term haloperidol: dopamine, acetylcholine, serotonin, alpha-noradrenergic and naloxone receptors. *Life Sciences* **21**: 1751-1758.

Müller-Vahl KR, Schneider U, Emrich HM (1999). Nabilone increases choreatic movements in Huntington's disease. *Mov Disord* **14**: 1038-1040.

Murray R, Correll CU, Reynolds GP, Taylor D (2017). Atypical antipsychotics: recent research findings and applications to clinical practice: Proceedings of a symposium presented at the 29th Annual European College of Neuropsychopharmacology Congress, 19 September 2016, Vienna, Austria. *Ther Adv Psychopharmacol* **7**: 1-14.

Natesan S, Reckless GE, Nobrega JN, Fletcher PJ, Kapur S (2006). Dissociation between in vivo occupancy and functional antagonism of dopamine D2 receptors: comparing aripiprazole to other antipsychotics in animal models. *Neuropsychopharmacology* **31**: 1854-1863.

Navarro G, Carriba P, Gandía J, Ciruela F, Casadó V, Cortés A, Mallol J, Canela EI, Lluis C, Franco R (2008). Detection of heteromers formed by cannabinoid CB1, dopamine D2, and adenosine A2A G-protein-coupled receptors by combining bimolecular fluorescence complementation and bioluminescence energy transfer. *Scientific World Journal* **8**: 1088-97.

Navarro G, Cordomí A, Zelman-Femiak M, Brugarolas M, Moreno E, Aguinaga D, Perez-Benito L, Cortés A, Casadó V, Mallol J, Canela EI, Lluís C, Pardo L, García-Sáez AJ, McCormick PJ, Franco R (2016). Quaternary structure of a G-protein-coupled receptor heterotetramer in complex with Gi and Gs. *BMC Biol* **5**:14-26.

Navarro G, McCormick PJ, Mallol J, Lluís C, Franco R, Cortés A, Casadó V, Canela EI, Ferré S (2013). Detection of receptor heteromers involving dopamine receptors by the sequential BRET-FRET technology. *Methods Mol Biol* **964**: 95-105.

Naydenov AV, Sepers MD, Swinney K, Raymond LA, Palmiter RD, Stella N (2014). Genetic rescue of CB1 receptors on medium spiny neurons prevents loss of excitatory striatal synapses but not motor impairment in HD mice. *Neurobiol Dis* **71**: 140-150.

Nelson AB, Kreitzer AC (2014). Reassessing Models of Basal Ganglia Function and Dysfunction. *Annual review of neuroscience* **37**: 117-135.
Neve KA, Seamans JK, & Trantham-Davidson H (2004). Dopamine receptor signaling. *J Recept Signal Transduct Res* **24**: 165-205.

Newcombe RG (1981). A life table for onset of Huntington's chorea. *Ann Hum Genet* **45**: 375-385.

Ng Cheong Ton JM, Gerhardt GA, Friedemann M, Etgen AM, Rose GM, Sharpless NS, Gardner EL (1988). The effects of delta 9-tetrahydrocannabinol on potassium-evoked release of dopamine in the rat caudate nucleus: an in vivo electrochemical and in vivo microdialysis study. *Brain Res* **451**: 59-68.

Nguyen VH, Wang H, Verdurand M, Zavitsanou K (2012). Differential treatment regimen-related effects of HU210 on CB1 and D2-like receptor functionality in the rat basal ganglia. *Pharmacology* **89**: 64-73.

 Noble EP (2003). D2 dopamine receptor gene in psychiatric and neurologic disorders and its phenotypes. *Med Genet B Neuropsychiatr Genet* **116**: 103-25.

Nobles M, Benians A, Tinker A (2005). Heterotrimeric G proteins precouple with G protein-coupled receptors in living cells. *PNAS USA* **102**: 18706-18711. doi:10.1073/pnas.0504778102.

Nurnberg B, Gudermann T, Schultz G (1995). Receptors and G proteins as primary components of transmembrane signal transduction Part 2 G proteins: Structure and function. *J Mol Med* **73**: 123-32.

Nyiri G, Szabadits E, Cserép C, Mackie K, Shigemoto, Freund TF (2005) GABAB and CB1 cannabinoid receptor expression identifies two types of septal cholinergic neurons. *Eur J Neurosci* **21**: 3034-3042.

O'Dowd BF, Ji X, Alijaniaram M, Rajaram RD, Kong MM, Rashid A, Nguyen T, George SR (2005). Dopamine receptor oligomerization visualized in living cells. *J Biol Chem* **280**: 37225-35.

Oldham WM, Hamm HE (2008). Heterotrimeric G protein activation by G-protein-coupled receptors. *Nature Rev Mol Cell Biol* **9**:60-71.

Ong WY, Mackie K (1999). A light and electron microscopic study of the CB1 cannabinoid receptor in primate brain. *Neuroscience* **92**: 1177-91.

Orio L, Edwards S, George O, Parsons LH, Koob GF (2009). A role for the endocannabinoid system in the increased motivation for cocaine in extended-access conditions. *J Neurosci* **29**: *4846-57.*

Orru M, Bakesová J, Brugarolas M, Quiroz C, Beaumont V, Goldberg SR, Lluís C,Cortés A, Franco R, and Casadó V, et al. (2011) Striatal pre- and postsynaptic profile of adenosine A(2A) receptor antagonists. *PLoS ONE* 6:e16088.

Pacher P, Batkai S, Kunos G (2006). The endocannabinoid system as an emerging target of pharmacotherapy. *Pharmacol Rev* **58**: 389-462.

Paleacu D, Anca M, Giladi N (2002). Olanzapine in Huntington's disease. *Acta Neurol Scand* 105: 441-444.

Pan B, Hillard CJ, Liu QS (2008). D2 dopamine receptor activation facilitates endocannabinoid-mediated long-term synaptic depression of GABAergic synaptic transmission in midbrain dopamine neurons via cAMP-protein kinase A signaling. *Neurosci* **28**: 14018-14030.

Paoletti P, Vila I, Rifé M, Lizcano JM, Alberch J, Ginés S (2008). Dopaminergic and glutamatergic signaling crosstalk in Huntington's disease neurodegeneration: the role of p25/cyclin-dependent kinase 5. *J Neurosci* **28**: 10090-101.

Pellissier LP, Barthet G, Gaven F, Cassier E, Trinquet E, Pin JP, Marin P, Dumuis A, Bockaert J, Banères JL, et al. (2011) G protein activation by serotonin type 4 receptor dimers: evidence that turning on two protomers is more efficient. *J Biol Chem* **286**: 9985-9997.

Pertwee RG (2008). The diverse CB1 and CB2 receptor pharmacology of three plant cannabinoids: Δ9-tetrahydrocannabinol, cannabidiol and Δ9-tetrahydrocannabivarin. *Br J Pharmacol* **153**: 199-215.

Pertwee RG (2012). Targeting the endocannabinoid system with cannabinoid receptor agonists: pharmacological strategies and therapeutic possibilities. *Philos Trans R Soc* **367**: 3353-3363.

Pertwee RG, Fernando SR, Nash JE, Coutts AA (1996). Further evidence for the presence of cannabinoid CB1 receptors in guinea-pig small intestine. *Br J Pharmacol* **118**: 2199-205.

Petersén A, Gil J, Maat-Schieman ML, Björkqvist M, Tanila H, Araújo IM, Smith R, Popovic N, Wierup N, Norlén P, Li JY, Roos RA, Sundler F, Mulder H, Brundin P (2005). Orexin loss in Huntington's disease. *Hum Mol Genet* 14: **39**-47.

Pfeiffer M, Koch T, Schroder H, Laugsch M, Hollt V, Schulz S (2002). Heterodimerization of somatostatin and opioid receptors cross modulates phosphorylation, internalization, and desensitization. *J Biol Chem* **277**: 19762- 72.

Pfleger KD, Eidne KA (2005). Monitoring the formation of dynamic G-protein-coupled receptor-protein complexes in living cells. *Biochem J* **385**: 625-37.
Philip F, Sengupta P, Scarlata S (2007). Signaling through a G Protein-coupled receptor and its corresponding G protein follows a stoichiometrically limited model. *J Biol Chem* **282**:19203-19216.

Pickel VM , Chan J , Kearn CS, Mackie K (2006). Targeting Dopamine D2 and Cannabinoid-1 (CB1) Receptors in Rat Nucleus Accumbens. *J Comp Neurol* **495**: 299-313.

Pickel VM, Chan J, Kash TL, Rodriguez JJ, Mackie K (2004). Compartment-specific localization of cannabinoid 1 (CB1) and μ-opioid receptors in rat nucleus accumbens. *Neuroscience* **127**: 101-112.

Pinna A, Bonaventura J, Farré D, Sánchez M, Simola N, Mallol J, Lluís C, Costa G, Baqi Y, Müller CE, Cortés A, McCormick P, Canela EI, Martínez-Pinilla E, Lanciego JL, Casadó V, Armentero MT, Franco R (2014). L-DOPA disrupts adenosine A(2A)-cannabinoid CB(1)-dopamine D(2) receptor heteromer cross-talk in the striatum of hemiparkinsonian rats: biochemical and behavioral studies. *Exp Neurol* **253**: 180-91.

Piomelli D (2003). The molecular logic of endocannabinoid signalling. *Nat Rev Neurosci* **4**: 873-84.

Pisterzi LF, Jansma DB, Georgiou J, Woodside MJ, Chou JT, Angers S, et al (2010). Oligomeric size of the m2 muscarinic receptor in live cells as determined by quantitative fluorescence resonance energy transfer. *J Biol Chem* **285**:16723-16738.

Pistis M, Ferraro L, Pira L, Flore G, Tanganelli S, Gessa GL, Devoto P (2002). Δ9-Tetrahydrocannabinol decreases extracellular GABA and increases extracellular

glutamate and dopamine levels in the rat prefrontal cortex: An in vivo microdialysis study. *Brain Res* **948**: 155-158.

Polo GC, Delgado CE, Cachorro MA, Posadas JR, Pérez NM, Formoso A D (2015). Energy balance in Huntington's disease. *Ann Nutr* **67**: 267-73.

Prinster SC, Hague C, Hall RA (2004). Heterodimerization of G Protein-Coupled Receptors: Specificity and Functional Significance. *Pharmacological Reviews* **57**: 289-298.

Przybyla JA, Watts VJ (2010). Ligand-Induced Regulation and Localization of Cannabinoid CB1 and Dopamine D2L Receptor Heterodimers. *J Pharmacol Exp Ther* 332: 710-719.

Qin K, Dong C, Wu G, Lambert NA (2011). Inactive-state pre-assembly of G(q)-coupled receptors and G(q) heterotrimers. *Nat Chem Biol* **7**: 740-747.

Ramsay D, Kellett E, McVey M, Rees S, Milligan G (2002). Homo- and hetero-oligomeric interactions between G-protein-coupled receptors in living cells monitored by two variants of bioluminescence resonance energy transfer (BRET): hetero-oligomers between receptor subtypes form more efficiently than between less closely related sequences. *Biochem J* **365**: 429-40.

Rangel-Barajas C, Coronel I, Florán B (2015). Dopamine Receptors and Neurodegeneration. *Aging Dis* **6**: 349-68.

Rashid AJ, So CH, Kong MM, Furtak T, El-Ghundi M, Cheng R, O'Dowd BF, George SR (2007). D1-D2 dopamine receptor heterooligomers with unique pharmacology are coupled to rapid activation of Gq/11 in the striatum. *Proc Natl Acad Sci U S A* **104**: 654-9.

Rasmussen SG, Choi HJ, Rosenbaum DM, Kobilka TS, Thian FS, Edwards PC, Burghammer M, Ratnala VR, Sanishvili R, Fischetti RF, Schertler GF, Weis WI, Kobilka BK (2007). Crystal structure of the human beta2 adrenergic G-protein-coupled receptor. *Nature* **450**: 383-7.

Rayport S, Sulzer D (1995). Visualization of antipsychotic drug binding to living mesolimbic neurons reveals D2 receptor, acidotropic, and lipophilic components. *J Neurochem* **65**: 691-703.

Rebois RV, Robitaille M, Pétrin D, Zylbergold P, Trieu P, Hébert TE (2008). Combining protein complementation assays with resonance energy transfer to detect multipartner protein complexes in living cells. *Methods* **45**: 214-8.

Richfield EK, O'Brien CF, Eskin T, Shoulson I (1991). Heterogeneous dopamine receptor changes in early and late Huntington's disease. *Neurosci Lett* **132**: 121-6.

Rios CD, Gomes I, Devi LA (2006). μ opioid and CB$_1$ cannabinoid receptor interactions: Reciprocal inhibition of receptor signaling and neuritogenesis. *Br J Pharmacol,* **148**: 387-95.

Rios CD, Jordan BA, Gomes I, Devi LA (2001). G-protein-coupled receptor dimerization: Modulation of receptor function. *Pharmacol Ther* **92**: 71-87.

Robison G, Sullivan B, Cannon JR, Pushkar Y (2015). Identification of dopaminergic neurons of the substantia nigra pars compacta as a target of manganese accumulation. *Metallomics* **7**: 748-55.

Rocheville M, Lange DC, Kumar U, Patel SC, Patel RC, Patel YC (2000). Receptors for dopamine and somatostatin: formation of hetero-oligomers with enhanced functional activity. *Science* **288**: 154-7.

Rodriguez JJ, Mackie K, Pickel VM (2001). Ultrastructural localization of the CB1 cannabinoid receptor in mu-opioid receptor patches of the rat Caudate putamen nucleus. *J Neurosci* **21**: 823-33.

Roos RA, Hermans J, Vegter-van der Vlis M, van Ommen GJ, Bruyn GW (1993). Duration of illness in Huntington's disease is not related to age at onset. *J Neurol Neurosurg Psychiatry* **56**: 98-100.

Ross CA, Tabrizi SJ (2011). Huntington's disease: from molecular pathogenesis to clinical treatment. *Lancet Neurol* **10**:83-98.

Ross RA (2007). Allosterism and cannabinoid CB(1) receptors: the shape of things to come. *Trends Pharmacol Sci* **28**: 567-572.

Ross RA (2010). Huntington's disease: a clinical review. *Orphanet J Rare Dis* **5**: 40.

Ross SB (1991). Synaptic Concentration of Dopamine in the Mouse Striatum in Relationship to the Kinetic Properties of the Dopamine Receptors and Uptake Mechanism. *J Neurochem* **56**: 22-9.
Ross SB, Jackson DM (1989). Kinetic properties of the accumulation of 3H-raclopride in the mouse brain in vivo. *Naunyn Schmiedebergs Arch Pharmacol* **340**: 6-12.

Rovira X, Vivó M, Serra J, Roche D, Strange PG, and Giraldo J (2009). Modelling the interdependence between the stoichiometry of receptor oligomerization and ligand binding for a coexisting dimer/tetramer receptor system. *Br J Pharmacol* **156**: 28-35.

Rozenfeld R, Bushlin I, Gomes I, Tzavaras N, Gupta A, Neves S, Battini L, Gusella GL, Lachmann A, and Ma'ayan A, et al. (2012). Receptor heteromerization expands the repertoire of cannabinoid signaling in rodent neurons. *PLoS ONE* **7**: e29239.

Rozenfeld R, Gupta A, Gagnidze K, Lim MP, Gomes I, Lee-Ramos D, Nieto N, Devi LA (2011). AT1R-CB1R heteromerization reveals a new mechanism for the pathogenic properties of angiotensin II. *EMBO J* **30**: 2350-63.

Rummel-Kluge C, Komossa K, Schwarz S, Hunger H, Schmid F, Kissling W, Davis JM, Leucht S (2012). Second-generation antipsychotic drugs and extrapyramidal side effects: a systematic review and meta-analysis of head-to-head comparisons. *Schizophr Bull* **38**: 167-77.

Ryberg E, Vu HK, Larsson N, Groblewski T, Hjorth S, Elebring T, Sjögren S, Greasley PJ (2005). Identification and characterisation of a novel splice variant of the human CB1 receptor. *FEBS Lett* **579**: 259-64.

Sagredo O, Pazos MR, Satta V, Ramos JA, Pertwee RG, Fernandez-Ruiz J (2011). Neuroprotective effects of phytocannabinoid-based medicines in experimental models of Huntington's disease. *J Neurosci Res* **89**: 1509-1518.
Sagredo O, Pazos MR, Valdeolivas S, Fernandez-Ruiz J (2012). Cannabinoids: novel medicines for the treatment of Huntington's disease. *Recent Pat CNS Drug Discov* **7**: 41-48.

Sagredo O, Ramos JA, Decio A, Mechoulam R, Fernandez-Ruiz J (2007). Cannabidiol reduced the striatal atrophy caused 3-nitropropionic acid in vivo by mechanisms independent of the activation of cannabinoid, vanilloid TRPV1 and adenosine A2A receptors. *Eur J Neurosci* **26**: 843-851.

Sahlholm K, Zeberg H, Nilsson J, Ögren SO, Fuxe K, Århem P (2016). The fast-off hypothesis revisited: A functional kinetic study of antipsychotic antagonism of the dopamine D2 receptor. Eur Neuropsychopharmacol 26:467-76.

Sampaio-Maia B, Serrão MP, da Silva PS (2001). Regulatory pathways and uptake of L-DOPA by capillary cerebral endothelial cells, astrocytes, and neuronal cells. *Am J Physiol Cell Physiol* **280**: C333-C342.

Sawaguchi T, Goldman-Rakic PS (1994). The role of D1-dopamine receptor in working memory: local injections of dopamine antagonists into the prefrontal cortex of rhesus monkeys performing an oculomotor delayed-response task. J *Neurophysiol* **71**:515-528.

Scavone JL, Mackie K, Van Bockstaele EJ (2010). Characterization of cannabinoid-1 receptors in the locus coeruleus: relationship with mu-opioid receptors. *Brain Res* **1312**:18-31.

Scheerer P, Park JH, Hildebrand PW, Kim YJ, Krauss N, Choe HW, Hofmann KP, Ernst OP (2008). Crystal structure of opsin in its G-protein-interacting conformation *Nature* **455**: 497-502.

Schindler CW, Carmona GN (2002). Effects of dopamine agonists and antagonists on locomotor activity in male and female rats. *Pharmacol Biochem Behav* **72**: 857-63.

Scigliano G, Ronchetti G (2013). Antipsychotic-induced metabolic and cardiovascular side effects in schizophrenia: a novel mechanistic hypothesis. *CNS Drugs* **27**: 249-57.

Seeman P (2010). Dopamine D2 receptors as treatment targets in schizophrenia. *Clin Schizophr Relat Psychoses* **4**: 56-73.

Seeman P, Ulpian C (1988). Dopamine D1 and D2 receptor selectivities of agonists and antagonists. *Adv Exp Med Biol* **235**:55-63.

Seibenhener ML, Wooten MC (2015). Use of the Open Field Maze to measure locomotor and anxiety-like behavior in mice. *J Vis Exp* **6**:96.
Sharma S, Taliyan R (2015). Transcriptional dysregulation in Huntington's disease: The role of histone deacetylases. *Pharmacol Res* **100**: 157-169.

Shenoy SK, Drake MT, Nelson CD, Houtz DA, Xiao K, Madabushi S, Reiter E, Premont RT, Lichtarge O, Lefkowitz RJ (2006). Beta-arrestin-dependent, G protein-independent ERK1/2 activation by the beta2 adrenergic receptor. *J Biol Chem* **281**: 1261-73.

Shire D, Calandra B, Rinaldi-Carmona M, Oustric D, Pessègue B, Bonnin-Cabanne O, Le Fur G, Caput D, Ferrara P (1996). Molecular cloning, expression and function of the murine CB2 peripheral cannabinoid receptor. *Biochim Biophys Acta* **1307**: 132-6.

Shire D, Carillon C, Kaghad M, Calandra B, Rinaldi-Carmona M, Le Fur G, Caput D, Ferrara P (1995). An amino-terminal variant of the central cannabinoid receptor resulting from alternative splicing. *Journal of Biological Chemistry* **270**: 3726-3731.

Shuen JA, Chen M, Gloss B, and Calakos N (2008) Drd1a-tdTomato BAC transgenicmice for simultaneous visualization of medium spiny neurons in the direct and indirect pathways of the basal ganglia. *J Neurosci* **28**:2681-2685.

Shyu YJ, Liu H, Deng X, Hu, CD (2006). Identification of new fluorescent protein fragments for bimolecular fluorescence complementation analysis under physiological conditions. *Biotechniques* **40**:61-6.

Sibley DR, Monsma FJ Jr (1992). Molecular biology of dopamine receptors. *Trends Pharmacol Sci* **13**: 61-9.

Sim-Selley LJ (2003). Regulation of cannabinoid CB1 receptors in the central nervous system by chronic cannabinoids. *Crit Rev Neurobiol* **15**: 91-119.

Sim-Selley LJ, Martin BR (2002). Effect of chronic administration of R-(+)-[2,3-dihydro-5-methyl-3-[(morpholinyl)methyl]pyrrolo[1,2,3-de]-1,4-benzoxazinyl]-(1-

naphthalenyl)methanone mesylate (WIN55,212-2) or Δ9-tetrahydrocannabinol on cannabinoid receptor adaptation in mice. *J Pharmacol Exp Ther* **303**: 36-44.

Sleno R, Devost D, Pétrin D, Zhang A, Bourque K, Shinjo Y, Aoki J, Inoue A, Hébert TE (2017). Conformational biosensors reveal allosteric interactions between heterodimeric AT1 angiotensin and prostaglandin F2α receptors. *J Biol Chem* **5**: 3137-3148.

Smith JS, Rajagopal S (2016). The β-Arrestins: Multifunctional Regulators of G Protein-coupled Receptors. *J Biol Chem* **291**: 8969-77.

Smith NJ , Milligan G (2010). Allostery at G Protein-Coupled Receptor Homo- and Heteromers: Uncharted Pharmacological Landscapes. *Pharmacol Rev* **62**: 701-725.

Smith SK, Limbird LE (1981). Solubilization of human platelet alpha-adrenergic receptors: Evidence that agonist occupancy of the receptor stabilizes receptor–effector interactions. *Proc Natl Acad Sci USA* **78**: 4026-4030.

Smith TH, Sim-Selley LJ, Selley DE (2010). Cannabinoid CB1 receptor-interacting proteins: novel targets for central nervous system drug discovery?. *Br J Pharmacol* **160**: 454-66.

Smith Y, Villalba R (2008). Striatal and extrastriatal dopamine in the basal ganglia: an overview of its anatomical organization in normal and Parkinsonian brains. *Mov Disord* **23**: S534-47.

Soares-Cunha C, Coimbra B, Sousa N, Rodrigues AJ (2016). Reappraising striatal D1- and D2-neurons in reward and aversion. *Neurosci Biobehav Rev* **68**: 370-86.

Söderberg O, Gullberg M, Jarvius M, Ridderstråle K, Leuchowius KJ, Jarvius J, Wester K, Hydbring P, Bahram F, Larsson LG, Landegren U (2006). Direct observation of individual endogenous protein complexes in situ by proximity ligation. *Nat Methods* **3**:995-1000.

Söderberg O, Leuchowius KJ, Gullberg M, Jarvius M, Weibrecht I, Larsson LG, Landegren U (2008). Characterizing proteins and their interactions in cells and tissues using the in situ proximity ligation assay. *Methods* **45**: 227-32.

Solinas M, Justinova Z, Goldberg SR, Tanda G (2006). Anandamide administration alone and after inhibition of fatty acid amide hydrolase (FAAH) increases dopamine levels in the nucleus accumbens shell in rats. *J Neurochem* **98**:408-19.

Stamer WD, Golightly SF, Hosohata Y, Ryan EP, Porter AC, Varga E, Noecker RJ, Felder CC, Yamamura HI (2001). Cannabinoid CB1 receptor expression, activation and detection of endogenous ligand in trabecular meshwork and Ciliary process tissues. *Eur J Pharmacol* **431**; 277-86.

Stella N, Piomelli D (2001). Receptor-dependent formation of endogenous cannabinoids in cortical neurons. *Eur J Pharmacol* **425**: 189-96.

Stella N, Schweitzer P, Piomelli D (1997). A second endogenous cannabinoid that modulates long-term potentiation. *Nature* **388**:773-778.

Stocchi F, Torti M, Fossati C (2016). Advances in dopamine receptor agonists for the treatment of Parkinson's disease. *Expert Opin Pharmacother* **14**: 1889-902.

Stowe RL, Ives NJ, Clarke C, van Hilten J, Ferreira J, Hawker RJ, Shah L, Wheatley K, Gray R (2008). Dopamine agonist therapy in early Parkinson's disease. *Cochrane Database Syst Rev* **16**: CD006564.

Straiker AJ, Maguire G, Mackie K, Lindsey J (1999). Localization of cannabinoid CB1 receptors in the human anterior eye and retina. *Invest Ophthalmol Vis Sci* **40**: 2442-8.

Strathmann M, Simon MI (1990). G protein diversity: a distinct class of alpha subunits is present in vertebrates and invertebrates *Proc Natl Acad Sci U S A* **87**: 9113-7.

Sugiura T, Kodaka T, Nakane S, Kishimoto S, Kondo S, Waku K (1998). Detection of an endogenous cannabimimetic molecule, 2-arachidonoylglycerol, and cannabinoid CB1 receptor mRNA in human vascular cells: is 2-arachidonoylglycerol a possible vasomodulator?. *Biochem Biophys Res Commun* **243**: 838-43.

Sugiura T, Kondo S, Sukagawa A, Nakane S, Shinoda A, Itoh K, Yamashita A, Waku K (1995). 2-Arachidonoylglycerol: a possible endogenous cannabinoid receptor ligand in brain. *Biochem Biophys Res Commun* **215**: 89-97.

Szabo B, Siemes S, Wallmichrath I (2002). Inhibition of GABAergic neurotransmission in the ventral tegmental area by cannabinoids. *Eur J Neurosci* **15**: 2057-2061.

Szalai B, Hoffmann P, Prokop S, Erdélyi L, Várnai P, Hunyady L (2014). Improved methodical approach for quantitative BRET analysis of G Protein Coupled Receptor dimerization. *PLoS One* **9**: 10.

Takahashi H, Kato M, Takano H, Arakawa R, Okumura M, Otsuka T, Kodaka F, Hayashi M, Okubo Y, Ito H, Suhara T (2008). Differential contributions of prefrontal and hippocampal dopamine D(1) and D(2) receptors in human cognitive functions. *J Neurosci* **28**: 12032-12038.

Tanda G, Pontieri FE, Di Chiara G (1997). Cannabinoid and heroin activation of mesolimbic dopamine transmission by a common mu1 opioid receptor mechanism. *Science* **276**: 2048-50.

Terrillon S, Barberis C, Bouvier M (2004). Heterodimerization of V1a and V2 vasopressin receptors determines the interaction with β-arrestin and their trafficking patterns. *Proc Natl Acad Sci USA* **101**: 1548-1553.

Terrillon S, Bouvier M (2004). Roles of G-protein-coupled receptor dimerization. *EMBO Rep* **5**: 30-4.

Tolkovsky AM, Levitzki A (1978). Mode of coupling between the beta-adrenergic receptor and adenylate cyclase in turkey erythrocytes. *Biochemistry* **17**: 3795.

Tohgo A, Pierce KL, Choy EW, Lefkowitz RJ, Luttrell LM (2002). β-arrestin scaffolding of the ERK cascade enhances cytosolic ERK activity but inhibits ERK mediated transcription following angiotensin AT1A receptor stimulation. *J Biol Chem* **277**, 9429-36.

Tomlinson CL, Stowe R, Patel S, Rick C, Gray R, Clarke CE (2010). Systematic review of levodopa dose equivalency reporting in Parkinson's disease. *Mov Disord* **25**: 2649-53

Tost H, Alam T, Meyer-Lindenberg A (2010). Dopamine and Psychosis: Theory, Pathomechanisms and Intermediate Phenotypes. *Neurosci Biobehav Rev* **34**: 689-700.

Toyama Y, Kano H1, Mase Y, Yokogawa M, Osawa M, Shimada I (2017). Dynamic regulation of GDP binding to G proteins revealed by magnetic field-dependent NMR relaxation analyses. *Nat Commun* **8**:14523.

Trettel F, Rigamonti D, Hilditch-Maguire P, Wheeler VC, Sharp AH, Persichetti F, Cattaneo E, MacDonald ME (2000). Dominant phenotypes produced by the HD mutation in STHdh (Q111) striatal cells. *Hum Mol Genet* **9**: 2799-280.

Trifilieff P, Rives M-L, Urizar E, Piskorowski RA, Vishwasrao HD, Castrillon J, Schmauss C, Sla¨ttman M, Gullberg M, Javitch JA (2011). Detection of antigen interactions ex vivo by proximity ligation assay: endogenous dopamine D2-adenosine A2A receptor complexes in the striatum. *Biotechniques* **51**: 111-118.

Tschoner A, Engl J, Laimer M, Kaser S, Rettenbacher M, Fleischhacker WW, Patsch JR, Ebenbichler CF (2007). Metabolic side effects of antipsychotic medication. *Int J Clin Pract*. **61**: 1356-70.

Tsou K, Brown S, Sañudo-Peña MC, Mackie K, Walker JM (1998). Immunohistochemical distribution of cannabinoid CB_1 receptors in the rat central nervous system. *Neuroscience* **83**: 393-411.

Turu G, Hunyady L (2010). Signal transduction of the CB1 cannabinoid receptor. *J Mol Endocrinol* **44**: 75-85.

Uchigashima M, Narushima M, Fukaya M, Katona I, Kano M, Watanabe M (2007). Subcellular arrangement of molecules for 2-arachidonoyl-glycerol-mediated retrograde signaling and its physiological contribution to synaptic modulation in the striatum. *J Neurosci* **27**: 3663-76.

Ücok A, Gaebel W (2008). Side effects of atypical antipsychotics: a brief overview. *World Psychiatry* **7**: 58-62.

Urizar E, Yano H, Kolster R, Galés C, Lambert N, Javitch JA (2011). CODA-RET reveals functional selectivity as a result of GPCR heteromerization. *Nat Chem Biol* **7**: 624-30.

Usiello A, Baik JH, Rouge-Pont F, Picetti R, Dierich A, LeMeur M, Piazza PV, Borrelli E (2000). Distinct functions of the two isoforms of dopamine D2 receptors. *Nature* **408**: 199-203.

Valdeolivas S, Navarrete C, Cantarero I, Bellido ML, Muñoz E, Sagredo O (2015). Neuroprotective properties of cannabigerol in Huntington's disease: studies in R6/2 mice and 3-nitropropionate-lesioned mice. *Neurotherapeutics* **12**: 185-99.

Valdeolivas S, Satta V, Pertwee RG, Fernandez-Ruiz J, Sagredo O (2012). Sativex-like combination of phytocannabinoids is neuroprotective in malonate-lesioned rats, an inflammatory model of Huntington's disease: role of CB1 and CB2 receptors. ACS Chem. *Neurosci* **3**: 400-406.

Vallone D, Picetti R, Borrelli E (2000). Structure and function of dopamine receptors. *Neurosci Biobehav Rev* **24**: 125-132.

van der Burg JM, Bacos K, Wood NI, Lindqvist A, Wierup N, Woodman B, Wamsteeker JI, Smith R, Deierborg T, Kuhar MJ, Bates GP, Mulder H, Erlanson-Albertsson C, Morton AJ, Brundin P, Petersén A, Björkqvist M (2008). Increased metabolism in the R6/2 mouse model of Huntington's disease. *Neurobiol Dis* **29**: 41-51.
van der Lee MM, Blomenröhr M, van der Doelen AA, Wat JW, Smits N., Hanson B. J., van Koppen CJ, Zaman GJ (2009). Pharmacological characterization of receptor redistribution and β-arrestin recruitment assays for the cannabinoid receptor 1. *J Biomol Screen* **14**: 811-823.

van der Westhuizen ET, Valant C, Sexton PM, Christopoulos A (2015). Endogenous allosteric modulators of G protein-coupled receptors. *J Pharmacol Exp Ther* **353**: 246-60.

Van Oostrom JC, Dekker M, Willemsen AT, De Jong BM, Roos RA, Leenders KL (2009). Changes in striatal dopamine D2 receptor binding in pre-clinical Huntington's disease. *Eur J Neurol* **16**: 226-231.

Vemuri VK, Janero DR, Makriyannis A (2008). Pharmacotherapeutic targeting of the endocannabinoid signaling system: drugs for obesity and the metabolic syndrome. *Physiol Behav* **93**: 671-686.

Videnovic A (2013). Treatment of huntington disease. *Curr Treat Options Neurol* **15**: 424-38.
Vidi PA, Chen J, Irudayaraj JM Pisterzi, Watts VJ (2008). Adenosine A(2A) receptors assemble into higher-order oligomers at the plasma membrane. *FEBS Lett* **582**: 3985-3990.

Vidi PA, Przybyla JA, Hu CD, Watts VJ (2010). Visualization of G protein-coupled receptor (GPCR) interactions in living cells using bimolecular fluorescence. Curr Protoc Neurosci Chapter 5:Unit 5.29.

Vilardaga JP, Nikolaev VO, Lorenz K, Ferrandon S, Zhuang Z, Lohse MJ (2008). Conformational cross-talk between alpha2A-adrenergic and mu-opioid receptors controls cell signaling. *Nat Chem Biol* **4**: 126-131.

Vonsattel JP, Myers RH, Stevens TJ, Ferrante RJ, Bird ED, Richardson EP Jr (1985). Neuropathological classification of Huntington's disease. *J Neuropathol Exp Neurol* **44**: 559-577.

Vrecl M, Drinovec L, EllingC, Heding A (2006). Opsin oligomerization in a heterologous cell system. *J Recept Signal Transduct Res* **26**: 505-26.

Wager Miller J, Westenbroek R, Mackie K (2002). Dimerization of G protein-coupled receptors: CB1 cannabinoid receptors as an example. *Chem Phys Lipids* **121**: 83-9.

Walker JM, Huang SM, Strangman NM, Tsou K, Sañudo-Peña MC (1999). Pain modulation by release of the endogenous cannabinoid anandamide. *Proc Natl Acad Sci U S A* **96**:12198-203.

Walters DE, Carr LA (1986). Changes in brain catecholamine mech- anisms following perinatal exposure to marihuana. *Pharmacol Biochem Behav* **25**: 763-768.
Wang GJ, Volkow ND, Thanos PK, Fowlwe JS (2009). Imaging of Brain Dopamine Pathways: Implications for Understanding Obesity. *J Addict Med* **3**: 8-18.

Wang X, Dow-Edwards D, Keller E, Hurd YL (2003). Preferential limbic expression of the cannabinoid receptor mRNA in the human fetal brain. *Neuroscience* **118**: 681-94.
Ward RJ, Pediani JD, Godin AG, Milligan G (2015). Regulation of oligomeric organization of the serotonin 5-hydroxytryptamine 2C (5-HT2C) receptor observed by spatial intensity distribution analysis. *J Biol Chem* **290**: 12844-57.

Weeks R. A., Piccini P., Harding A. E., Brooks D. J. (1996). Striatal D1 and D2 dopamine receptor loss in asymptomatic mutation carriers of Huntington's disease. *Ann Neurol* **40**: 49-54.

Wilkie TM (2001). Treasures throughout the life-cycle of G-protein-couple receptors. *Trends in Pharmacological Sciences* **22**: 396-397.

Wilson R, Nicoll RA (2001). Endogenous cannabinoids mediate retrograde signalling at hippocampal synapses. *Nature* **410**: 588-92.

Wootten D, Christopoulos A, Sexton PM (2013). Emerging paradigms in GPCR allostery: implications for drug discovery. *Nat Rev Drug Discov* **12**: 630-644.

Wu B, Chien EY, Mol CD, Fenalti G, Liu W, Katritch V, Abagyan R, Brooun A, Wells P, Bi FC, Hamel DJ, Kuhn P, Handel TM, Cherezov V, Stevens RC (2010). Structures of the CXCR4 chemokine receptor in complex with small molecule and cyclic peptide antagonists. *Science* **330**: 1066-1071.

Wu DF, Yang LQ, Goschke A, Stumm R, Brandenburg LO, Liang YJ, Höllt V, Koch T (2008). Role of receptor internalization in the agonist-induced desensitization of cannabinoid type 1 receptors. *J Neurochem* **104**: 1132-1143.

Wurch T, Matsumoto A, Pauwels PJ (2001). Agonist independent and –dependent oligomerization of dopamine D(2) receptors by fusion to fluorescent proteins. *FEBS Lett* **507**: 109-113.

Wyant KJ, Ridder AJ, Dayalu P (2017). Huntington's Disease-Update on Treatments. *Curr Neurol Neurosci Rep* **17**: 33.

Xiao JC, Jewell JP, Lin LS, Hagmann WK, Fong TM, Shen CP (2008). Similar in vitro pharmacology of human cannabinoid CB1 receptor variants expressed in CHO cells. *Brain Res* **1238**: 36-43.

Zawarynski P, Tallerico T, Seeman P, Lee SP, O'dowd BF, George SR (1998). Dopamine D2 receptor dimers in human and rat brain. *FEBS Lett* **441**: 383-386.

Ziegler N, Batz J, Zabel U, Lohse MJ, Hoffmann C (2011). FRET-based sensors for the human M1-, M3-, and M5-acetylcholine receptors. *Bioorganic & Medicinal Chemistry* **19**: 1048-1054.

Zuccato C, Cattaneo E (2014). Huntington's disease. *Handb Exp Pharmacol* **220**: 357-409.

Zurn A, Zabel U, Vilardaga JP, Schindelin H, Lohse MJ, Hoffmann C (2009). Fluorescence resonance energy transfer analysis of α2A-adrenergic receptor activation reveals distinct agonist-specific conformational changes. Molecular Pharmacology **75**: 534-541.

Zylbergold P, Hébert TE (2009). A division of labor: asymmetric roles for GPCR subunits in receptor dimers. *Nat Chem Biol* **5**: 608-9.

APPENDIX A OF COPYRIGHT PERMISSIONS

June 22, 2017

Amina M. Bagher
Pharmacology Department
Dalhousie University
5850 College St.
Halifax, NS B3H 4R2
Canada

Email: amina.bagher@dal.ca

Dear Amina Bagher:

This is to grant you permission to include the following article in your dissertation entitled "ALLOSTERIC INTERACTIONS WITHIN CANNABINOID RECEPTOR 1 (CB1) AND DOPAMINE RECEPTOR 2 LONG (D2L) HETEROMERS" for Dalhousie University:

> AM Bagher, RB Laprairie, MEM Kelly, and EM Denovan-Wright (2016), Antagonism of Dopamine Receptor 2 Long Affects Cannabinoid Receptor 1 Signaling in a Cell Culture Model of Striatal Medium Spiny Projection Neurons, *Mol Pharmacol*, 89(6):652-666; DOI: https://doi.org/10.1124/mol.116.103465

On the first page of each copy of this article, please add the following:

> Reprinted with permission of the American Society for Pharmacology and Experimental Therapeutics. All rights reserved.

In addition, the original copyright line published with the paper must be shown on the copies included with your thesis.

Sincerely yours,

Richard Dodenhoff
Journals Director